2010

A Molecular Mechanism for Endocytic Recycling of the M5 Muscarinic Acetylcholine Receptor

Jacob T. Bendor

A MOLECULAR MECHANISM FOR ENDOCYTIC RECYCLING OF THE M5 MUSCARINIC ACETYLCHOLINE RECEPTOR

A Thesis Presented to the Faculty of

The Rockefeller University

in Partial Fulfillment of the Requirements for

the degree of Doctor of Philosophy

by

Jacob T. Bendor

June 2010

A MOLECULAR MECHANISM FOR ENDOCYTIC RECYCLING OF THE M5 MUSCARINIC ACETYLCHOLINE RECEPTOR

Jacob T. Bendor, Ph.D.

The Rockefeller University 2010

Muscarinic acetylcholine receptors (MRs), a family of five G protein-coupled receptors (GPCRs), play an essential role in the regulation of mammalian physiology. In the brain, MR-mediated neurotransmission is required for the control of movement and motivated behavior by the basal ganglia, and MR dysfunction may contribute to schizophrenia, Alzheimer's disease, and motor disorders. Functional studies of the muscarinic receptors have been hampered by a lack of selective pharmacology, poor receptor immunoreactivity and a wide, overlapping pattern of expression. MRs are characterized by the presence of a large third intracellular loop domain (i3), the sequence of which is divergent between MR subtypes. The i3 is known to determine signaling and trafficking characteristics of GPCRs by binding to defined subsets of regulatory and effector proteins. In an effort to discover novel, subtype-specific muscarinic receptor regulatory mechanisms, we performed yeast two-hybrid protein-protein interaction screens with the five MR i3 regions. An interaction between M5 and the Arf GAP protein AGAP1 was detected, and was observed to be specific to the M5 subtype. This interaction was confirmed *in vitro*, and was shown to mediate the binding of the AP-3 adaptor complex to the M5 i3. Immunocytochemical and live cell imaging of primary rat hippocampal neurons revealed co-localization of M5 and AGAP1- or AP-3-positive vesicles after treatment with a muscarinic agonist. Activity-induced receptor

trafficking studies demonstrated that interaction with AGAP1 and activity of AP-3 were required for the endocytic recycling of M5 in neurons, the lack of which resulted in down-regulation of cell surface receptor density. M5 has been shown to be expressed in the dopaminergic neurons of the ventral midbrain and to function in the presynaptic modulation of dopamine release in the striatum. Results from dopamine release studies suggest that the abrogation of AGAP1-mediated recycling decreases the magnitude of presynaptic M5-mediated release potentiation. Our study demonstrates a novel, neuron-specific trafficking function for AGAP1 and AP-3, and suggests the presence of a previously unknown receptor recycling pathway that may underlie mechanisms of sustained sensitivity of GPCRs.

ACKNOWLEDGEMENTS

First, I would like to thank Paul Greengard for inviting me into his lab, for his mentorship and wisdom, and for his continuing encouragement to follow this challenging project wherever it may lead. I am also deeply indebted to Marc Flajolet for his guidance, optimism, and the wealth of technical and practical knowledge I gained from working with him. I thank my thesis committee members, Cori Bargmann and Jeff Friedman, for their suggestions and perceptive advice throughout all stages of my project. I also thank my outside committee member, Michael Ehlers, for his time and comments.

I would like thank the many Greengard Lab members who have provided me with technical, analytical and moral support during my stay. In particular, I thank my medical diploma student Markus Brandstetter for his contributions to this project. I also thank Angus Nairn for helpful discussion and advice, and both Elisabeth Griggs and Alison North for their assistance in the acquisition and presentation of imaging data. In addition, I thank my collaborators Hugh Hemmings, Robert Westphalen, David Sulzer, and José Lizardi-Ortiz for their time, expertise and invaluable data.

Finally, I would like to sincerely thank all of my friends who have provided camaraderie and assistance during the course of my studies. I give particular thanks to Tina Schwabe for her patience, encouragement, and help with preparation of this Thesis. Most importantly, I thank my parents and brothers for their unwavering support.

TABLE OF CONTENTS

LIST OF FIGURES

LIST OF TABLES

LIST OF ABBREVIATIONS

ACh	acetylcholine
ACh	activation domain
Arf	adenosine-5'-diphosphate ribosylation factor
ATP	adenosine-5'-triphosphate
BCS	bovine calf serum
BSA	bovine serum albumin
cAMP	3'-5'-cyclic adenosine monophosphate
CFU	colony-forming units
CPM	counts per minute
CSM	complete supplement mixture
CV	fast-scan cyclic voltammetry
ddH_2O	double-distilled water
DIV	days in vitro
DMEM	Dulbecco's modified Eagle's medium
DMF	dimethylformamide
DMSO	dimethyl sulfoxide
DNA BD	DNA binding domain
DOI	domain of interaction
DPM	decays per minute
DPM	decays per minute
DSP	dithiobis[succiniminyl propionate]
DTT	dithiothreitol,
EDTA	ethylenediaminetetraacetic acid
EGTA	ethylene glycol tetraacetic acid
ELISA	enzyme-linked immunosorbent assay
ER	endoplasmic reticulum
EtOH	ethanol
FBS	fetal bovine serum
GABA	gamma-aminobutyric acid
GAP	GTPase-activating protein
GDP	guanosine-5'-diphosphate
GEF	GTP exchange factor
GFP	green fluorescent protein
GPCR	G protein-coupled receptor
GRK	G protein-coupled receptor kinase
GST	glutathione-S-transferase
GTP	guanosine-5'-triphosphate
HBSS	Hank's buffered salt solution,
HEPES	4-(2-hydroxyethyl)-1-piperazineethanesulfonic acid
HOAc	acetic acid
IgG	immunoglobulin G

IPTG	isopropyl β-D-1-thiogalactopyranoside
LN_2	liquid nitrogen
MeOH	methanol
MOPS	3-(N-morpholino)propanesulfonic acid,
MR	muscarinic acetylcholine receptor
NAcc	nucleus accumbens
nAchR	nicotinic acetylcholine receptor
ORF	open reading frame
PBS	phosphate-buffered saline
PCR	polymerase chain reaction
PIP_2	phosphatidylinositol-4,5-bisphosphate
PMSF	phenylmethylsulfonyl fluoride
RGS	regulator of G protein signaling
SDS	sodium docecyl sulfate
SNc	substantia nigra pars compacta
TBS	tris-buffered saline
TGN	trans-Golgi network
tris	tris(hydroxymethyl)aminomethane
UAS	upstream activation sequence
UTR	untranslated region
VTA	ventral tegmental area
X-Gal	5-bromo-4-chloro-3-indolyl β-D-galactoside
Y2H	yeast two-hybrid
YNB	yeast nitrogen base
YPD	yeast extract-peptone-dextrose media

INTRODUCTION

1.1 Acetylcholine and cholinergic neurotransmission

Acetylcholine, the first molecule identified as a chemical neurotransmitter, plays an essential role in the physiology of animals. In the peripheral nervous system (PNS), acetylcholine (ACh) mediates the execution of voluntary movements via its release from motor neuron axon terminals at the neuromuscular junction. Also in the PNS, ACh functions as the post-ganglionic neurotransmitter of the parasympathetic nervous system, innervating heart, smooth muscle and glandular tissue, and serving to stimulate functions such as bronchial constriction, heart rate decrease, salivation, digestive peristalsis and blood vessel dilation. ACh further serves as the pre-ganglionic neurotransmitter for both the parasympathetic and sympathetic divisions of the PNS. In the central nervous system (CNS), ACh plays a neuromodulatory role in nearly every region of the brain. ACh neurotransmission is implicated in such processes as arousal, reward, learning, and memory. In addition, ACh is known to exhibit hormone-like activity, with autocrine and/or paracrine functions described in such non-innervated tissues as skin, lymphocytes, and the endothelium, as well as in cancer cells (Wessler et al., 2003; Wess et al., 2007; Cheng et al., 2008). The ubiquity of ACh is further demonstrated by its identification as a phylogenetically ancient molecule; ACh and its synthetic enzyme choline acetyltransferase (ChAT) have been detected in protozoa, algae, and even bacteria, and ACh is seen to

modulate such fundamental cellular processes as proliferation, migration, and morphology (Wessler et al., 1999).

In the CNS, cholinergic projection and interneurons provide widespread, diffuse innervation of nearly every brain region. Cholinergic afferents project from areas of the basal forebrain and brainstem; these neurons are further subdivided into eight nuclei based on location and targets (Ch1-Ch8), with anatomy generally conserved across mammalian species (Mesulam, 2004). The basal forebrain nuclei provide the majority of cholinergic projection neuron innervation in the CNS. Cholinergic neurons in the medial septal nucleus (Ch1) and the vertical nucleus of the diagonal band (Ch2) innervate the hippocampus, Ch3 neurons of the horizontal limb of the diagonal band project to the olfactory bulb, while cholinergic afferents originating in the nucleus basalis of Meynert (Ch4) project widely to the cerebral cortex, with particularly dense innervation of the sensory and limbic cortices in humans. In the brain stem, cholinergic projection neurons in the pedunculopontine (Ch5) and laterodorsal tegmental (Ch6) nuclei project to the thalamus and regions of the basal ganglia, while Ch7 and Ch8 neurons of the medial habenula and parabigeminal nucleus project to midbrain regions. In contrast to this system of cholinergic projection neurons, the striatum receives little input from cholinergic afferents, but is characterized by extensive intrinsic innervation by giant aspiny cholinergic interneurons. As judged by staining for cholinergic markers (ChAT and the extracellular ACh degradative enzyme acetylcholine esterase (AChE)), the striatum is in fact the

brain region most heavily innervated by the cholinergic system (Zhou et al., 2002a).

The cellular effects of ACh are mediated by two classes of receptors: nicotinic (nAchR) and muscarinic (mAchR; MR), so named for their sensitivity to the tobacco alkaloid nicotine and the mushroom toxin muscarine, respectively. Nicotinic acetylcholine receptors are a family of homo- and hetero-pentameric ligand-gated cation channels. In muscles, nAchRs are expressed post-synaptically at the neuromuscular junction, and their activation by ACh results in contraction. nAchRs mediate fast excitatory neurotransmission in PNS ganglia, while in the CNS, nAchRs serve a neuromodulatory function, most notably in the terminals of basal ganglia dopaminergic neurons (Dajas-Bailador and Wonnacott, 2004; Zhang and Sulzer, 2004). Muscarinic acetylcholine receptors, on the other hand, are metabotropic receptors belonging to the G protein coupled receptor superfamily; activation of MRs by ACh stimulates production of intracellular second messenger molecules, which in turn mediate cellular effects. MRs, of which five subtypes are known to exist in mammals, are expressed in a complex, overlapping pattern in both the CNS and periphery; in fact, nearly every cell type is known to express multiple MR subtypes (Wess et al., 2007). Adding to this complexity is the fact that MRs couple to multiple signaling pathways, leading to both convergent and divergent second messenger pathway activation in ACh-stimulated cells (Nathanson, 2000). In the following sections, we will discuss the structure, second messenger coupling, distribution, and regulatory characteristics of the muscarinic receptors in the context of this functional complexity.

1.2 G protein-coupled receptors: general characteristics

G protein-coupled receptors (GPCRs) are a structurally conserved gene superfamily, constituting the largest and most functionally diverse group of proteins in mammals and representing over 30% of identified drug targets to date (Oldham and Hamm, 2008). GPCRs are multiple-pass integral membrane proteins consisting of seven transmembrane α-helices, an extracellular N-terminus, a cytoplasmic C-terminal tail and three each of both extracellular and cytoplasmic loop regions positioned between the transmembrane helices. The GPCR superfamily is generally divided into five main subgroups based on phylogeny: class A (rhodopsin-like), class B (secretin receptor-like) class C (metabotropic glutamate receptor-like), adhesion receptor-like and Frizzled family receptors (Fredriksson et al., 2003; Foord et al., 2005). The rhodopsin-like group contains by far the greatest number of member GPCRs, including the muscarinic acetylcholine receptors. Among members of this group, structural and sequence motifs are highly conserved, implying shared mechanisms of function (Rosenbaum et al., 2009). GPCRs are activated by a variety of extracellular stimuli, including light (rhodopsin), volatile odorants and pheromones (olfactory and vomeronasal receptors, respectively) as well as small molecule, peptide, protein, ion and lipid ligands.

The classical mechanism by which GPCRs transduce extracellular signals to the cell interior relies on activation of heterotrimeric G proteins. In the resting state, GDP-bound Gα (a small GTPase protein) forms a complex with Gβ and Gγ

subunits. Upon activation, the GPCR is able to function as a GDP exchange factor (GEF) for the heterotrimeric G protein, catalyzing the exchange of GDP for GTP by the Gα subunit and leading to dissociation of activated Gα and the Gβγ dimer, thus allowing activation of effector proteins by Gα-GTP. A recently described crystal structure of the light-sensitive GPCR opsin in a pseudo-active state suggests that activation-induced conformational changes in the GPCR allow direct binding to Gα (Scheerer et al., 2008). Signaling is terminated upon hydrolysis of GTP to GDP by Gα, and subsequent re-assembly with the inhibitory Gβγ dimer into the inactive heterotrimeric complex. As the intrinsic GTPase activity of Gα is low, termination of signaling is accelerated by the presence of RGS (regulator of G-protein signaling) proteins, which function as GTPase activating proteins (GAPs) for Gα (Hepler, 1999). In addition, GPCRs typically undergo a stereotyped series of desensitization events subsequent to activation, including phosphorylation by GPCR kinases, binding of β-arrestin, and uncoupling of receptors from G-proteins; we describe this process in detail in section 1.3 of this chapter.

In contrast to the nearly 800 identified GPCRs in the human genome, far fewer G protein subtypes exist. Functional categorization of Gα subunits reveals four classes of G-protein heterotrimers: Gi/o, Gs, Gq, and G12 (Simon et al., 1991). $G\alpha_{i/o}$ and $G\alpha_{s}$ are negatively and positively coupled, respectively, to the production of cyclic AMP (cAMP) by adenylate cyclase. The second messenger cAMP, in turn, activates protein kinase A (PKA), which is able to act upon a wide variety of downstream targets, including enzymes, ion channels (Ca^{2+} and K^{+}),

transcriptional regulators, and the signal integration protein DARPP-32 in the medium spiny neurons of the striatum (Greengard, 2001). Activated $G\alpha_q$ stimulates the phospholipase C beta (PLC-β)-mediated cleavage of phosphatidylinositol-4,5-bisphosphate (PIP_2), thereby generating the second messengers diacylglycerol (DAG) and inositol triphosphate (IP_3). Diffusible IP_3 stimulates intracellular Ca^{2+} release by the gating of channels located in the endoplasmic reticulum, while membrane-bound DAG, along with Ca^{2+}, activates protein kinase C (PKC). Ca^{2+} and PKC, in turn, act upon a number of downstream targets, including ion channels and the mitogen-activated protein (MAP) kinases. $G\alpha_{12}$ class proteins appear to signal mainly through Rho GEF to affect cellular morphology and motility by downstream modulation of actin cytoskeleton dynamics (Worzfeld et al., 2008). Coupling specificity between G proteins and GPCRs is thought to arise from binding domains present on the cytoplasmic face of the receptors (Kostenis et al., 1997; Kostenis et al., 1999; Oldham and Hamm, 2008). Factors complicating this model of GPCR signal transduction include 1) GPCRs may couple to multiple G protein subtypes (Maudsley et al., 2007); 2) GPCRs also stimulate non-Gα mediated signaling, such as the modulation of voltage-gated calcium channels by Gβγ and activation of the MAP kinase pathway by β-arrestin (McDonald et al., 2000; Dolphin, 2003); and 3) GPCRs may exist as functional heterodimers (Satake and Sakai, 2008).

1.3 The muscarinic acetylcholine receptor family

The muscarinic acetylcholine receptors are a family of five rhodopsin-type (group A) GPCRs in mammals (Bonner et al., 1987). The family can be further subdivided into two groups based on G protein coupling: muscarinic receptors 1 (M1), 3 (M3) and 5 (M5) signal predominantly through Gq, while MRs 2 (M2) and 4 (M4) couple to Gi. The MR family is distinguished structurally by the presence of large third intracellular loop (i3) regions which are conserved in sequence across species but highly divergent between subtypes, save for juxtamembrane regions likely involved in G protein recognition and / or binding (figure 1.1) (Wess et al., 1995; Wess et al., 1997). In contrast, the extracellular and transmembrane regions of the MRs, including the presumed ligand binding domain, show strong sequence similarity across subtypes (figure 1.1). As a consequence of this similarity, the pharmacological specificity of cholinergic agonists and antagonists with respect to receptor subtype is poor; in addition, divergent regions of MRs appear to offer low antigenicity, precluding the successful development of subtype-specific antibodies (Wess et al., 2003; Jositsch et al., 2009). Combined with the widespread, overlapping distribution pattern of MRs, these technical limitations have greatly hampered functional studies of individual muscarinic receptors *in vivo*. The investigation of MR function in a subtype-selective manner has instead relied upon the use of single or double MR knockout mice (Wess et al., 2007). Below, we summarize the current knowledge of MR subtype function in the CNS and periphery based on knockout loss-of-function and MR binding site studies combined with tissue-

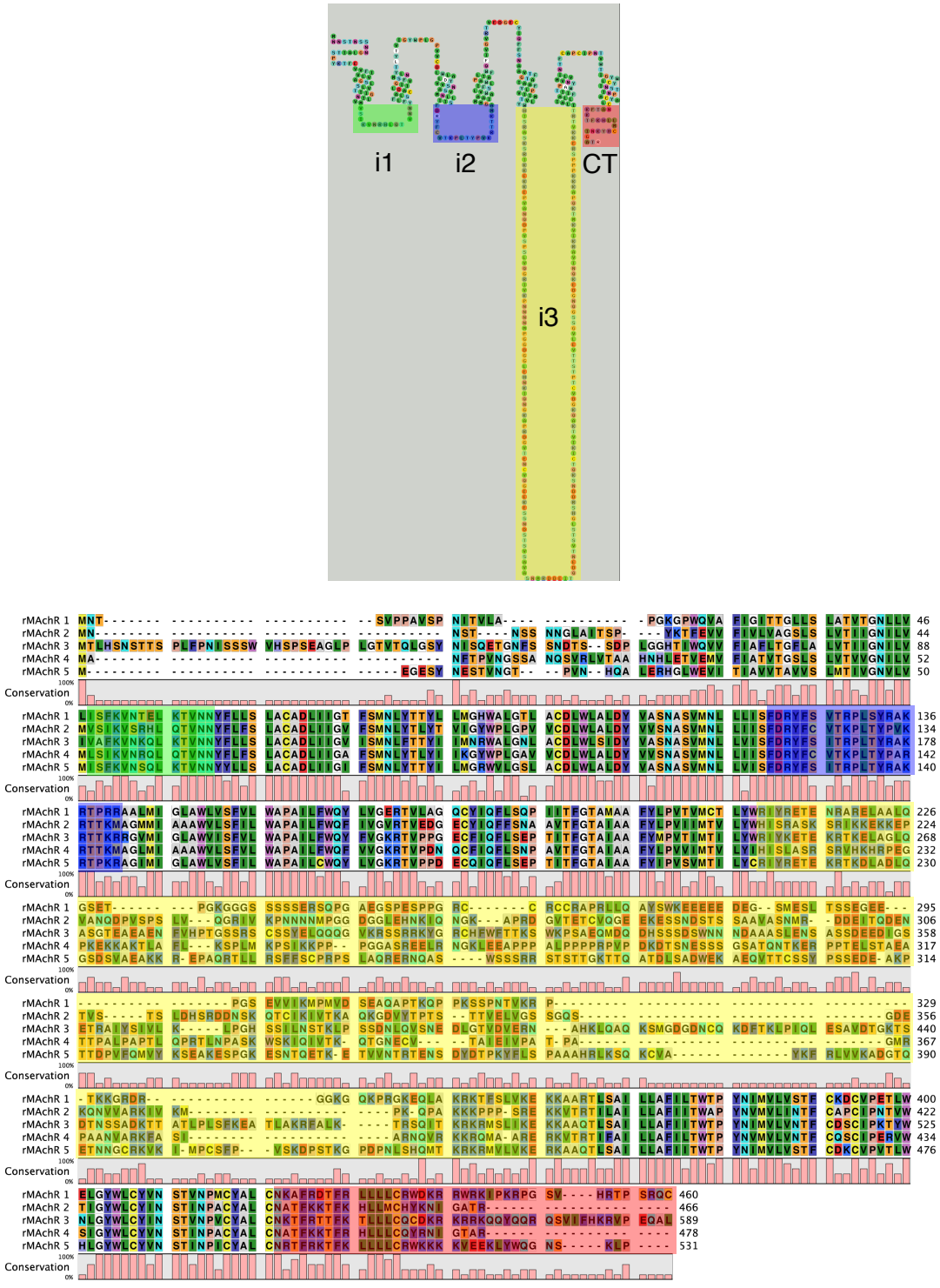

Figure 1.1 Muscarinic acetylcholine receptor topology and sequence alignment. Top: Snake plot of rat M4 illustrating extracellular, transmembrane, and cytoplasmic domains (from www.GPCR.org). i1,i2, i3: first, second and third intracellular loops, respectively; CT, C-terminal tail. Bottom: Alignment of five rat muscarinic receptor amino acid sequences, with i1, i2, i3, and CT regions highlighted. Residues are colored according to shared physical properties.

specific and global gene expression data (Oki et al., 2005; Regard et al., 2008; Ito et al., 2009).

1.3.1 *M1*

The M1 receptor is the most highly expressed muscarinic receptor subtype in the CNS, constituting the majority of MR radioligand binding sites and the entirety of ACh-stimulated Gq activation in the cortex and hippocampus (Porter et al., 2002; Oki et al., 2005). Activation of post-synaptic M1 receptors is generally excitatory, and appears to exert this neuromodulatory effect through a number of distinct mechanisms. First, activation of M1 (and other Gq-coupled receptors including M3 and M5) leads to membrane depolarization by inhibition of the voltage-dependent, outwardly-rectifying M-current (I_M). I_M is mediated by KCNQ2/3 K^+ channels, which require PIP_2 for activation; stimulation of PLC-β by M1 / $G\alpha_q$ hydrolyzes PIP_2 and deactivates this hyperpolarizing current (Zhang et al., 2003). Second, M1 activation can inhibit the activity of a number of voltage gated Ca^{2+} channels through a slow-acting mechanism involving diffusible second messengers such as PIP_2 and/or PKC activation (Liu et al., 2006; Perez-Burgos et al., 2008). M1 receptors mediate the neuromodulatory effects of ACh in cortical pyramidal neurons (Gulledge et al., 2009) and post-synaptic M1 receptors in CA3 neurons are required for induction of hippocampal gamma-oscillations (Fisahn et al., 2002). Additionally, M1 is the sole MR responsible for ACh-induced MAP kinase activation in the hippocampus, a process implicated in the mechanism of long-term plasticity (Berkeley et al., 2001). Outside of the

CNS, M1 receptor expression is low, although deficits in PNS functions such as salivation and blood pressure homeostasis were observed in M1 knockout mice (Bymaster et al., 2003). Behaviorally, M1-/- mice are moderately hyperactive, display subtle learning and memory deficits, and are insensitive to the seizure-inducing muscarinic agonist pilocarpine (Hamilton et al., 1997; Miyakawa et al., 2001; Bymaster et al., 2003).

1.3.2 *M2*

M2 receptors are the predominant MR expressed in heart myocytes, where they mediate the rate-slowing and atrial contraction strength-decreasing effects of ACh release by parasympathetic afferents. The cardiac effects of M2 are mainly transduced by Gβγ-stimulated opening of GIRK K^+ channels, leading to membrane hyperpolarization. M2 receptors are also expressed in smooth muscles, where they serve to potentiate the M3-mediated contractile effects of ACh via a cAMP-related mechanism (Stengel et al., 2000). M2 is widely expressed in the CNS, and appears to function as the primary autoreceptor for ACh at cholinergic neuron terminals outside of the striatum (Zhang et al., 2002a). The autoinhibitory effects of M2 are largely mediated by fast-acting Gβγ binding-induced inhibition of N- and P/Q- type Ca^{2+} channels (Shapiro et al., 2001). M2 also serves as an inhibitory autoreceptor and modulatory receptor at post-ganglionic parasympathetic and sympathetic nerve terminals, respectively (Zhou et al., 2002b; Trendelenburg et al., 2003). The M2 -/- mouse exhibits reduced sensitivity to the analgesia-inducing muscarinic agonist oxotremorine, altered

neuronal plasticity in the hippocampus, and deficits in memory and behavioral flexibility (Gomeza et al., 1999a; Tzavara et al., 2003; Seeger et al., 2004).

1.3.3 *M3*

M3 receptors are expressed in nearly all smooth muscle and glandular tissues, and are the primary MRs mediating the effects of ACh released by the parasympathetic PNS on blood vessels, the eye, the gastrointestinal, reproductive and urinary tracts, and in exocrine glands (Bymaster et al., 2003). In addition, M3 plays a key role in the regulation of glucose homeostasis by mediating the IP3-dependent potentiation of glucose-stimulated insulin release by pancreatic islet β cells (Gautam et al., 2006). M3 receptors are expressed widely in the CNS, but appear to play a minor role in the regulation of neuronal excitability, although hypothalamic dysfunction has been noted in the M3 -/- mouse (Yamada et al., 2001b; Gautam et al., 2009). Aside from exhibiting peripheral abnormalities associated with PNS dysfunction (and the glucose homeostasis phenotype described above in a β cell conditional knockout model), $M3^{-/-}$ mice exhibit feeding deficits, reduced serum leptin levels, and are abnormally small and lean (Yamada et al., 2001b; Gautam et al., 2009).

1.3.4 *M4*

M4 receptors are expressed at low levels outside of the CNS, where they play a minor, M2-like functional role in peripheral tissues and may be important for the motility of keratinocytes during wound healing (Zhou et al., 2002b;

Bymaster et al., 2003; Trendelenburg et al., 2003; Chernyavsky et al., 2004). In the brain, M4 is a low-abundance autoinhibitory receptor at cortex and hippocampal cholinergic terminals, likely functioning similarly to M2 via a Ca^{2+} channel mechanism (Zhang et al., 2002a). However, M4 is expressed at high levels in the striatum, where it functions both pre- and post-synaptically (discussed in further detail in section 1.2.8) (Zhang et al., 2002b; Oki et al., 2005). M4 -/- mice exhibit modest M2-like deficits in muscarinic agonist-induced analgesia, but are markedly hyperlocomotive and hypersensitive to the effects of D1 dopamine receptor agonists (Gomeza et al., 1999b; Gomeza et al., 2001).

1.3.5 *M5*

The M5 receptor is the least abundant muscarinic receptor expressed in mammals. M5 comprises less than 2% of the total MR population in the brain and is functionally undetectable in peripheral tissues, though low levels of M5 mRNA have been reported in skin and in some cancer cell lines (Kohn et al., 1996; Oki et al., 2005; Ito et al., 2009). However, M5 is the only muscarinic receptor for which expression is detected in the midbrain dopaminergic neurons of the substantia nigra pars compacta (SNc) and ventral tegmental area (VTA) (Weiner et al., 1990; Wess et al., 2007). Both somatodendritic and pre-synaptic M5 receptors mediate the ability of ACh to potentiate dopamine release from SNc and VTA neurons (Yamada et al., 2001a; Forster et al., 2002). In addition, M5 is the sole MR responsible for the dilatory action of ACh on cerebral arteries and arterioles, a function mediated by the M3 receptor elsewhere in the body

(Yamada et al., 2001a). The M5 -/- mouse exhibits mild cognitive defects, decreased sensitivity to amphetamine and morphine, reduced cocaine self-administration, and altered sensorimotor gating (Basile et al., 2002; Wang et al., 2004; Thomsen et al., 2005; Araya et al., 2006).

1.3.6 *Muscarinic receptor distribution and function in the striatum*

The basal ganglia (BG), a group of subcortical nuclei composed of the substantia nigra, pallidum, subthalamic nucleus, and striatum, play a critical role in the processing and integration of neuronally encoded information to produce motivated behaviors. The striatum is the major input nucleus of the BG, consisting mainly (90-95%) of GABAergic medium spiny neurons (MSNs) projecting to the BG output nuclei. The striatum can be divided functionally and anatomically along a dorsolateral to medioventral axis: dorsolateral areas, receiving glutamatergic afferents from sensorimotor cortex and dopaminergic input from the SNc, function mainly in the execution of movement and in spatial and procedural memory, while the medioventral striatum (including the nucleus accumbens) receives glutamatergic afferents mainly from limbic areas (including the hippocampus and amygdala) and dopaminergic input from the VTA, and plays a central role in motivation, reward, and the pathophysiology of drug addiction (Voorn et al., 2004). Striatal anatomy can be further subdivided on the basis of MSN efferent pathways, illustrated in figure 1.2: “direct” striatonigral MSNs directly innervate the BG output nuclei (the substantia nigra pars reticulata (SNr) and globus pallidus internal capsule (GPi)), while “indirect” striatopallidal

MSNs project to an intervening inhibitory nucleus (the globus pallidus external capsule, or GPe) and ultimately innervate the SNr/GPi indirectly via the subthalamic nucleus (STN). Importantly, direct pathway MSNs express excitatory D1 dopamine receptors, while indirect MSNs express inhibitory D2 receptors. This segregated expression pattern allows dopamine to potentiate the MSNs' disinhibition-mediated activation of thalamocortical output pathways (figure 1.2). The balance of non-MSN neurons in the striatum is composed of GABAergic and cholinergic interneurons. The giant aspiny cholinergic interneurons, comprising 2% of the total neuronal population of the striatum, are tonically active and provide both volumetric and synaptic innervation of MSNs through highly arborized axons (Pisani et al., 2007). The interaction between cholinergic and dopaminergic activity in the striatum plays a major role in the regulation of MSN activity and plasticity, and in turn is required for proper coordination of motivated locomotor activity (Pisani et al., 2007).

Figure 1.2 (following page), Cholinergic innervation and muscarinic receptor expression in the basal ganglia. Red, green, yellow and blue represent GABAergic, glutamatergic, cholinergic, and dopaminergic neurons and terminals, respectively. Small squares and circles represent dopamine and muscarinic receptors, respectively, with subtype noted by number. Green receptors are excitatory, while red receptors are inhibitory. Circles indicate neuron somatodendritic compartments, and axon terminals are indicated by triangles; non-synaptic terminals indicate volumetric ACh release (striatum) or diffuse innervation (thalamostriatal and thalamocoritical pathways, and cholinergic innervation of the cortex). GPe, globus pallidus external capsule; STN, subthalamic nucleus, SNr, substantia nigra pars reticulata, GPi, globus pallidus internal capsule, SNc, substantia nigra pars compacta, VTA, ventral tegmental area; MSN, medium spiny neuron.

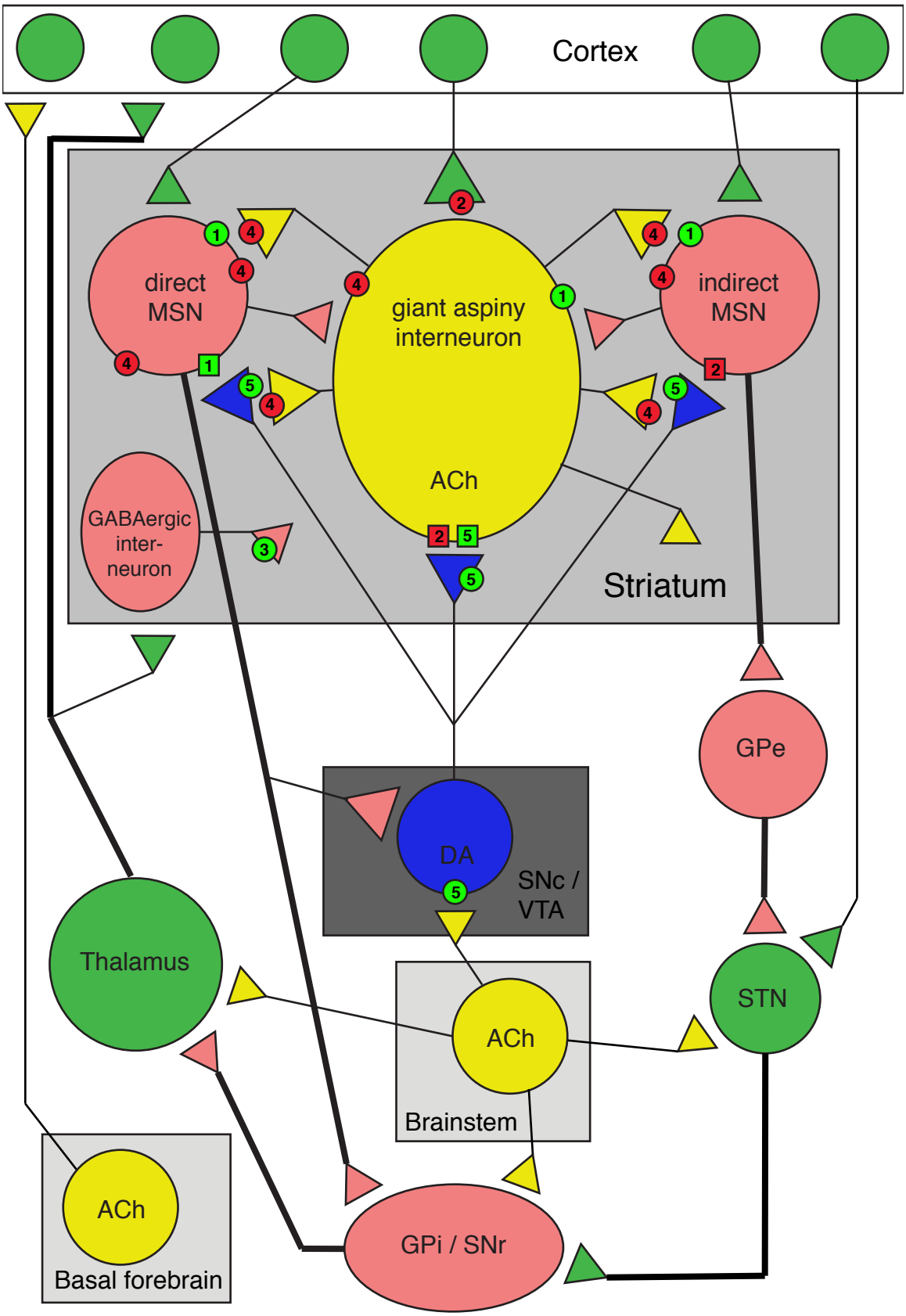
Cortex
direct MSN
giant aspiny interneuron
indirect MSN
ACh
GABAergic inter-neuron
Striatum
GPe
DA
SNc / VTA
Thalamus
STN
ACh
Brainstem
ACh
Basal forebrain
GPi / SNr

Muscarinic receptors are expressed in a complex, overlapping pattern in the striatum, and play a central role in the mediation of ACh's effects upon BG function (figure 1.2). Giant aspiny interneurons receive input from SNc and VTA dopaminergic neurons and co-express the D2 and D5 dopamine receptor subtypes. Activation of D2 receptors inhibit, while activation of D5 receptors stimulate, the firing rate and ACh release of aspiny interneurons; however, the *in vivo* coordination of these actions on individual cholinergic neurons is unknown (Yan et al., 1997; Yan and Surmeier, 1997). Medium spiny neurons express dendritic M1 and M4 muscarinic receptors, with anatomical and functional evidence suggesting preferential expression of M4 receptors on direct pathway MSNs (Santiago and Potter, 2001). MSN M1 activation is generally excitatory, although M1-stimulated Ca^{2+} / PKC activity can inhibit voltage-gated calcium channels (Calabresi et al., 2000). Post-synaptic M4 activation is seen to inhibit GABA release by medium spiny projection neurons. However, M4 also plays a key, striatum-specific autoinhibitory role at cholinergic interneuron terminals, functioning to reduce the ACh input to M1- and M4- expressing MSNs (Zhang et al., 2002a). M2 and M3 are present at low levels in the striatum, with neurotransmitter release-modulating functions reported for these receptors at corticostriatal glutamatergic and GABAergic interneuron terminals, respectively (Zhang et al., 2002b). In addition, cholinergic neurons themselves likely express somatodendritic M1 and M4 muscarinic receptors, with volumetrically released ACh providing input (Pisani et al., 2007).

Further complicating the system of muscarinic receptor function in the striatum is the fact that ACh can also exert influence on the release of dopamine by nigrostriatal and mesolimbic neurons (figure 1.2). Studies of evoked dopamine release in MR knockout mice have shown that M4 and M5 receptors mediate the ability of ACh to potentiate evoked DA release in the striatum; M4 likely exerts an indirect, trans-synaptic effect via receptors expressed on MSNs or cholinergic interneuron terminals, while ACh activation of dopaminergic terminal-localized M5 receptors is able to modulate dopamine release directly. M3 receptor activation was seen to indirectly inhibit evoked dopamine release, while a dopamine-modulatory role for M1 and M2 receptors was not observed (Zhang et al., 2002b). In addition, muscarinic receptor M5, the only MR detectably expressed in midbrain dopaminergic neurons, was seen to mediate the ability of ACh released from brainstem afferents to stimulate prolonged dopamine release from mesolimbic neuron terminals (Forster et al., 2002). Thus, while the overall effect of ACh on MSNs is to oppose the stimulatory action of dopamine on the disinhibition of thalamic output nuclei, the possibility of single-neuron co-expression of excitatory and inhibitory MRs, the opposing effects of pre- and post-synaptically localized M4, and the complex nature of ACh-regulated DA release leaves great uncertainty as to the precise roles of MR subtypes on striatal function. Adding a final layer of complexity is the role of muscarinic receptors in the regulation of DARPP-32 in MSNs; although not directly examined, activation of the Gq-coupled M1 and Gi-coupled M4 receptors may lead to inhibition of PKA activity and altered intracellular Ca^{2+} levels, thus

modulating DARPP-32's protein phosphatase-1 mediated effects on downstream receptor or transcriptional effectors (Svenningsson et al., 2004). The exact role of muscarinic receptor in the function of the striatum and BG is thus incompletely understood, and underscores the the need for development of cell-specific and MR subtype-selective experimental tools.

1.3.7 *Muscarinic receptors and CNS disease / dysfunction*

Muscarinic receptor dysfunction has been implicated in a number of diseases of the CNS. In Alzheimer's disease (AD), selective death of basal forebrain neurons leads to reduced cholinergic innervation of the hippocampus and cortex (Auld et al., 2002). Although the M1-/- mouse exhibited only modest cognitive dysfunction, transgenic AD-model mice treated with an M1-preferring agonist showed both improvements in cognitive function and reductions in β-amyloid and Tau pathologies in the cortex and hippocampus (Caccamo et al., 2006) and systemic administration of the non-selective muscarinic receptor antagonists scopolamine or atropine results in profound learning and memory inhibition in rodents and humans (Fibiger et al., 1991). In addition, M2 -/- mice show substantial learning and memory deficits, and decreased short- and long-term potentiation in hippocampal synapses (Tzavara et al., 2003; Seeger et al., 2004).

Although the pathophysiology of schizophrenia is most closely associated with dysfunction in mesolimbic neurotransmission, extra-dopaminergic symptom characteristics and the well-described interaction between the cholinergic and

dopaminergic systems suggest that ACh function may be clinically significant. The following observations argue for a role of muscarinic receptors in schizophrenia: 1) Post-mortem and *in vivo* imaging studies have identified decreased MR binding site density in the cortex, hippocampus and striatum of schizophrenic patients; 2) High doses of muscarinic antagonists lead to psychosis-like states, and N-desmethylclozapine, a metabolite of the widely used atypical antipsychotic clozapine, shows strong subtype-selective partial agonism towards M1 (Sur et al., 2003); 3) genetic linkage studies have implicated the M5-encoding *Chrm5* gene as a schizophrenia susceptibility locus; and 5) M5 -/- mice show alterations in schizophrenia-related sensorimotor gating behaviors (Wang et al., 2004; Thomsen et al., 2007). Knockout mouse and genetic linkage studies have also implicated muscarinic receptors in the etiology of pain, drug addiction, type 2 diabetes, and PNS-related disorders (Wess et al., 2007).

Despite the potential of muscarinic receptors as drug targets for the treatment of CNS diseases, the utility of such compounds has been limited by the undesirable parasympathetic-related side-effect profile of MR agonists and antagonists. The successful development of subtype-specific muscarinic drugs has been greatly hampered by the high conservation among MRs of the ACh (orthosteric) binding site. Thus, although targeting of predominantly neuronally-expressed MRs (M1, M4, and M5) could significantly reduce PNS-related off-target effects, only non-selective muscarinic agonists and antagonists, as well as cholinergic transmission-enhancing AChE inhibitors, are currently in clinical use. Aside from their obvious utility in research applications and in the treatment of

diseases directly related to muscarinic receptor dysfunction, such subtype-specific MR drugs could also show efficacy in the treatment of Parkinson's disease, for which non-selective muscarinic antagonists were the first accepted treatment and are currently used to alleviate dystonia symptoms. Parkinson's disease is a movement disorder characterized by the death of SNc nigrostriatal dopaminergic neurons, leading to relative hyperactivity of the striatal cholinergic system. M4-targeted drugs could alleviate hypercholinergia either by antagonism of post-synaptic M4 receptors distributed preferentially on direct pathway MSNs, or by stimulating interneuron M4 autoreceptors and decreasing striatal ACh tone. Additionally, development of M5-specific agonists could prove useful in the treatment of age-related cognitive impairment by increasing cerebral blood flow.

1.4 Regulation of muscarinic receptor function

The regulation of GPCR signaling efficacy in time and space is central to the ability of a cell to both respond and adapt to outside stimuli. The steady-state density of cell surface receptor molecules, and the degree to which termination of ligand-induced GPCR signaling events is followed by receptor resensitization, are crucial in determining the effects of sustained stimulation on cellular physiology (Hanyaloglu and von Zastrow, 2008). In neurons, such sensitivity-tuning mechanisms are important for plasticity events underlying learning and memory (Wang et al., 2005; Wang et al., 2009a). Despite the large number of GPCRs expressed in mammals, the basic mechanisms regulating nascent receptor delivery, plasma membrane sorting in polarized cells, steady-state cell

surface density, desensitization, resensitization and down-regulation of GPCRs are generally conserved. Nonetheless, important receptor-, tissue-, and subcellular compartment-specific regulatory details exist. A common theme binding these GPCR-modulating mechanisms is the importance of protein-protein interactions between receptors and trafficking, anchoring, or signal-regulating molecules. As with functional studies of muscarinic receptors, however, the lack of subtype-specific antibodies and ligands has left us with a limited understanding of the mechanisms governing the regulation of muscarinic receptors *in vivo*. Below, we discuss the regulation of MRs in the context of more thoroughly characterized GPCR systems.

1.4.1 *Cell-surface delivery of newly synthesized MRs*

GPCRs newly translated in the endoplasmic reticulum are delivered to the plasma membrane via the Golgi complex largely through the unregulated secretory pathway (figure 1.3) (Achour et al., 2008). Although the regulation of nascent GPCR expression is far less understood than the endocytic trafficking of mature cell surface receptors, a number of protein-protein binding events influencing plasma membrane delivery have been identified. For example, interaction between the third intracellular loops of serotonin receptors 5-HT1B and 5-HT4 and the annexin II light chain protein p11 increases the cell surface expression of these receptors in a functionally significant manner (Svenningsson et al., 2006; Warner-Schmidt et al., 2009). Similar chaperone-like interactions negatively or positively influencing surface expression of GPCRs have been

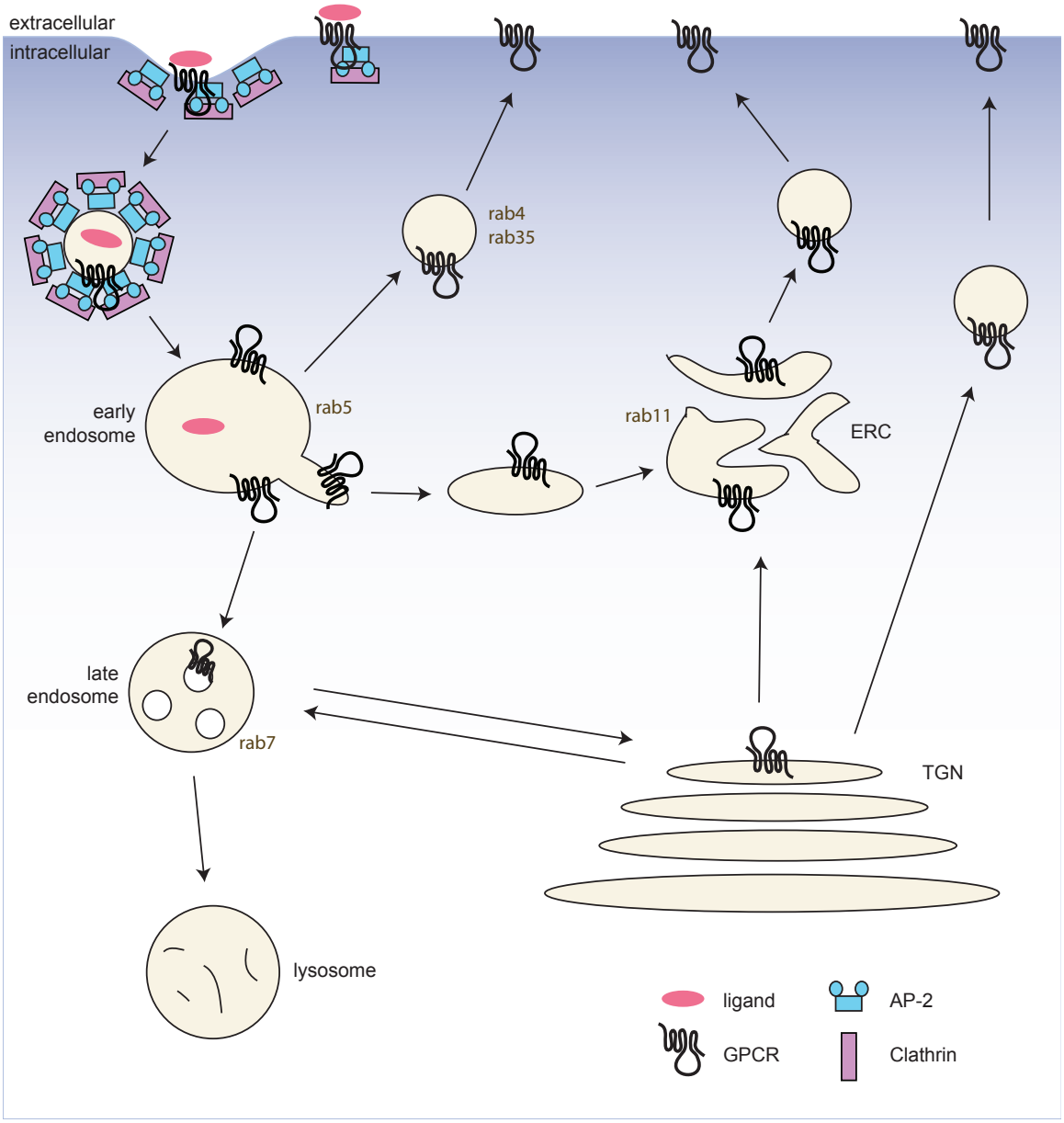

Figure 1.3 Summary of canonical GPCR trafficking pathways. Upper left, clathrin-dependent endocytosis of an activated GPCR. After endocytic vesicle uncoating, internalized receptors are delivered to the early endosome and are sorted to the degradative pathway via the rab7-positive late endosome (bottom left) or to the recycling pathway via a fast, rab4/rab35-dependent pathway (middle left) or through a slow pathway via the rab11-positive endocytic recycling compartment (ERC; middle right). Newly synthesized GPCR molecules are delivered to the plasma membrane from the trans-golgi network (TGN) via the unregulated secretory pathway (right) or through a regulated TGN-to-endosome pathway (middle right).

described for the dopamine D1 receptor (DRiP78), the angiotensin AT2 receptor (ATBP50), and the thromboxane A2 receptor (RACK1) (Bermak et al., 2001; Wruck et al., 2005; Parent et al., 2008). Heterooligomerization of GPCRs can also influence plasma membrane delivery: cell surface expression of the $GABA_BR1$ receptor is dependent upon co-expression, and physical interaction with, the $GABA_BR2$ receptor (Margeta-Mitrovic et al., 2000). Finally, regulated delivery of D1 dopamine and δ-opioid receptors to the cell surface from intracellular pools has been described, and may represent a mechanism of receptor sensitization (Achour et al., 2008).

A secondary, TGN-to-endosome mediated pathway of GPCR trafficking may also play a role in the regulated expression of newly synthesized receptors. Subcellular transport of GPCRs and other integral membrane protein cargo is mediated by a complex system of intracellular membrane trafficking, the details of which are still being elucidated. The basic mechanism of intracellular receptor trafficking is as follows: Adaptor proteins, heterotetrameric complexes of which four are known to be expressed in mammals (AP-1 through AP-4), are recruited to specific intracellular membrane compartments, in many cases by interaction with GTP-bound Arf (ADP ribosylation factor) proteins. There, the adaptor proteins are able to simultaneously bind to both cytoplasmic receptor domains containing specific amino acid motifs and membrane coat proteins, the most common of which is clathrin. Cargo-containing, coated membrane buds are “pinched-off” from host membranes through the action of accessory proteins such as dynamin, endophillin and amphiphysin. Endosomal vesicles are then

transported to specific locations via interaction with motor proteins and the cellular cytoskeleton, and cargo proteins delivered to target membranes by coat disassembly and vesicle fusion. The identity and functional characteristics of transport vesicles are regulated by membrane phospholipid content, and by the presence of specific Rab family proteins; these membrane-associated small GTPases recruit other functional and scaffolding proteins to specific vesicular compartments. Rabs switch between GTP-bound “on” and GDP-bound “off” states, the cycling of which is regulated by the presence of specific GEF and GAP proteins. TGN-to-endosome mediated transport of nascent GPCRs to the cell surface likely proceeds via an AP-1 and clathrin-dependent process, whereby the AP-1 complex recruits targeted receptors by binding to signal sequences present in intracellular regions (Nakatsu and Ohno, 2003). Such a process may underlie the motif-dependent delivery of the V2R vasopressin and α2B adrenergic receptors to the cell surface, and in the targeting of GPCRs to apical or basolateral domains in polarized cells (Dong and Wu, 2006).

Little is known regarding mechanisms regulating the cell surface delivery of newly translated muscarinic receptors. It has been shown, however, that in the polarized Madin-Darby canine kidney cell line, M2 is targeted to the apical plasma membrane domain, while M3 is targeted basolaterally via a dominant sorting signal present in the third intracellular loop (Nadler et al., 2001). Additionally, a phenylalanine-rich motif in the M2 receptor C-terminal tail was shown to bind the ER-associated protein DRiP78, leading to intracellular receptor sequestration in an exogenous expression system (Bermak et al., 2001).

1.4.2 *Stabilization of MRs in the plasma membrane*

The cell surface localization and two-dimensional diffusion characteristics of GPCRs are regulated by interaction with scaffolding proteins, among other mechanisms. Such regulation is particularly important in neurons, where localization of GPCRs to synaptic compartments and stabilization of receptors at the cell surface play a critical role in synaptic plasticity. The scaffolding protein PSD-95 is the best characterized of these molecules; it is localized almost exclusively at the post-synaptic density, and serves to organize and stabilize synaptic proteins, most notably AMPA and NMDA glutamate receptors (Kim and Sheng, 2004). PSD-95 can bind directly to the β1 adrenergic receptor via a C-terminal tail PDZ-binding domain, and indirectly to metabotropic glutamate receptors mGluR1 and mGluR5 via the scaffolding adaptor protein Homer; both of these interactions were shown to stabilize the receptors at the cell surface (Xiao et al., 1998; Hu et al., 2000). A second example of a scaffolding protein / GPCR interaction is the binding of the dopamine D2 and α2 adrenergic receptors via their i3 loops to spinophilin, an actin- and protein phosphatase-1-binding protein. This interaction was shown to stabilize receptors in the basolateral membrane domain of polarized cells, and to regulate GPCR-stimulated Ca^{2+} signaling by the concurrent binding of RGS2 (Brady et al., 2003; Wang et al., 2005). To date, however, no specific interactions between scaffolding proteins and muscarinic receptors have been identified.

1.4.3 *Agonist-induced desensitization and internalization*

After activation, nearly all GPCRs undergo a similar series of molecular events that serve to desensitize the receptor to further stimulation. In ligand gated receptors, the process was first identified in, and is best characterized for the β2 adrenergic receptor (β2AR) (Lohse et al., 1990; Gainetdinov et al., 2004; Hanyaloglu and von Zastrow, 2008). Upon ligand binding and G protein heterotrimer dissociation, GPCRs undergo a conformational change leading to phosphorylation on serine and threonine residues present on the C-terminal tail and i3 loop by G protein-coupled receptor kinases (GRKs). This phosphorylation induces binding of β-arrestin to cytoplasmic regions of the receptor, and serves to uncouple the GPCR from its cognate G protein complex by steric hindrance, leading to rapid desensitization of signaling. The GPCR-bound β-arrestin molecule also functions to bind adaptor protein AP-2 complex subunits, thus recruiting the desensitized receptor to PIP_2, clathrin and AP-2 enriched structures known as clathrin-coated pits. Upon further binding of AP-2 subunits to tyrosine-containing motifs on the GPCR C-terminal tail, recruitment of clathrin by AP-2 to the nascent vesicle, and membrane scission by a dynamin-dependent mechanism, the receptor-β-arrestin complex is internalized into a clathrin-coated vesicle (figure 1.3). Variations to this generalized mechanism exist, however, and likely depend on the differential receptor-regulatory protein interactions based on the presence or absence of specific protein-protein binding motifs on GPCR

cytoplasmic regions. Examples include constitutively internalized receptors, clathrin-, β-arrestin and/or dynamin-independent receptor internalization, dileucine motif-dependent internalization, and non-GRK mediated receptor phosphorylation (Pals-Rylaarsdam et al., 1997; Budd et al., 2000; Marchese et al., 2008). In addition, 1) heterologous (ligand binding-independent) GPCR phosphorylation activity can influence receptor / G protein coupling, and 2) the degree to which receptors undergo activity-induced phosphorylation may regulate the strength of β-arrestin binding, leading to differential downstream resensitization characteristics (Daaka et al., 1997; Marchese et al., 2008).

With the exception of M5, the phosphorylation and agonist-induced internalization characteristics of the muscarinic acetylcholine receptors have been investigated in heterologous expression systems. Muscarinic receptors M1 through M4 are phosphorylated by GRK2 in an agonist-dependent manner, exhibit desensitization of G protein signaling after prolonged stimulation, and undergo agonist-induced internalization and sequestration, events that require the presence of the i3 loop region (van Koppen and Kaiser, 2003). However, the mechanistic details of these events differ between subtypes. Whereas M1, M3 and M4 internalize via a β-arrestin- and clathrin-dependent mechanism, M2 receptor internalization is β-arrestin-, dynamin- and clathrin-independent, although overexpression of β-arrestin or β-arrestin-2 was able to increase the rate of M2 endocytosis (Pals-Rylaarsdam et al., 1997). In cardiac myocytes, internalization of endogenous M2 receptors was seen to be caveolin-dependent; however, M2 expressed exogenously in HEK-293 cells was not observed to

internalize through caveolae (Pals-Rylaarsdam et al., 1997; Dessy et al., 2000). Additional subtype specificity exists on the level of receptor phosphorylation. For example, the kinase CK1α plays a major role in the agonist-induced phosphorylation of exogenously expressed M3. This phosphorylation event appears to attenuate Gq, but not MAP kinase pathway coupling, and does not stimulate receptor internalization (Budd et al., 2000; Luo et al., 2008). Agonist-induced phosphorylation of M3 by CK2 and GRK6 has also been observed; however, involvement of these kinases was apparently expression system and cell type-dependent (Willets et al., 2003; Torrecilla et al., 2007). A recent study has also demonstrated constitutive, non-agonist stimulated and i3 loop-independent internalization of M3 receptors expressed in HeLa cells (Scarselli and Donaldson, 2009). Finally, the i3 loops of M1, M3 and M5 were shown to bind selectively to the G protein signaling attenuator RGS2. In M1, this receptor binding activity was required for the antagonism of agonist-stimulated PLCβ activity, suggesting that protein-protein binding mediated recruitment of RGS molecules to MRs may serve as a general mechanism of signaling desensitization (Bernstein et al., 2004). Taken together, current evidence points to the regulation of muscarinic receptor desensitization and internalization by heterogenous, cell- and subtype-specific mechanisms, the details of which remain unclear.

1.4.4 *Endocytic recycling*

Resensitization of agonist-internalized GPCRs begins with dissociation of β-arrestin, receptor dephosphorylation, and delivery of receptors to the Rab5-and phosphatidylinostiol-3-phosphate- positive early endosome. From this structure, signaling-competent receptors can be recycled to the cell surface through two general pathways (figure 1.3). In the fast recycling route, Rab4 / Rab35 endosomes return receptors to the plasma membrane directly from early endosomes. In the slow endocytic recycling route, which is more highly regulated and the most common pathway for GPCR recycling, receptors are first delivered to the typically perinuclear, Rab11-positive tubulovesicular endocytic recycling compartment (ERC) before returning to the plasma membrane via recycling endosomes (Grant and Donaldson, 2009). The ERC is likely composed of membrane and cargo proteins derived from matured membrane tubules extending from the early endosome; therefore, ERC-mediated receptor recycling is to some extent iterative / constitutive (Maxfield and McGraw, 2004). However, sorting signal-mediated protein interactions do play a role in the targeting of GPCRs for recycling, although the exact nature of these signals and interacting proteins remain poorly characterized. Recycling of the β1 and β2 adrenergic, the lutropin LH, and the κ-opioid receptors was seen to depend on interaction of distinct C-terminal tail motifs with PDZ domain-containing proteins (including PSD-95, NHERF-1, and GIPC) (Cao et al., 1999). In addition, a recycling motif present in the dopamine D1 C-terminal tail was shown sufficient to re-route a second receptor from the degradative to recycling pathways when fused to its C-

terminus (Vargas and Von Zastrow, 2004). In neurons, the endocytic recycling system is specialized; for example, rab11-positive recycling endosomes are present in dendrites and axons, and their translocation to dendritic spines plays a critical role in the mechanism of long-term potentiation (Park et al., 2004; Park et al., 2006; Wang et al., 2008). The neuronal endocytic recycling system serves a key function in the maintenance of axon / somatodendritic polarity by the targeted sorting of endocytosed plasma membrane proteins.

The endocytic recycling of muscarinic receptors has not been extensively studied. Agonist-internalized M1, M3 and M4 receptors expressed exogenously in HEK-293 cells were observed to undergo efficient endocytic recycling and signaling resensitization (Vogler et al., 1998; Krudewig et al., 2000). The endocytic recycling of M4 receptors was shown to depend on a 21-amino acid region in the i3 loop; fusion of this motif to a recycling-negative muscarinic receptor conferred upon it recycling activity (Krudewig et al., 2000; Hashimoto et al., 2008b). In addition, endocytic recycling of endogenous, predominantly M3-like muscarinic receptors in SH-SY5Y neuroblastoma cells was observed (Szekeres et al., 1998a); however, desensitization and resensitization of M3 receptors expressed exogenously in CHO cells was seen to proceed independently of receptor internalization and recycling (Tobin et al., 1992). Thus, similar to desensitization, endocytic recycling of muscarinic receptors appears to be subtype- and cell-specific but is poorly characterized in endogenous systems.

1.4.5 *Lysosomal targeting and down-regulation*

Upon agonist-induced endocytosis, GPCRs may be targeted for proteolytic degradation in lysosomes as opposed to cell surface recycling-based resensitization (figure 1.3). Degradative pathway targeting results in a decrease of overall receptor protein levels and forms a major component of the GPCR down-regulation response, a process distinct from that of rapid receptor desensitization and central to cellular adaptations to chronic stimulation, including those observed in the drug-addicted brain. The sorting of lysosomally-targeted GPCRs to Rab7-positive late endosomes occurs mainly at the early endosome level and is dependent on a number of relatively well-characterized protein-protein interactions between trafficking molecules and targeting motifs present in GPCR cytoplasmic regions. Many GPCRs contain lysosomal sorting signals in their C-terminal tails conforming to tyrosine-based YXXΦ (with Φ representing bulky hydrophobic residues) or dileucine-based [D/E]XXXL[L/I] motifs (Bonifacino and Traub, 2003). These signals confer lysosomal targeting by binding to adaptor protein complexes, and are critical to the constitutive degradation of endocytosed GPCRs. Similarly, the binding of GPCR-associated sorting proteins (GASPs) with C-terminal tail sequences is required for lysosomal targeting of endocytosed δ-opioid receptors, as well as a variety of other GPCRs (Whistler et al., 2002; Heydorn et al., 2004). Finally, covalent addition of ubiquitin to cytoplasmic lysine residues of GPCRs can serve as a degradative signal, functioning to direct sorting to lysosomes via the late endosome / multivesicular body through interaction with ESCRT complex proteins (Marchese et al., 2008).

In β2 adrenergic receptor-expressing cells treated chronically with agonist, receptor ubiquitination leads to diversion of endocytosed β2AR from the recycling to the lysosomal pathway, resulting in proteolytic down-regulation of the receptor (Shenoy et al., 2001).

YXXΦ and DXXXLL lysosomal targeting sequence-like motifs are present in the C-terminal tails of muscarinic receptors M2/M4 and M1, respectively. In addition, GASP-1 and GASP-2, members of a 10-protein family sharing a GPCR interaction domain, were observed to bind M1 and M2 C-terminal tails *in vitro* (Simonin et al., 2004) However, among the M1-M4 receptor subtypes, only M2 has been shown to undergo degradative down-regulation (Krudewig et al., 2000). Mutation of the M2 C-terminal tail tyrosine residue was seen to reduce receptor down-regulation but did not effect agonist-induced endocytic sequestration (Goldman and Nathanson, 1994). Down-regulation of muscarinic receptor binding sites was observed in cultured chick retina and rat cerebellar granule neurons after chronic agonist stimulation (Siman and Klein, 1983; Xu and Chuang, 1987). Finally, cocaine self-administration was shown to down-regulate muscarinic receptor binding sites in the mouse striatum; however, the magnitude this down-regulation was paradoxically increased in GASP-1$^{-/-}$ mice (Boeuf et al., 2009). As is the case with other aspects of muscarinic receptor regulation, the study of MR down regulation in a cell- and receptor-specific manner remains complicated by overlapping subtype expression patterns and a lack of appropriate experimental tools.

1.5 Summary and study rationale

Muscarinic receptors influence the function of nearly every cell in the mammalian body. As metabotropic G protein-coupled receptors that transduce the effects of extracellular acetylcholine, MRs mediate such varied physiological responses as cell growth and motility, glandular secretion, smooth muscle contraction, neuronal excitability, synaptic plasticity, and dopamine release. The five muscarinic receptors share with other GPCRs common signaling and regulatory pathways; therefore, the general characteristics governing activity of the MR family are well known. However, an understanding of MR subtype-specific functional mechanisms remains elusive. Muscarinic receptors are highly similar in sequence throughout much of their structure, including that of the orthosteric ligand binding domain; as a result, few truly subtype-selective small molecule agonists and antagonists have been identified. In addition, the MRs have proven particularly resistant to the development of subtype-selective antibodies useful for the identification and analysis of receptors expressed *in vivo*. In combination with the fact that nearly every cell type expresses at least two distinct MRs, this lack of subtype-selective tools has greatly limited our ability to precisely study muscarinic receptor signaling and regulation. The physiological effects of ACh are clearly not homogenous with respect to tissue and cell type; thus, our knowledge of this ubiquitous and fundamental neurotransmitter system remains incomplete.

The structure of muscarinic receptors is notable for the presence of a large third intracellular (i3) loop region whose sequence, in contrast to that of the remaining structural domains, is highly divergent between subtypes. In other GPCRs, the i3 loop region has been shown to mediate the binding of signaling, regulatory and trafficking proteins. These protein-protein interactions are largely responsible for determining the effector coupling, distribution, and re- or de-sensitization characteristics of a given GPCR. Although many of these protein binding events are determined by the presence of conserved amino acid motifs on the receptor i3 loop regions, the precise nature of most protein-GPCR interactions are unknown. Given the strongly divergent nature of the muscarinic receptor i3 loops, we reasoned that subtype-specific receptor-protein interactions may exist, and that knowledge of such interactions could shed light upon signaling and/or regulatory mechanisms heretofore unknown as a result of the paucity of MR experimental tools. In addition, identification of muscarinic receptor-interacting proteins could provide novel intracellular targets for the subtype- or tissue-specific modulation of MRs *in vivo*. In an effort to discover such MR-interacting proteins, we performed a series of unbiased yeast two-hybrid protein-protein interaction screens using as “baits” the five MR i3 loop regions. A protein identified in the M5 i3 loop screen, AGAP1, was subsequently shown to be a *bona fide*, subtype-selective M5 receptor interacting protein. We further demonstrated that interaction with AGAP1 was required for the endocytic recycling of M5, and that this trafficking proceeded through a novel, tissue-specific mechanism. Physiological experiments suggest that interaction with

AGAP1 is required for the normal function of the M5 muscarinic receptor in the regulation of striatal dopamine release.

2 IDENTIFICATION OF NOVEL MUSCARINIC RECEPTOR BINDING PROTEINS BY YEAST TWO-HYBRID SCREEN

2.1 Summary

Muscarinic acetylcholine receptors are GPCRs characterized by the presence of large, unstructured third intracellular loops that are divergent in sequence between receptor subtypes. Binding of proteins to intracellular regions of GPCRs is required for normal signaling, desensitization, and trafficking functions. In an effort to uncover proteins regulating muscarinic receptor function in a subtype-specific manner, we performed yeast two-hybrid screens employing as “baits” the third intracellular loop regions of the five muscarinic receptors. Using a diploid mating strategy, we achieved full coverage of the rat and human brain cDNA “prey” libraries used in the screens. Based on confirmation of positive interactions by prey plasmid retransformation and by identification and analysis of positive clone cDNA sequences, we selected three putative muscarinic receptor- interacting candidate proteins for further study.

2.2 Introduction

The yeast two-hybrid (Y2H) system allows for detection of protein-protein interactions by transcriptional activation of reporter genes (Fields and Song, 1989; Chien et al., 1991). The genesis of the Y2H system was based on the following observations: First, the DNA binding and transcriptional activator functions of eukaryotic transcriptional regulatory proteins were shown to be

separable and functionally compartmentalized (Hope and Struhl, 1986; Keegan et al., 1986). Second, it was shown that fusion of DNA-binding repressors with transcriptional activator proteins (Gal4) or fragments thereof could allow activation of transcription downstream of the bound repressor sequence (Brent and Ptashne, 1985; Ma and Ptashne, 1988). Finally, it was observed that native transcriptional activators need not directly bind DNA; for example, the herpes simplex VP16 protein activates transcription by binding to DNA-bound host proteins (Triezenberg et al., 1988), and c-Fos activates transcription as part of the AP-1 complex by binding to c-Jun (Curran and Franza, 1988).

In the first demonstrated example of the Y2H assay, a fusion of the Gal4p DNA binding domain (BD; $Gal4_{1-147}$) and the protein kinase SNF1 was co-expressed in the yeast *Saccharomyces cerevisiae* with the Gal4p transcription activation domain (AD; $Gal4_{768-881}$) in fusion with SNF4, a known binding partner of SNF1 (Fields and Song, 1989). The yeast strain used included a *lacZ* transgene under control of a Gal4 binding sequence (UAS_G) and carried mutations for the Gal4 AD and BD plasmid markers *HIS3* and *LEU2* (Fields and Song, 1989). Whereas co-expression of the Gal4-AD and Gal4-BD was unable to activate transcription from UAS_G, binding of the fused proteins SNF1:Gal4-BD and SNF4:Gal4-AD in the yeast nucleus was able to reconstitute GAL4 activity, allowing colorimetric detection of the *lacZ* protein product β-galactosidase. Subsequently, the Y2H system was shown to be able to reconstitute a known homo-dimeric interaction by using a SIR4:GAL4-BD fusion protein to screen a GAL4-AD-yeast genomic DNA library (Chien et al., 1991).

A number of important improvements to the Y2H system have since been developed. The modern Y2H screen was introduced with the addition of an auxotrophic reporter gene under Gal4 transcriptional control, *GAL1-HIS3*, to the *lacZ* reporter described above. This system allowed for the successful screening of a GAL4-AD-human lymphocyte cDNA library for clones interacting with a GAL4-BD-"bait" fusion protein by positive growth selection and colorimetric confirmation (Durfee et al., 1993). Next, Y2H "interaction trap" screening systems employing a bacterial LexA-based DNA BD and reporter genes under transcriptional control of the *lexA* operator (LexA-OP) were developed (Gyuris et al., 1993; Vojtek et al., 1993; Zervos et al., 1993). Such screening systems are compatible with bait libraries fused with yeast GAL4, viral VP16, and bacterial B42 ADs (Ruden et al., 1991; Vojtek et al., 1993; Dagher and Filhol-Cochet, 1997). Advantages of the LexA system include lack of endogenous DNA binding sites and protein binding partners for the bacterial DNA-BD, avoidance of the toxic effects of GAL4 overexpression, and ease of titering reporter gene sensitivity by varying copy number of the upstream LexA-OP sequences (Gyuris et al., 1993; Toby and Golemis, 2001). In addition, the development of Y2H screens in diploid yeast after mating of bait and prey strains provided a simplified method for the exhaustive coverage of library complexity (Bendixen et al., 1994; Fromont-Racine et al., 1997).

The strength of the Y2H system is illustrated clearly by the number of studies employing the technique for the identification and characterization of novel protein-protein interactions. Y2H screens have yielded important findings

pertaining to signaling cascades. For example, the small GTPase H-Ras was shown to interact directly with its kinase effectors c-Raf and A-Raf (Vojtek et al., 1993); the G1 and S phase protein phosphatase Cdi1 was discovered to interact with the cyclin-dependent kinase Cdk2 (Gyuris et al., 1993). Y2H screen results have led to insight into the regulation of cytoskeletal dynamics; the rho GEF Lfc was identified as a binding partner of the actin- and protein phosphatase 1-binding protein spinophilin and was shown to regulate dendritic spine morphology through this interaction (Ryan et al., 2005). Using cytosolic protein fragments as baits, functionally significant protein-protein interactions of transmembrane molecules have also been identified. Most notably, a Y2H screen identified the postsynaptic density protein PSD-95 as a binding partner for the C-terminal tail of the NMDA receptor subunit NR2 (Kornau et al., 1995). Similar screens identified the small GTPase RhoA as a binding partner of the delayed rectifier potassium channel Kv1.2, which was shown to play a central role in the receptor-mediated tyrosine kinase mechanism of Kv1.2 suppression (Cachero et al., 1998) and RGS2 as a TRPV6 Ca^{2+} channel interactor and functional inhibitor (Schoeber et al., 2006). More recently, large-scale Y2H screening programs have yielded genome-level binary protein-protein interaction maps (interactomes) for *S. cerevisiae* (Yu et al., 2008) *Plasmodium falciparum* (LaCount et al., 2005) *Caenorhabditis elegans* (Li et al., 2004) and an inter-species map between herpesviral and human proteomes (Uetz et al., 2006).

Of particular significance to our current project are the success of Y2H screens in the identification of novel GPCR-binding proteins. Numerous studies

utilizing cytoplasmic fragments of GPCRs as Y2H baits have uncovered protein-protein interactions shown subsequently to affect the signaling, localization, and stimulation-dependent and -independent trafficking properties of the receptors. For example, Y2H screens using GPCR c-terminal tail baits have demonstrated the following functionally significant interactions: The α1a adrenergic receptor and ezrin, affecting agonist-induced receptor recycling (Stanasila et al., 2006); the prostacyclin IP receptor and PDE6δ, involved in receptor trafficking and recycling (Wilson and Smyth, 2006); and the thromboxane A2β receptor and RACK1, shown to be important for ER-to-plasma membrane receptor delivery (Parent et al., 2008). Similarly, the literature contains examples of GPCR i3 loop interactions uncovered by Y2H screens, including the binding of the protein kinase C-zeta interacting protein (ZIP) to dopamine receptor D2, mediating receptor down-regulation by trafficking to lysosomes (Kim et al., 2008); up-regulation of the D3 dopamine receptor through binding to ALG-2 interacting protein 1 (AIP1) (Zhan et al., 2008) and filamin-A (Lin et al., 2001); and promotion of agonist-induced endocytosis of the β1 adrenergic receptor though binding to endophilin 1/2/3 (Tang et al., 1999).

Our laboratory has successfully utilized the Y2H screen in numerous studies identifying novel binding partners of brain-expressed GPCRs. p11, an S100 family protein, was discovered in a Y2H screen to interact with the 5HT1b serotonin receptor i3 loop, to regulate 5HT1b surface expression and signaling properties, and to be required for the 5HT1B-mediated behavioral response to antidepressant drugs in mice (Svenningsson et al., 2006). A subsequent directed

Y2H study identified the 5HT4 serotonin receptor as a second p11 binding partner; interaction with the i3 loop regulated receptor activity and drug responses in a manner similar to that of 5HT1b (Warner-Schmidt et al., 2009). A second Y2H screen using the c-terminal tail of the adenosine A_{2A} receptor identified an interaction with the tyrosine kinase fibroblast growth factor receptor (FGFR); this interaction was demonstrated to underlie the synergistic effects of FGF / adenosine co-stimulation on MAP kinase signaling, dendritic spine morphogenesis, and synaptic plasticity (Flajolet et al., 2008). Additionally, a Y2H screen performed with the c-terminal tail of the metabotropic glutamate receptor mGluR5 identified binding to the neuron-specific protein norbin (neurochondrin); this interaction was shown to potentiate mGluR5 surface expression, and to affect mGluR5-related synaptic plasticity and behavior (Wang et al., 2009b).

The Y2H system holds a number of significant advantages over other biochemical or genetic protein-protein interaction screening techniques with regard to its ability to detect GPCR-interacting molecules. Most notable of the competing methodologies, affinity purification and mass spectrometry (AP-MS) allow for proteomic identification of individual proteins from isolated complexes (Domon and Aebersold, 2006; Gingras et al., 2007). Affinity matrices composed of glutathione-S-tansferase (GST) fusions of cytosolic GPCR fragments immobilized on glutathione resins have been used to purify and identify serotonin 5HT2C C-terminal tail- and muscarinic M4 i3 loop- binding proteins by MALDI-TOF MS (Becamel et al., 2002; McClatchy et al., 2002). In addition, immunoprecipitation of native metabotropic glutamate mGluR5 receptors from rat

brain was used to identify co-purified proteins by liquid chromatography-tandem mass spectrometry (Farr et al., 2004). Compared to the Y2H system, however, AF-MS is inherently less sensitive to both low-affinity and low-abundance protein interactions; the Y2H system is sensitive to interactions with Kd constants as high as 10^{-7}, and, as it is a genetic screen, is unaffected by physiological target protein abundance (Phizicky et al., 2003). Affinity purification by GST-fusion protein is limited to recombinant proteins well-expressed in *Escherichia coli*, and is prone to high non-specific binding (Maurice et al., 2008; Daulat et al., 2009). In addition, immunoprecipitation strategies are hampered by the need to solubilize receptors under detergent conditions that may disrupt GPCR-protein interactions, and the fact that few high-affinity GPCR antibodies exist (the latter point especially true for the muscarinic receptors) (Daulat et al., 2009). Other well-characterized protein-protein interaction methods, such as phage-display and protein microarrays, have not as of yet been utilized in a whole-genome / whole-proteome screen for GPCR-interacting proteins (Smith, 1985; Stephen and Lane, 1992; Heydorn et al., 2004; Fam et al., 2005).

An important consideration in the design of a Y2H screen for GPCR-interacting proteins is the fact that full-length receptors are inappropriate as baits. As alluded to above, soluble cytoplasmic regions, either C-terminal tails or intracellular transmembrane loops, are most commonly employed as DNA-BD fusions in Y2H studies. Useful bait fusion proteins must also be able to enter the yeast nucleus, and must lack intrinsic transcriptional activation activity (Toby and Golemis, 2001). As described in section 1, while rat muscarinic receptors contain

relatively short (from 23 to 42 amino acid) C-terminal tails, their i3 cytoplasmic loops are large (157 to 240 amino acid), lack secondary structure (Rasmussen et al., 2007; Rosenbaum et al., 2007) and are divergent in sequence between receptor subtypes (table 1.1). The i3 loops of muscarinic receptors have previously been shown to be substrates for agonist dependent-phosphorylation (Tobin and Nahorski, 1993; Budd et al., 2000; Torrecilla et al., 2007), involved in activity-induced receptor internalization (Maeda et al., 1990), and required for basolateral membrane sorting of MRs (Nadler et al., 2001). The i3 loop has also been shown to be important for coupling of muscarinic receptors to signaling pathways (Singer-Lahat et al., 1996; Wess et al., 1997; Mitchell et al., 2003) and to mediate binding of $G\alpha_{i/o}$ and $G\beta\gamma$ subunits (Wess et al., 1997; Wu et al., 2000) and regulatory proteins such as RGS2 (Bernstein et al., 2004) to MRs. Thus, in an effort to identify novel binding proteins of the five muscarinic receptors, we performed Y2H screens using i3 loop-DNA BD proteins as baits.

Figure 2.1 Summary of Y2H screen strategy (following page). The use of mating type MATa yeast strains (CG1945, L40) for expression of MRi3-DNA BD "bait" fusions in concert with the expression of a brain cDNA library-AD fusion in a mating type MATα strain (Y187) provided for simplified library coverage by formation of bait / prey diploids through mating. The presence of dual transcriptional reporters allowed for confirmation of *HIS3*+ clones by assay for *lacZ* expression by the colorimetric X-Gal assay. Doubly-positive, sequenced clones were verified by retransformation in the appropriate reporter strain with positive (MRi3-pASIIΔΔ) or negative (empty pASIIΔΔ) controls and X-Gal lift assay.

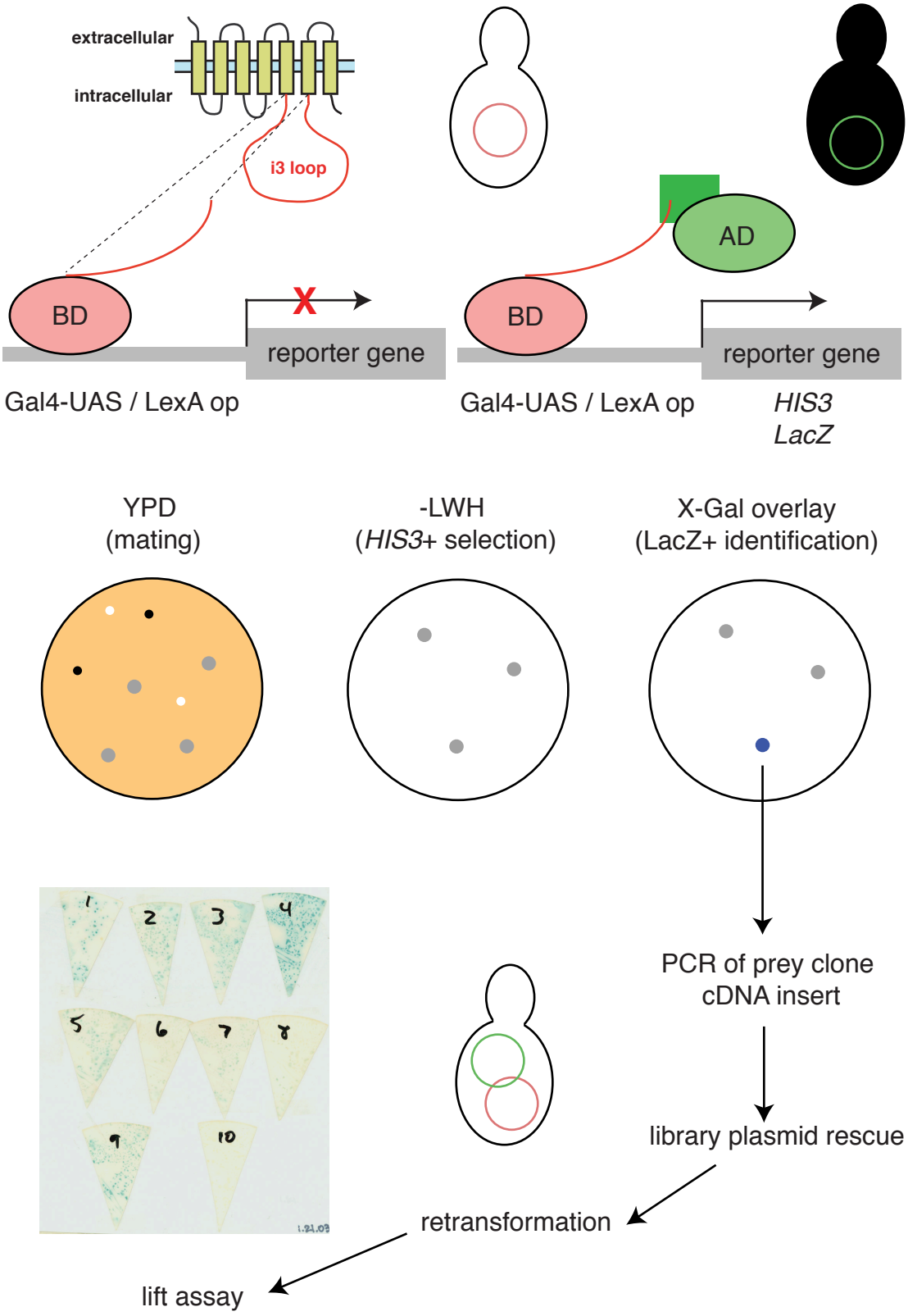
extracellular
intracellular
i3 loop
BD
X
reporter gene
Gal4-UAS / LexA op
AD
BD
reporter gene
Gal4-UAS / LexA op
HIS3
LacZ
YPD
(mating)
-LWH
(HIS3+ selection)
X-Gal overlay
(LacZ+ identification)
PCR of prey clone
cDNA insert
library plasmid rescue
retransformation
lift assay

2.3 Results

Y2H screens were performed on rat brain cDNA libraries (BD Clontech) with rat MRi3 baits for subtypes M1, M2, M4, and M5. A human M3i3 bait sequence was used to screen a human brain cDNA library (BD Clontech), as the hM3 cDNA clone was previously available in the laboratory. The bait DNA BD protein contained an intrinsic nuclear localization signal (NLS), while the prey Gal4 AD protein was fused with the SV40 T antigen NLS (Durfee et al., 1993). Before performing screens, we first checked for bait fusion protein toxicity by examining yeast colony growth rates on -Trp media. All bait strains exhibited normal growth rates (data not shown). Bait strains were then plated on -Trp-His

Table 2.1 Y2H screen characteristics. Screens were performed on rat or human MRi3 loops in fusion with the Gal4 or LexA DNA binding domains. Total diploid colony forming units (CFUs) indicate the number of prey clones screened. *HIS3+* / *lacZ+* clones with in-frame ORF fusions were identified by sequencing.

	screen type	clones screened (total diploid CFUs)	positive clones (His + / β-Gal+)	positive clones in-frame
rM1	Gal4	$2.5x10^7$	49	25
rM1	LexA	$5.6x10^7$	126	26
rM2	Gal4	$2.7x10^7$	7	0
rM2	LexA	$4.7x10^7$	15	10
hM3	Gal4 (human)	$1.8x10^7$	64	27
rM4	Gal4	$2.0x10^8$	234	37
rM5	Gal4	$1.8x10^7$	32	11

media to confirm that bait protein fusions did not exhibit reporter gene autoactivation; no colony growth was observed (data not shown).

Screens were first performed with the Gal4 system according to the strategy outlined in figure 2.1. After mating of prey and bait strains, library coverage was estimated by quantifying diploid colony growth on -Leu-Trp media; in all cases, mating efficiency was sufficient for full coverage of pACT2 cDNA library complexity (Table 2.1). Where indicated, screens were repeated in the higher-sensitivity LexA system using MRi3 loop - LexA DNA BD fusion baits in the L40 strain, allowing use of the pACT2-containing library strains (table 2.1). Screen results for each MRi3 bait are described below.

2.3.1 *rM1*

A screen of 25 million rat brain cDNA clones with a GAL4 DNA BD-rM1i3 fusion bait yielded 49 doubly-positive yeast colonies (*HIS3*+, *lacZ*+) (table 2.1). Twenty five of these positive colonies were identified by PCR as containing a pACT2 library clone falling within a gene-coding open reading frame (ORF) (table 2.1). Of the seven genes represented, one was of a recognized Gal4 screen false-positive (*Asrgl1*) (M. Flajolet, personal communication), and one coded for DNA-binding zinc finger protein (*Zfp61*); along with *Rpsp* and *Cenpc*, these clone plasmids were not rescued (table 2.2). Three pACT2 library clones were rescued and amplified: one (coding for *Kat5*) was β-Gal negative upon retransformation with pASIIΔΔ-rM1i3 in Y187 yeast, while one (coding for *Ppp3r1*) exhibited false-positive activation with empty pASIIΔΔ co-transformation and β-Gal lift assay

Table 2.2 rM1i3 screen results. Identity of *HIS3+* / *lacZ+* clones as determined by PCR are listed in columns 1 and 2, with total number of clones for each gene indicated. "+", β -Gal+; "-", β -Gal- after prey plasmid rescue and retransformation in yeast strain Y187 with bait plasmid (M1) or empty vector control (ctl). Gene names without + / - entries indicate positive clones from the rM1i3 screens for which prey plasmid isolation was either unsuccessful or not attempted. Green / red indicates successful / unsuccessful control experiment result, respectively. Format applies to results listed in tables 2.3-2.6.

ID	description	# clones	rescue M1	rescue ctl
(Gal4 screen)				
Olfm2	olfactomedin 2	4	+	-
Kat5	lysine acetyltransferase 5	1	-	
Ppp3r1	calcineurin B type I	10	+	+
Zfp61	zinc finger protein 61	3		
Rpsp	30S ribosomal protein S16	2		
Asrgl1	asparaginase like 1	4		
Cenpc	centromere autoantigen C	1		
(LexA screen)				
Olfm2	olfactomedin 2	3	+	-
Kat5	lysine acetyltransferase 5	4	+	-
8 genes represented by 1-2 clones		9	-	-
Ywhab	tyrosine 3-monooxygenase/tryptophan 5-monooxygenase activation protein, beta polypeptide (14-3-3β)	3		
Sharpin	SHANK-associated RH domain interactor	1		
Sdhd	succinate dehydrogenase complex, subunit D	1		
Apoe	apolipoprotein E	1		
XM_347156		1		
xm_222273		1		
rgd1560070		1		
xm_216178		1		

(table 2.2). A rescued clone, representing one of four positive clones coding for a fragment of the *Olfm2* ORF, passed positive and negative retransformation lift assays (table 2.2). *Olfm2*, coding for the Noelin-2 (Ofactomedin-2) protein, is a member of the olfactomedin family of secreted glycoproteins (Barembaum et al., 2000).

In an effort to obtain a greater number of M1i3-interacting clones, we repeated the rM1i3 screen using an LexA-rM1i3 fusion as bait in the L40 strain. The protein-protein interaction detection sensitivity of the LexA screen was anticipated to be higher, as *HIS3* activation in L40 is less stringent than in CG1945, and because the bait plasmid pLEX9 contained a LexA-OP-*lacZ* reporter (Vojtek et al., 1993). The rM1i3-LexA screen covered 56 million independent library clones, of which 126 were *HIS*+ / *lacZ*+. PCR analysis showed 26 of these positive clones to contain in-frame ORF cDNAs (table 2.1). pACT2-library plasmid rescue failed for clones representing the genes *Ywhab* and *Sharpin*, and was not attempted for *Sdhd*, *Apoe*, and 4 uncharacterized genes (table 2.2). 10 pACT2 library clones were successfully rescued; of these, 8 were β-Gal negative upon retransformation with rM1i3-pLexA (table 2.2). In the X-Gal lift assay, two clones were β-Gal+ / β-Gal- upon retransformation with pLex9-rM1i3 and empty pLex9 vector, respectively: *Olfm2*, representing 3 of the 26 total positive screen colonies, and *Kat5*, representing 4 of the positive colonies (table 2.2). *Kat5* encodes lysine acetyltransferase 5 / TIP60, a histone acetyltransferase shown to function in DNA damage repair, transcriptional

control, and chromatin remodeling (Squatrito et al., 2006). *Olfm2* / Noelin-2 is described above.

2.3.2 *rM2*

An initial screen of 27 million independent rat brain cDNA library clones with a Gal4 DNA BD-rM2i3 bait yielded 7 *His*+ / *lacZ*+ colonies (Table 2.1). However, PCR analysis indicated no clones representing in-frame ORF sequences (table 2.1). We thus repeated the screen in the less-stringent LexA system, as described above. The LexA-rM2i3 screen covered 47 million independent rat brain cDNA library clones, and yielded 15 *His*+ / *lacZ*+ colonies. Of these, 10 clones represented in-frame ORF sequences, covering 3 genes (table 2.1, 2.3). Rescue and retransformation in L40 yeast with pLex9-rM2i3 gave negative β-Gal activation results for two of the recovered clones, representing the genes *Ppp1ca* and *Cldn10* (table 2.3). The remaining rescued

Table 2.3, rM2i3 screen results

ID	description	# clones	rescue M2	ctl
(Gal4 screen)				
-		0		
(LexA screen)				
snx20	sorting nexin 20	8	+	-
Ppp1ca	protein phosphatase 1, catalytic subunit, alpha isoform	1	-	-
Cldn10	claudin 10	1	-	-

clone, encoding a 3' fragment of *Snx20*, represented 8 of the 10 positive / ORF in-frame screen colonies and was β-Gal+ / β-Gal- upon retransformation with pLex9-rM2i3 and empty pLex9 vector, respectively (table 2.3). SNX20 (sorting nexin 20) is a member of the sorting nexin family, and was recently shown to bind to and regulate the distribution of P-selectin glycoprotein ligand-1 (PSGL-1) (Worby and Dixon, 2002; Schaff et al., 2008).

2.3.3 *hM3*

A screen of 28 million human brain cDNA clones with a GAL4 DNA BD-hM3i3 fusion bait yielded 64 doubly-positive yeast colonies (*HIS3*+, *lacZ*+) (table 2.1). Twenty seven of these 64 positive clones were found by PCR analysis to contain in-frame human ORF sequences, covering 17 unique genes (table 2.1,

Table 2.4 hM3i3 screen results

ID	description	# clones	rescue M3	rescue ctl
Mllt3	myeloid/lymphoid or mixed-lineage leukemia; translocated to, 3	1	+	-
Pou2f1	POU class 2 homeobox 1	3	+	+
PCDHGA5	protocadherin gamma subfamily A, 5	1	+	+
KIAA1012		1	+	+
9 genes covered		12	-	
Psmc1	proteasome (prosome, macropain) 26S subunit, ATPase, 1	3		
THUMPD3	THUMP domain containing 3	2		
Aff4	AF4/FMR2 family, member 4	2		
Ranbp9	RAN binding protein 9	2		

2.4). pACT2 library plasmids covering 13 of these genes were rescued and retransformed in Y187 yeast with pASIIΔΔ-hM3i3 bait constructs; of these, 9 clones failed to activate β-Gal activity in the lift assay (table 2.4). Rescued clones containing coding sequences for *Pou2f1*, *PCDHGA5*, and *KIAA1012* were *lacZ*+ with both hM3i3 and control (empty vector) baits, indicating false-positive interactions (table 2.4). One clone, containing coding sequence from the gene *Mllt3* and representing a single positive colony from the hM3i3 screen, was β-Gal+ / β-Gal- upon retransformation with positive and negative control baits, respectively (table 2.4). MLLT3 encodes a transcription factor implicated in the pathology of leukemia and in the fating of human erythroid cell types (Iida et al., 1993; Pina et al., 2008). Rescue of prey plasmids encoding an additional 4 genes (*Psmc1*, *THUMPD3*, *Aff4*, and *Ranbp9*) was not successful (table 2.4).

2.3.4 *rM4*

A screen of 200 million human brain cDNA clones with a GAL4 DNA BD-rM4i3 fusion bait yielded 234 doubly-positive yeast colonies (*HIS3*+, *lacZ*+) (table 2.1). Thirty seven of the 234 positive clones were found by PCR to contain in-frame ORF sequences, covering 11 unique genes (table 2.1, 2.5). pACT2 bait plasmids for 6 positive clones (representing 31 of the 37 total positive colonies from the screen) were rescued and amplified for use in the retransformation lift assay in Y187 yeast. A rescued clone encoding *Ube2i* failed to show *lacZ* activation when co-expressed with the Gal4 DNA BD-rM4i3 bait fusion protein (table 2.5). Rescued pACT2 clones coding for segments of NRBP2, Pclo, and

Ccar1 were indicated as false-positives, as co-transformation with empty pASIIΔΔ vector led to β-Gal activity (table 2.5). Rescued prey clones encoding 3‘ fragments of the *UHRF1BP1L* and *Rbp3* ORFs (representing 2 and 14 of the 31 identified in-frame positive clones, respectively) were confirmed in the retransformation lift assay as β-Gal+ with the rM4i3 bait and β-Gal- with empty vector. UHRF1BP1L, or UHRF1 binding protein like 1 (also annotated as KIAA0701), is uncharacterized; however, the UHRF1 protein is known to function as an E3 ubiquitin ligase and to affect cell proliferation (Bronner et al., 2007). Rbp3 (retinol binding protein 3; also known as Interphotoreceptor retinol-binding

Table 2.5 rM4i3 screen results. (*) Isolation of *Dynlt1*-encoding prey plasmid from yeast clones was not successful; indicated results are for full-length rat *Dynlt1* coding sequence amplified by PCR from a rat brain cDNA library and cloned into the pACT2 prey vector.

ID	description	# clones	rescue M4	rescue ctl
UHRF1BP1L	UHRF1 binding protein 1-like (KIAA0701)	14	+	-
Rbp3	retinol binding protein 3, interstitial	2	+	-
NRBP2	nuclear receptor binding protein 2	4	+	+
Pclo	piccolo (presynaptic cytomatrix protein)	3	+	+
Ccar1	cell division cycle and apoptosis regulator 1	5	+	+
Ube2i	ubiquitin-conjugating enzyme E2I	3	-	-
Dynlt1	dynein light chain Tctex-type 1	2*	-	+
E4f1	E4F transcription factor 1	1		
Zcchc17	zinc finger, CCHC domain containing 17	1		
Nap1l5	nucleosome assembly protein 1-like 5	1		
Sult4a1	sulfotransferase family 4A, member 1	1		

protein / IRBP) is an extracellular glycoprotein found in the interphotoreceptor matrix of the retina, and functions to shuttle chromophore molecules between cells of the retinal pigment epithelium and photoreceptors (Liou et al., 1982; Jin et al., 2009). Clones representing 4 genes (*E4f1*, *Zcchc17*, *Nap1l5*, and *Sult4a*) were not rescued. Rescue of a clone encoding *Dynlt1* failed; however, the full-length cDNA for this gene was amplified from a rat brain cDNA library by PCR and was cloned into the pACT2 prey plasmid for use in the retransformation lift assay. *Dynlt1* exhibited *lacZ* reporter activity with empty pASIIΔΔ bait plasmid, but not with the rM4i3 bait construct (table 2.5).

2.3.5 *rM5*

A screen of 18 million human brain cDNA clones with a GAL4 DNA BD-rM5i3 fusion bait yielded 32 doubly-positive yeast colonies (*HIS3*+, *lacZ*+) (table 2.1). Eleven of these 32 positive clones were found by PCR analysis to contain in-frame ORF sequences, representing 4 unique genes (table 2.1, 2.6). A clone containing a 3‘ fragment of the *AGAP1* ORF (representing 4 of the 11 total

Table 2.6 rM5i3 screen results.

ID	description	# clones	rescue M5	rescue ctl
AGAP1	AGAP1 / centaurin, gamma 2	4	+	-
Ddrgk1	DDRGK domain containing 1	3		
RGD1566093	similar to Fusion (involved in t(12;16) in malignant liposarcoma)	2		
E4f1	E4F transcription factor 1	2		

characterized positive screen colonies) was rescued and confirmed to interact with the Gal4 DNA BD-rM5i3 bait in the X-gal lift assay; the negative control co-transformation with empty bait vector showed no *lacZ* activation (table 2.6). AGAP1 (also known as centaurin γ2 / Centg2) is a phospoinositide-dependent Arf GAP shown to regulate endocytic trafficking (Nie et al., 2002; Nie et al., 2003). Rescue of pACT2 plasmids from the remaining prey clones (representing three additional genes; *Ddrgk1*, *RGD1566093*, and *E4f1*) was not attempted (table 2.6).

2.4 Discussion

In this section, we have described screens performed with the yeast two-hybrid system in an effort to detect proteins interacting with the five muscarinic acetylcholine receptors. The prey / bait strain mating protocol, as opposed to co-transformation techniques, allowed us to easily generate a high number (>18 million) of diploid clones in each screen (Bendixen et al., 1994; Fromont-Racine et al., 1997). As the oligo-dT-primed pACT2 cDNA libraries used contained approximately 3.6 million independent clones (BD Clontech), our screens achieved multiple-fold coverage of the approximately 1.2 million in-frame Gal4 AD-cDNA fusions potentially present. For each receptor, a number of potential interacting clones were isolated and identified by PCR sequencing. Narrowing this list of candidate MR-interacting proteins was necessary in order to focus our subsequent experimental efforts.

There are important limitations to the Y2H method that must be considered in order to properly evaluate candidate MR-interacting clones (Phizicky and Fields, 1995; Toby and Golemis, 2001; Lin et al., 2005; Daulat et al., 2009). First, unlike proteomic approaches, the Y2H system is sensitive only to binary protein-protein interactions; multi-protein complexes are not detected. Second, in order to activate transcription of reporter genes, bait-prey interactions occur in the yeast nucleus. Prey fusion proteins unable to translocate to the nucleus, such as proteins containing transmembrane domains, will not be detected in Y2H screens. Third, expression of mammalian proteins in yeast may be inefficient or lead to toxicity and growth retardation. Although we observed no toxic effects of either the DNA BD-MRi3 or AD-cDNA library fusions, it was impossible to determine to what extent library clones were under-represented as a result of poor expression or slow yeast growth. Expression of bait or prey proteins as hybrid fusions may interfere with their native structure and/or function. Additionally, proteins expressed in yeast may be subject to misfolding, and may lack characteristic post-translational modifications such as phosphorylation, glycosylation, and nitrosylation found in their native environment. Finally, as described earlier, the Y2H system is compatible only with soluble proteins. This necessitated the use of cytoplasmic fragments of the MRs, rather than the full-length receptors as bait, and implied that library cDNAs containing coding regions for protein transmembrane domains were not represented in the screens.

The presence of false-negative results are a result of the Y2H technical considerations listed above. There are a number of known, physiological GPCR-protein interactions that would not be expected to be detected in our screening system. For example, binding of G proteins to GPCRs requires both formation of heterotrimeric complexes and interaction to second and third intracellular loop regions present in the native receptor conformation (Bluml et al., 1994; Wess et al., 1995) Homo- and hetero- dimerization and oligomerization of native receptors has been described for muscarinic receptors (Zeng and Wess, 1999; Park and Wells, 2003) as well as for GPCRs such as $GABA_B$ (Kaupmann et al., 1998; Margeta-Mitrovic et al., 2000), β2-adrenergic and opioid receptors (Jordan et al., 2001) and many others (Gurevich and Gurevich, 2008); these interactions would not be indicated in the Y2H system, although detection of transmembrane receptor association by cytoplasmic domain interactions is possible (Flajolet et al., 2008). In addition, binding of β-arrestin to GPCRs occurs only after activation and receptor phosphorylation by GRKs (Lohse et al., 1990; Luttrell and Lefkowitz, 2002), post-translational modifications that are unlikely to be present in MRi3 loops expressed in yeast. Indeed, we did not detect in our Y2H screens a number of proteins demonstrated previously (by alternate methodologies) to interact with MRi3s, such as RGS2, SET, and eEF1A2 (McClatchy et al., 2002; Bernstein et al., 2004; Simon et al., 2006). Thus, the absence of clones present in our Y2H screens was not diagnostic of absence of interaction with a given gene product. Nevertheless, for the reasons described earlier, we considered Y2H screens employing i3 loop regions as a desirable methodology for the

detection of physiologically and functionally relevant MR- interactions. It should be noted, however, that in the period since the performance of our screens, a number of technologies have come into use that address some of the difficulties inherent to the study of MR protein-protein interactions, such as the high-affinity tandem affinity purification technique (TAP) for the purification of protein complexes associated with tagged, full-length MRs (Daulat et al., 2007; Lyssand et al., 2008).

Additional characteristics of the Y2H system are responsible for the occurrence of false-positive clones in screens. First, prey protein fusions exhibiting binding to the Gal4 or LexA DNA BDs could indicate interaction by reporter gene activation despite lack of binding to the i3 loop portion of the bait fusion protein. We therefore confirmed interacting clones by retransformation of rescued plasmids in the presence of both bait (DNA BD-i3 loop) and negative control (empty bait vector) plasmids. Clones displaying β-Gal activity in the presence of DNA-BD alone were excluded from further consideration (tables 2.2-2.6). Second, the Y2H transcriptional activation reporter system is sensitive to interference by bait fusions exhibiting transcriptional activation activity, and bait fusion proteins displaying DNA binding affinity. We confirmed that our DNA BD-MRi3 bait fusion proteins did not activate transcription of *HIS3* by observing lack of growth on -His media of bait plasmid-transfected yeast strains. Based on known or predicted function of sequenced positive clones, we also excluded from further consideration genes encoding transcription factors, transcriptional transactivators, or proteins with other known DNA-binding activity. These clones

included the transcription factor E4f1 from the M4 and M5 screens; the zinc-finger proteins Zcchc17 and Zfp61 from the M4 and Gal4-M1 screens, respectively; the centromere autoantigen Cenpc (Earnshaw et al., 1987) from the M1i3-Gal4 screen; and the transcription factors Mllt3 and Aff4 from the M3 screen (tables 2.2-2.6).

A third factor responsible for the occurrence of false-positive results in Y2H screens is the fact that, while able to interact when co-localized in the yeast nucleus, putative interacting proteins may not co-localize spatially or temporally under normal physiological conditions in the mammalian cell. Thus, for positive clones with known or predicted function, we considered functional plausibility as a factor in the ranking of candidates for priority of further study. Based on the false-positive selection criteria described above, no rescued candidate clones remained from the M3 screen. Candidates remaining for the other four MRi3 screens are discussed in the following paragraphs.

In the initial M1i3 screen in the Gal4 system, the only rescued clone passing positive and negative retransformation controls encoded a C-terminal fragment of the secreted glycoprotein Olfactomedin / Noelin 2 (Barembaum et al., 2000). Noelin 1/2 has been shown to be expressed during development in the brain, retina and other structures in the chick, mouse, and zebrafish, and to be important for early and late brain developmental events (Barembaum et al., 2000; Moreno and Bronner-Fraser, 2002; Lee et al., 2008). Mutations in human *Olfm2* have also been implicated in the genetics of a form of glaucoma (Funayama et al., 2006). Based on this knowledge of Noelin 2 distribution and function, a

functional interaction with M1 was determined to be physiologically unlikely, and we considered the interaction with M1i3 to be false-positive. In the hope of identifying additional M1i3-interacting proteins, we repeated the screen with the higher-sensitivity LexA reporter system. Two positive clones emerged from this screen: Noelin 2 and the lysine acetyltransferase Kat5. Kat5, also known as TIP60, is a histone acetyltransferase that functions as part of the conserved NuA4 complex which was shown to be recruited to chromatin by binding to to the transcription factor MYC, and to play a role in the DNA damage response pathway and in tumorigenesis (Frank et al., 2003; Squatrito et al., 2006; Gorrini et al., 2007; Bhoumik et al., 2008). These functions also led us to discount the Kat5 interaction with M1i3 as a probable false-positive result. Thus, no rescued clones emerged as likely physiological binding partners of M1 from our screens, although it was interesting to note the reproducibility of our screen results: Noelin 2 was identified as a positive clone in both screens, and Kat5, the confirmed positive clone from the LexA screen, was also identified as a *HIS3*+ / *lacZ*+ clone in the initial Gal4 screen, although re-transformation failed to display β-Gal activation (table 2.2). It is also worth noting the greater number of false-positive clones obtained in the LexA screen as opposed to the Gal4, which is consistent with the greater stringency of the Gal4 reporter system and illustrates the tradeoffs between sensitivity and false-positive rate that is important to consider in the design and analysis of Y2H screens (Phizicky and Fields, 1995; Toby and Golemis, 2001).

The M2i3 screen performed in the Gal4 system yielded no positive in-frame clones, and was thus repeated in the LexA system. Eight positive clones encoding a C-terminal fragment of SNX20 (sorting nexin 20) were confirmed to interact with M2i3 by plasmid rescue and retransformation (table 2.3). SNX20, also annotated as SLIC-1, is a member of the sorting nexin family, proteins characterized by the presence of a phosphoinositide-binding phox homology (PX) domain (Xu et al., 2001; Worby and Dixon, 2002). Proteins in the sorting nexin family, of which 33 members have been identified in mammals, have been shown to function in endocytosis, endosomal sorting of cargo proteins, regulation of endosomal structure, and coordination of endosomal signaling (Worby and Dixon, 2002; Cullen, 2008). A recent study (employing the Y2H screen technique, but subsequent to the analysis of our results) demonstrated SNX20 binding to the P-selectin glycoprotein ligand-1 (PSGL-1) cytoplasmic tail; this binding is thought to regulate the endosomal distribution of PSGL-1 (Schaff et al., 2008). As functionally significant interactions of trafficking molecules with GPCRs are well established (Tan et al., 2004) and since sorting nexins have been shown to bind to and regulate the trafficking of low-density lipoprotein receptors, EGF receptors, and protease-activated receptor 1 (Kurten et al., 1996; Stockinger et al., 2002; Wang et al., 2002), among others, we considered the identified interaction of SNX20 with M2i3 as a physiologically plausible result and an intriguing candidate for further study.

The M4i3 screen yielded two positive clones that passed subsequent retransformation controls: *Rbp3* (interstitial retinol-binding protein) and

UHRF1BP1L (table 2.5). Rbp3, known more commonly as interphotoreceptor retinol binding protein (IRBP), is a glycoprotein secreted by photoreceptor cells into the interphotoreceptor matrix of the retina (Liou et al., 1982; Gonzalez-Fernandez, 2003). IRBP functions to shuttle all-*trans*-retinol and 11-*cis*-retinaldehyde molecules between cells of the retinal pigment epithelium and photoreceptors, and is critical for resensitization of photoreceptors after light exposure (Carlson and Bok, 1992; Qtaishat et al., 2005; Jin et al., 2009). Based on the extracellular distribution and described function of IRBP, we discounted this M4i3 screen clone as a likely false-positive result.

Fourteen clones encoding two different C-terminal fragments of UHRF1BP1L (UHRF1 binding protein 1-like) were detected and confirmed by rescue and retransformation in our M4i3 screen. UHRF1BP1L, also annotated as KIAA0701, is an uncharacterized protein with no putative functional domains, named for its sequence similarity to the uncharacterized protein UHRF1BP1. UHRF1, known also as ICBP90 and Np95, is a multidomain protein containing a RING-finger ubiquitin E3 ligase domain, and was shown to bind directly to methylated DNA sequences and to be important for the maintenance of histone and DNA methylation states (Bronner et al., 2007; Sharif et al., 2007; Hashimoto et al., 2008a). Though false-positive Y2H results as a result of multiple protein complex formation is unlikely, the relation of UHRF1BP1L to a known DNA-binding protein was of concern. Nevertheless, as down-regulation of β2 adrenergic receptors has been shown to be mediated by ubiquitination by an E3

ligase (Shenoy et al., 2001), and since the function of UHRF1BP1L is unknown, we selected UHRF1BP1L for further study with respect to its binding to M4.

The M5i3 screen yielded positive clones encoding a C-terminal fragment of AGAP1 that passed positive and negative retransformation control experiments (table 2.6). AGAP1 (an acronym for **A**rf GAP containing **G**TP binding protein-like domain, **a**nkyrin repeats and **p**leckstrin homology domain 1), also annotated as centaurin γ2, is a member of both the AZAP and centaurin protein families (Jackson et al., 2000; Nie et al., 2002). AGAP1 is a phosphoinositide-dependent GAP for members of the small GTPase protein family Arf, proteins that function to regulate mechanisms of intracellular membrane trafficking and actin cytoskeleton dynamics (Nie et al., 2002). AGAP1 was shown to bind to and regulate the function of the AP-3 adapter / coat protein complex, in turn affecting the trafficking of the lysosome-associated protein LAMP1 (Nie et al., 2003). A number of AZAP and centaurin family proteins have been shown to affect trafficking of plasma membrane receptors: ACAP1 binds to sorting signals on the transferrin receptor and integrin β1, promoting their endocytic recycling (Dai et al., 2004; Li et al., 2005); ASAP1 accelerates the recycling of internalized EGF receptors (Nie et al., 2006); and centaurin α1 inhibits internalization of the β2 adrenergic receptor (Lawrence et al., 2005). In addition, the protein PIKE-L / centaurin γ1 mediates the anti-apoptotic effects of the metabotropic glutamate receptor mGluR1 activation via Homer-coupled binding to the mGluR1 C-terminal tail (Rong et al., 2003). Taken together, the known functions of AGAP1 and AZAP / centaurin family proteins led us to

consider an interaction between M5 and AGAP1 as physiologically plausible, and so we selected AGAP1 for continued study.

Based on the criteria described above for selecting candidates by the likelihood of their physiologically relevant interaction with MRs, there were a number of notable clones identified in our screens for which prey plasmid rescue failed. From the M1i3-LexA screen, Ywhab- (14-3-3β) and Sharpin- coding clones were not rescued (table 2.2). The Sharpin protein localizes to the post-synaptic density and interacts with Shank (Lim et al., 2001), while 14-3-3 proteins serve as molecular scaffolds for signaling regulation, and bind to phosphoserine motifs and the β1 adrenergic receptor (Tutor et al., 2006; Obsilova et al., 2008). In addition, it is possible that clones such as *Ppp1ca* (coding for the catalytic subunit of protein phosphatase 1a) that failed to exhibit β-Gal activity upon retransformation with bait plasmid were displaying an MRi3 interaction weak enough to activate transcription of *HIS3*, but not the more stringent *lacZ* (table 2.3). Nonetheless, the group of three candidate MRi3-interacting proteins described above - SNX20, AGAP1, and to a lesser extent UHRF1BP1L - were deemed sufficiently promising to allow us to proceed with experiments examining the characteristics of their binding to MRs.

3 ANALYSIS OF THE M5-AGAP1 PROTEIN-PROTEIN INTERACTION

3.1 Summary

The binding characteristics of muscarinic receptor- interacting protein candidates identified in Y2H screens were investigated using complementary protein-protein interaction techniques. We performed deletion mapping using directed Y2H assays to confirm candidate / MR i3 loop interactions, and to determine minimum domains of interaction. The interaction between M5i3 and AGAP1 was determined to be unique to the M5 receptor subtype, and was shown to require a 23-residue region in the M5i3 loop. Similar mapping experiments demonstrated that AGAP1 was unique among its most closely related family members in its association with M5i3, and that a 60-residue region in the split pleckstrin homology domain region was required for M5i3 binding. *In vitro* binding of exogenously expressed AGAP1 to recombinant GST-MRi3 fusion proteins recapitulated a M5-specific binding pattern across MR subtypes. GST-fusion proteins containing fragments of M5i3 and AGAP1 were also able to interact, in a DOI-specific manner, with AGAP1 and full-length M5, respectively. Endogenous AGAP1 from rat brain lysate bound to a GST-M5i3 fusion protein, as did members of the heteromeric AP-3 adaptor complex. Parallel protein-protein interaction experiments with SNX20 and M2i3, and with UHRF1BP1L and M4i3 did not provide strong evidence for specific interaction of these proteins. The results provide support for a subtype-specific interaction of M5 with AGAP1, and

suggest utility of a M5 DOI-deletion mutant receptor as a tool for the study of AGAP1-dependent M5 function.

3.2 Introduction

The validation of putative interacting proteins identified in yeast two-hybrid screens by independent protein-protein interaction techniques is critical. The Y2H system is subject to artifactual false-positive results as a result of the yeast nuclear environment, misfolding of mammalian proteins, and DNA BD / AD fusion junction effects (Van Criekinge and Beyaert, 1999; Lin et al., 2005). While no protein-protein interaction technique is free from false-positive interference, the use of complementary techniques (genetic and biochemical; *in vitro* and *in vivo*) provides the strongest evidence for the existence of a physiological protein complex. "Pull-downs" from cell or tissue lysates using immobilized affinity matrices of recombinantly expressed glutathione-S-transferase (GST) fusion proteins are a commonly used and well-characterized method for detecting and analyzing protein-protein or protein-complex interactions (Lee and Liu, 2005; Chen et al., 2006; Flajolet et al., 2008; Warner-Schmidt et al., 2009). Co-immunoprecipitation of solubilized receptors expressed exogenously in tissue culture cells or from endogenous sources is an additional method commonly employed to verify and study the binding of protein or complexes with receptors, and is particularly well-suited to the detection of receptor-protein complexes from native tissues (Hall, 2005; Svenningsson et al., 2006; Daulat et al., 2007; Daulat et al., 2009). A number of other *in vitro* techniques are also available for the

confirmation and analysis of putative protein binding partners, including protein and peptide arrays (Kung and Snyder, 2006), “Far Western” overlay blots and arrays (Mahlknecht et al., 2001; Hall, 2004) and peptide competition binding assays (Badtke et al., 2006).

Protein-protein interactions are commonly dependent on amino acid motifs or conserved functional binding domains. A large number of short peptide sequences conferring binding affinity to trafficking, signaling or scaffold proteins have been characterized; examples include dileucine and YXXΦ (Φ representing the bulky hydrophobic residues L,I,V,M, or F) motif binding to AP-1 and AP-2 adaptor protein complexes, respectively (Rapoport et al., 1997; Rapoport et al., 1998) and proline-rich motif binding to the WW and SH3 domains (Pawson and Nash, 2003). Similarly, many conserved functional domains capable of binding proteins (as well as lipids and ions) have been described; as these domains are typically able to fold correctly independent of N- and C- terminal context, they exhibit modular function and occur repeatedly throughout the proteome (Pawson and Nash, 2003). Common protein-protein interaction domains include PDZ, found in the post-synaptic density scaffold protein PSD-95 and important for the assembly of excitatory synapses (Kim and Sheng, 2004), and the proline-rich peptide-binding SH3 domain (Kaneko et al., 2008).

In the current study, two of the putative MR-interacting proteins identified by Y2H screen contain conserved binding domains. SNX20 contains a phox homology (PX) domain, a defining characteristic of the entire sorting nexin family (Worby and Dixon, 2002). PX domains are mainly implicated in the binding of

phospholipids and phosphoinositides (Xu et al., 2001), although instances of protein-protein interactions mediated by PX domains have been observed (Worby and Dixon, 2002; Abdul-Ghani et al., 2005). The PX domain of of SNX20 was shown to bind most strongly to phosphatidylinositol 4-phosphate, phosphatidylinositol 5-phosphate, and phosphatidylinositol 3,5-bisphosphate; in addition, PX phospholipid binding was seen to be required for endosomal localization of SNX20 (Schaff et al., 2008). AGAP1 contains multiple functional domains, two of which (pleckstrin homology (PH) and ankyrin repeat) potentially participate in protein-protein interactions (see figure 3.2A). The PH domain is found in a variety of signaling and membrane-associated molecules; it is known to bind phospholipids, but is also able to participate in protein-protein interactions with Arf1 and G-protein βγ subunits (Lodowski et al., 2003; Godi et al., 2004; Lemmon, 2004). In AGAP1, the PH domain is split by intervening sequence into N- and C- terminal halves (Nie et al., 2002). The C-terminal end of AGAP1 also contains a series of ankyrin repeats; the ankyrin domain occurs widely and is able to mediate binding to a diverse array of protein targets (Li et al., 2006).

The primary goal of the experiments described in this chapter was to confirm the presence of protein-protein interaction between muscarinic receptors and the three putative MR-binding proteins identified by Y2H screening. We used the complementary protein-protein interaction experimental techniques of directed Y2H, GST pull-down and co-immunoprecipitation to investigate the binding of AGAP1, SNX20, and UHRF1BP1L to muscarinic receptors M5, M2, and M4, respectively. Using a similar experimental approach, we also

determined the specificity of MR-candidate protein interactions with respect to MR subtype and interacting protein family members. Finally, we performed Y2H domain-of-interaction mapping of MRi3 loops and candidate interacting proteins in an effort to determine residues or regions responsible for their binding. In doing so, our hope was 1) to gain insight into the molecular and/or cellular implications of MR-protein interactions by identifying known amino acid motifs or interaction domains mediating binding, and 2) to develop molecular tools for subsequent study of the function of MRs in a loss-of-interaction context.

3.3 Results

3.3.1 *AGAP1 interaction with M5i3 is subtype-specific and is mediated by discrete binding domains*

We first investigated the specificity of the putative AGAP1- M5i3 interaction by Y2H lift assay. Co-transformation of Y187 yeast with the AGAP1-coding pACT2 clone obtained from the Y2H screen and with pASIIΔΔ bait plasmid encoding each of the five MRi3s (or empty vector) revealed *lacZ* reporter gene activation only with the M5i3 bait (figure 3.1A). We then sought to map the domain of M5i3 critical to interaction with AGAP1 by deletion mutagenesis and directed Y2H assays, an approach used successfully in previous domain of interaction (DOI) studies (Miller et al., 2004; Lin et al., 2005; Flajolet et al., 2008; Hsu et al., 2009). First, we determined that a prey plasmid encoding a rat AGAP1 fragment spanning residues 552 to 645 was able to activate β-Gal activity with a full length M5i3 bait in the Y2H lift assay (table 3.1B). Next, we

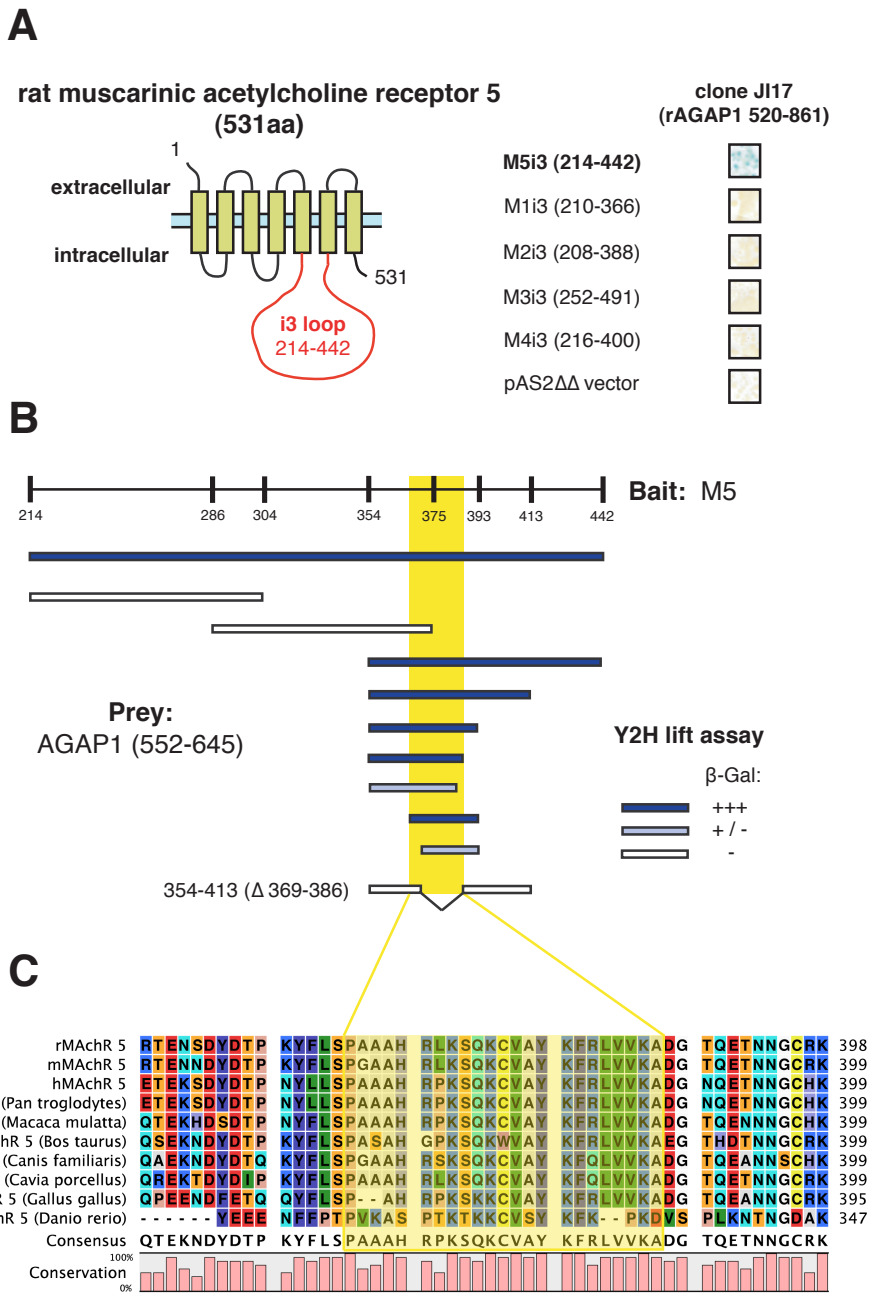

Figure 3.1 AGAP1 interacts with a defined region of the M5 i3 loop in a receptor subtype-specific manner. **(A)** Right, X-Gal lift assay results for Y2H interaction assay between rat MRi3-Gal4 bait proteins and the rat AGAP1 clone isolated in the M5i3 screen. pAS2ΔΔ, negative control. **(B)** Cartoon summarizing X-Gal lift assay results from Y2H interaction assays. M5(214-442) represents the rM5 i3 loop region. Truncation and deletion mutants were assayed for AGAP1(542-645) interaction as indicated. Dark blue, strong *lacZ* activation; light blue, weak *lacZ* activation; white, negative result. **(C)** Multiple species alignment of the identified M5 i3 domain of interaction with AGAP1. R, m, h; rat, mouse, human, respectively. Yellow box indicates minimum domain of interaction. Residues are colored by shared amino acid characteristics.

used PCR cloning to construct a series of three M5i3 deletion mutants spanning the 229-residue length of the i3 loop. Only the C-terminal end fragment, M5 (354-442), displayed interaction with AGAP1 (552-645) (figure 3.1B). We then constructed a series of deletion mutants in order to determine the C-terminal extent of the putative AGAP1-M5i3 binding domain. While the M5 (354-386) i3 loop bait fragment displayed X-Gal staining intensity with AGAP1 (552-645) prey equal to that of the full-length i3 sequence, an M5 fragment truncated by a further 3 residues (M5 (354-383)) produced greatly reduced X-Gal staining (figure 3.1B). Using a similar N-terminal end truncation approach, we observed that an M5 (364-393) bait fragment exhibited full-length i3 X-Gal staining intensity, while truncation by a further 5 residues (M5 (369-393)) greatly reduced reporter activity (figure 3.1B). Thus, a 23-amino acid region of M5i3 was identified as a possible minimum domain of interaction with AGAP1 in the Y2H assay. To confirm this result, we constructed an M5i3 bait construct spanning the identified binding region but deleted for an 18-amino acid stretch within this region, M5 (354-413 Δ369-386). This deletion-mutant bait construct showed no *lacZ* activation in the Y2H assay with the AGAP1 (552-645) prey, indicating successful disruption of the AGAP1 binding domain (figure 3.1B). Multiple-species alignment of the M5 amino acid sequences available in Genbank revealed the putative critical region of interaction to be strongly conserved suggesting the presence of a functionally significant domain (figure 3.1C). This 23-residue M5i3 sequence displayed no homology with sequences of the other four MRs (figure 1.1).

We next used deletion mutagenesis and the Y2H lift assay to investigate the residues on AGAP1 required for interaction with the M5 i3 loop. The pACT2 clone (JI17) isolated from the M5i3 Y2H screen encoded a C-terminal fragment of rat AGAP1 spanning residues 520-861 (figure 3.2A). A series of truncation mutants spanning the C-terminal region of AGAP1 covered by the JI17 clone were tested against the full-length M5i3 bait. An AGAP1 fragment (552-646) that included the entire C-terminal half of the split PH domain was found to interact strongly with M5i3 in the X-Gal lift assay (figure 3.2A). Further refinement of the M5i3-interacting domain of AGAP1 indicated that a 59-amino acid region spanning residues 552-609 was the minimum domain sufficient for M5i3 binding in the Y2H assay. The entire C-terminal half of the split PH domain was required for M5i3 interaction, as an N-terminal truncation of 8 amino acids was sufficient to eliminate *lacZ* reporter activation (figure 3.2A). Alignment of the rat AGAP1 (552-609) region sequence with that of other species revealed very high conservation, with >98% amino acid identity between rat, mouse and human sequences (figure 3.2B).

3.3.2 *M5i3 alanine mutagenesis reveals residues critical for AGAP1 interaction*

Based on the previous results, we performed site-directed mutagenesis of residues falling within the M5i3 domain identified as critical for interaction with AGAP1. We identified charged and/or bulky hydrophobic residues in this region that displayed strong conservation across species, and constructed a series of alanine point mutants of the M5 (332-419) bait construct (figure 3.2B, figure

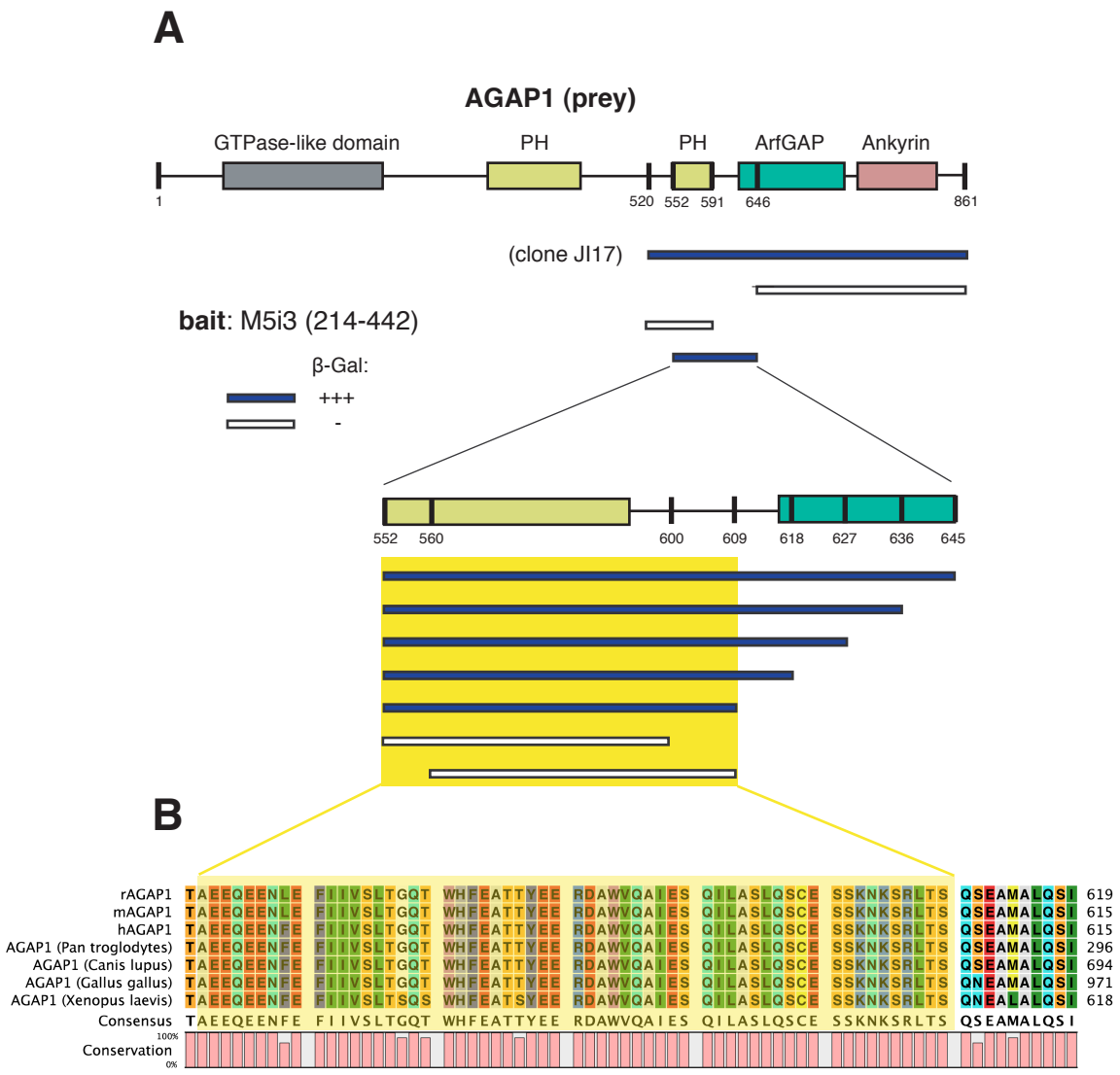

Figure 3.2 AGAP1 domain-of-interaction mapping. **(A)** Cartoon summarizing X-Gal lift assay results from Y2H interaction assays. Top, AGAP1 functional domains. Below, rat AGAP1 truncation mutants were assayed for M5i3 interaction as indicated. Dark blue, strong *lacZ* activation; white, negative result. **(B)** Multiple species alignment of the identified AGAP1 domain of interaction with M5i3. R, m, h; rat, mouse, human, respectively. Yellow box indicates minimum domain of interaction. Residues are colored by shared amino acid characteristics.

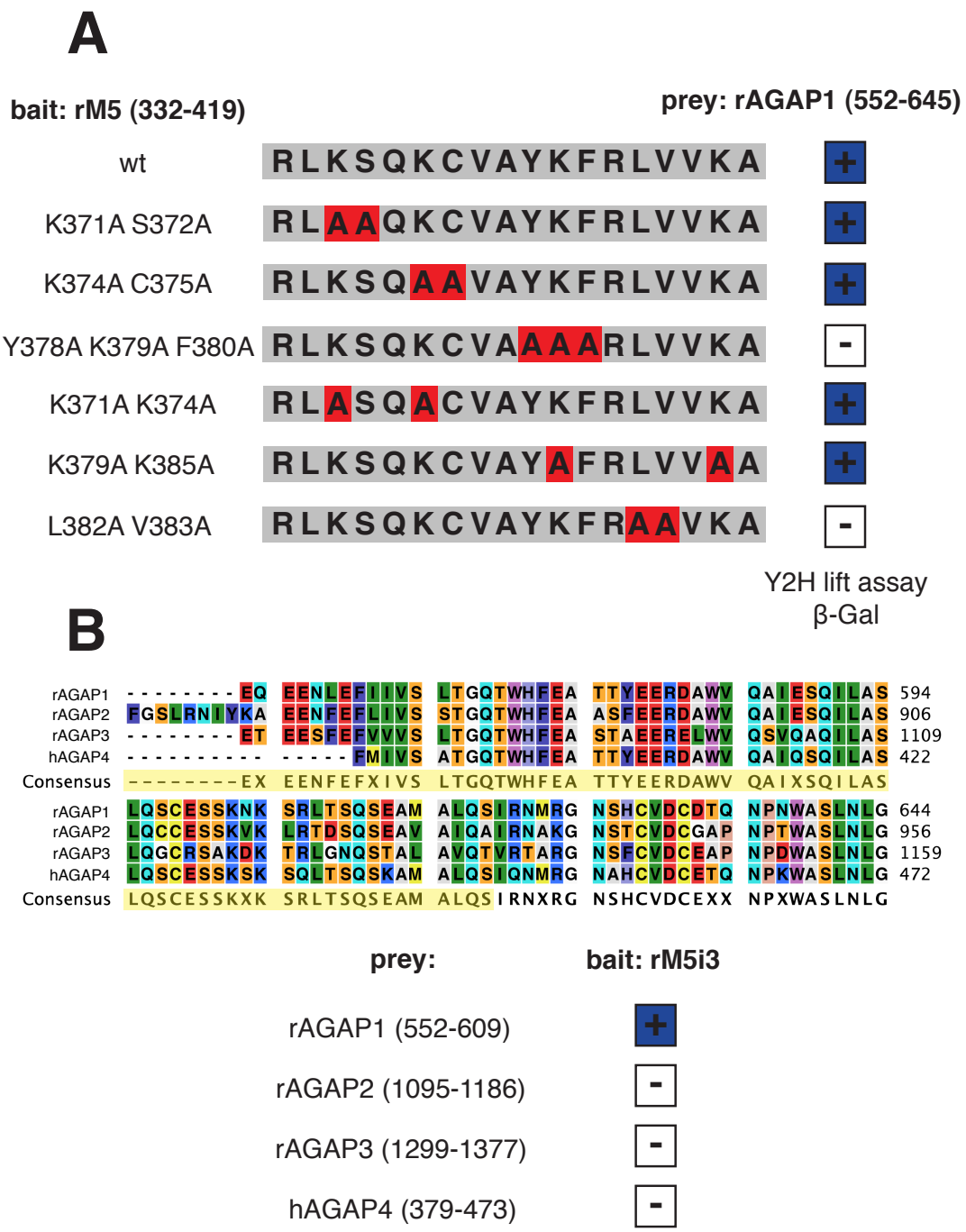

Figure 3.3 Specificity of the AGAP1 / M5 i3 interaction. (A) Alanine point mutants were generated from the rat M5 (332-419) bait construct and tested for interaction with rat AGAP1 (552-645) in the Y2H lift assay. Dark blue, strong *lacZ* activation; white, negative result. **(B)** Top, multiple species sequence alignment of rat AGAP1, 2 and 3, and human AGAP4. Yellow box, consensus sequence corresponding to the AGAP1 domain of interaction with M5i3. Residues are colored by shared amino acid characteristics. Bottom, Y2H X-Gal lift assay results. Dark blue, strong *lacZ* activation; white, negative result.

3.3A). The Y2H lift assay identified two series of mutations, Y378A K379A F380A and L382A V383A, that completely eliminated AGAP1 interaction as measured by β-Gal activity (figure 3.3A). Notably, the mutated YKF and LV sequences resembled YXXΦ and LL motifs, respectively, which are known to target membrane proteins for endosomal and lysosomal compartments via interaction with adaptor protein complexes (Canfield et al., 1991; Vowels and Payne, 1998; Bonifacino and Traub, 2003).

3.3.3 *M5i3 interaction with AGAP family proteins is limited to AGAP1*

The AGAP subfamily contains four characterized proteins: AGAP1, AGAP2 (Centaurin γ1) AGAP3 (Centaurin γ3) and AGAP4 (MRIP2 / Centaurin γ-like family 1). AGAP4 is present only in humans, and is included in the Centaurin γ-like family of 7 genes and pseudogenes present as a result of a likely gene duplication event on chromosome 10q (Kahn et al., 2008). We cloned regions of AGAP family members homologous to the C-terminal split PH domain-containing AGAP1 region of interaction (AGAP1 (552-609) from rat brain cDNA library (AGAP2 and AGAP3) and human brain cDNA library (AGAP4), and tested them for interaction with the rat M5i3 bait in the Y2H lift assay (figure 3.3B). Only AGAP1 displayed X-Gal staining, indicating that the putative interaction between M5 and AGAP1 is AGAP subtype-specific (figure 3.3B).

3.3.4 *AGAP1 interacts with M5i3* in vitro

In order to confirm the Y2H assay M5i3 / AGAP1 interaction results in a complementary system, we performed *in vitro* binding studies using recombinant MRi3 proteins as affinity matrices. MRi3 regions for the five rat MRs were expressed in *E. coli* as N-terminal fusions of the Glutathione-S-transferase protein (GST). Recombinant GST proteins were purified and immobilized by affinity chromatography with a glutathione-conjugated resin. The GST-MRi3 (or native GST) affinity matrices were then used in "pull-down" assays to examine interaction with AGAP1 proteins, with detection by autoradiography or immunoblot. We first used an *in vitro* transcription-translation kit to produce [35S]Met-labeled protein from the JI17 clone DNA template (AGAP1 520-861). This AGAP1 fragment was seen to interact most strongly with the GST-M5i3 protein, though binding to GST-M3i3 and GST-M4i3 was also observed. No binding to native GST was apparent (figure 3.4A). Next, we exogenously expressed full-length AGAP1 with a C-terminal myc tag in COS-7 cells. Pull-downs of AGAP1-myc- containing lysates and analysis by anti-myc immunoblot again showed AGAP1 to interact with GST-M5i3 but not native GST, with weaker interactions between AGAP1 and GST-M1i3, GST-M3i3 and GST-M4i3 observed (figure 3.4A).

We next performed pull-down experiments to confirm the Y2H domain-of-interaction mapping data described above. We purified GST fusion proteins

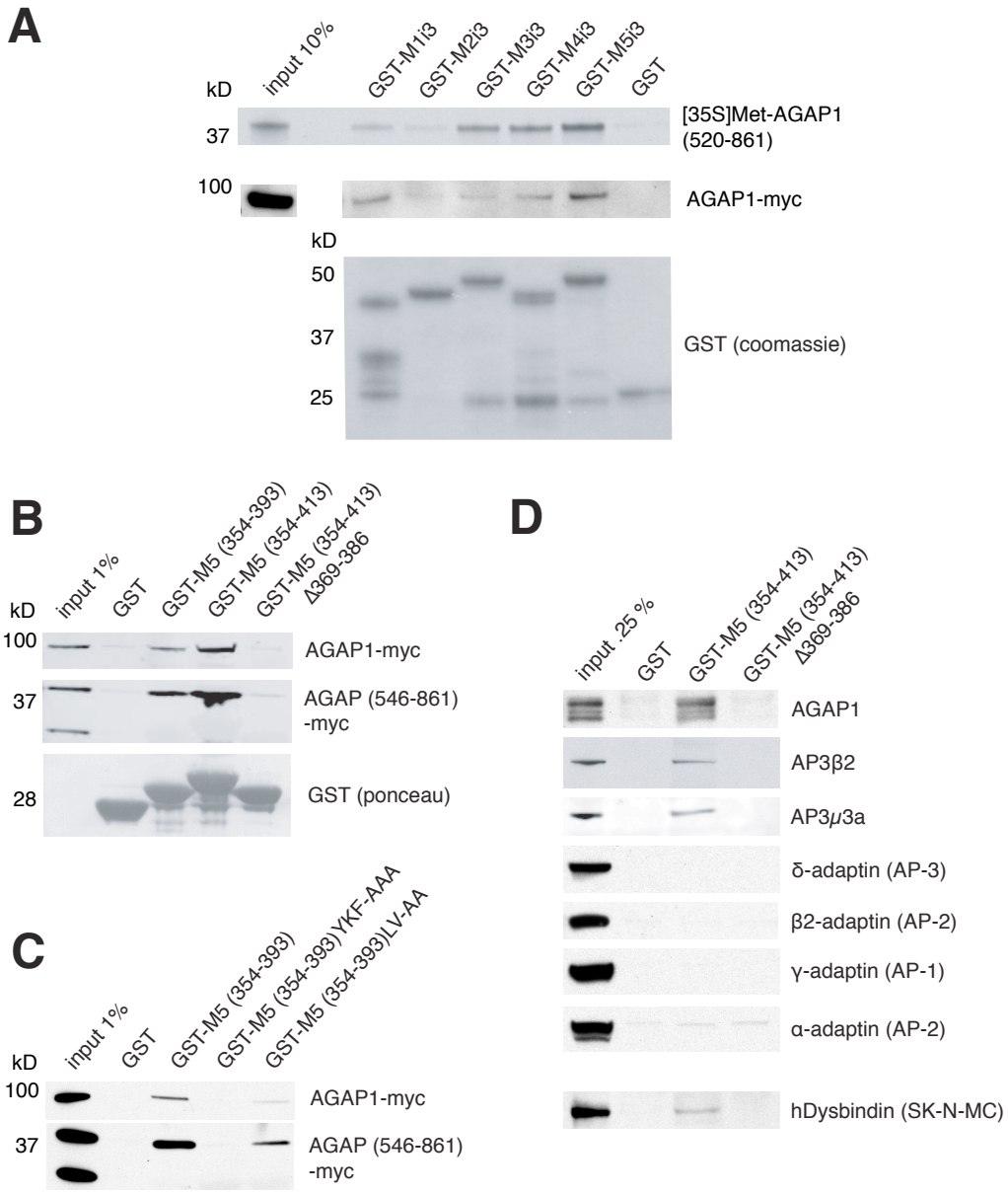

Figure 3.4 AGAP1 interacts with M5 *in vitro*. **(A)** through **(D)** Cell or tissue lysates were incubated with indicated GST-fusion proteins immobilized on glutathione resin, and bound proteins were detected by immunoblot or autoradiography. Where indicated, GST proteins were detected by coomassie blue or ponceau red stains. Molecular weights are listed in kilodaltons (kD). **(A)** Top, autoradiograph of *in vitro* synthesized [35S]methionine-labeled rat AGAP1(520-861) protein. Middle, immunoblot detecting myc-tagged AGAP1 expressed in COS-7 cells. **(B)** and **(C)** Lysates from COS-7 cells expressing myc-tagged rat AGAP1 proteins were incubated with indicated M5i3-GST truncation or point mutant proteins. **(D)** Indicated GST proteins were incubated with rat brain lysate (top 7 panels) or human neuroblastoma SK-N-MC cell lysate (bottom panel).

containing M5i3 fragments with (M5 (354-393), M5 (354-413)) and without (M5 (354-413) Δ369-386) the critical domain of interaction with AGAP1 as determined above by Y2H assay. These immobilized proteins were then used in pull-down assays with lysates from COS-7 cells overexpressing full-length or truncated (546-861) AGAP1 tagged with the myc epitope. Immunoblot revealed that both M5 (354-393) and M5 (354-413) proteins were able to pull down full-length AGAP-myc, whereas the domain of interaction deletion mutant and native GST were not (figure 3.4B). This pattern of interaction was also observed for the AGAP1 (546-861)-myc protein, a truncation mutant missing the GLD and N-terminal half of the split PH domain, but retaining the critical domain of M5i3 interaction identified in Y2H experiments (figure 3.4B). Interestingly, exogenous expression of the AGAP1 (546-861) protein yielded a second myc-immunoreactive band, likely corresponding to a predicted 21-kD truncation protein formed by translation from a strong internal translation initiation site (AGAP1 (675-861)). This lower band exhibited no binding to the GST-M5i3 proteins, consistent with the absence of the M5 domain-of-interaction in this hypothesized protein (figure 3.4B).

Finally, GST-M5i3 fusion proteins containing the alanine point mutations identified in Y2H experiments as sufficient to disrupt AGAP1 binding were tested for interaction with AGAP1-myc and AGAP1 (546-861)-myc in the pull-down assay. While the Y378A K379A F380A mutation was observed to eliminate binding of AGAP1 proteins, the L382A V383A mutation reduced, but did not completely eliminate, AGAP1 interaction with M5i3 (figure 3.4C). Taken together,

the Y2H and *in vitro* binding data therefore strongly supported the M5i3 YKF sequence as critical for binding of AGAP1.

3.3.5 *Endogenous AGAP1 and AP-3 interact with M5i3* in vitro

Using the GST, GST-M5 (354-413) and GST-M5 (354-413 Δ369-386) recombinant affinity matrices described above, we next attempted to detect interaction of M5i3 with endogenous proteins in rat brain lysate by pull-down and immunoblot analysis. Consistent with our previous data, we observed interaction of GST-M5 (354-413), but not GST-M5 (354-413 Δ369-386) or native GST, with AGAP1 (figure 3.4D). Interestingly, the AGAP1 antibody used in this study detected by immunoblot a multiplet band running at the predicted AGAP1 protein size (94.5 kD), the significance of which is unknown (figure 3.4D).

AGAP1 has been shown to specifically bind to, and to influence the activity of, the AP-3 adaptor protein complex (Nie et al., 2003; Nie et al., 2005). Heterotetrameric adaptor complexes mediate trafficking of membrane-bound cargo proteins by binding to both target and vesicle coat proteins, as well as phospholipids and accessory proteins such as the Arf small GTPases (Nakatsu and Ohno, 2003; Lefrancois et al., 2004). The AP-3 adaptor complex, consisting of the adaptin subunits δ, β3, *μ*3, and σ3, is present in mammals as ubiquitous (AP-3a) and neuron-specific (AP-3b) isoforms (Dell'Angelica et al., 1997; Newell-Litwa et al., 2007). Whereas the ubiquitous AP-3 complex is important for trafficking of proteins to late endosomes, lysosomes, and lysosomal-like compartments such as melanosomes and platelet dense granules, the neuron-

specific form of AP-3 is required for the biogenesis of, and trafficking of certain membrane proteins to, endosomally-derived synaptic vesicles (Ooi et al., 1997; Bonifacino and Dell'Angelica, 1999; Blumstein et al., 2001; Salazar et al., 2004b). Using antibodies directed at subunits of AP-3a and AP-3b, we tested the hypothesis that an AGAP1/AP-3 complex could interact with the M5i3 loop. Subunits of both the ubiquitous (μ3A) and neuron-specific (β3B / β-NAP) AP-3 adaptor complexes were detected in pull-downs using GST-M5 (354-413), but not GST-M5 (354-413 Δ369-386) or native GST (figure 3.4D). However, M5i3 interaction with the AP-3 large subunit δ-adaptin was not observed (figure 3.4D). The association of the AP-3 adaptor complex with M5i3 appeared to be specific, as AP-1 and AP-2 complex subunits did not bind to GST-M5 (354-413) (figure 3.4D).

The AP-3 adaptor complex interacts physically and functionally with the heteromeric complex BLOC-1 (biogenesis of lysosome-related organelles complex 1) (Salazar et al., 2006; Salazar et al., 2009). Mutations in human genes encoding members of either the AP-3 complex or BLOC-1 are responsible for Hermansky-Pudlak syndrome, a genetically heterogeneous set of related autosomal recessive disorders characterized by albinism, platelet storage pool deficits, and prolonged bleeding (Wei, 2006). A mutation in one of these genes, *DTNBP1*, is responsible for Hermansky-Pudlak syndrome type 7 (Li et al., 2003). The *DTNBP1* gene product dysbindin (dystrobrevin binding protein 1) is an essential member of BLOC-1, and was shown to bind directly to AP-3 via the μ3A subunit (Li et al., 2003; Taneichi-Kuroda et al., 2009). In order to determine

whether dysbindin was part of the AGAP1/AP-3 complex that we observed to interact with M5i3 *in vitro*, we tested lysate prepared from cultured SK-N-MC neuroblastoma cells in the GST-M5i3 pull-down assay (use of human tissue was necessitated by the lack of rat- or mouse- immunoreactivity of our commercially-sourced dysbindin antibody). Immunoblotting for human dysbindin revealed modest but specific binding to GST-M5 (354-413) (figure 3.4D). Taken together, our *in vitro* binding data confirm the the Y2H results indicating a subtype-specific and domain-delineated interaction between M5 and AGAP1, and suggest that AGAP1 binding may be mediating the interaction of a larger AP-3 / BLOC-1 -containing complex with the M5i3 loop.

3.3.6 *Intact AP-3 or phospholipid binding activity of AGAP1 is not required for its interaction with M5i3*

We investigated whether AP-3 could play a role in mediating the binding of AGAP1 to M5. Although false-positive interaction in the Y2H assay as a result of an endogenous multi-protein complex is unlikely, our *in vitro* pull-down experiments could not exclude the possibility that the observed interaction of AGAP1 to M5 was indirect, perhaps as a result of AP-3 binding to the YXXΦ or dileucine-like motifs in the M5i3 domain of interaction. As an indirect measure of this, we performed co-immunoprecipitations of full-length and truncated forms of myc-tagged AGAP1 expressed in HEK-293T cells. Full-length AGAP1 was seen to co-immunoprecipitate the AP-3 subunit μ3A, as previously reported (figure 3.5A) (Nie et al., 2003). However, the AGAP1(546-861) mutant, in which the

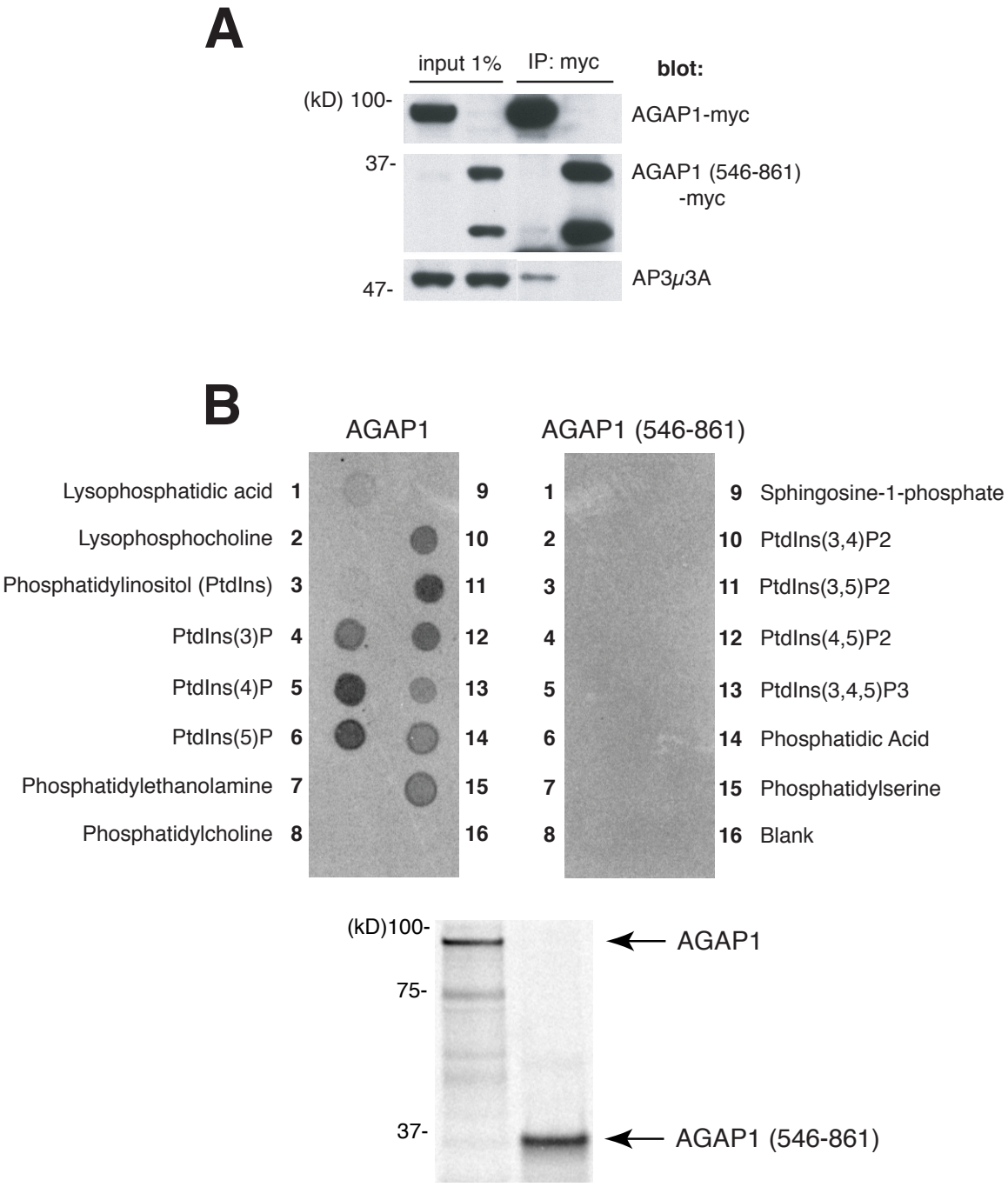

Figure 3.5 AGAP1 interacts with AP-3 and phospholipids. (A) Myc-tagged rat AGAP1 proteins were expressed in NIH-3T3 cells, immunoprecipitated with anti-myc antibodies, and immunoprecipitates were analyzed by immunoblot. **(B)** Top, Phospholipid dot-blot arrays were incubated with [35S]methionine-labeled AGAP1 proteins as indicated, and bound proteins were visualized by autoradiography. Bottom, [35S]methionine-labeled AGAP1 proteins used above were analyzed by SDS-PAGE and autoradiography.

GLD and N-terminal half of the split PH domain are deleted, was unable to co-immunoprecipitate AP-3 μ3A (figure 3.5A). As both full-length and truncated forms of AGAP1 were able to bind to M5i3 in the pull-down and Y2H assays, the co-immunoprecipitation data indicated that AP-3 binding was not required for the interaction of AGAP1 with M5.

AGAP1 exhibits phosphoinositide-dependent Arf GAP activity, and contains a PH domain, a functional motif known to exhibit phospholipid binding activity (Nie et al., 2002; Lemmon, 2004). To investigate the role of phospholipids in the interaction of AGAP1 with M5, we performed a lipid array overlay assay using [35S]Met-labeled full-length AGAP1 and the AGAP1(546-861) N-terminal deletion mutant prepared by *in vitro* coupled transcription-translation. Full-length AGAP1 showed binding to a variety of phospholipids, phosphatidic acid, and phosphatidylserine, with strongest apparent binding to phosphatidylinositol-4-phosphate and phosphatidylinositol-(3,5)-bisphosphate (figure 3.5B). However, AGAP1(546-861), in which the split PH domain is disrupted but the domain of M5i3 interaction is maintained, displayed no phospholipid binding (figure 3.5B). Thus, we determined that AGAP1 does indeed bind phospholipids via its split PH domain, but that this activity is dispensable for binding to M5.

3.3.7 *Studies of M5 / AGAP1 interaction by co-immunoprecipitation*

In an effort to demonstrate interaction of M5 receptors with AGAP1 under physiological conditions, we attempted to co-immunoprecipitate M5 and AGAP1

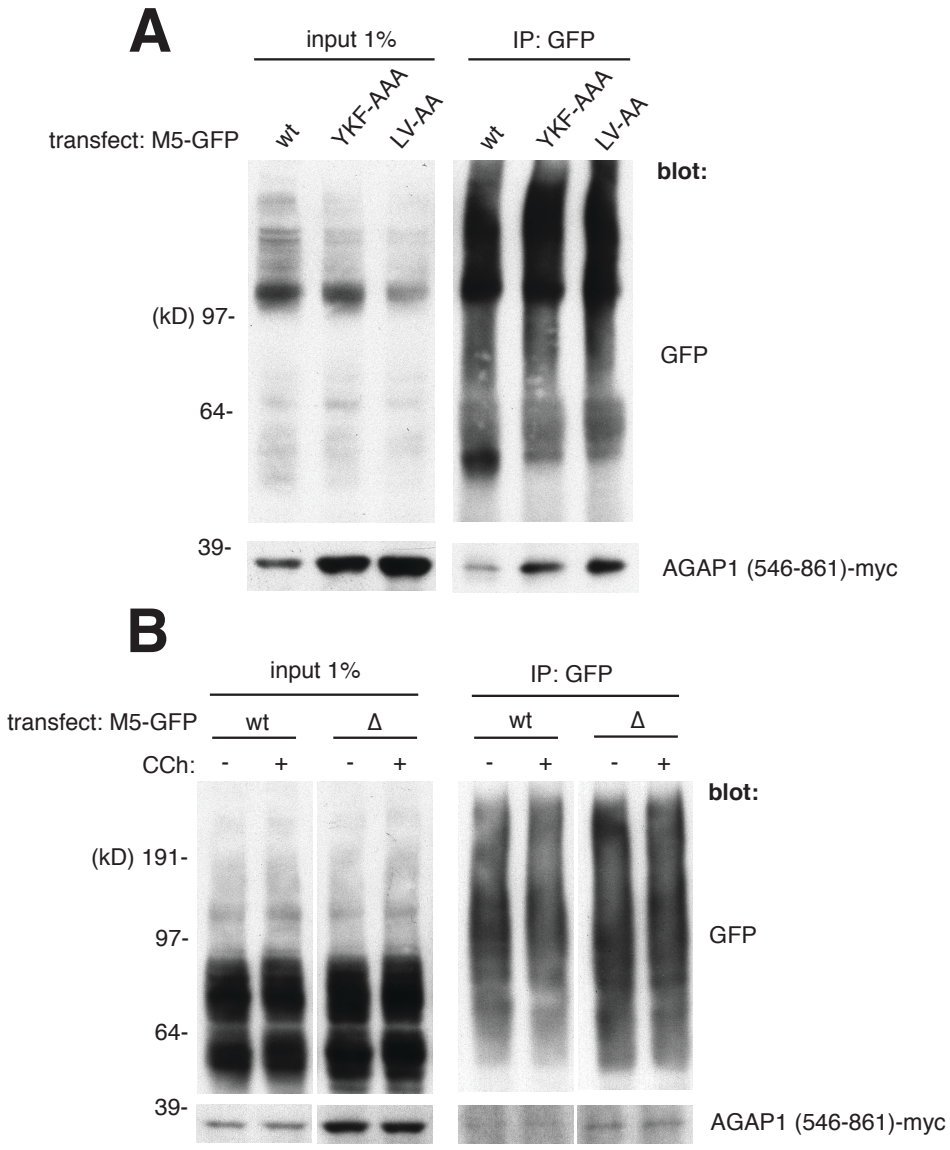

Figure 3.6 Co-immunoprecipitation studies of AGAP1-M5 interaction. COS-7 cells co-expressing rat AGAP1(546-861) and wild-type, point-, or domain-of-interaction- mutant rat M5-GFP receptors were left untreated (A) or were treated as indicated with carbachol (CCh; 1mM) for 30 minutes. Lysates were incubated with anti-GFP antibodies, and immunoprecipitates were analyzed by immunoblot for GFP and myc tags. M5-GFP receptors present in COS-7 cell lysates were detected predominantly as dimers **(A)** or monomers **(B)**.

proteins from intact cells. As no specific antibodies appropriate for immunoprecipitation from native tissue sources exist for M5, we performed the experiments using M5 receptors fused with GFP on their C-termini expressed in exogenous cell systems. A number of different detergent conditions for M5 solubilization were employed, including a digitonin-cholate system described previously as yielding monomeric, non-denatured receptors (Haga and Haga, 1985; Peterson et al., 1995). Although small amounts of AGAP1(546-861)-myc were seen to co-immunoprecipitate with M5-GFP expressed in tissue culture cells using anti-GFP antibodies, the specificity of this association did not reflect our *in vitro* binding data: neither the Y378A K379A F380A nor Δ369-386 M5 mutations were able to interfere with apparent AGAP1(546-861)-myc binding (figure 3.6). The specific co-immunoprecipitation of AGAP1 with M5-GFP after agonist (carbachol) stimulation of M5 (figure 3.6B), in the presence of a protein cross-linking reagent, or using primary cultured rat neurons as the exogenous expression system was not observed (data not shown). We therefore were unable to corroborate our Y2H and *in vitro* binding data with demonstration of specific M5/AGAP1 co-immunoprecipitation.

3.3.8 *Domain mapping and* in vitro *binding: SNX20 and M2i3*

Using a strategy similar to that described for the study of AGAP1/M5 interaction, we investigated the characteristics and specificity of the putative interaction of the M2 i3 loop with SNX20. Y2H domain-of-interaction mapping confirmed the positive interaction with the pACT2 prey clone isolated in the Y2H

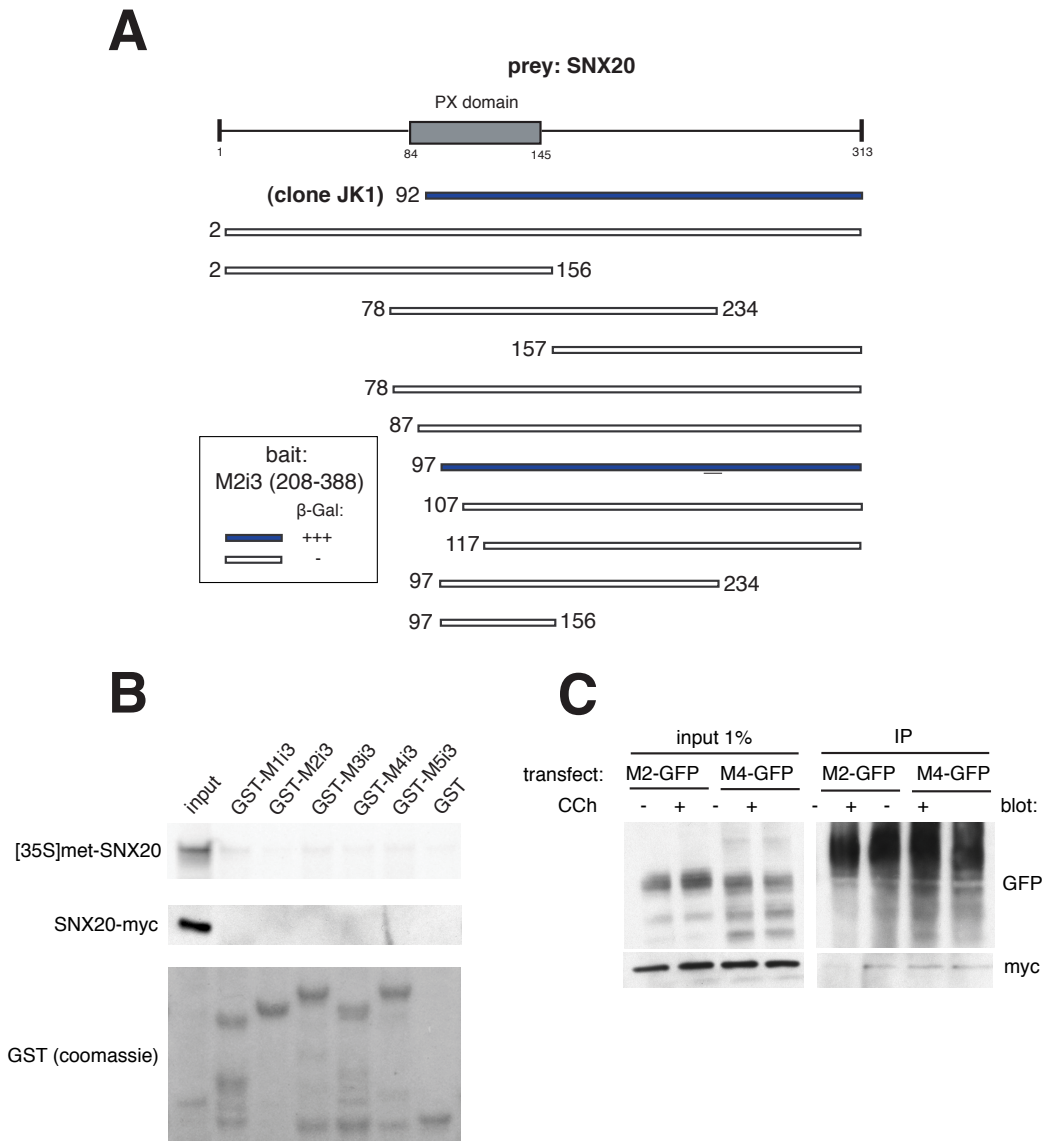

Figure 3.7 SNX20 domain-of-interaction mapping and *in vitro* binding. **(A)** Cartoon summarizing X-Gal lift assay results from Y2H interaction assays. Top, SNX20 sequence indicating position of the PX domain. Below, rat SNX20 truncation mutants were assayed for M2i3 interaction as indicated. Dark blue, strong lacZ activation; white, negative result. **(B)** [35S]methionine labeled SNX20 synthesized in vitro (top; input = 10% of total) or lysate of COS-7 cells expressing myc-tagged SNX20 (middle; input = 1% of total) were incubated with GST-fusion proteins immobilized on glutathione resin, and bound proteins were detected by autoradiography or immunoblot, respectively. Total GST proteins were detected by coomassie blue staining (lower panel). **(C)** Rat M2-GFP or M4-GFP receptors were co-expressed in COS-7 cells with myc-tagged SNX20, cells were treated as indicated, and MR-GFP proteins immunoprecipitated after cross-linking. Immunoprecipitates were analyzed by immunoblot with GFP and myc tag antibodies as indicated.

screen (JK1, encoding SNX20 residues 92-313) (figure 3.7A). We observed no reporter gene activation by JK1 when co-expressed with the LexA-M1i3 bait in L40 yeast (data not shown). Despite extensive coverage of the SNX20 protein by truncation mapping, we were able to identify only a single mutant, SNX20(97-313), that exhibited *lacZ* activation with the pLexA-M2i3 bait in the Y2H lift assay (figure 3.7A). Additionally, truncation mutants containing both the SNX20(97-313) domain and an intact PX domain showed no interaction with M2i3 in this assay (figure 3.7A). We therefore surmised that either SNX20 interaction with M2i3 was dependent on a large protein domain and that the presence of an active PX domain was able to interfere with the readout of this interaction in yeast, or that the observed SNX20-M2i3 interaction was a result of an artifactual sequence present at the fusion junction between the DNA-BD and M2i3 proteins.

We next attempted to detect binding of full-length SNX20 to GST-M2i3 *in vitro*. Using either [35S]Met-labeled SNX20 prepared by *in vitro* coupled transcription-translation or lysate from tissue culture cells overexpressing epitope-tagged SNX20-myc, we performed GST pull-down assays with the five GST-MRi3 proteins or native GST as affinity matrices. Neither [35S]Met-SNX20 or SNX20-myc displayed specific binding to M2i3 (figure 3.7B). We also attempted to co-immunoprecipitate M2-GFP receptors with SNX20-myc expressed in tissue culture cells, with and without carbachol treatment and using the cell-permeable protein crosslinker DSP prior to solubilization. Using GFP antibodies for immunoprecipitation, no specific co-immunoprecipitation of

SNX20-myc was observed (figure 3.7B). Taken together, our data do not provide strong biochemical support for the existence of a physiological interaction between SNX20 and M2.

3.3.9 *Domain mapping and* in vitro *binding: UHRF1BP1L and M4i3*

The M4i3 Y2H screen yielded β-Gal positive prey clones encoding UHRF1BP1L with two distinct AD-fusion N-terminal junctions: clones JA54 (UHRF1BP1L(2034-1469)) and JA71 (UHRF1BP1L(1123-1469)) (figure 3.8A). These clones were observed to activate *lacZ* reporter activity with the M4i3 bait, but not the remaining four MRi3 baits, in the Y2H lift assay (data not shown). However, UHRF1BP1L fragments with N-terminal truncations between (residue 1116) or past (residue 1188) the junctions present in the JA54 and JA71 clones failed to display interaction with M4i3 (figure 3.8A).

We performed a GST-MRi3 pull-down experiment using COS-7 cell lysate, in which endogenous UHRF1BP1L (KIAA0701) protein was detectable by immunoblot using a commercial antibody. Although weak interaction of UHRF1BP1L with GST-M4i3 was observed, stronger pull-down with the GST-M3i3 and GST-M5i3 affinity matrices was apparent, in contrast to the M4i3 interaction specificity observed in the Y2H system (figure 3.8B). We also attempted to detect interaction of endogenous UHRF1BP1L in COS-7 cells with exogenously expressed M4-GFP by DSP cross-linking and immunoprecipitation with GFP antibodies. We observed no co-immunoprecipitation of UHRF1BP1L protein with M4-GFP, either with or without carbachol treatment prior to receptor

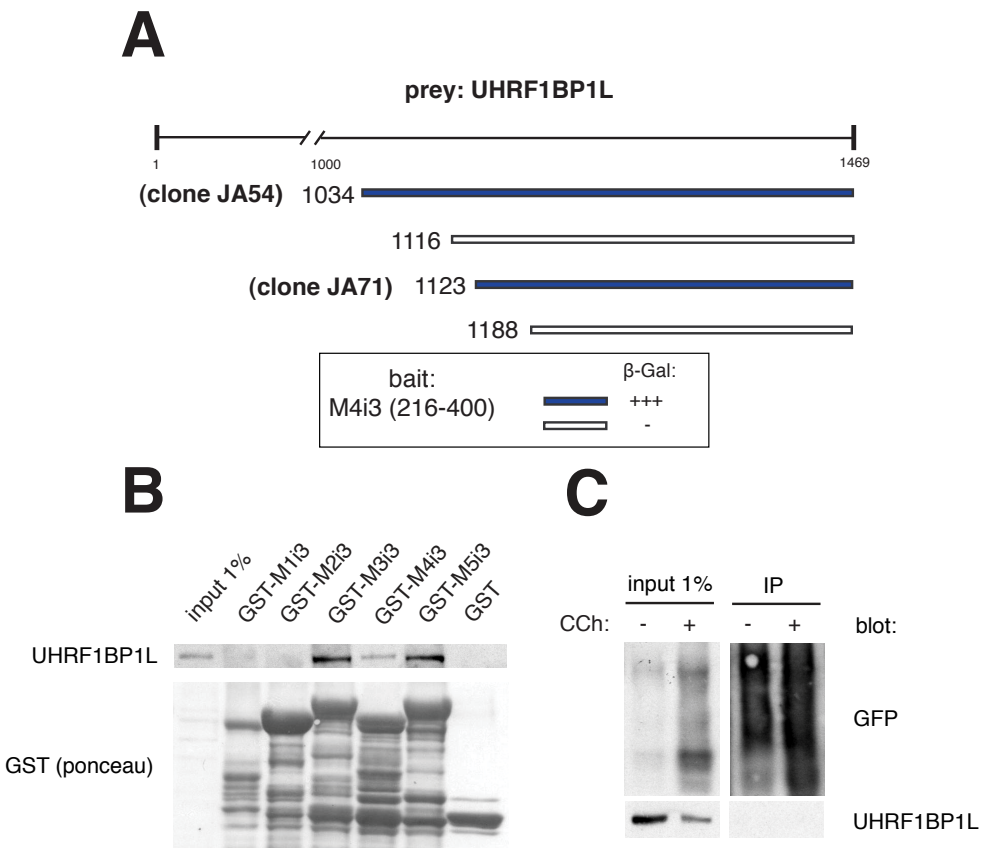

Figure 3.8 UHRF1BP1L domain-of-interaction mapping and in vitro binding. **(A)** Cartoon summarizing X-Gal lift assay results from Y2H interaction assays. Rat UHRF1BP1L-encoding clones derived from the M2i3 Y2H screen, or UHRF1BP1L truncation mutants were assayed for M2i3 interaction as indicated. Dark blue, strong lacZ activation; white, negative result. **(B)** Lysate from COS-7 cells expressing myc-tagged rat UHRF1BP1L was incubated with GST-fusion proteins immobilized on glutathione resin, and bound proteins were detected by immunoblot, respectively. **(C)** Rat M4-GFP receptors were co-expressed in COS-7 cells with myc-tagged UHRF1BP1L, cells were treated as indicated, and MR-GFP proteins immunoprecipitated after cross-linking. Immunoprecipitates were analyzed by immunoblot with GFP and myc tag antibodies as indicated.

solubilization (figure 3.8C). Thus, the *in vitro* binding studies combined with our Y2H data do not strongly support the existence of a specific, domain-delineated interaction between M2i3 and URHF1BP1L.

3.4 Discussion

In this chapter, we provide biochemical evidence for the physical interaction of muscarinic receptor M5 with AGAP1. The observed interaction was unique to the M5 muscarinic receptor subtype, and was mediated by a conserved 23-residue region on the M5 i3 cytoplasmic loop sharing no sequence homology with muscarinic receptors 1 through 4. Similarly, three closely-related AGAP proteins did not exhibit M5i3 interaction, and the AGAP1 domain mediating this binding is highly conserved in sequence across species. We are the first to report direct binding between an AGAP protein and a GPCR, although a related AZAP family protein ACAP1 has been shown to interact with a number of non-GPCR transmembrane receptors (Dai et al., 2004; Li et al., 2005). We also observed that, at least *in vitro*, the M5i3 domain critical for interaction with AGAP1 was able to bind subunits of the ubiquitous and neuron-specific isoforms of the AP-3 adaptor complex. As the interaction between AGAP1 and M5 was apparently direct, and since AGAP1 is known to bind directly to AP-3 (Nie et al., 2003), we surmised that AGAP1 was mediating binding of AP-3 to M5i3. This suggested the possibility that *in vivo*, the identified interaction domain of M5i3 mediates binding of an AGAP1/AP-3 trafficking complex to the receptor, perhaps implicating the identified protein-protein interaction in the regulated trafficking of

M5. Indeed, we also detected binding of dysbindin protein to the M5i3 AGAP1-interaction domain; dysbindin is a sub-member of BLOC-1, a complex known to interact physically and functionally with AP-3 (Li et al., 2003; Taneichi-Kuroda et al., 2009). It should be cautioned, however, that our *in vitro* data does not distinguish between binding of a native, pre-formed AGAP1/AP-3/BLOC-1 super-complex to M5i3 and recruitment of AP-3 / BLOC-1 components to M5i3-bound AGAP1; in addition, we did not observe M5i3 binding of the large AP-3 subunit δ-adaptin in our assays.

Site-directed mutagenesis implicated a YKF motif in M5i3 as critical for AGAP1 binding to M5i3. Phenylalanine- and tyrosine- residue clusters on the transferrin receptor cytoplasmic tail were similarly shown to be critical for ACAP1 binding and/or endocytic recycling of the receptor (McGraw et al., 1991; Dai et al., 2004). The YKF sequence resembles, but does not fulfill the functional identity of, the commonly occurring and well-characterized YxxΦ sorting signal, which targets host proteins for endocytosis and localization to lysosomes or lysosome-like compartments via interaction with adaptor protein complex *μ* subunits (Rapoport et al., 1997; Ohno et al., 1998; Bonifacino and Traub, 2003). We also identified by site-directed mutagenesis a leucine-valine residue pair whose mutation interfered with AGAP1 binding. Although lacking the upstream acidic residues, this motif resembles the [DE]XXXL[LI] and DXXLL dileucine-type sorting signals known to mediate receptor internalization, lysosomal targeting and TGN-to-endosome transport by binding to adaptor protein complex subunits (Johnson and Kornfeld, 1992; Letourneur and Klausner, 1992; Bonifacino and

Traub, 2003; Janvier et al., 2003). Notably, dileucine and dileucine-like (LI, LV) motifs lacking upstream acidic residues have been shown to function as AP-1- and AP-3-binding lysosomal targeting motifs in yeast and mammals (Rapoport et al., 1998; Vowels and Payne, 1998; Kyttala et al., 2005). Although our Y2H and *in vitro* binding data demonstrate direct binding of AGAP1 to M5i3, and though AP-3 subunits bind AGAP1, our data cannot discount the possibility of a direct AP-3 / M5i3 interaction, perhaps mediated by the leucine-valine motif.

Co-immunoprecipitation of endogenous proteins from native tissue sources is typically considered the "gold-standard" for proof of molecular interaction *in vivo* (Hall, 2005). Such an experiment is not possible in the case of M5, as no antibodies currently exist that are appropriate for either immunoprecipitation or immunoblotting, and the receptor is expressed at very low levels in the brain and periphery (Wess et al., 2003). We investigated a number of N-terminal, C-terminal, and internal epitope tags on the M5 receptor for their suitability in immunoprecipitation and immunoblotting experiments in exogenous expression systems; a C-terminal GFP tag was identified as most appropriate. However, we were unable to identify conditions under which the wild-type M5-GFP receptor, but not the Y378A K379A F380A, L382A V383A or Δ369-386 M5-GFP receptors, was able to co-immunoprecipitate either truncated or full-length forms of AGAP1. Detergent solubilization of M5 receptors was a continuing technical difficulty; the degree to which the non-denaturing digitonin-cholate system purified monomeric or oligomeric forms of M5 protein was reagent batch-dependent (see figure 3.6), and more stringent solubilization conditions were

avoided in fear of disrupting the putative AGAP1-M5 complex. Attempts to stabilize the putative low-affinity AGAP1-M5 complex by chemical cross-linking also failed, in part due to insolubility of AGAP1 proteins after DSP treatment and poor reduction of the disulfide crosslink bond under conditions necessary to avoid M5 aggregation during SDS-PAGE. However, due to the agreement between *in vitro* binding and Y2H interaction data and the existence of clearly-delineated interaction domains, we took our results to indicate the existence of a low-affinity interaction between M5 and AGAP1. Weak protein-protein interactions are typical of the transient binding of trafficking or signaling complexes with their cellular targets (Vaynberg and Qin, 2006). Indeed, physiologically relevant trafficking complex binding to receptor targeting motifs has been revealed by a combined Y2H / GST pull-down strategy (Voglmaier et al., 2006) and binding of targeting motif-containing peptides to adaptor complex proteins was shown to require cryopreservation and/or photo-crosslinking for detection (Rapoport et al., 1997; Rapoport et al., 1998).

Our data do not provide strong support for the existence of the putative SNX20-M2i3 and UHRF1BP1L-M4i3 interactions detected in the Y2H screens. DOI mapping and *in vitro* binding results cannot rule out the possibility that the detected interactions were false-positive artifacts of the Y2H system, bait or prey fusion proteins, or some combination thereof. In the case of SNX20, it is curious that the presence of a functional PX domain abrogates *lacZ* reporter activity in the Y2H lift assay. The possibility exists that phospholipid binding activity of the AD-SNX20 prey fusion prevents nuclear localization, M2i3 interaction, or AD

activity in yeast. Nonetheless, based on the strength of the interaction data, our experimental focus from this point forward was on the functional consequences of the AGAP1 / M5 protein-protein interaction. As co-immunoprecipitation data were lacking, we chose to employ the domain-of-interaction deletion mutant (Δ369-386) to study AGAP1 interaction-dependent M5 function, since this mutant was most likely to maintain the AGAP1 binding loss-of-function observed in yeast and *in vitro*.

4 AGAP1 & M5: DISTRIBUTION

4.1 Summary

We demonstrate in this chapter co-localization of M5 receptors with AGAP1 in endosomal-like compartments of cultured neurons. Exogenous co-expression of AGAP1-myc and M5-GFP in rat primary hippocampal neurons revealed a population of partially overlapping AGAP1- and M5- positive puncta after agonist induced internalization of M5. Live imaging in cultured neurons indicated a dynamic relationship between mobile, M5-GFP- and AGAP1- or AP-3B-positive vesicles. Co-immunostaining in cultured neurons confirmed transit of agonist-internalized M5 through AP-3-positive endosomes and the recycling and/or degradative trafficking pathways. Results obtained from membrane fractionation of rat brain tissue are consistent with the association of AGAP1 with AP-3 endosomes. As AGAP1 is likely a ubiquitously expressed protein, our results support the cellular and sub-cellular co-localization of AGAP1 and M5, further arguing for their physical interaction *in vivo*. Our data also suggest a functional role for AGAP1 in the activity-induced trafficking of M5 in neurons.

4.2 Introduction

The M5 muscarinic receptor is by far the lowest expressed and most poorly characterized MR in mammals. Though the lack of subtype-selective ligands and antibodies appropriate for detection of M5 by immunohistochemistry

or immunoblotting has hampered investigation of the receptor, a number of studies have demonstrated functionally significant expression of M5. In the mouse, M5 mRNA was detected almost exclusively in the brain, with particular enrichment in the hypothalamus, hippocampus, and striatum, although small amounts of M5 transcript were detected both in mouse skin and in a human melanoma cell line (Kohn et al., 1996; Regard et al., 2008). Radioligand detection of MR sites immunoprecipitated from rat brain using subtype-selective antibodies suggested that M5 receptors contribute to less than 2% of the total MR population, a result confirmed more recently in the M5 knockout mouse (Yasuda et al., 1993; Oki et al., 2005). *In situ* hybridization studies in mouse and rat brain confirm a low overall level of M5 transcription; interestingly, however, M5 mRNA, but not M1-4 mRNA, was detected in the midbrain dopaminergic neurons of the SNc and VTA (figure 4.1) (Weiner et al., 1990; Lein et al., 2007). Phenotypic (loss-of-function) analysis of the M5 knockout mouse has indicated functional expression of M5 in two main areas: first, in both pre- and post-synaptic terminals of midbrain dopaminergic neurons innervating the dorsal and ventral striatum (Yeomans et al., 2001; Forster et al., 2002; Zhang et al., 2002b), and second, in cerebral arteries and arterioles (Yamada et al., 2001a). The subcellular distribution of M5 has not been directly investigated. However, MR 1-4 have been shown to localize to the plasma membrane of tissue culture cells, and undergo the stereotypical GPCR trafficking cycle of agonist-induced internalization, followed by either endocytic recycling or targeting for lysosomal degradation, depending on subtype (Tolbert and Lameh, 1996; Volpicelli et al.,

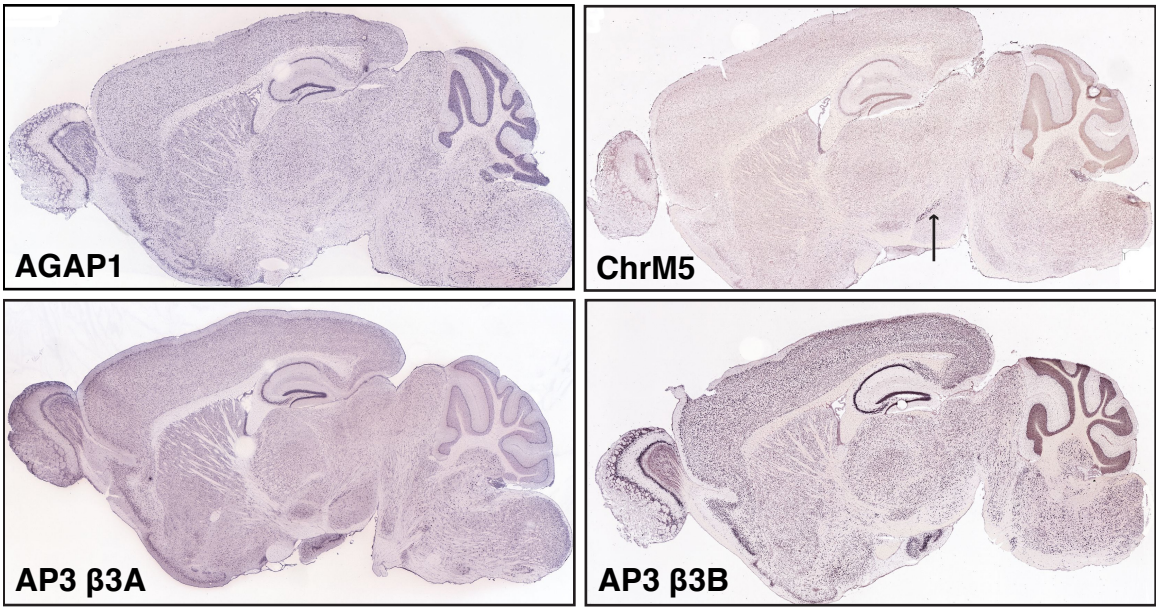

Figure 4.1 Allen Mouse Brain Atlas in situ hybridization data. Sagittal C57BL/6J mouse brain sections labeled with digoxigenin-conjugated riboprobes for indicated genes were obtained from the on-line Allen Mouse Brain Atlas (Seattle (WA): Allen Institute for Brain Science. ©2009. Available from: http://mouse.brain-map.org). Arrow indicates substantia nigra pars compacta region labeled with ChrM5 riboprobe.

2001; Delaney et al., 2002; Popova and Rasenick, 2004).

AGAP1 is an AP-3-associated Arf GAP protein expressed widely in mammalian tissues. Expression of AGAP1 mRNA was detected at equal levels in a variety of human organs, including brain, by RT-PCR (Nie et al., 2005). Northern blot analyses of AGAP1 mRNA isolated from human and mouse tissues have described the presence of large (9 kb), medium (4.5 kb) and small (2.4 kb) transcripts expressed at various levels in a number of tissues; as Genbank indicates a message length of 9.5 kb and 4.5 kb for mouse and human AGAP1 mRNAs, these results likely indicate the presence of splice forms, the significance of which is unclear (Xia et al., 2003; Meurer et al., 2004). AGAP1 protein was also detected in lysates from human cell lines derived from lymphocyte, epithelial, gastric, liver, and glial sources (Nie et al., 2005). In the mouse brain, AGAP1 mRNA is highly expressed in the fore- and mid-brain during development (Xia et al., 2003), and exhibits a ubiquitous and uniform pattern of expression in adults (figure 4.1) (Lein et al., 2007). Epitope-tagged AGAP1 expressed exogenously in tissue culture cells was shown to exhibit either a uniform or punctate distribution pattern, apparently depending on host cell type and overexpression levels (Nie et al., 2002; Xia et al., 2003). These AGAP1 puncta were shown by biochemical and immunocytological methods to correspond to a population of AP-3-positive endosomes (Nie et al., 2003).

The heterotetrameric adaptor protein complex AP-3 exists as ubiquitous and neuron-specific isoforms. The ubiquitous AP-3A, composed of the large adaptin subunits δ and β3A, the medium subunit μ3A, and the small subunit σ3A/

B, is expressed in all mammalian cells and tissues, including the brain (figure 4.1) (Dell'Angelica et al., 1997; Lein et al., 2007). The neuron-specific AP-3B isoform shares the δ and σ3A/B subunits with the ubiquitous form, and includes the neuron-specific subunit proteins β3B / β-NAP and μ3B (Newman et al., 1995; Seong et al., 2005). β3B is likely expressed in all CNS and peripheral neurons (figure 4.1) (Newman et al., 1995; Lein et al., 2007). AP-3 is distributed subcellularly in both cytosolic and membrane-bound pools, the latter consisting of clathrin- and non-clathrin- coated vesicles seen to associate by biochemical and immunofluorescence techniques with TGN- and endosome-like structures (Dell'Angelica et al., 1997; Simpson et al., 1997; Dell'Angelica et al., 1998). An immuno-electron microscopy study of δ-adaptin in tissue culture cells found AP-3 localized to early endosome-associate membrane tubules co-localized with the lysosome-target protein LAMP1, but found no evidence for AP-3 localization in the TGN (Peden et al., 2004). In neurons, distribution of the ubiquitous AP-3A isoform is apparently restricted to neuronal soma, whereas the neuron-specific AP-3B is distributed in axons and dendrites, and is associated with nerve terminal vesicles (Newman et al., 1995; Seong et al., 2005).

Using biochemical methods, we identified AGAP1 as an M5-interacting protein, potentially present as a part of an AGAP1/AP-3 complex. In this chapter, we describe experiments examining the cellular and subcellular distribution of M5, AGAP1, and AP-3. As antibodies appropriate for immunocytological labeling of AGAP1 and M5 are not available, we used epitope tags for the immunofluorescent localization of M5 and AGAP1 expressed exogenously, under

both basal and agonist-stimulation conditions expected to induce internalization and endocytic traffic of the M5 receptor. Using a similar strategy, we also studied the distribution of M2 and SNX20. We used both tissue culture cells and rat primary hippocampal neurons for exogenous expression, the latter due to the possible involvement of the functionally divergent, neuron-specific AP-3B complex in the interaction of AGAP1 with M5. In primary neurons, we took advantage of the recently developed monomeric red fluorescent protein derivative mCherry (Shaner et al., 2004), along with M5-GFP, to perform two-color live imaging of M5, AGAP1, or AP-3. Finally, we investigated the distribution of M5, AP-3 and AGAP1 in comparison to membrane-associated endosomal markers in an effort to further characterize the distribution of these proteins. The main goal of this chapter's experiments was to confirm the temporal and spatial co-localization of M5 and AGAP1, and possibly AP-3, that is required for the existence *in vivo* of the proteins' physical interaction. A secondary goal was to gain knowledge as to the functional implications of AGAP1 interaction with M5, with particular attention paid to trafficking pathways.

4.3 Results

4.3.1 *AGAP1 mRNA exhibits widespread expression in mouse tissues and brain subregions*

We first analyzed mouse AGAP1 mRNA distribution by Northern blot to confirm the widespread pattern of AGAP1 expression described previously in human and mouse tissues (Xia et al., 2003; Meurer et al., 2004; Nie et al., 2005).

Using a [33P]-labeled antisense riboprobe targeting the 3'-UTR of mouse AGAP1, we detected hybridization signals in most of the tissues represented (figure 4.2A). An AGAP1 transcript of approximately 9.5 kilobases (kb) was expressed predominantly in brain, while a 4.4 kb message was most prevalent in kidney, and a smaller, approximately 3.5 kb transcript was detected only in testis (figure 4.2A). Additionally, immunoblot detection of AGAP1 protein revealed AGAP1 expression in all tested tissue sources, including tissue culture cells derived from a variety of species (human, rat, mouse, chinese hamster, african green monkey) and pre- and post-natal rat and mouse brain tissues (data not shown), in agreement with previous reports examining AGAP1 expression in human cell lines (Nie et al., 2005).

Next, we performed *in situ* hybridizations of adult mouse brain tissues using the same [33P]-labeled AGAP1 3'-UTR antisense riboprobe described above. AGAP1 mRNA was detected widely, with an autoradiography signal consistent with brain subregion cell body density (figure 4.2B). A control sense-strand riboprobe prepared from the AGAP1 3'-UTR template produced no signal (data not shown). The uniform expression of AGAP1 mRNA in the rodent brain is consistent with previously published mouse brain gene expression atlas data (figure 4.1) (Lein et al., 2007). Thus, the expression of AGAP1 mRNA and protein products was confirmed to be widespread in mammals both across tissues and within the brain.

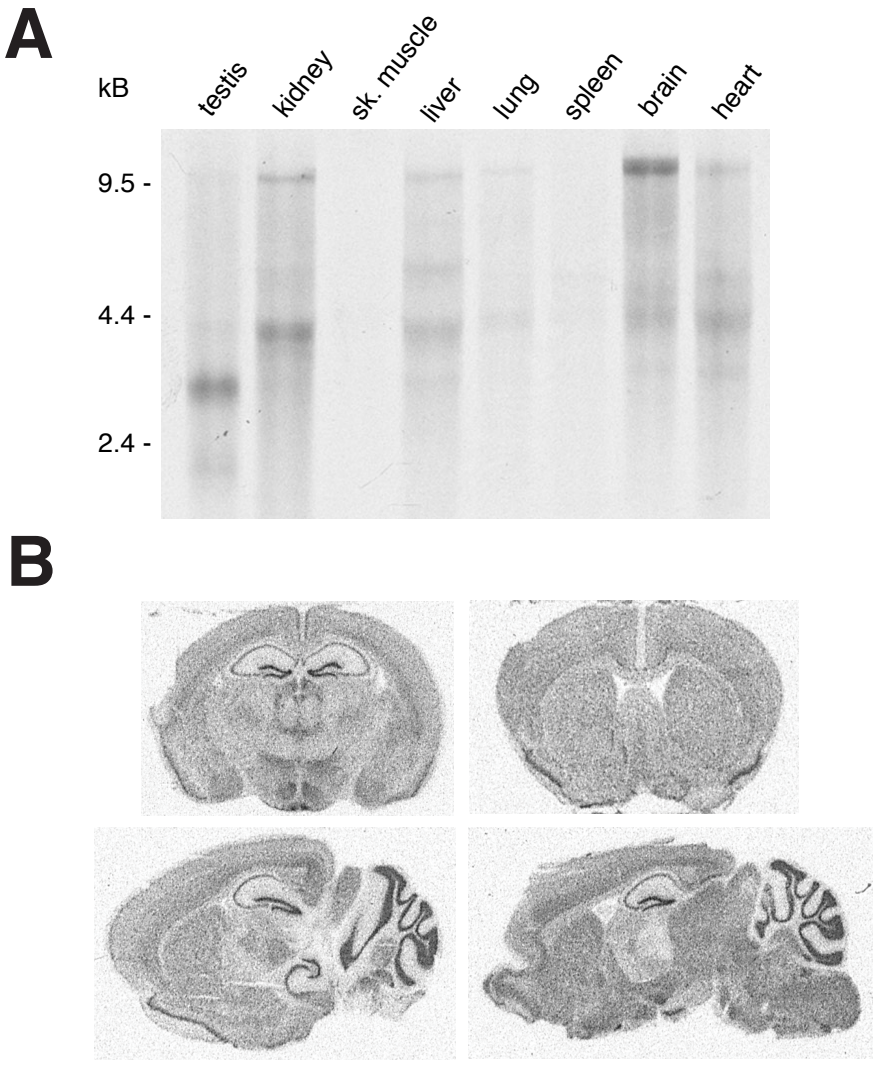

Figure 4.2 AGAP1 mRNA expression. (A) Mouse Multiple Tissue Northern blot hybridized with [33P]-labeled AGAP1 antisense riboprobe. Transcript size is indicated in kilobases. **(B)** Autoradiograph of C57BL/6 mouse brain coronal (top) and sagittal (bottom) sections labeled by in situ hybridization using the [33P] AGAP1 riboprobe from (A).

4.3.2 *Exogenously expressed M5-GFP and AGAP1-myc do not extensively co-localize in tissue culture cells*

In the next series of experiments, we aimed to investigate by confocal microscopy the degree to which M5 receptors and AGAP1 co-localize when overexpressed in mammalian tissue culture cells. Since detection of endogenous M5 and AGAP1 proteins in cultured cells was not possible due to the lack of antibodies suitable for immunocytochemistry, we performed immunofluorescence experiments using exogenously expressed epitope-tagged M5 and AGAP1 proteins. An M5 receptor tagged at the cytosolic C-terminus with GFP was seen to localize predominantly at the plasma membrane when expressed in a variety of mammalian tissue culture lines (CHO, COS-7, HEK293T) after fixation and detection with anti-GFP antibodies (figure 4.3A). In addition, treatment of M5-GFP -transfected cells with the muscarinic agonist carbachol (CCh) led to a predominantly intracellular, punctate GFP immunofluorescence pattern, consistent with agonist-induced internalization of surface M5 receptors into endocytic vesicles, as has been described in similar systems for muscarinic receptor subtypes 1-4 (Tolbert and Lameh, 1996; Volpicelli et al., 2001; Delaney et al., 2002; Popova and Rasenick, 2004).

In previous studies, exogenously expressed AGAP1 protein exhibited either a uniform/cytosolic or punctate distribution, apparently depending on the degree to which the protein was overexpressed (Nie et al., 2002; Nie et al., 2003; Xia et al., 2003). In experiments examining the immunocytological distribution of overexpressed rat AGAP1-myc, we observed a mainly uniform expression

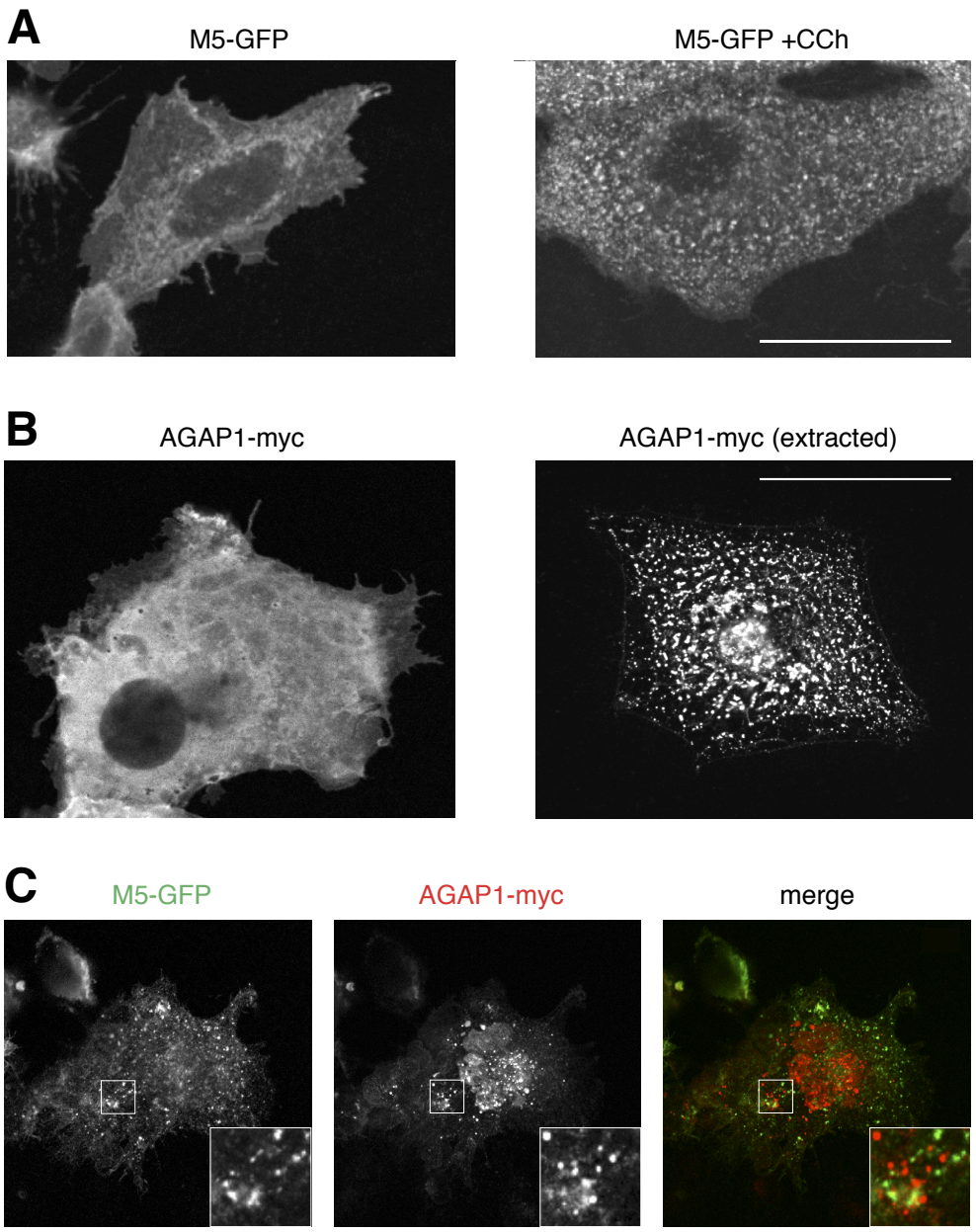

Figure 4.3 Immunofluorescence staining of AGAP1 and M5 in tissue culture cells. **(A)** CHO cells were transiently transfected with M5-GFP construct, treated with (right) or without (left) 100μM carbachol for 30 minutes, fixed, immunostained for GFP and imaged by confocal microscopy. **(B)** COS-7 cells were transiently transfected with AGAP1-myc construct, extracted with detergent (right) or not (left), fixed, immunostained for myc tag and imaged by confocal microscopy. **(C)** COS-7 cells were transiently co-transfected with M5-GFP and AGAP1-myc constructs. Cells were treated with 100μM carbachol for 1 hour, extracted with detergent, fixed, immunostained for GFP (green) and myc tag (red) and imaged by confocal microscopy. Scale bars = 50μm.

pattern consistent with cytosolic localization (figure 4.3B). In some cases, higher expression levels of AGAP1-myc led to what appeared to be a punctate localization pattern, as had been previously reported (Nie et al., 2003); however, AGAP1-enriched puncta were localized to numerous peripheral membrane blebs of cells displaying unusual gross morphology, indicating that such cells may have been apoptotic (Coleman et al., 2001). In some cases (including that of the AZAP protein ACAP1), cytosol extraction prior to fixation and immunostaining can reveal the otherwise-obscured membrane-bound pool of membrane-associated proteins (Morris and Cooper, 2001; Dai et al., 2004). We observed a punctate, vesicular-like distribution of AGAP1-myc when overexpressing cells were subjected to a mild detergent extraction before fixation (figure 4.3B).

We next investigated whether M5 and AGAP1 co-localized under conditions in which subcellular vesicle-like distribution patterns were evident. We co-expressed M5-GFP and AGAP1-myc in tissue culture cells, treated with CCh to induce M5 internalization, and performed cytosol extraction before fixation and immunostaining. Although both M5-GFP and AGAP1-myc were seen to localize mainly to subcellular puncta, little overlap was observed between the M5- and AGAP1- positive compartments in this expression system (figure 4.3C).

4.3.3 AGAP1-myc co-localizes with endocytosed M5-GFP in primary cultured neurons

Our previous data confirmed the biochemical association of AGAP1 with the AP-3 adaptor complex (Nie et al., 2003). The neuron-specific isoform of AP-3

exhibits distinct functions from that of ubiquitous AP-3, and the complex isoforms are expressed in neurons in a spatially-segregated manner (Seong et al., 2005; Newell-Litwa et al., 2007). Immunocytological studies have indicated association of AGAP1 protein with AP-3-positive endocytic compartments in tissue culture cells; however, the subcellular localization of AGAP1 in neurons has not been reported (Nie et al., 2003; Nie et al., 2005). In order to investigate both the localization and spatial overlap of M5 and AGAP1 in neurons, we transfected primary rat embryonic hippocampal neurons with AGAP1-myc and M5-GFP, and analyzed cells by confocal microscopy. M5-GFP was seen to localize to the soma, dendrites, and axons of transfected neurons (figure 4.4A). Whereas M5-GFP was localized mainly to the plasma membrane of neurons, treatment of cells with CCh led to an endosomal-vesicle-like distribution of M5-GFP (figure 4.4B). Detergent extraction prior to fixation revealed a punctate, vesicular-like distribution of AGAP1-myc in neuronal soma and processes that was otherwise

Figure 4.4 Co-localization of agonist-internalized M5 with AGAP1 and AP-3 in cultured neurons (following page). (A) Neurons were transfected with AGAP1-myc and M5-GFP plasmids, fixed and immunostained for myc tag (red) and GFP (green), and imaged by confocal microscopy. Scale bar = 20 μm. **(B and C)** Neurons were transfected as in (A) and treated without (ctl) or with 1mM carbachol (CCh) for indicated times. Cells were fixed, immunostained for GFP (green) and myc (red) and imaged by confocal microscopy. In (C), cytosolic extraction with 0.03% saponin was performed prior to fixation to visualize the membrane-bound pool of exogenously expressed AGAP1-myc. Yellow arrows indicate green / red puncta overlap. Scale is bar in top panel of (B) = 5 μm and applies to all images in (B) and (C). **(D)** Neurons were transfected with M5-GFP and treated without (ctl) or with 1mM CCh for 60 minutes, followed by fixation and immunostaining for GFP (green) and the AP-3a / AP-3b subunit δ-Adaptin (red) Yellow arrows indicate green / red puncta overlap. Scale is identical to (B).

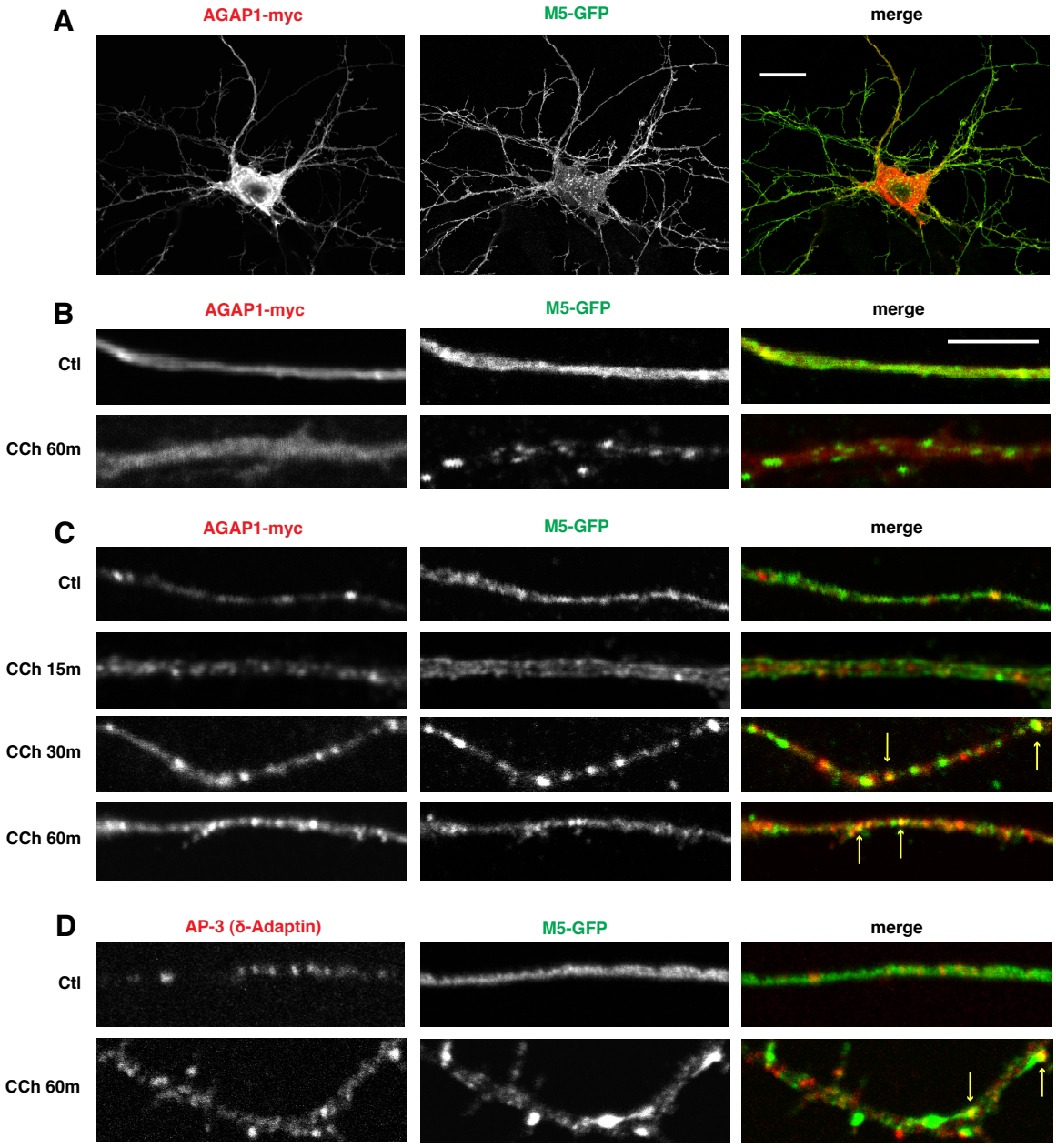
A
AGAP1-myc
M5-GFP
merge
B
AGAP1-myc
M5-GFP
merge
Ctl
CCh 60m
C
AGAP1-myc
M5-GFP
merge
Ctl
CCh 15m
CCh 30m
CCh 60m
D
AP-3 (δ-Adaptin)
M5-GFP
merge
Ctl
CCh 60m

obscured by the predominant cytosolic AGAP1 pool (figure 4.4C). In cells fixed after 30 or 60 minutes of CCh treatment, we observed overlap of M5-GFP- and AGAP1- positive puncta in neuronal projections (figure 4.4C). We therefore concluded that in neurons, agonist-internalized M5 co-localized with AGAP1, possibly in an endocytic vesicle compartment.

4.3.4 *Agonist-internalized M5-GFP appears in AP-3-positive vesicles*

In an effort to confirm the identity of vesicular compartments containing internalized M5 and AGAP1 as AP-3-positive endosomes, we performed CCh agonist treatments and immunostaining on M5-GFP- and/or AGAP1- transfected primary rat hippocampal neurons as described above. Staining with a δ-Adaptin antibody as a marker for AP-3, we observed in neuronal processes some instances of overlap between agonist-internalized M5-GFP and AP-3 puncta, suggesting transit of M5-GFP through AP-3-positive endosomal compartments (figure 4.4D). However, we were unable to confirm the identity of AGAP1-containing puncta as AP-3 endosomes, as both AGAP1 overexpression and cytosol extraction appeared to interfere with the normal pattern of AP-3 distribution, as indicated by δ-adaptin and *μ*3A immunostaining (data not shown).

4.3.5 Live imaging in cultured neurons reveals association of M5- and AGAP1- or β3B- positive vesicles

To further investigate the dynamic relationship between the population of M5-, AGAP1-, and AP-3- positive endosomes observed in immunofluorescent

staining of fixed specimens, we performed live imaging studies of GFP- or mCherry- tagged proteins expressed in primary cultured rat hippocampal neurons. In apparent axons and dendrites of transfected neurons, near-simultaneous two-color live imaging revealed mobile populations of M5-GFP- and AGAP1-mCherry- positive puncta (figure 4.5A). In general, vesicular motility was observed to be highest in axon-like processes, and AGAP1-mCherry puncta appeared less mobile than those containing M5-GFP. In some cases, we were able to observe events resembling fission of doubly-positive compartments into separate M5-GFP and AGAP1-mCherry compartments, and transient overlap of highly mobile M5-GFP and AGAP1-mCherry vesicles (figure 4.5A). Although not extensively observed, the results were consistent with the co-localization of M5 and AGAP1 in an endosome-like vesicular compartment.

We also investigated the association of M5-GFP and AP-3 vesicles using the neuron-specific AP-3B complex marker mCherry-AP3β3B expressed in primary cultured neurons. Although mCherry-AP3β3B puncta were difficult to detect, we did observe instances of apparent juxtaposition of AP-3- and M5-GFP-positive vesicles both with and without CCh agonist treatment; in addition,

Figure 4.5 Live imaging of M5, AGAP1 and AP-3 β3B in cultured neurons (following page). Primary cultured rat hippocampal neurons were cotransfected with M5-GFP (green) and AGAP1-mCherry (A; red) or mCherry-AP3β3B (B and C; red) plasmids, treated with 1mM carbachol for 1 hour (A and C), and imaged by two-color spinning disk confocal microscopy at two second intervals. Images on right depict time-lapse series of enlarged areas from images at left. Red, green and yellow arrows indicate mobile GFP, mCherry, or GFP + mCherry puncta, respectively. Scale bars = 10μm.

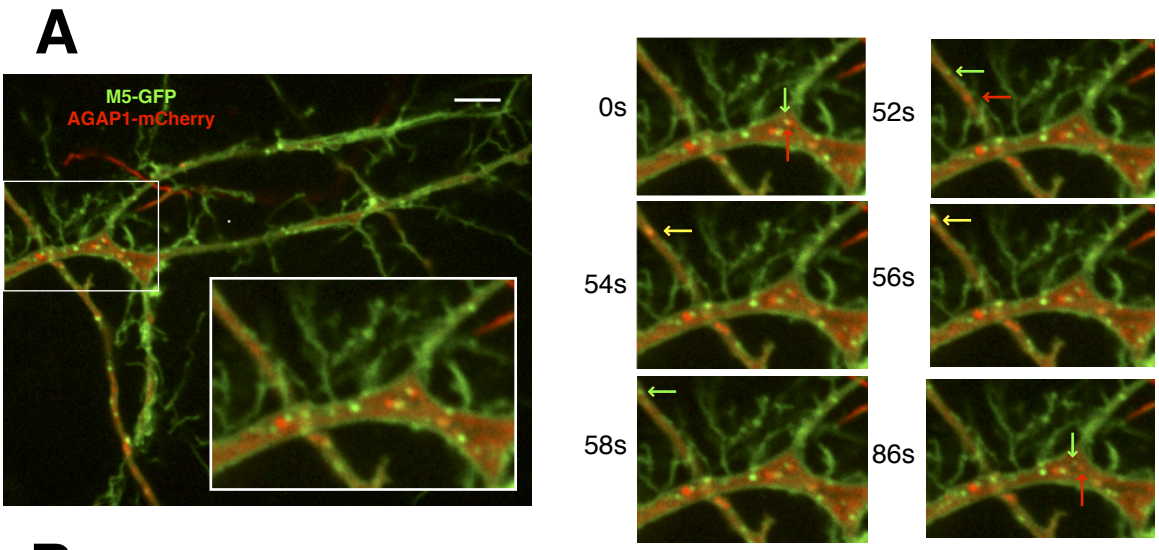
A
M5-GFP
AGAP1-mCherry
0s
52s
54s
56s
58s
86s

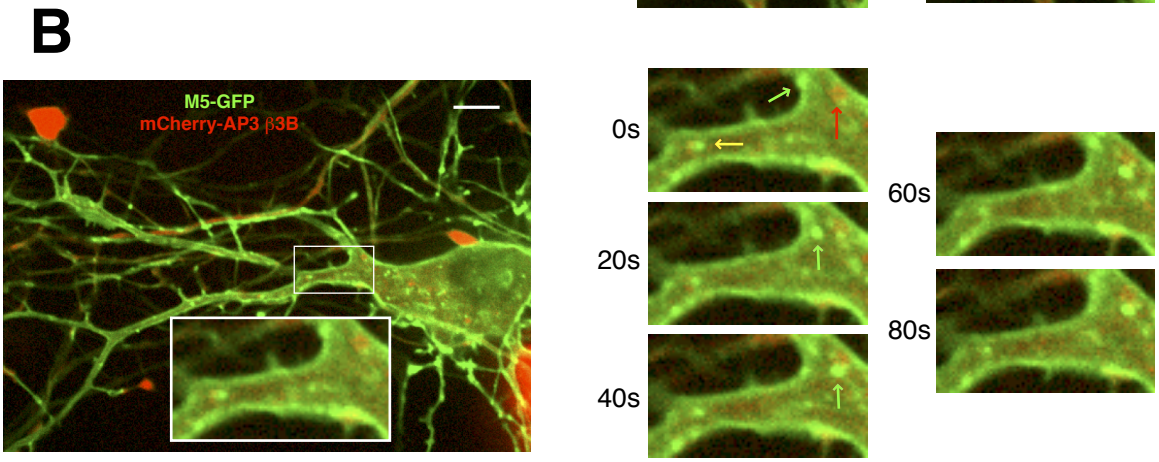
B
M5-GFP
mCherry-AP3 β3B
0s
60s
20s
80s
40s

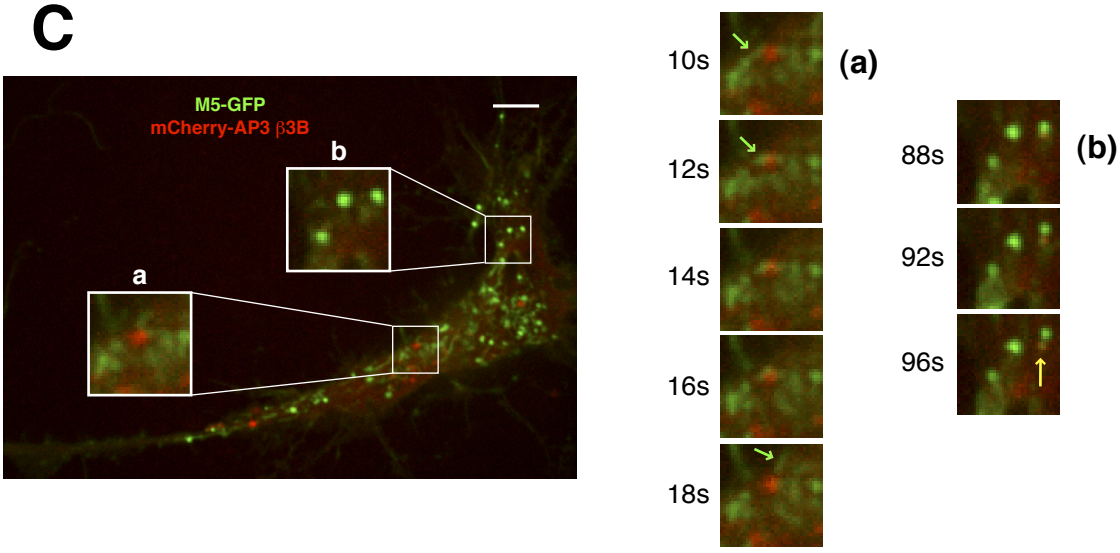
C
M5-GFP
mCherry-AP3 β3B
b
a
10s
(a)
12s
14s
16s
18s
88s
(b)
92s
96s

fission-like events between these vesicles were observed (figure 4.5B,C). In both of these cases, although cytosolic expression was apparent in neuronal projections, AP3β3B puncta were clearly visible only in soma or soma-proximal areas. In addition, the appearance of M5-GFP in dynamic, tubular-like structures after agonist treatment in an imaged cell soma is indicative of their presence in tubular-vesicular recycling endosomes (Stoorvogel et al., 1996; Grant and Donaldson, 2009). Although these results are consistent with the co-localization of M5- and AP-3- positive vesicle populations, we were unable to successfully image simultaneously AGAP1-mCherry and AP-3 (using GFP-AP3β3A and GFP-AP3β3B markers) in single neurons. Additionally, despite previous reports suggesting that the distribution in neurons of the ubiquitous AP-3 isoform was restricted to soma (Seong et al., 2005), we observed in neurons expressing both GFP-AP3β3A and mCherry-AP3β3B somatic, dendritic and axonal localization of these ubiquitous and neuron-specific AP-3 isoform markers, respectively (figure 4.6C).

4.3.6 *Agonist-internalized M5-GFP traffics through characterized endocytic compartments*

We next performed co-immunostainings of primary cultured neurons expressing M5-GFP to investigate the endocytic compartments encountered by agonist-internalized receptor. After 60 minutes of CCh treatment, numerous puncta co-labeled for M5-GFP and transferrin receptor (TfrR) are apparent (figure 4.6A). TfrR is a constitutively recycled receptor with distribution in neurons

restricted to the somatodendritic compartment (West et al., 1997a); thus, internalized M5-GFP is trafficked at least partially through this recycling pathway. We also observed in CCh-treated neurons some instances of co-localization of M5-GFP with the early endosome marker rab5 in dendrite-like compartments, but little overlap between M5-GFP and the late endosome marker rab7 (figure 4.6A). Thus, our data suggested that endocytosed M5 may traffic mainly through the recycling pathway.

4.3.7 AP-3 endosomes are perisynaptically localized in axons

Our previous data demonstrated overlap of M5-GFP and AGAP1 puncta in axon-like neuronal processes, although the AP-3 content of these puncta was not determined (figure 4.4B). The neuron-specific isoform of AP-3 as been shown to function in the biogenesis of synaptic vesicles from endosomes and in the targeting of synaptic vesicle proteins such as the vesicular zinc (ZnT3) and GABA (VGAT) transporters (Faundez et al., 1998; Blumstein et al., 2001; Nakatsu et al., 2004; Salazar et al., 2004b). In addition, the neuronal AP-3

Figure 4.6 Distribution of M5 and endocytic markers in cultured rat hippocampal neurons (following page). (A) Neurons were transfected with M5-GFP plasmid, treated with 1mM carbachol for 30 (Transferrin receptor, TfrR) or 60 (Rab5, Rab7) minutes, fixed, co-immunostained for GFP (green) and with antibodies as indicated (red) and imaged by confocal microscopy. Scale bars, 20μm (top) and 5μm (bottom). **(B)** Neurons were fixed and co-immunostained for Synapsin I (red) and δ -Adaptin (green) and imaged by confocal microscopy. Scale is identical to (A). **(C)** Primary cultured rat hippocampal neurons were co-transfected with mCherry-AP3β3B (red) and GFP-AP3β3A (green) plasmids and imaged by two-color spinning disk confocal microscopy. Scale bar, 10μm.

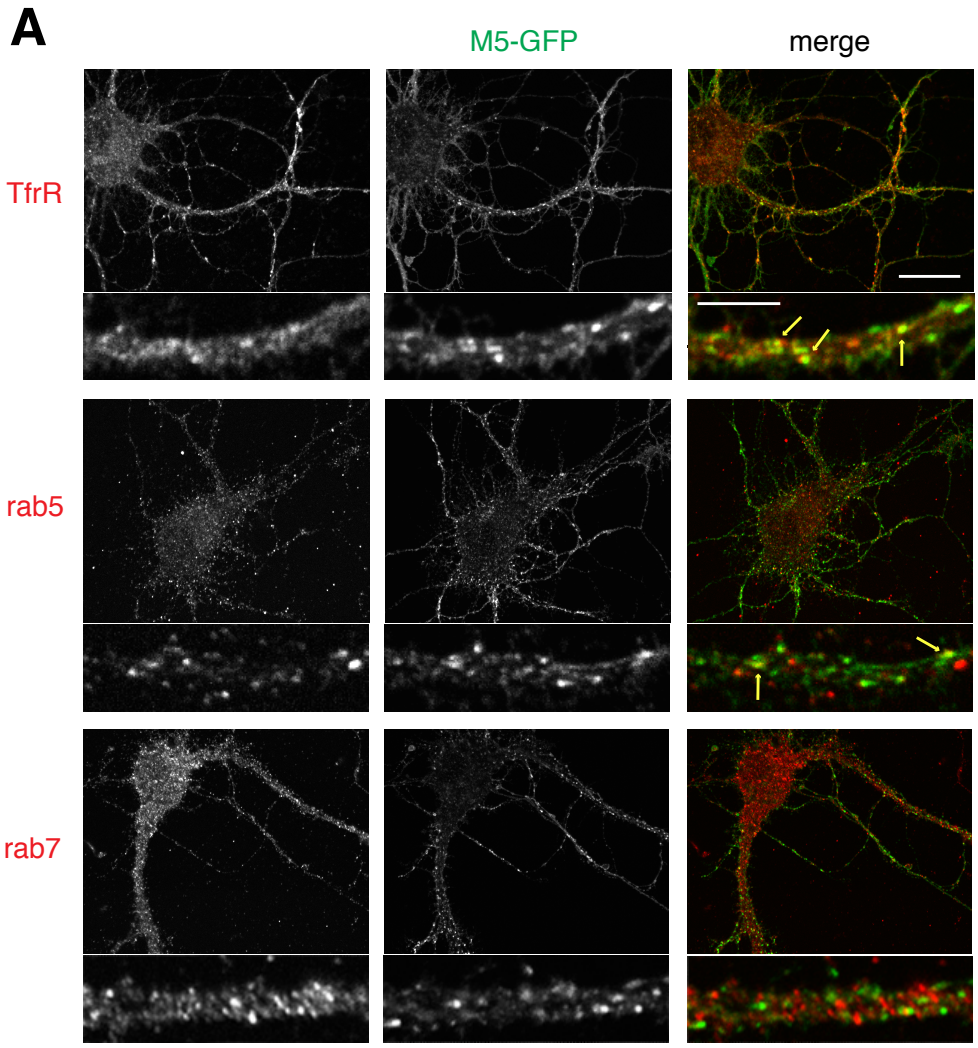
A
M5-GFP
merge
TfrR
rab5
rab7

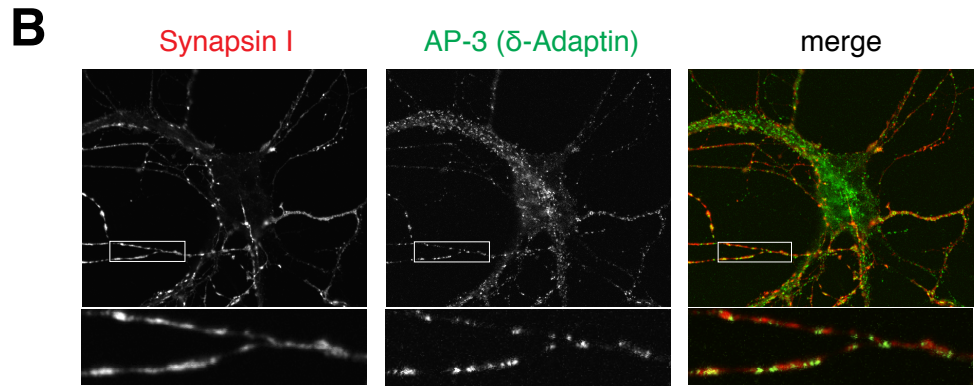
B
Synapsin I
AP-3 (δ-Adaptin)
merge

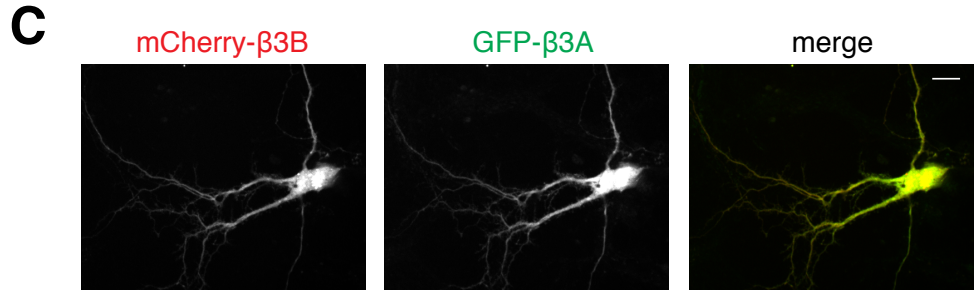
C
mCherry-β3B
GFP-β3A
merge

subunit β3B (β-NAP) was shown to associate with nerve terminal vesicles (Newman et al., 1995). To investigate the distribution of AP-3 endosomes in axons, we performed co-immunostaining of long-term cultures of primary rat hippocampal neurons containing mature synapses. We observed numerous instances of AP-3-positive puncta juxtaposed, but not superimposed, with synapsin I-positive varicosities of thin, aspiny projections, consistent with a perisynaptic distribution of AP-3 endosomes in axons (figure 4.6B). As AP3β3A/B antibodies appropriate for immunostaining were not available, however, we were unable to determine whether the observed AP-3 endosomes were of the ubiquitous or neuron-specific subtype.

4.3.8 *Subcellular fractionation analysis of AGAP1 and AP-3 content of rat brain membranes*

In order to take advantage of the wider array of antibodies available for immunoblotting of native AGAP1 and AP-3 proteins, we performed a biochemical separation of rat brain membranes by iodixanol step gradient centrifugation (Lee et al., 2003). Immunoblot analysis of separated membrane fractions revealed a distribution of AGAP1, the ubiquitous AP-3 isoform marker *μ*3A, and the neuron-specific AP-3 marker β3B roughly similar to that of the early, late and recycling endosome markers Rab5, Rab7, and Rab11 (figure 4.7). The fractional distribution of the TGN-associated, AP-1 adaptor subunit γ-adaptin and the integral plasma membrane protein Na+,K+ ATPase β2 were distinct (figure 4.7). We noted 1) that the pattern of AGAP1 membrane association resembled that of

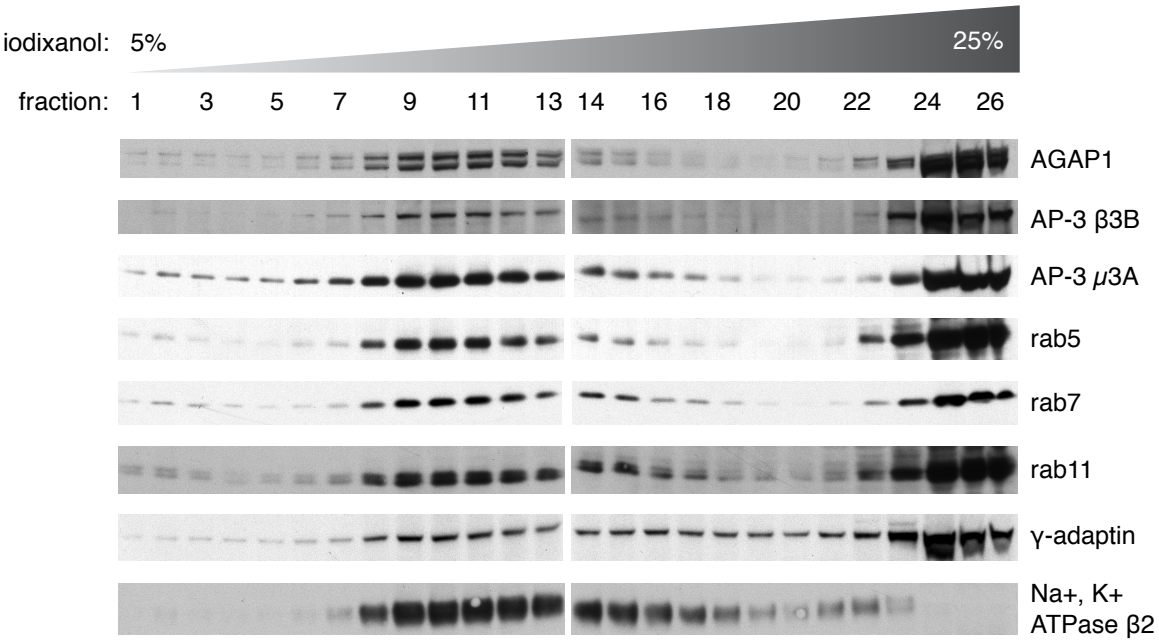

Figure 4.7 Subcellular fractionation analysis of AGAP1 and AP-3 content of rat brain membranes. Total rat brain membranes were separated by iodixanol density gradient centrifugation as described. Membrane fractions were analyzed for protein content by immunoblot as indicated.

AP3β3B most closely, 2) AP3μ3A exhibited a considerable distribution in low-density membrane fractions, and 3) AP-3β3B, rab7 and γ-adaptin shared peak immunoreactivity at fraction 24 (figure 4.7). Thus, the fractionation data confirm that AGAP1 is associated with AP-3 like endosomal membranes, and suggest that neuron-specific AP-3 endosomes may differ physically from that of ubiquitous AP-3 endosomes, perhaps resembling late endosomal or TGN-like compartments.

4.3.9 Agonist-internalized M2-GFP associates with SNX20-positive vesicles

Finally, we investigated the subcellular distribution of muscarinic receptor M2 and its putative interactor SNX20. Expression of SNX20 in COS-7 cells revealed a predominant distribution in vesicle-like structures, with some cytosolic, perinuclear, and nuclear staining variously present, consistent with reports published subsequent to the performance of these experiments (figure 4.8) (Schaff et al., 2008). While M2 receptors C-terminally tagged with GFP exhibited plasma membrane localization in untreated cells, agonist stimulation with CCh induced internalization and redistribution to endosome-like compartments (figure 4.8). Extensive co-localization of M2-GFP- and SNX20- positive vesicles was apparent after 15 and 60 minutes of agonist treatment (figure 4.8). Thus, although our biochemical data was inconclusive with regard to the physical interaction of M2i3 and SNX20, the current results strongly suggest that agonist-induced internalization of M2 leads to trafficking through an SNX20-positive endosomal compartment.

4.4 Discussion

Our data provide qualitative evidence for the co-localization of agonist-internalized M5 muscarinic receptors with AGAP1 in an endosomal compartment. The demonstration of such co-localization was a primary goal of this chapter's experiments, and suggests that AGAP1 and M5 are temporally and spatially juxtaposed in a manner consistent with, or conducive to, their physical interaction. Although we were unable to study the distribution of natively

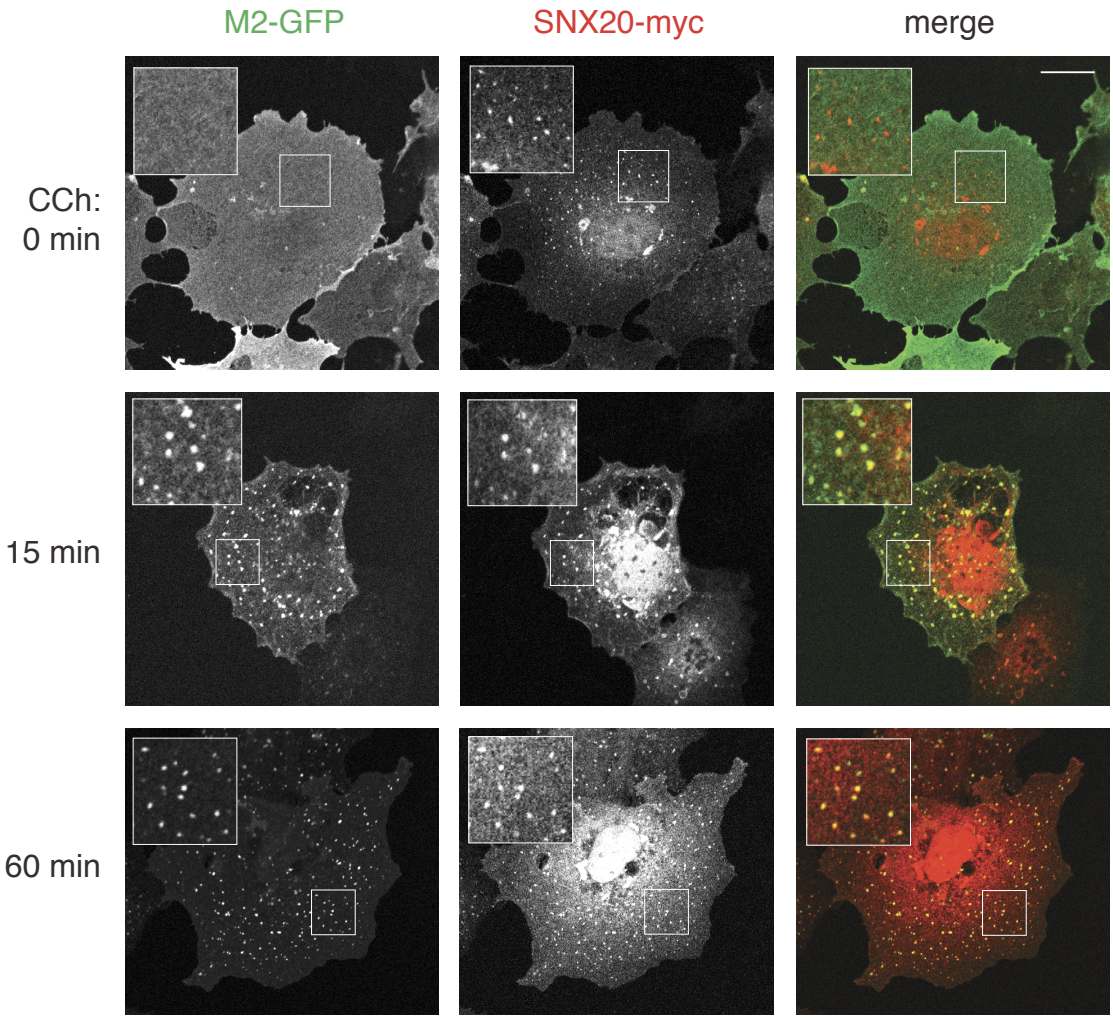

Figure 4.8 Co-localization of agonist-internalized M2 with SNX20 in COS-7 cells. COS-7 cells were transiently co-transfected with M2-GFP and SNX20-myc constructs, treated with 100μM carbachol for 0 (top) 15 (middle) or 60 (bottom) minutes, fixed, immunostained for GFP (green) and myc tag (red) and imaged by confocal microscopy. Scale bar = 20 μm.

expressed M5 receptors, the use of epitope-tagged GPCRs in exogenous expression systems has been widely used to study the constitutive and activity-dependent trafficking of a number of receptors (Cao et al., 1999; Oksche et al., 2000; Hanyaloglu and von Zastrow, 2008). In light of our biochemical data demonstrating a specific, but likely low-affinity interaction between M5 and AGAP1, our observation of a partially-overlapping pool of AGAP1- and agonist-internalized M5- positive vesicles, including apparent instances of fusion, fission, and budding-like events in AGAP1-mCherry and/or M5-GFP vesicles in live neurons, suggests that AGAP1 may play a functional role in the trafficking of M5. Importantly, 1) this vesicular overlap was observed only in neurons, and 2) associative evidence supports the identification of AGAP1 vesicles as AP-3 endosomes. As the function of neuronal AP3B is distinct from that of AP3 in non-neuronal tissues (Newell-Litwa et al., 2007), our results suggest that an AGAP1/ AP-3B complex may mediate the activity-induced trafficking of M5 by binding to recognition sequences in the M5 i3 loop. Interestingly, we also observed apparent interaction of M5-GFP- and mCherry-AP3β3B in unstimulated neurons, perhaps due to the presence of constitutive receptor endocytosis. To our knowledge, interaction-mediated trafficking of a membrane protein by AGAP1 has not been described; however, the AZAP family Arf GAP ACAP1 was shown to direct the endocytic recycling of TfrR and integrin β1 by binding to sorting signals present in their cytoplasmic regions (Dai et al., 2004; Li et al., 2005), and interaction with AP-3 was shown to direct the intracellular localization of the cannabinoid CB1 receptor in neurons (Rozenfeld and Devi, 2008) and is known

to mediate the sorting of lysosome-targeted proteins such as LAMP1 and CD63 (Dell'Angelica et al., 1999; Peden et al., 2004). In addition, we observed in tissue culture cells a clear co-localization of agonist-internalized M2-GFP with SNX20 in vesicle-like structures; in light of the inconclusive SNX20-M2 biochemical data, however, we continued to focus our experimental efforts on the study of the M5-AGAP interaction.

Although M5 co-localization with AGAP1 and AP-3 was apparent in neurons, we were unable to extend these findings to the determination of the functional ramifications of AGAP1 / M5 interaction. Our efforts were compromised by a number of technical limitations inherent to the experimental system we employed. First, AGAP1 overexpression was seen to adversely effect cell morphology and viability in both tissue culture and primary neuronal cells, likely as a result of its effect on the critical secretory pathway regulator Arf1 and by its previously reported actin cytoskeleton-modulating function (Nie et al., 2002; D'Souza-Schorey and Chavrier, 2006). Additionally, we did not observe restriction of the AP-3A complex (visualized with β3A fluorescent fusion proteins) to the soma of cultured neurons, as has been previously described (Seong et al., 2005); overexpression may have played a role in this distribution pattern. Second, visualization of membrane-associated exogenous AGAP1 or AP3β3 in the presence of M5 required either cytosol extraction in fixed cells, or the use of mCherry fusions in live cells. Cytosol extraction left only a minority of neurons morphologically intact, and the mCherry tag provided a low contrast signal, and though reportedly monomeric, was seen to induce immobile aggregates when

fused to the proteins investigated in this study (the vesicular association of both AP3β3A and B were more readily visualized with GFP fusion tags; however, M5-mCherry aggregated to an unacceptable degree). Third, as the localization and trafficking characteristics of native M5 have not been described, it was impossible to determine whether the C-terminal GFP tag interfered with the normal trafficking of the receptor. It should be noted, however, that M5-GFP was clearly plasma-membrane localized and underwent agonist-induced internalization, and that the GFP tag was seen to offer superior performance to that of a number of extracellular and intracellular epitope tagging strategies attempted on M5. Although we attempted to investigate the effect of AGAP1 interaction on localization and/or activity-induced trafficking of M5 through the use of the AGAP1 interaction (Δ369-386) deletion mutant, no gross differences were apparent, and due to the selective nature of neurons imaged, quantitative analysis was not successful. We thus elected to pursue a biochemical approach to the study of AGAP1/AP-3 - dependent M5 function and activity-induced trafficking, as described in the following chapter.

5 REGULATION OF M5 ENDOCYTIC RECYCLING BY AGAP1

5.1 Summary

We studied the effect of AGAP1 interaction loss-of-function on the steady-state and activity-induced trafficking of the M5 muscarinic receptor. In tissue culture cells, the total protein level and cell surface expression of the AGAP1 domain-of-interaction mutant M5Δ was higher than that of wild-type receptor. AGAP1 knockdown decreased surface expression of both M5wt and M5Δ. Both mutant and wild-type M5 receptors underwent agonist-induced internalization and subsequent endocytic recycling to the plasma membrane after washout, the magnitude of which was similar between M5wt and M5Δ. In primary cultured neurons, however, the M5Δ receptor displayed a significant endocytic recycling deficit as compared to wild-type. Knockdown of AGAP1 or the neuron-specific AP-3 subunit β3B reduced the extent of M5wt recycling, as did treatment with the AP-3 inhibitor brefeldin-A. In addition, chronic agonist treatment in cultured neurons significantly increased down-regulation of cell surface M5Δ compared to wild-type. The results demonstrate a novel, neuron-specific function of AGAP1 / AP-3 in the mechanism of M5 receptor endocytic recycling. This function suggests that *in vivo*, AGAP1 interaction is required for sustained M5 signaling in neurons.

5.2 Introduction

Cell-surface receptor density and localization is a key determinant of GPCR signaling sensitivity. As described in chapter 1, trafficking of GPCRs to and from the plasma membrane by functionally and spatially defined classes of subcellular membrane vesicles or endosomes regulates the surface expression of receptors in both a constitutive and activity-dependent manner. The Rab and Arf families of small GTPases regulate the trafficking of transmembrane proteins by recruitment of effector proteins in their GTP-bound “on” state, serving to regulate the formation, motion, fission, fusion, and functional identity of subcellular membrane vesicles (D'Souza-Schorey and Chavrier, 2006; Stenmark, 2009). The heterotetrameric adaptor protein complexes are a class of Arf effectors that mediate transmembrane protein traffic by binding to both signal sequences in cargo proteins and to membrane coat proteins (Nakatsu and Ohno, 2003). In the current report, we have described a physical interaction between the Arf GAP AGAP1 and the i3 intracellular loop of the M5 muscarinic receptor. As AGAP1 binds to the adaptor protein complex AP-3 (Nie et al., 2003) and was observed to interact with M5 as part of an AGAP1-containing complex, we hypothesized that *in vivo*, AGAP1 functions as an adaptor complex scaffold protein by binding to recognition sequences in the M5 i3 loop and targeting the receptor for AP-3-dependent trafficking.

Much of the initial knowledge of AP-3’s cellular function has resulted from study of spontaneously occurring mutants in flies, humans, and mice. The *Drosophila melanogaster* eye color mutant *garnet* exhibits a reduced number of

pigment granules in the eye and other tissues as a result of a near-null mutation in the δ-adaptin coding *Ap3d1* gene (Ooi et al., 1997). Similarly, the mouse coat color mutants *mocha* and *pearl* were found to result from null mutations in the *Ap3d1* and *Ap3b1* (coding for the ubiquitously expressed AP3 β3A subunit) genes, respectively (Kantheti et al., 1998; Feng et al., 1999). Both *pearl* and *mocha* are categorized as platelet storage pool deficiency phenotypes, characterized by hypopigmentation, lysosome abnormalities, and deficient storage ability of platelet dense granules leading to prolonged bleeding (Lane and Deol, 1974; Novak et al., 1984; Kantheti et al., 1998; Feng et al., 1999). In humans, the Hermansky-Pudlak syndrome (HPS) is a collection of related autosomal recessive platelet storage pool deficiency disorders (Wei, 2006). Of the 8 genetically unique forms of HPS yet described, one (HPS-2) is caused by a near-null mutation in the *Ap3b1* gene, while another (HPS-7) is due to a mutation in *DTNBP1*, encoding dysbindin, a member of the AP-3 associated BLOC-1 complex (Dell'Angelica et al., 1999; Li et al., 2003).

The ubiquitously expressed AP-3A isoform functions mainly to traffic membrane proteins to lysosomes and lysosome-like organelles (figure 5.1). In fibroblasts derived from HPS-2 patients (in which function of the ubiquitous AP-3 complex is disrupted), the lysosomal membrane proteins Lamp-1, Lamp-2 and CD63 were seen to mis-localize to the plasma membrane (Dell'Angelica et al., 1999). Similarly, intact AP-3 function in yeast was shown to be required for vacuole localization of membrane proteins containing a lysosome targeting sequence (Vowels and Payne, 1998). An AP-3-dependent trafficking mechanism

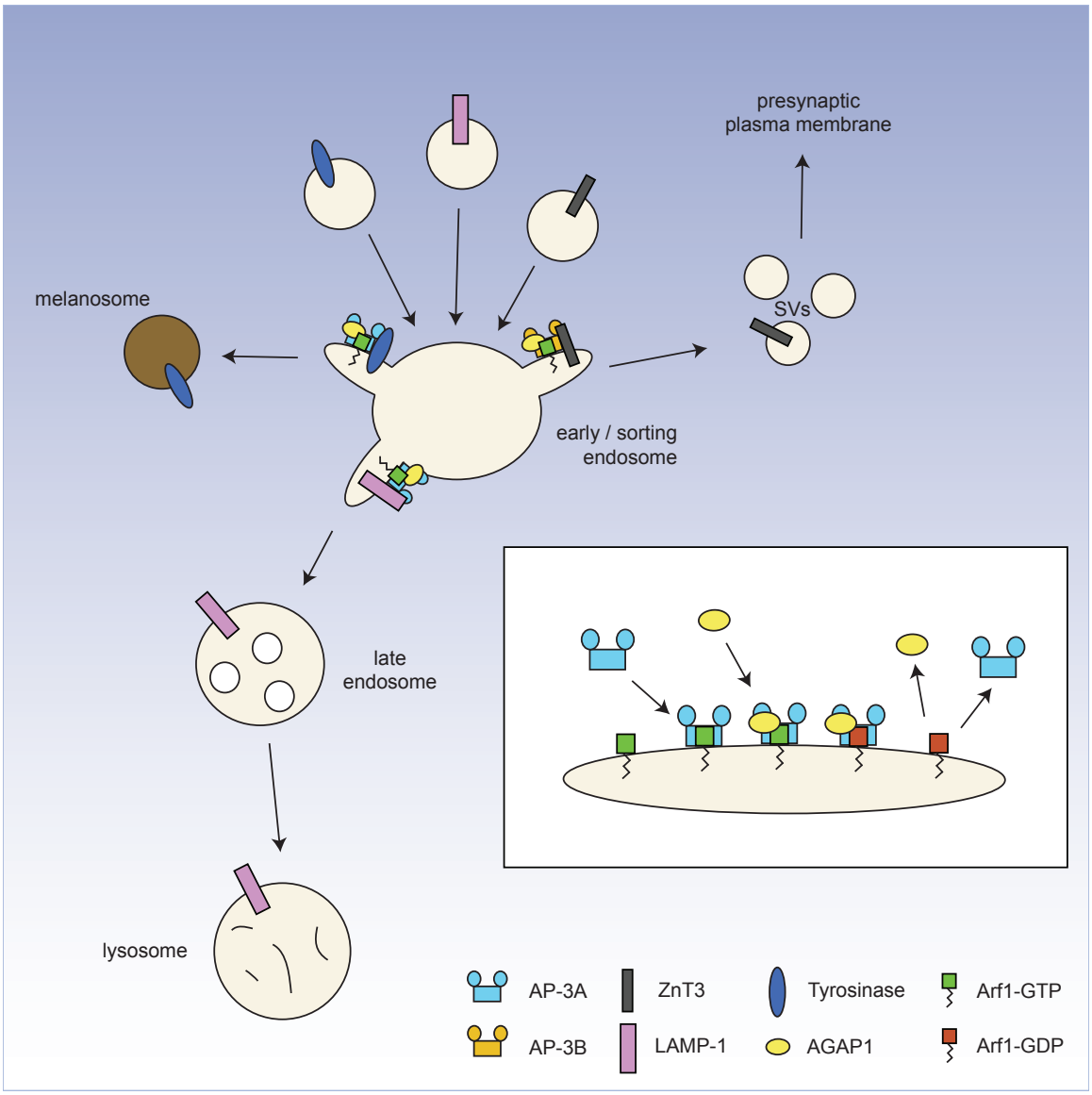

Figure 5.1 AP-3-dependent trafficking pathways. Inset, GTP-bound Arf1 recruits AP-3 to membranes. Subsequent binding of AGAP1 catalyzes hydrolysis of GTP to GDP, resulting in dissociation of AP-3 (and AGAP1) and release of integral membrane cargo proteins. Top, endocytosed membrane proteins are delivered to early / sorting endosomes and are trafficked to specific cellular compartments by recognition of sorting motifs by AP-3. The ubiquitously expressed AP-3A isoform targets membrane proteins such as Tyrosinase or LAMP-1 to melanosomes or the lysosome limiting membrane, respectively. The neuron-specific isoform AP-3B is responsible for both biogenesis of endosomally-derived synaptic vesicles (SVs) and for delivery of proteins such as ZnT3 to these SVs.

has also been demonstrated for cannabinoid CB1 receptor localization to late endosome-like compartments (Rozenfeld and Devi, 2008), delivery of Notch to the limiting (outer) lysosomal membrane in *Drosophila* (Wilkin et al., 2008), and the targeting of tyrosinase to melanosomes (Huizing et al., 2001). AP-3-dependent targeting to lysosomes or lysosome-like organelles is mediated by recognition of dileucine-like or tyrosine-based sorting signals present on cytoplasmic regions of cargo proteins (Ohno et al., 1998; Vowels and Payne, 1998; Bonifacino and Traub, 2003; Janvier et al., 2003). An immuno-EM study identified AP-3 localized to membrane buds emanating from early endosome-associated, recycling compartment-like tubular structures; no AP-3 immunoreactivity was detected in the TGN, however (Peden et al., 2004). The lysosomal membrane protein Lamp-1, apparently in transit from the plasma membrane, was seen to co-localize with AP-3 at these budding structures (Peden et al., 2004). Additionally, although some AP-3 trafficking events appear to proceed via non-clathrin coated vesicles, AP-3 is able to bind clathrin *in vitro* and is seen to partially co-localize to clathrin-positive vesicular structures (Dell'Angelica et al., 1998; Vowels and Payne, 1998; Peden et al., 2004). Thus, the current model of AP-3-dependent sorting suggests that targeted proteins first undergo delivery to the plasma membrane, followed by endocytosis and trafficking from the early endosome to a recycling endosome-like structure, after which target proteins are sorted to and sequestered in distinct clathrin or non-clathrin coated vesicles by AP-3 (in concert with the associated trafficking

complex BLOC-1), followed finally by delivery to lysosomal or lysosome-like organelle membranes.

The neuron-specific AP-3B isoform, consisting of the ubiquitously expressed δ and σ3 subunits and neuron-specific μ3B and β3B, is functionally distinct from the ubiquitous AP-3A complex (figure 5.1). *In vitro* studies demonstrated that AP-3B, but not AP-3A, is able to mediate the formation of synaptic vesicles from endosomes (Faundez et al., 1998; Blumstein et al., 2001). In *Ap3b2*$^{-/-}$, *Ap3m2*$^{-/-}$ or *Ap3d1*$^{-/-}$ (*mocha)* mutant mice, the zinc transporter ZnT3 and the vesicular GABA transporter VGAT are absent from a subpopulation of synaptic vesicles, resulting in impaired GABA release and reduced zinc content in the hippocampus and cortex (Kantheti et al., 1998; Nakatsu et al., 2004; Salazar et al., 2004b). In addition, the chloride channel ClC-3, the vesicular glutamate channel Vglut1, TI-VAMP and phosphatidylinositol-4-kinase type IIα were seen to be absent from a subpopulation of synaptic vesicles in cells derived from *mocha* mice or after disruption of AP-3 targeting with by the Arf GEF inhibitor brefeldin-A (Martinez-Arca et al., 2003; Salazar et al., 2004a; Salazar et al., 2005a; Salazar et al., 2005b; Scheuber et al., 2006). *Ap3b2*$^{-/-}$, *Ap3m2*$^{-/-}$ and *mocha* mice are hyperactive and epileptic (Newell-Litwa et al., 2007). *Mocha* mice display deficient spontaneous and evoked glutamate release in hippocampal synapses (Scheuber et al., 2006) and decreased synaptic vesicle recycling rates under high-frequency stimulation conditions (Voglmaier et al., 2006); in addition, GABAergic neurotransmission was seen to be disrupted in *Ap3m2*$^{-/-}$ mice (Nakatsu et al., 2004). It should be noted, however, that the

phenotypic penetrance of the *Ap3b2*$^{-/-}$ and *Ap3m2*$^{-/-}$ mutations does not reach that of *mocha* (*Ap3d1*$^{-/-}$), suggesting a neuron-specific functional role for the ubiquitous AP-3A complex (Newell-Litwa et al., 2007). Additionally, the assembly of neuron-specific and ubiquitous β3 and μ3 subunits into AP-3A and AP-3B heterotetramers may not be exclusive (Peden et al., 2002).

AP-3 is targeted to membranes via recruitment by GTP-bound Arf1 (Lefrancois et al., 2004). The proper function of AP-3 in the transport of cargo proteins requires its coating and uncoating of membrane vesicles in a regulated manner. The Arf1 GAP AGAP1 plays a key role in this process, as release of the AP-3 coat requires hydrolysis of GTP to GDP by Arf1, and the intrinsically low GTPase activity of Arf1 necessitates stimulation by GAPs (Nie et al., 2002; Nie and Randazzo, 2006). AGAP1 binds directly to the AP-3 complex via its PH domain, spatially coordinating Arf1 GAP activity with the AP-3 coat (Nie et al., 2003). Up- or down- regulation of AGAP1 levels interferes with the targeting of AP-3 to vesicles and with the trafficking of the lysosomal cargo protein Lamp-1 (Nie et al., 2003). In addition, the PH domain of AGAP1 confers upon it membrane lipid-binding activity and phospholipid-dependent GAP activity, and AGAP1 / AP-3 binding was seen to be specific with regard to related adaptor protein complexes (Nie et al., 2002; Nie et al., 2005). Although AGAP1 thus plays an indirect role in the AP-3-dependent trafficking of target proteins, an intrinsic cargo recognition or AP-3-independent trafficking function of AGAP1 has not been described. However, the related AZAP protein ACAP1 was demonstrated to bind to recognition sequences in the cytoplasmic tails of the

transferrin receptor and integrin β1, and to be required for their endocytic recycling to the plasma membrane (Dai et al., 2004; Li et al., 2005). In addition, the AGAP1-related protein centaurin α1 was shown to inhibit the agonist-induced internalization of the β2 adrenergic receptor (Lawrence et al., 2005).

Although the steady state and activity-induced trafficking characteristics of muscarinic receptors 1 through 4 have been described, the trafficking pattern of the M5 receptor is unknown. In this chapter, we describe experiments investigating the basal and agonist-induced trafficking of M5 in exogenous cellular expression systems. We employed both the AGAP1 region-of-interaction deletion mutant M5(Δ369-386) (M5Δ) and RNAi-mediated knockdown of endogenous AGAP1 to study the effects of AGAP1 interaction loss-of-function on the trafficking of M5. Knockdown of ubiquitous and brain-specific AP-3 subunits was used to investigate the hypothesized involvement of this trafficking pathway on M5 regulation. We took advantage of the availability of a hydrophilic, cell-impermeant muscarinic antagonist radioligand [3H]-N-methyl-scopolamine to quantitatively monitor cell surface M5 receptor density in intact, living cells (Toews, 2000). This approach allowed for the measurement of M5 surface density under basal conditions, and allowed us to indirectly monitor the rate of internalization and endocytic recycling of M5 receptors after agonist stimulation.

5.3 Results

5.3.1 *Transfected M5(Δ369-386) is expressed at higher levels than M5wt in tissue culture cells*

We first examined the effect of the AGAP1 domain-of-interaction (DOI) i3 loop deletion on the expression of M5 in mammalian tissue culture cells. HEK-293T or CHO cells were transiently transfected with equal quantities of M5wt-GFP and M5Δ-GFP coding plasmids, and then assayed for total M5 protein content by GFP immunoblot 48 hours later. We observed, on average, a nearly 2.5-fold greater amount of M5Δ-GFP than M5wt-GFP protein present in cell lysates, a pattern also present with M5 receptors extracellularly-tagged with the HA epitope, and in cell lines stably expressing wild-type and Δ369-386 M5 (figure 5.2A; data not shown). Next, to determine whether the mutant M5 receptor also exhibited an increased abundance at the cell surface compared to wild-type, we performed radioligand binding experiments on intact, transiently transfected HEK-293T cells using the cell-impermeant tritiated muscarinic antagonist [3H]-N-methyl-scopolamine ([3H]NMS) to quantitatively label extracellular M5 ligand binding sites (we previously detected negligible specific [3H]NMS binding to the cell lines used in these experiments). We observed a significantly higher surface expression of the non-GFP-tagged AGAP1 DOI mutant M5Δ compared to M5wt (figure 5.2B).

The increased total and surface levels of deletion-mutant receptor protein suggested that AGAP1 interaction may function to decrease expression of M5 in our system. To test this, we performed siRNA-mediated knockdown concurrent

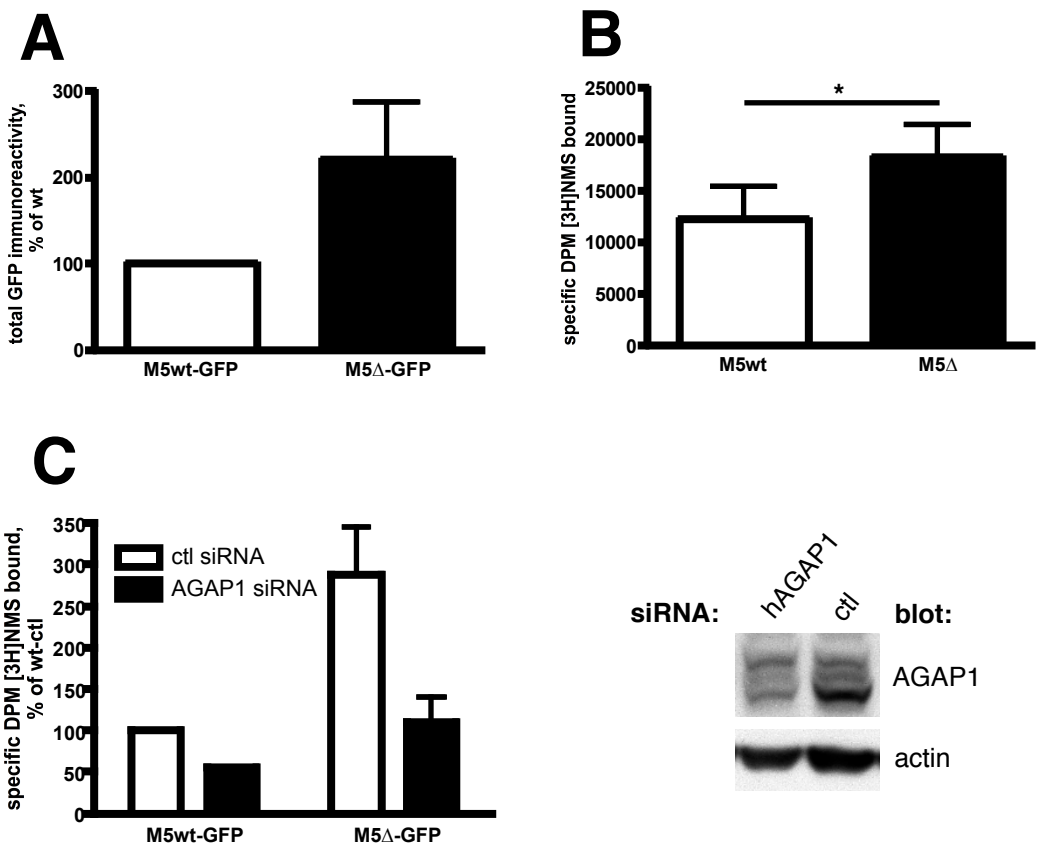

Figure 5.2 Expression of wild-type and Δ369-386 M5 receptors in HEK-293T cells. **(A)** HEK-293T cells were transiently transfected with GFP-tagged wild-type or domain-of-interaction deletion mutant constructs, and lysates were analyzed by quantitative immunoblot for GFP with data normalized to M5wt-GFP. **(B)** HEK-293T cells were transiently transfected with M5wt or M5Δ constructs, and cell surface muscarinic receptor density was assayed by [3H]NMS radioligand binding. **(C)** HEK-293T cells were transiently transfected with siRNA targeting AGAP1 or with non-targeting control, and 24 hours later transfected with M5wt-GFP or M5Δ-GFP constructs. Left, surface receptors density was assayed as in (B). Right, representative immunoblot displaying AGAP1 knockdown. Lower panels, Actin loading controls. (*): $P < 0.05$, paired two-tailed Student's ratio T-test.

to exogenous expression of M5wt- or M5Δ- GFP, and assayed for surface MR sites by [3H]NMS binding in HEK-239T cells. We predicted that, due to the inability of the DOI mutant receptor to physically interact with AGAP1, knockdown of AGAP1 would increase surface expression of M5wt but not effect M5Δ levels. As with rat brain tissue, the AGAP1 antibody detected a multiplet band by immunoblot in lysate from the human HEK-293T cell line; siRNA targeting hAGAP1 was able to knock down AGAP1 expression with moderate efficacy compared to transfection of a non-targeting siRNA duplex (figure 5.2C). However, AGAP1 knockdown decreased cell-surface binding of [3H]NMS in both M5wt-GFP and M5Δ-GFP transfected cells (figure 5.2C). We also observed a decrease in M5wt-, M5Δ, and M3-GFP total protein levels after AGAP1 knockdown (data not shown). This result argued against an AGAP1-related mechanism for the increased expression of M5Δ compared to wild-type receptor in this system.

5.3.2 *M5wt and M5Δ exhibit similar patterns of activity-induced trafficking in HEK-293T cells*

We asked whether deletion of the AGAP1 ROI in M5 could affect activity-induced trafficking of the receptor. We expressed wild-type and Δ369-386 M5 receptors exogenously in HEK-293T or CHO cells, treated cells with the cholinergic agonist carbachol (CCh) for various times in the presence of the translation inhibitor cycloheximide (to eliminate interference from the appearance of newly-synthesized M5 protein) and assayed intact cells for surface M5

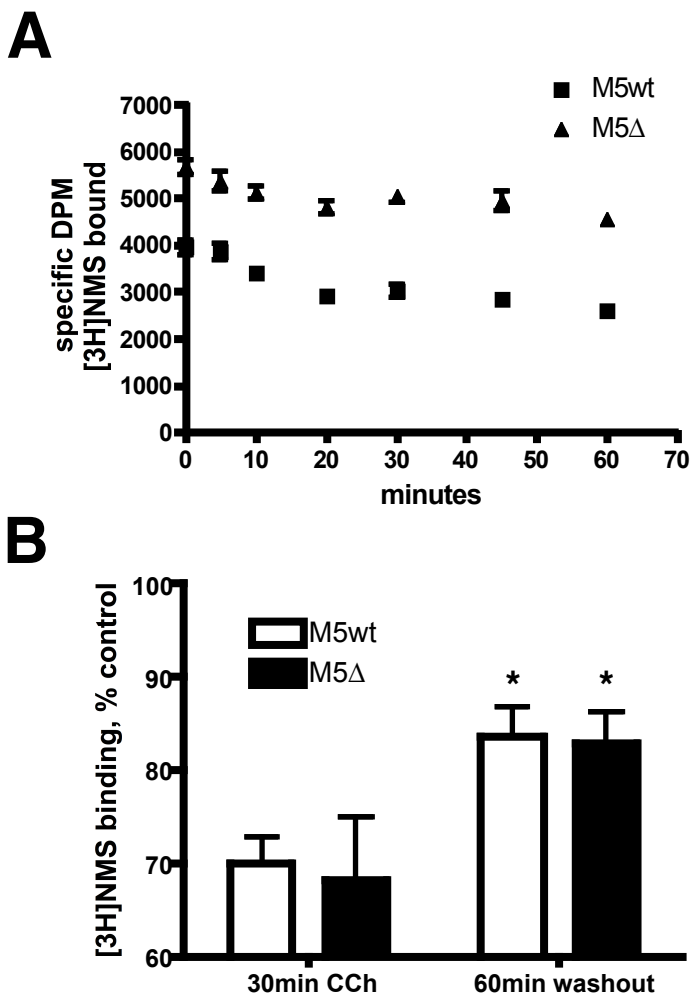

Figure 5.3 Activity-induced trafficking of M5 receptors in HEK-293T cells. HEK-293T cells were transiently transfected with M5wt or M5Δ contructs, and cell surface M5 receptors were assayed by [3H]NMS radioligand binding as described. **(A)** Time course of M5 receptor internalization after treatment with 0.1mM carbachol (CCh) for indicated periods. **(B)** Receptor recycling assay. M5-expressing cells were left untreated, or treated with 0.1mM CCh for 30 minutes with or without a subsequent 60 minute washout period. Cell surface M5 receptors were assayed as in (A), with data expressed as a percent of untreated control values. (*): $P < 0.05$, two-way ANOVA (treatment).

receptor binding sites by [3H]NMS radioligand binding. In these experiments, we observed a time-dependent reduction of cell-surface [3H]NMS binding after CCh incubation for both M5wt and M5Δ, confirming the agonist-induced internalization of these receptors (figure 5.4A). However, the temporal characteristics and magnitude of CCh-induced internalization did not differ between M5wt and M5Δ (figure 5.3A,B). Next, we examined endocytic recycling of agonist-internalized M5 expressed in HEK-293T cells using an experimental system similar to the one described above. Cycloheximide-pretreated cells were left untreated, treated with 100μM CCh for 30 minutes to induce M5 internalization, or CCh-treated followed by a 1-hour washout period to allow for endocytic recycling of internalized receptors. An increase of cell surface [3H]NMS binding sites after washout was taken as a quantitative measure of M5 recycling. Wild-type and deletion-mutant M5 receptors did not differ in the degree to which they were recycled to the cell surface after agonist-induced internalization (figure 5.3B). We therefore concluded that the AGAP1 ROI deletion, and presumably interaction with AGAP1, did not play a role in the activity-dependent trafficking of M5 in HEK-293T and CHO cells.

5.3.3 *Development of a primary cultured neuron system for the study of exogenous M5 receptor trafficking*

Our previous data suggested that the function of M5/AGAP1 interaction may be neuron-specific, as we observed activity-induced co-localization of M5-GFP-positive and AGAP1-positive vesicles in neurons only, and since the M5 i3

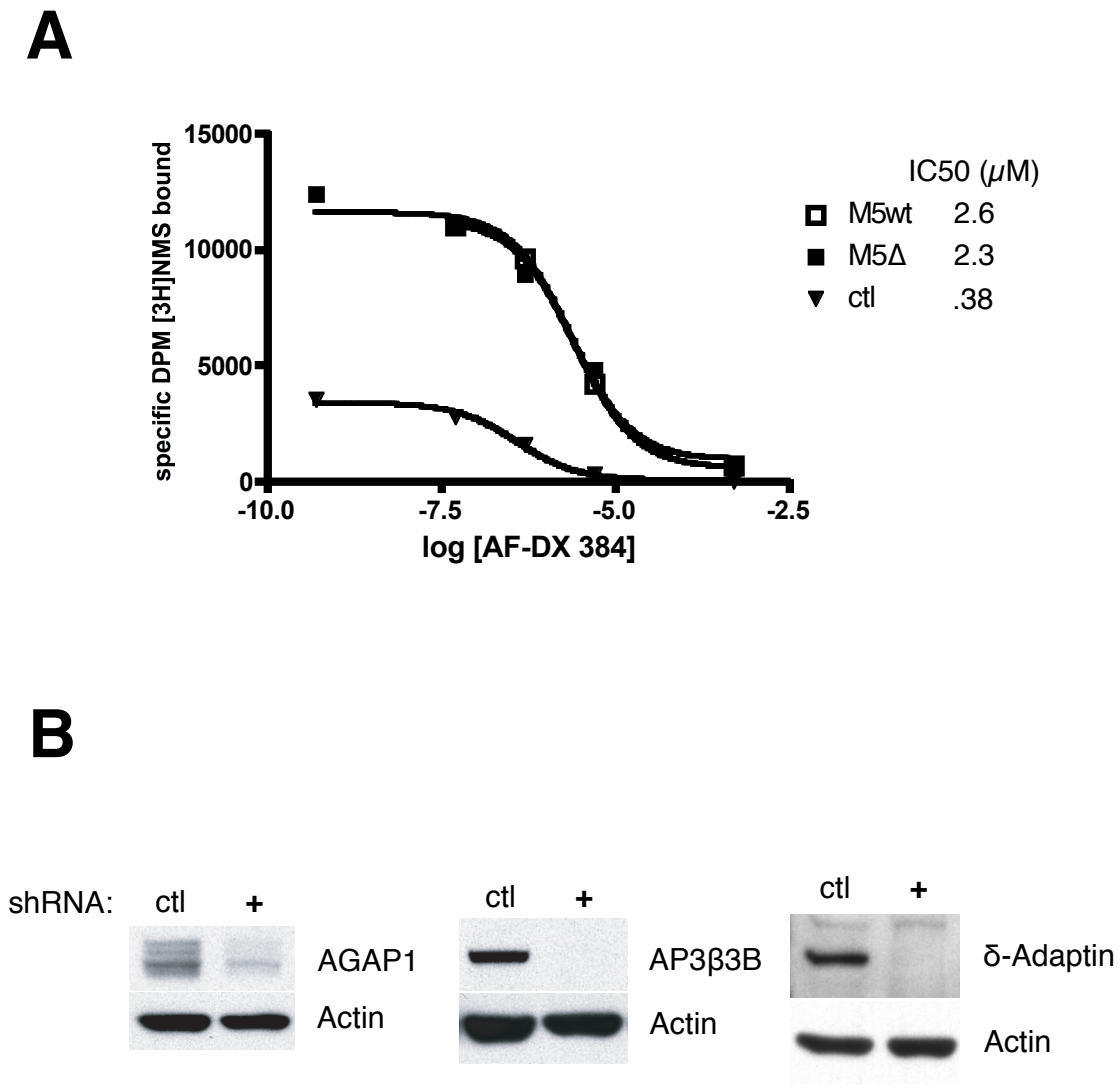

Figure 5.4 Primary cultured neuron radioligand binding assay development. **(A)** Rat embryonic cortico-hippocampal neurons were nucleofected with M5wt, M5Δ, or empty vector control plasmids (ctl) and cultured for 12 days. Radioligand binding was performed in the presence of various concentrations of AF-DX 384, and IC_{50} values for displacement of [3H]NMS binding were calculated by non-linear curve fitting to a one-site competition binding model (GraphPad Prism). **(B)** Representative immunoblots of AGAP1, AP3β3B and δ -Adaptin knockdown by target-specific shRNA constructs in nucleofected primary neuron cultures. Lower panels, Actin loading controls.

loop physically interacted with the neuron-specific AP3B complex, whose role in membrane protein trafficking is distinct from that of the ubiquitously expressed AP-3A complex (Danglot and Galli, 2007). We wished to study the trafficking of exogenously expressed M5 receptors in cultured neurons, as endogenous M5 sites are both low in abundance and pharmacologically indistinguishable from non-M5 MRs with currently available tools (Wess et al., 2007). We were able to achieve exogenous expression of wild-type and mutant M5 receptors in primary cultured cortico-hippocampal cultures using the nucleofection technique to introduce expression plasmids (Gartner et al., 2006). However, the detection of exogenous M5 by [3H]NMS radioligand binding was complicated by the presence of a considerable amount of endogenous muscarinic receptor binding sites; based on radioligand binding studies of MR knockout mouse cortex and hippocampus, these receptors are predominantly M1/M2 subtypes, with little to no endogenous M5 present (Oki et al., 2005). With the aim of improving the M5-to-non-M5 "signal-to-noise" ratio of our cell surface radioligand binding assay, we identified an antagonist, AF-DX 384, displaying 10-fold less binding affinity for the M5 receptor than endogenous, non-M5 sites present in nucleofected primary neurons, in accordance with previous pharmacological reports (figure 5.4A) (Dorje et al., 1991). Importantly, the binding affinity (measured by the concentration-dependent ability to displace [3H]NMS binding) of AF-DX 384 for M5wt and M5Δ was identical (figure 5.4A). Therefore, by preferentially displacing [3H]NMS binding to non-M5 sites, the inclusion of an appropriate concentration (5 μM) of AF-DX in the radioligand binding assay allowed for an M5-to-non-M5

signal sufficient to allow quantitative analysis of cell surface M5 site densities (figure 5.4A).

Next, we investigated the feasibility of performing RNAi-mediated knockdown experiments in primary cultured neurons. Though nucleofection of primary hippocampal neurons can, under ideal conditions, yield up to 70% of cells positive for transgene expression (Gartner et al., 2006), near-pure populations of nucleofected cells are most appropriate for gene knockdown experiments to be analyzed biochemically. Immunosorbent strategies for the enrichment of nucleofection-positive cells from a mixed population have been described (Tahvanainen et al., 2006). We observed previously that puromycin selection of primary neurons nucleofected with a plasmid encoding the puromycin resistance gene was able to effectively enrich for a transgene-expressing population of neurons (data not shown). We designed a series of puromycin-selectable short hairpin RNA (shRNA)-encoding plasmids targeting rat AGAP1, AP3β3B, and δ-adaptin sequences and tested them for knockdown efficiency in mature (12-14 DIV) rat cortico-hippocampal cultures after nucleofection and puromycin selection. With at least one shRNA per gene, we were able to effectively knock down endogenous protein levels, with nearly 100% efficiency observed for AP3β3B and δ-adaptin compared to a non-targeting control shRNA (figure 5.4B).

5.3.4 *Increased expression of M5Δ in primary neurons is not mediated by AGAP1 or AP-3*

Using the M5-specific radioligand assay and shRNA knockdown method described in the preceding section, we first investigated the effect of AGAP1/ AP-3 disruption on the steady-state surface expression of M5. As in tissue culture cells, nucleofection of equal quantities of M5wt- or M5Δ- coding expression plasmids resulted in a near two-fold greater surface expression of the AGAP1 DOI mutant as measured by cell-surface [3H]NMS radioligand binding (2-way ANOVA $p<.01$) (figure 5.5A,B,C). However, knockdown of either AGAP1 or the neuron-specific AP-3B subunit β3B had no effect on the surface expression of either the wild-type or deletion mutant receptor (figure 5.5A,B). Knockdown of ubiquitously expressed δ-adaptin, a component of both the AP-3A and AP-3B complexes, was seen to decrease M5 surface expression; however, M5wt and M5Δ receptors were affected to a similar extent (figure 5.5C). Thus, our data did not support a role for AGAP1 / AP-3 interaction in the steady-state surface expression of M5 in cultured neurons.

5.3.5 *M5wt, but not M5Δ, undergoes efficient endocytic recycling in cultured neurons*

We next investigated whether disruption of the AGAP1 binding site on the M5 i3 loop affected the activity-induced trafficking of the receptor in neurons. M5wt and Δ receptors were expressed exogenously in primary cortico-hippocampal neurons, subjected to agonist-induced internalization, recycling, or

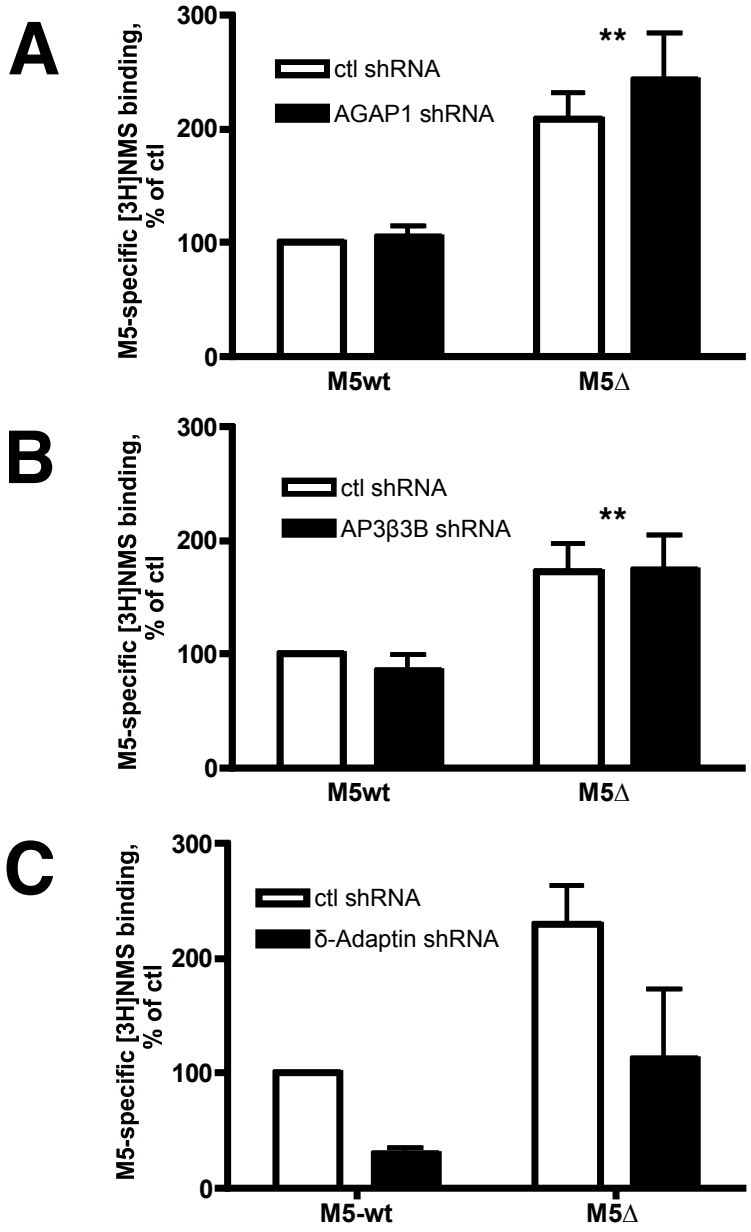

Figure 5.5 AGAP1- and AP-3-dependent surface expression of wild-type and Δ 369-386 M5 receptors in primary cultured neurons. Rat embryonic cortico-hippocampal neurons were co-nucleofected with M5wt, M5Δ, or empty vector control plasmids and targeting or non-targeting control shRNA plasmids and cultured for 13 days. Cell surface muscarinic receptors were assayed by [3H]NMS radioligand binding and M5-specific signal was calculated as described. Knockdown of AGAP1, AP3β3B and δ-Adaptin proteins was verified by immunoblot. (**): $P < 0.01$, two-way ANOVA (receptor).

control conditions as described in section 5.3.2, and assayed for surface [3H]NMS sites as described above. We observed that the M5Δ receptor was deficient in its ability to recycle to the cell surface after a 60 minute washout of agonist treatment as compared to M5wt (figure 5.6A). To control for the possibility that this recycling deficiency was related to the overall higher level of M5Δ present, we repeated the experiment under slightly altered nucleofection / culture conditions, in which we observed no difference in the steady-state surface expression of M5wt and M5Δ (figure 5.6B, inset). Although overall M5 endocytic recycling levels were slightly lower, the M5Δ recycling deficiency phenotype was maintained (figure 5.6B).

5.3.6 *Knockdown of AGAP1 or AP3β2 in neurons inhibits endocytic recycling of wild-type M5 receptors*

To confirm that the observed deficit in the ability of M5Δ to undergo endocytic recycling after activity-induced internalization was due to an AGAP1-dependent mechanism, we repeated the experiment described in section 5.3.5 after shRNA-mediated knockdown of endogenous AGAP1 protein (figure 5.4B). Although AGAP1 protein was not completely eliminated, we observed a significant decrease in the extent of recycling of M5wt in primary cultured neurons co-nucleofected with AGAP1 shRNA plasmid (figure 5.7A). Importantly, there was no significant difference in the degree to which the M5Δ receptor recycled after AGAP1 knockdown, as would be predicted for the interaction loss-of-function mutant with a mechanism of trafficking requiring recognition of i3 loop

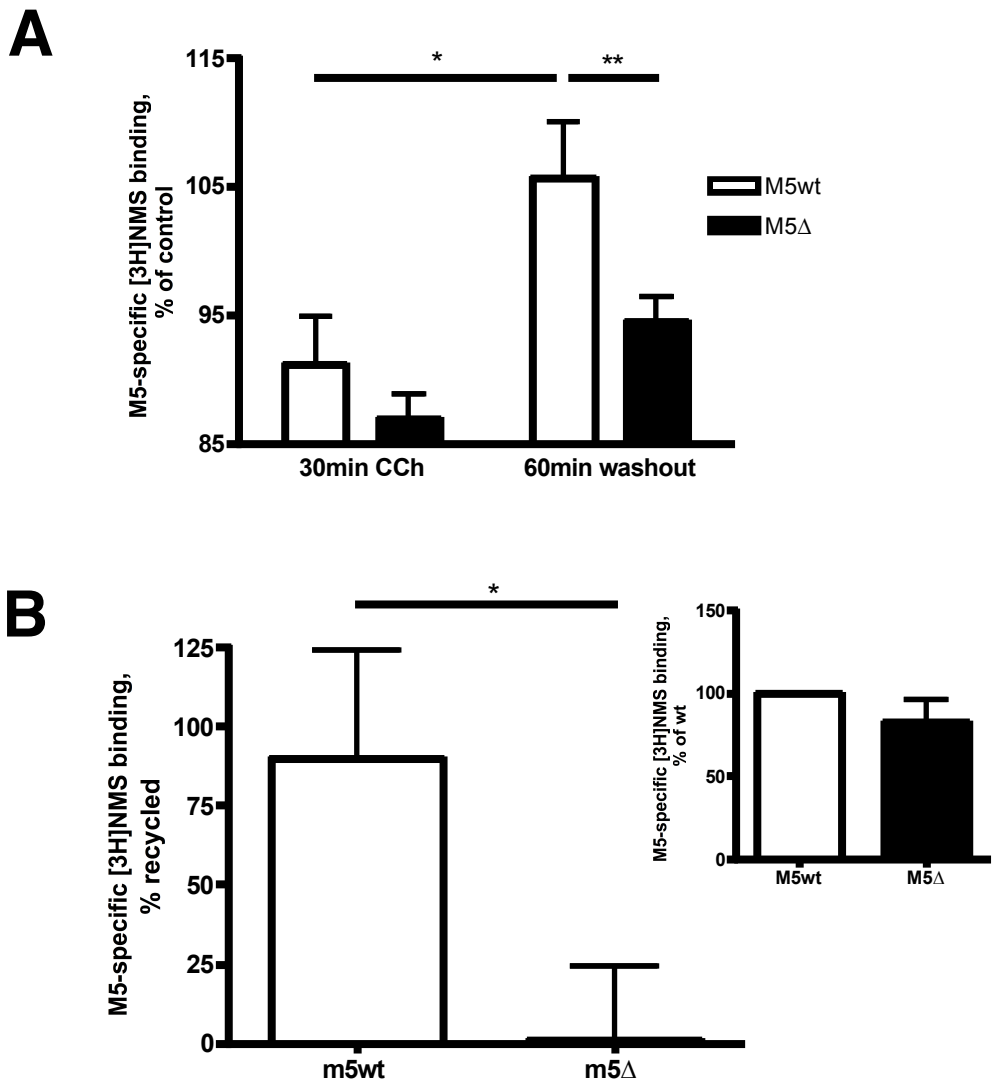

Figure 5.6 Deficient endocytic recycling of M5Δ receptors expressed in cultured neurons. (A) Rat embryonic cortico-hippocampal neurons were nucleofected with M5wt, M5Δ, or empty vector control plasmids and cultured for 13 days. Cells were left untreated, or treated with 0.1mM CCh for 30 minutes with or without a subsequent 60 minute washout period. Cell surface muscarinic receptors were assayed by [3H]NMS radioligand binding and M5-specific signal was calculated as described. Data are expressed as a percent of untreated control values. (*/**): $P< 0.05$/ $P< 0.01$, Bonferroni post-test / two-way ANOVA. **(B)** Experiment in (A) performed with equalized M5wt and M5Δ steady-state surface receptor levels (inset). Data are expressed as a percent of CCh-internalized receptors recycled after 1 hour washout. (*): $P< 0.05$, paired two-tailed Student's T-test.

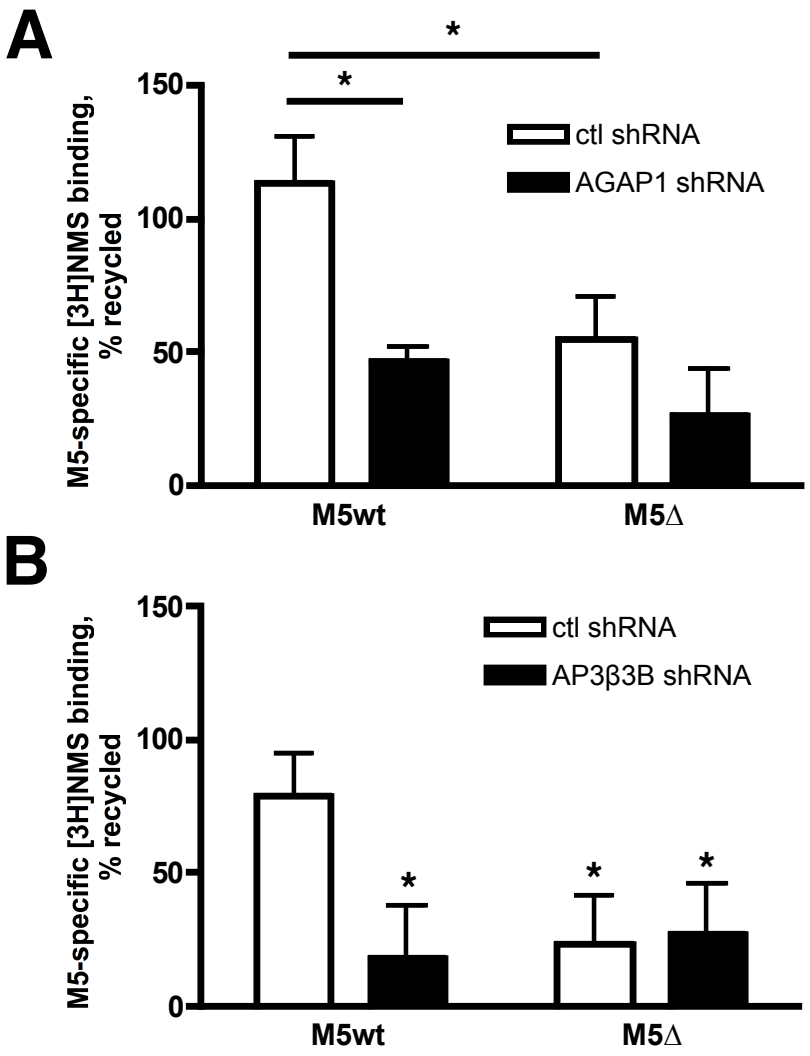

Figure 5.7 Knockdown of AGAP1 or AP3β3B inhibits endocytic recycling of M5 receptors in cultured neurons. Rat embryonic cortico-hippocampal neurons were co-nucleofected with M5wt, M5Δ, or empty vector control plasmids and targeting or non-targeting control shRNA plasmids and cultured for 13 days. Cells were left untreated, or treated with 0.1mM CCh for 30 minutes with or without a subsequent 60 minute washout period. Cell surface muscarinic receptors were assayed by [3H]NMS radioligand binding and M5-specific signal was calculated as described. Knockdown of AGAP1 and AP3β3B proteins was verified by immunoblot. Data are expressed as a percent of CCh-internalized receptors recycled after 1 hour washout. (A)(*): $P < 0.05$, Bonferroni post-test / two-way ANOVA. (B)(*): $P < 0.05$, one-sample T-test (versus 100).

sorting signals by AGAP1 (figure 5.7A).

To test whether the endocytic recycling of M5wt was AP-3-dependent, we performed the same experiment after knockdown of the neuron-specific AP-3B subunit β3B. Similar to the AGAP1 results, AP3β3B knockdown reduced recycling of agonist-internalized M5wt, but did not effect M5Δ (figure 5.7B). Although the reduction in receptor recycling values did not reach significance by two-way ANOVA, AP3β3B knockdown significantly reduced M5wt, but not M5Δ recycling as measured by the Student's T-test ($p<.05$) and only M5wt co-nucleofected with non-coding shRNA did not differ significantly from a hypothesized recycling rate of 100% (one-sample T-test, $p<.05$). Thus, we concluded that efficient endocytic recycling of M5 in neurons requires interaction with AGAP1 and AP-3B, likely as part of a single trafficking complex.

5.3.7 *Inhibition of AP-3 activity reduces endocytic recycling of M5 in an AGAP1 ROI-dependent manner*

The fungal metabolite brefeldin-A (BFA) is an Arf1 GDP exchange factor (GEF) that has been used previously to chemically inhibit the assembly, membrane targeting and/or function of the AP-3 complex (Donaldson et al., 1992; Ooi et al., 1998; Salazar et al., 2004b). To further test whether the mechanism of M5 endocytic recycling is AP-3- dependent, we performed the M5 internalization / recycling assay in primary cortico-hippocampal neuron cultures nucleofected with wild-type or deletion-mutant M5 receptors after a 2 hour pre-incubation with BFA or vehicle. BFA treatment was able to eliminate M5wt recycling, but had no effect

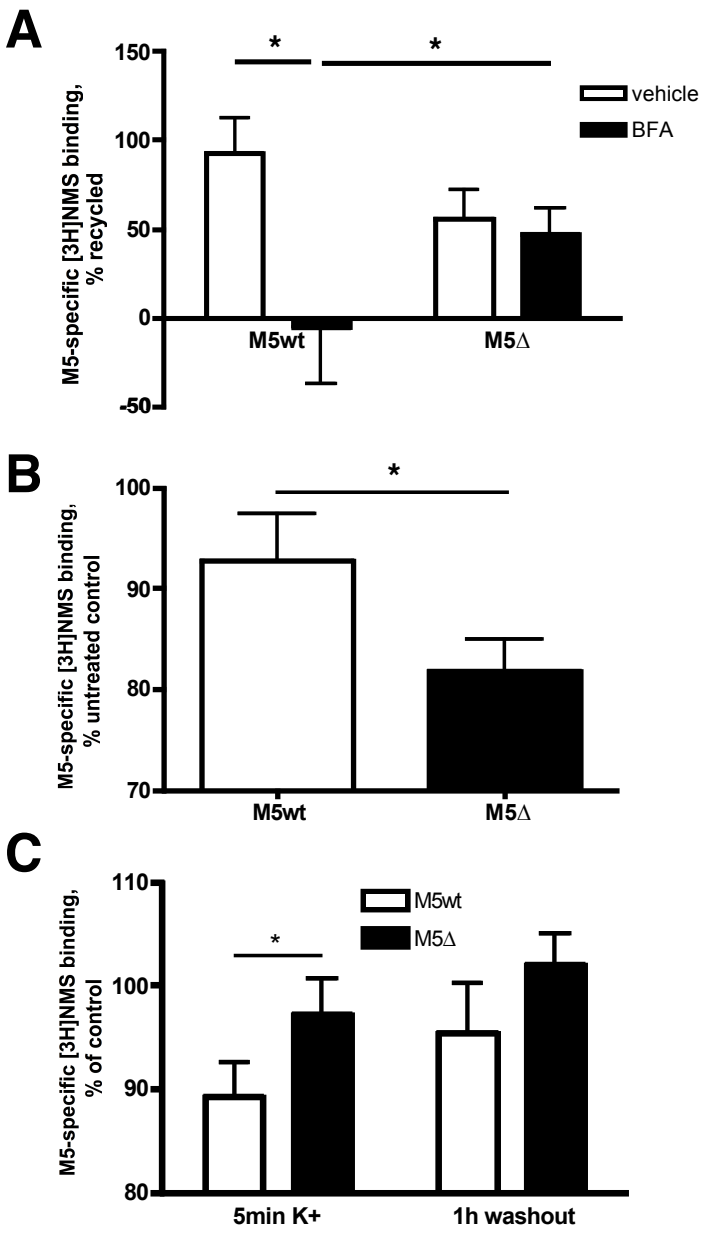

Figure 5.8 Activity-induced trafficking characteristics of M5 receptors in cultured neurons. Rat embryonic cortico-hippocampal neurons were nucleofected with M5wt, M5Δ, or empty vector control plasmids, cultured for 13 days, and treated as indicated. Cell surface muscarinic receptors were assayed by [3H]NMS radioligand binding and M5-specific signal was calculated as described. **(A)** Cultures were pre-treated with 5μM brefeldin-A (BFA) for two hours before assaying for endocytic recycling as in figure 5.7. Data are expressed as a percent of CCh-internalized receptors recycled after 1 hour washout. (*): P< 0.05, Bonferroni post-test / two-way ANOVA. **(B)** Cultures were treated for 4 days with 10μM CCh and assayed for cell-surface M5 receptor binding. (*): P< 0.05, paired two-tailed Student's T-test. **(C)** Cultures were treated with 45mM KCl for 5 minutes, with and without a subsequent 1 hour washout. (*): P< 0.05, paired two-tailed Student's T-test.

on the levels of M5Δ recycled to the cell surface after 1 hour washout from a 30-minute CCh treatment (figure 5.8A). This result further supports the hypothesis that M5 undergoes endocytic recycling via an AP-3-dependent mechanism, and suggests that residual recycling seen in the AGAP1 DOI deletion mutant may proceed by an alternate, AP-3 independent mechanism.

5.3.8 Down-regulation of cell surface M5 receptors after chronic agonist treatment is increased in the M5Δ mutant

Long-term activation of GPCRs can result in their down-regulation by targeting of agonist-stimulated receptors for lysosomal degradation (Tsao and von Zastrow, 2000). The striatum, in which M5 receptors are present in midbrain dopaminergic afferent terminals, is characterized by the presence of tonically active, extensively arborized cholinergic interneurons, and has the highest acetylcholine tone found in the CNS (Zhou et al., 2002a; Pisani et al., 2007). As the M5Δ receptor was observed to be deficient in its ability to undergo endocytic recycling after agonist-induced internalization, we asked whether its long-term activation could lead to down-regulation as a result of aberrant targeting to the lysosomal degradative pathway. We treated primary cultured neurons expressing wild-type of AGAP1 ROI mutant M5 receptors with a moderate dose (10μM) of the non-hydrolyzable ACh analogue carbachol for 4 days, and then assayed for cell surface M5 receptor sites by radioligand binding as described above. As a percentage of untreated controls, we observed a significantly greater reduction in the density of cell surface M5Δ receptors as compared to

M5wt (figure 5.8B). This result supports the hypothesis that AGAP1-mediated recycling is required for maintenance of surface M5 expression under sustained ACh stimulation conditions.

5.3.9 Chemical depolarization decreases surface density of M5 receptors expressed in primary cultured neurons

AP-3 is known to be required for the targeting of certain proteins (ZnT3, VGAT) to nerve-terminal synaptic vesicles (Nakatsu et al., 2004; Salazar et al., 2004b). One interpretation of our recycling data is that M5 is trafficked to a synaptic vesicle-like compartment via an AGAP1 / AP-3 sorting mechanism, and that stimulation with CCh serves to increase cell surface M5 density by depolarization-induced exocytosis of receptors held in subcellular stores. To test this, we expressed M5wt or M5Δ in cultured neurons, and 1) chemically induced depolarization with 45mM KCl for 5 minutes, 2) depolarized with KCl, followed by a 60-minute washout / recovery, or 3) left cells untreated. We observed a decrease in surface M5 [3H]NMS binding sites that was significantly greater after 5 minutes of KCl treatment in the wild-type as compared to deletion mutant receptors (Student's paired two-tail T-test, $p<.05$; however, 2-way ANOVA showed a significant difference ($p<.05$) only between M5wt and M5Δ groups) (figure 5.8C). After washout / recovery, surface levels of both mutant and wild-type M5 increased (figure 5.8C). These results do not support depolarization-dependent synaptic vesicle fusion as a mechanism for M5 surface expression

up-regulation. The significance of the differential response of M5wt and M5Δ to neuronal depolarization with regard to endocytic recycling is unclear.

5.3.10 M5Δ couples normally to downstream signaling pathways

To insure that the i3 loop AGAP1 ROI deletion (Δ369-386) did not interfere with the coupling of M5Δ to signaling effectors, we compared the Gq and MAP kinase responses of the M5 wild-type and M5Δ receptors. In HEK-293T cells transiently transfected with M5wt, M5Δ, or control expression plasmids, cells were stimulated with various concentrations of CCh, and PLC-β activation was assayed by the accumulation of the inositol-3-phosphate metabolite inositol-1-phosphate. No difference in agonist efficacy (EC_{50}) was observed between wild-type and mutant receptors, while signal magnitude was greater in M5Δ than wild-type, in line with its pattern of surface expression (figure 5.9A). Similarly, CCh was able to stimulate intracellular calcium release in cells stably transfected with both M5wt or M5Δ receptors, with a larger signal magnitude in the higher-expressing M5Δ line (figure 5.9B). We also observed that both M5wt and M5Δ were able to activate the MAP kinase pathway in HEK-293T cells (as measured by phosphorylation of Erk 1/2) after stimulation with CCh in a similar range of concentrations (figure 5.9C).

5.3.11 Analysis of M5 trafficking by subcellular membrane fractionation

Finally, we performed subcellular membrane fractionation of nucleofected cultured primary neurons in an effort to further understand the activity-induced

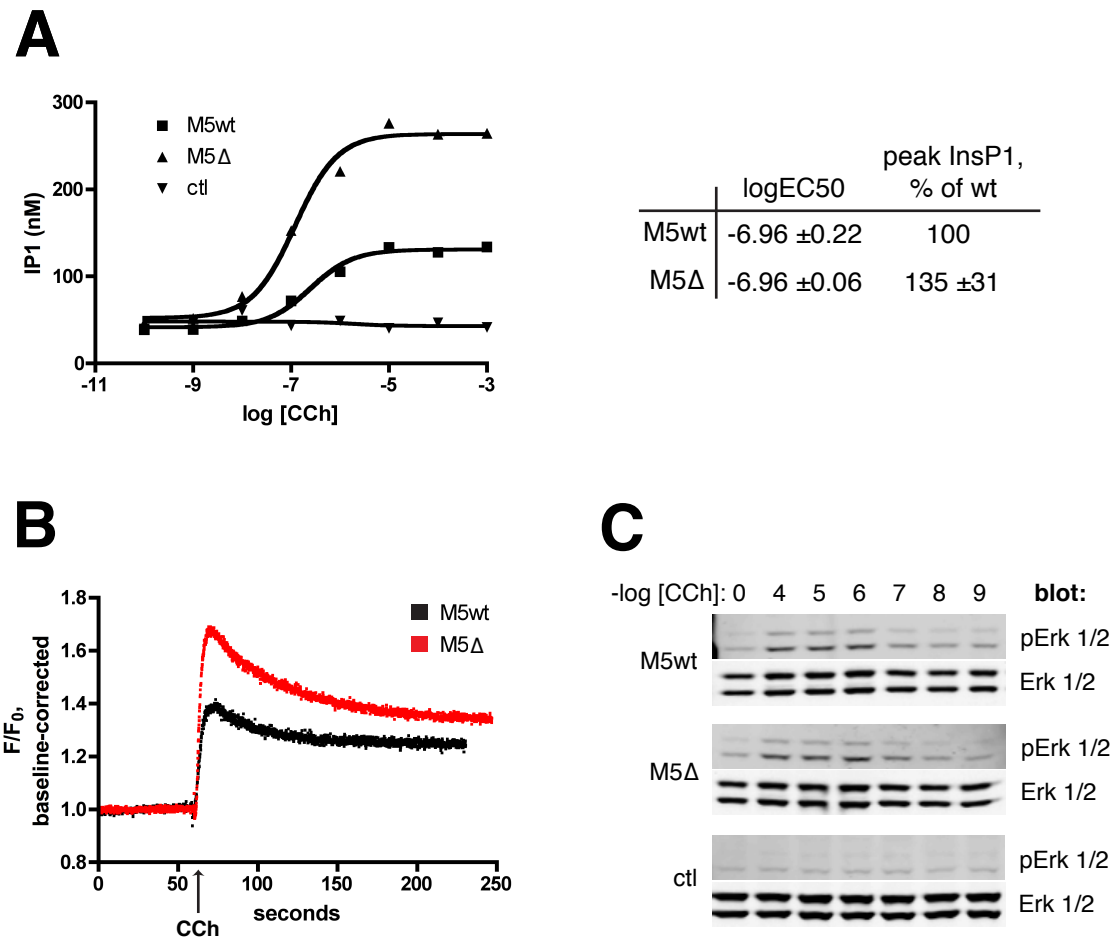

	logEC50	peak InsP1, % of wt
M5wt	-6.96 ±0.22	100
M5Δ	-6.96 ±0.06	135 ±31

Figure 5.9 The Δ369-386 mutation does not affect M5 signaling properties. **(A)** HEK-293T cells transiently transfected with M5wt, M5Δ or empty vectors were stimulated with various concentrations of CCh and assayed for inositol-1-phosphate accumulation as described. EC_{50} values were calculated by non-linear curve fitting to a sigmoidal dose-response model (GraphPad Prism). **(B)** HEK-293T cells stably expressing M5wt or M5Δ receptors monitored for intracellular Ca2+ concentration by Fluo-3 fluorometry. Cells were stimulated with CCh (1mM) at the indicated time point. **(C)** HEK-293T cells transiently transfected with M5wt, M5Δ or empty vectors were stimulated with various concentrations of CCh for 10 minutes. Activated (phospho-Tyr 202/204; pErk 1/2) and total Erk 1/2 were detected from cell lysates by immunoblot.

trafficking of M5 receptors. In the first experiment, primary cultured cortico-hippocampal neurons expressing wild-type or deletion-mutant M5-GFP were treated with CCh for 1 hour, homogenized, and then subject to glycerol velocity gradient centrifugation in order to synaptic vesicle-containing fractions (West et al., 1997b). The isolation of synaptic vesicle-containing membrane fractions was confirmed by immunoblot for synaptophysin; however, neither M5wt- nor M5Δ-GFP protein was detected in a pattern consistent with enrichment in a synaptic vesicle-like compartment, arguing against an AP-3 mediated endosome-to-synaptic vesicle pathway in the recycling of M5 to the cell surface (figure 5.10A).

In the second experiment, membrane fractionation was performed in an effort to confirm the hypothesis that agonist-internalized M5Δ is mistargeted to the late endosome / lysosome degradative pathway. Primary cultures expressing M5wt- or M5Δ-GFP were incubated with CCh in the presence of the lysosomal protease inhibitor leupeptin for 4 hours, and then fractionated by self-forming percoll density gradient centrifugation (Schaub et al., 2005). A dense membrane fraction corresponding to late endosomes / lysosomes was observed by immunoblot to be relatively enriched in the late endosome marker rab7, but showed little AGAP1 or plasma membrane marker (Na+,K+ ATPase β2) immunoreactivity (figure 5.10B). While small amounts of M5wt- and M5Δ-GFP protein were detected in the peak lysosomal membrane fraction, their overall lysosome-like distribution was similar (M5wt-GFP, 6.7% of total immunoreactivity; M5Δ-GFP, 4.1%) (figure 5.10B). We therefore could not conclude from this

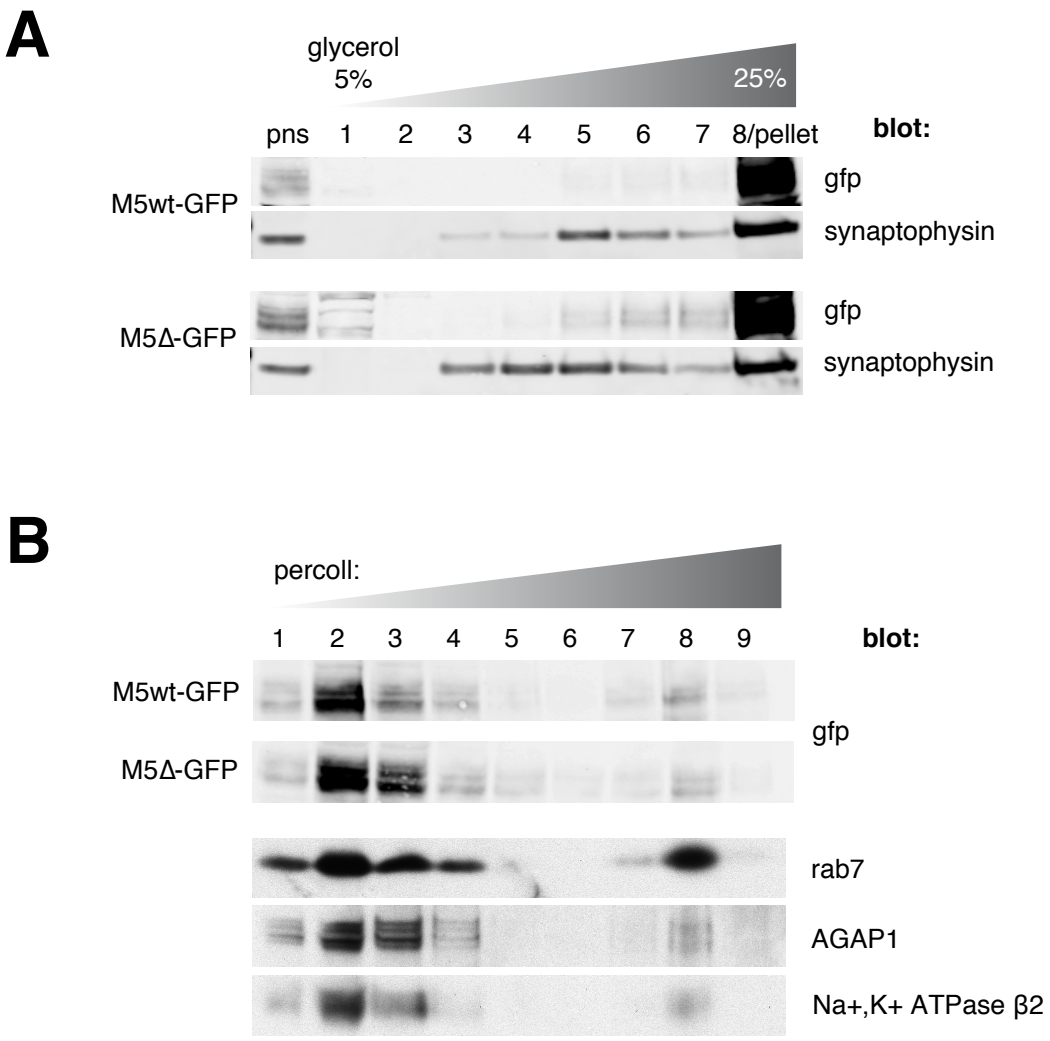

Figure 5.10 Analysis of M5 receptor trafficking in cultured neurons by subcellular fractionation. Rat embryonic cortico-hippocampal neurons were nucleofected with M5wt-GFP or M5Δ-GFP plasmids, and cultured, treated and fractionated as indicated. **(A)** 14 DIV cultures were treated with 0.1mM CCh for 1 hour and synaptic vesicle-like membranes were isolated by glycerol velocity gradient centrifugation. Isolated membranes and post-nuclear supernatant (PNS) were analyzed by immunoblot. **(B)** 21 DIV cultures were treated for 4.5 hours with 1mM CCh and 0.1mM leupeptin. Membranes were fractionated through a self-forming Percoll density gradient, and fractions were analyzed by immunoblot as indicated.

experiment that the AGAP1 DOI deletion mutant M5 receptor is targeted to the degradative pathway upon agonist induced stimulation.

5.4 Discussion

This chapter describes evidence of an AGAP1-dependent, neuron-specific mechanism for the recycling of agonist-internalized M5 muscarinic receptors to the plasma membrane. Induction of AGAP1 interaction loss-of-function by deletion of the M5 i3 loop region of interaction or by RNAi-mediated depletion of endogenous AGAP1 protein decreased the magnitude of cell surface M5 binding site reappearance after agonist-induced intracellular sequestration, indicating inhibition of M5 endocytic recycling. The recycling deficit was reproduced by both knockdown of the brain-specific AP-3B subunit β3B and by chemical inhibition of AP-3 membrane recruitment with the Arf GEF inhibitor brefeldin-A, demonstrating that M5 endocytic recycling proceeds through an AP-3-dependent pathway. Taken together with our biochemical and imaging data demonstrating physical, spatial and temporal interaction between M5 and an AGAP1/AP-3 complex, our results strongly suggest that efficient endocytic recycling of M5 is mediated by recognition of i3 loop trafficking motifs by an AGAP1/AP-3B complex, and that this mechanism is specific to the M5 muscarinic receptor subtype. This proposed mechanism, whereby AGAP1 serves as a cargo-interacting scaffold protein for the AP-3 complex, has not been described. However, AP-3 -dependent trafficking of the cannabinoid CB1 GPCR to intracellular compartments was reported (Rozenfeld and Devi, 2008), as was

endocytic recycling of membrane proteins by the AGAP1-related AZAP family protein ACAP1 (Dai et al., 2004; Li et al., 2005).

Further details of the mechanism by which AGAP1 and AP-3 mediate recycling of M5 receptors await elucidation. Muscarinic receptors M1-4 have been reported to undergo agonist-induced endocytosis via clathrin-dependent and -independent mechanisms (Tolbert and Lameh, 1996; Vogler et al., 1998; Delaney et al., 2002; Popova and Rasenick, 2004; Madziva et al., 2005). Though we did not determine the mechanism of M5 internalization, clathrin and non-clathrin endocytic routes may imply differing downstream trafficking pathways (Weigert et al., 2004). As we were unable to detect M5 recycling after short-duration agonist washout periods in pilot experiments (data not shown), the route of receptor recycling is likely not through the Rab4- / Rab35- dependent "fast" route, but rather via the Rab11-dependent "slow" endocytic recycling pathway (Grant and Donaldson, 2009). Since the slow pathway requires transit of cargo proteins through the tubulovesicular endocytic recycling compartment (ERC), and since ubiquitous AP-3A was seen to localize to membrane buds in ERC-like compartments (Peden et al., 2004), we speculate that in neurons, agonist internalized M5 is targeted to a recycling pathway by sorting from the ERC to an AGAP1/AP-3B-positive compartment. We found no evidence that internalized M5 is localized to synaptic vesicle-like structures; therefore, M5 may sort to recycling endosomes for transit back to the plasma membrane. In addition, our biochemical assays employed a heterogeneous neuronal cell population for exogenous expression, and could not distinguish between

trafficking events occurring in axonal and somatodendritic compartments. As neuron sub-class and axon-specific trafficking mechanisms are known to exist (Yap et al., 2008), studies employing purified cell populations and/or single-cell analysis could help identify the mechanisms of AGAP1-mediated M5 trafficking with further precision.

The mechanism responsible for the increased total and cell surface expression of M5Δ receptors compared to M5 wild-type remains unclear. The phenotype seemed to be unrelated to interaction with AGAP1 or AP-3, since knockdown of AGAP1 or β3B had no effect on steady-state M5 surface expression in neurons, and δ-adaptin and AGAP1 knockdown did not differentially effect M5 expression in neurons or tissue culture cells, respectively. It is possible that a second, unknown trafficking motif was inadvertently eliminated in the deletion of the AGAP1 ROI from the M5 i3 loop, or that mutation of the M5 coding sequence disrupted an miRNA binding site that served to down-regulate wild-type M5 *in vivo*. Although the degree of M5 overexpression in neurons was not high (M5 binding site density was comparable to that of endogenously expressed MRs), it is also possible that the increase in M5Δ expression compared to wild-type was related to transient expression conditions.

The use of primary cultured neurons as an exogenous expression system for radioligand assays, along with an enhanced protocol for RNAi-based expression knockdown in long-term cultures, were novel technical developments that proved crucial to the identification of the AGAP1-dependent endocytic recycling pathway. We used cell-surface radioligand binding as an indirect

measure of M5 trafficking, as related methodologies (including biotinylation, antibody feeding / stripping, and covalent receptor labeling) proved either unfeasible or lacking adequate sensitivity for use in this experimental system. Based on pilot experiments in tissue culture cells and primary cultured neurons, we chose time points for agonist treatment and receptor recycling (washout) conditions that corresponded to steady-state MR binding site labeling. It should be noted that 1) our assay could not identify the origin of binding sites appearing at the cell surface after agonist washout, and 2) the agonist-internalized receptor values reflect not the total percentage of cell surface receptors internalized, but rather the surface density reached by virtue of steady-state balance between rates of internalizing and recycling M5 (Szekeres et al., 1998b). Given the time frame of our primary neuron experiments compared to their time of culture, and since interference from newly synthesized receptors was reduced by cycloheximide inhibition in tissue culture cell experiments, M5 surface density values obtained after agonist washout almost certainly reflect the re-appearance of endocytically recycled receptors. Additionally, since we observed M5Δ to be deficient in terms of the magnitude of receptor reappearance after agonist washout, differential internalization rates are likely not confounding our interpretation of the recycling assay data.

We observed a significantly larger reduction in the steady-state surface expression of M5Δ receptors compared to wild-type after chronic (4-day) agonist treatment. This result implies that AGAP1-dependent endocytic recycling may play a role in the avoidance of M5 receptor down-regulation under conditions of

sustained stimulation. To test this hypothesis directly would require determination of the effects of AGAP1-mediated trafficking abrogation on signaling pathways coupled to M5 activation. The cultured neuron exogenous expression system is not appropriate for such experiments, as the presence of non-M5 muscarinic receptors and the stoichiometric effects of overexpression greatly complicate data interpretation. In addition, endogenous M5 receptors are expressed at very low abundance in neurons, and M5-selective agonists do not exist. The dopaminergic neurons of the ventral midbrain have been reported to express M5 receptors to the exclusion of other MR subtypes, and their activation potentiates the release of dopamine (Weiner et al., 1990; Yeomans et al., 2001). However, the heterogeneous nature of primary midbrain cultures precludes their use in biochemical assays of M5 effector activation. In the following chapter, we describe an experimental approach whereby dopamine release magnitude is examined as a functional readout of endogenous M5 receptor activity in genetic models of M5 and AP-3 dysfunction.

6 ACETYLCHOLINE-STIMULATED DOPAMINE RELASE: PHYSIOLOGICAL CONSEQUENCES OF AGAP1-MEDIATED M5 RECYCLING

6.1 Summary

Acetylcholine modulates the release of dopamine in the striatum through a complex pattern of muscarinic and nicotinic receptor-mediated mechanisms. In this chapter, we describe ongoing, collaborative experiments examining the role of AGAP1 / AP-3-mediated endocytic recycling on the function of M5 in the striatum. We use mouse models of M5 and AP-3 dysfunction to investigate stimulated dopamine release in the context of muscarinic receptor activation. We confirm *in vitro* and *ex vivo* that presynaptic M5 is required for the dopamine release-potentiating activity of muscarinic receptor agonists in the striatum. Preliminary data suggest that loss of AGAP1 / M5 i3 loop interaction leads to a long-term down-regulation of M5 signaling efficacy, resulting in decreased levels of stimulated dopamine release.

6.2 Introduction

The M5 muscarinic acetylcholine receptor mediates the ability of ACh to potentiate dopamine release from midbrain dopaminergic neurons. M5 is the only muscarinic receptor detectably expressed in ventral tegmental area (VTA) and substantia nigra pars compacta (SNc) dopaminergic neurons of the

nigrostriatal and mesolimbic pathways, respectively (Weiner et al., 1990). These midbrain dopaminergic neurons are innervated somatodendritically by brainstem Ch5/Ch6 cholinergic afferents, and receive modulatory ACh input at striatal presynaptic terminals through the synaptic or volumetric action of the giant aspiny cholinergic interneurons. An *in vivo* electrochemical study demonstrated that electrical stimulation of Ch5/Ch6 cholinergic nuclei resulted in a slowly activating, sustained release of dopamine in the nucleus accumbens (NAcc). This ACh-stimulated dopamine release event was observed in wild-type mice and rats, was blocked by the muscarinic receptor antagonist scopolamine, and was completely abolished in M5 -/- mice (Yeomans et al., 2001; Forster et al., 2002). In addition, infusion of either the muscarinic antagonist atropine or antisense oligonucleotides directed against M5 into the rat ventral midbrain was seen to decrease the behavioral sensitivity to rewarding hypothalamic stimulation, a process dependent on the mesolimbic dopamine system (Yeomans et al., 2001). Electrophysiological studies indicate that sustained activation of midbrain dopaminergic neuron muscarinic receptors increases firing rate and bursting activity as a result of depolarization, most likely through an inhibition of K^+ currents (Gronier and Rasmussen, 1998; Fiorillo and Williams, 2000).

M5 muscarinic receptors also mediate the presynaptic modulatory actions of ACh on dopaminergic neurons projecting to the striatum. In studies of superfused acute mouse striatal slices, the genetic ablation of M5 was seen to decrease the ability of a muscarinic receptor agonist to potentiate K^+-stimulated dopamine release. As this M5-mediated potentiation mechanism was insensitive

to the action potential blocker tetrodotoxin, receptors located at dopaminergic neuron terminals were implicated (Yamada et al., 2001a; Zhang et al., 2002b). Further support for a presynaptic M5 receptor mechanism came from studies of dopamine release from rat striatum synaptosomes (an isolated nerve terminal preparation); the muscarinic agonist oxotremorine-M was seen to be release-potentiating in the absence of intact neurons. In the synaptosomal system, MR-mediated dopamine release potentiation was dependent on KCNQ2/3 K^+ channel activity; thus, local depolarization via I_m inhibition is likely responsible for M5's activity at the dopaminergic presynaptic terminal (Martire et al., 2007).

In the preceding chapters, we demonstrated that interaction between AGAP1 and M5 is required for efficient endocytic recycling of agonist-internalized receptors in neurons. By maintaing cell surface pools of signaling-competent receptors, this endocytic recycling mechanism may underlie the ability of M5 to maintain activity under conditions of sustained stimulation. In this chapter, we describe experiments examining the role of AGAP1 / AP-3 mediated recycling of presynaptic M5 receptors in the potentiation of dopamine release. In collaboration with outside laboratories, we studied evoked striatal dopamine release using the techniques of synaptosome superfusion and fast scan cyclic voltammetry. While the former technique allows definitive isolation of presynaptic mechanisms, the latter electrochemical approach provides high temporal resolution and quantitative dopamine concentration measurements in a tissue system with intact local morphology. To model M5 activity and/or trafficking dysfunction, we used the M5 -/- (knockout) and the spontaneous δ-Adaptin-null

mocha mouse models. The development of an AGAP1 -/- mouse was not pursued, as we reasoned that genetic deletion of this protein would result in a generalized and severe secretory pathway disruption phenotype as a result of Arf1 dysregulation. Instead, we developed a mouse in which the previously characterized M5Δ receptor was expressed in place of wild-type M5. We hypothesized that inhibition of AGAP1 or AP-3 function would inhibit recycling of desensitized M5 receptors at striatal dopaminergic terminals, resulting in a decreased basal or activity-dependent sensitivity to MR-stimulated dopamine release.

6.3 Results

6.3.1 Generation of the M5 Δ369-386 mouse

In order to study the effect of AGAP1-mediated trafficking on the function of the M5 muscarinic acetylcholine receptor *in vivo*, we generated a mutant mouse in which the domain-of-interaction deleted M5 Δ369-386 receptor (M5Δ) was expressed in place of wild-type M5. A homologous recombination-based "knock-in" approach was used to replace the single-exon wild-type *Chrm5* coding sequence with the mutant *Chrm5*$^{\Delta 369\text{-}386}$ allele in C57BL/6 mouse ES cells. The targeting strategy was designed and M5Δ mutant mouse generation was performed by Ozgene Pty. Ltd. (Bentley, Australia) as summarized in figure 6.1A. Targeted ES cell colonies were sequenced to confirm deletion of the M5 369-386 coding region. Blastocyst injection of targeted ES cells resulted in germline transmission of the *Chrm5*$^{\Delta 369\text{-}386}$ allele. The resultant mouse was subsequently

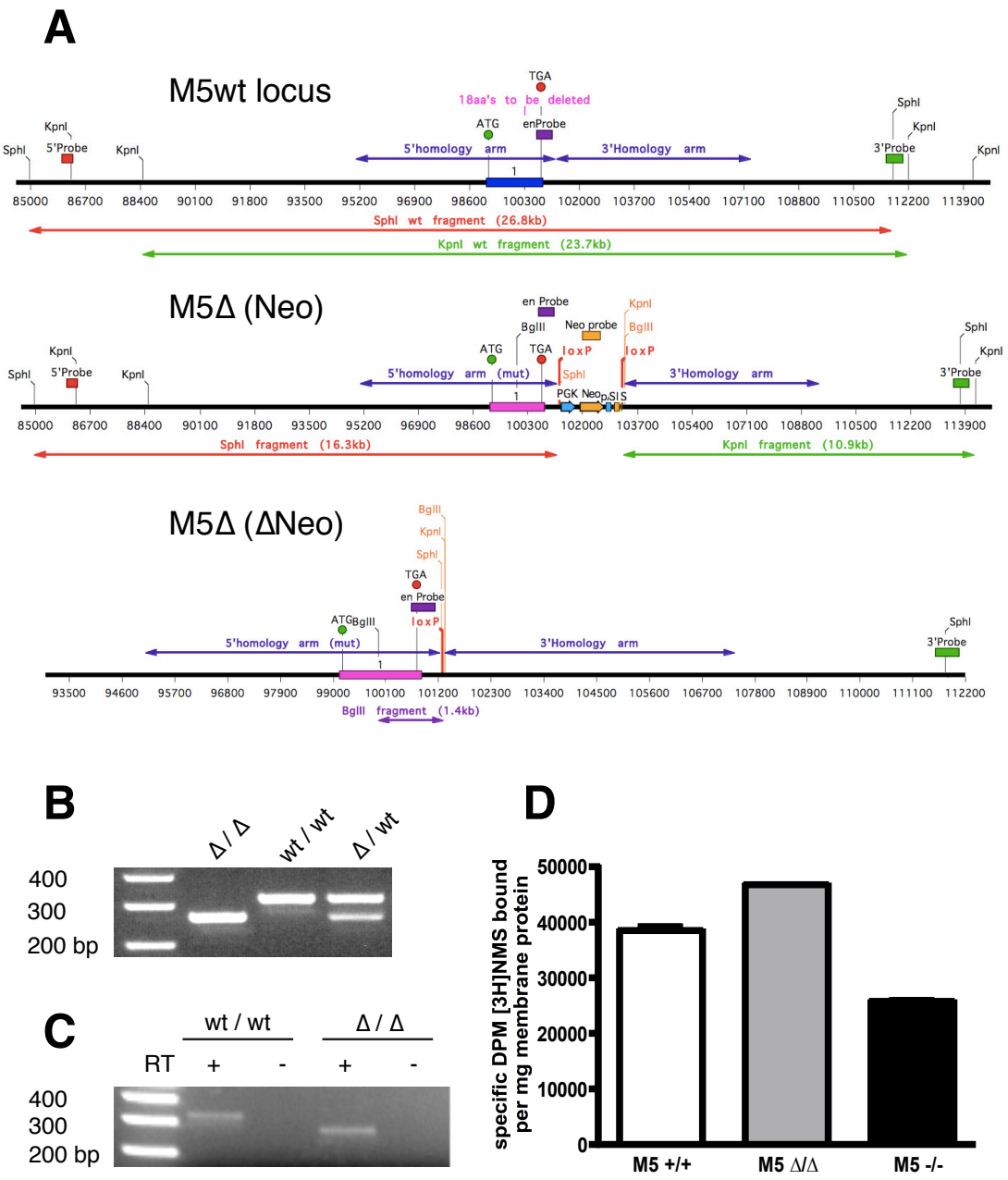

Figure 6.1 M5Δ369-386 knock-in mouse generation. **(A)** Targeting and screening strategy was designed by Ozgene, Pty. Ltd. Top, wild-type M5 (*Chrm5*) locus; middle, targeted (*Chrm5 Δ369-386* / M5Δ) locus; bottom, ΔNeo locus after Cre-mediated excision of LoxP-flanked selection cassette. Restriction fragment lengths indicate expected band sizes for Southern blot screening of targeted ES clones. (figures courtesy of Ozgene) **(B)** PCR genotyping of mice using primers flanking the Δ369-386 site. **(C)** RT-PCR from total RNA extracted from midbrains of M5 Δ/Δ and wt/wt mice. Primer set was identical to (C). RT, reverse transcriptase. **(D)** [3H]NMS binding to mouse cerebral blood vessel membranes isolated from mice of indicated genotypes. Data represent a single experiment performed in triplicate on tissue pooled from two animals.

mated to a Cre recombinase-expressing transgenic line to excise the loxP site-flanked neomycin selection cassette from the *Chrm5* locus (figure 6.1A). From these founder animals, a congenic C57BL/6 background M5Δ mouse colony was established. M5 *Δ/Δ* animals were healthy and fertile, and we observed no obvious phenotypic differences (gross appearance or home cage behavior) between *Δ/Δ*, *Δ/wt* and *wt/wt* mice. Polymerase chain reaction (PCR)-based genotyping of mouse tail genomic DNA using oligonucleotide primers flanking the deleted region of M5Δ369-386 yielded products of expected sizes for M5 *Δ/Δ*, *Δ/wt* and *wt/wt* mice (figure 6.1B). We next confirmed that the M5 *Δ* mRNA was expressed *in vivo* by reverse transcription PCR (RT-PCR) of total RNA isolated from midbrains of M5 *Δ/Δ* and *wt/wt* mice. Using the genotyping primer set, we detected PCR products of the expected sizes from reverse transcribed *Δ/Δ* and *wt/wt* mouse RNA (figure 6.1C). Confirmation of M5Δ protein expression was complicated by the lack of subtype-selective antibodies or radioligands appropriate for the detection of low-abundance native M5 receptors. Since M5 is the sole muscarinic receptor responsible for the dilatory effects of ACh on cerebral arteries and arterioles (Yamada et al., 2001a), we reasoned that an absence of M5 expression would be detectable in this tissue by quantification of the total MR population. To test this, we prepared membranes from cerebral blood vessels isolated by density centrifugation from M5 *wt/wt, Δ/Δ*, and *-/-* mouse brains and assayed for muscarinic receptor density by [3H]NMS radioligand binding. In a single experiment consisting of tissue pooled from two animals of each genotype, binding of [3H]NMS was greater in both *wt/wt and Δ/Δ*

blood vessel membranes than in *-/-*, consistent with the expression of M5 receptor protein in M5 *Δ/Δ* animals (figure 6.1D).

6.3.2 Expression of AP-3 and AGAP1 in dopaminergic neuron terminals

As we wished to study the effects of AGAP1- and AP-3-mediated endocytic recycling on presynaptic M5 receptor function at striatal dopaminergic terminals, we first examined the distribution of the AP-3 complex in primary cultured rat midbrain dopaminergic neurons. Mature (14 DIV) midbrain cultures yielded a heterogeneous population of neurons, of which 25-50% were positive for the dopaminergic marker tyrosine hydroxylase (TH) (figure 6.2A). We observed punctate δ-Adaptin staining in thin, aspiny processes of TH-positive neurons, consistent with the presence of AP-3 endosomes in the axons of dopaminergic neurons (figure 6.2A). Next, we prepared synaptosomes from wild-type mouse striatal tissue in order to confirm the presence of AP-3 and AGAP1 proteins in presynaptic terminal compartments. Immunoblot analysis of synaptosome-containing fractions detected the presence of AGAP1, ubiquitously expressed AP3*μ*3A, and brain-specific AP3β3B, with possible enrichment of AGAP1 and AP3β3B indicated (figure 6.2B). The results of these experiments were consistent with the imaging data presented in chapter four, which demonstrated δ-Adaptin localization in presynaptic-adjacent compartments of cultured hippocampal neurons.

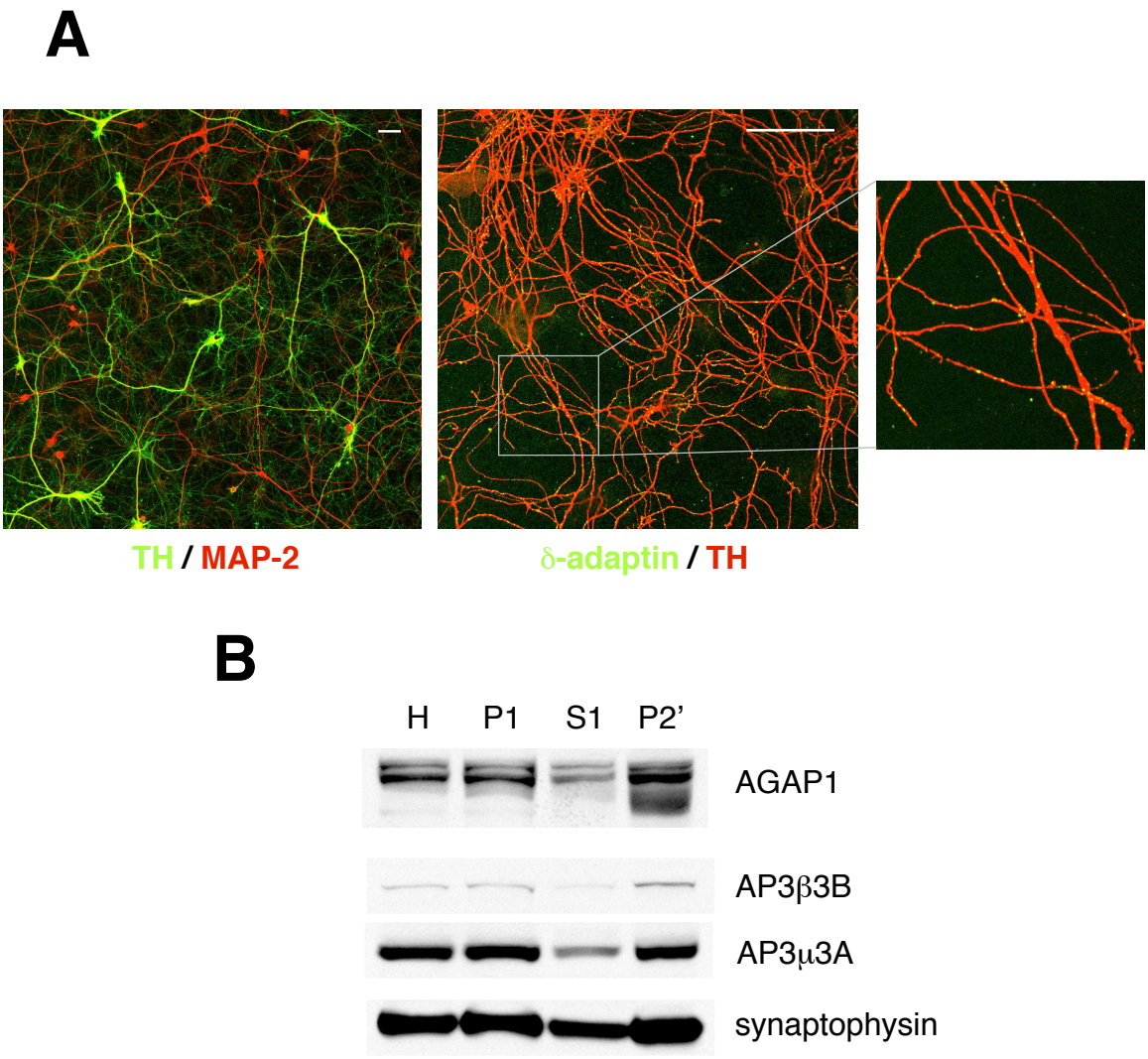

Figure 6.2 Expression of AGAP1 and AP-3 in dopaminergic neurons and nerve terminals. **(A)** Primary cultured rat ventral midbrain neurons were fixed, immunostained and imaged by confocal microscopy. Left: Cells immunostained for the dopaminergic neuron marker tyrosine hydroxylase (TH; green) and the pan-neuronal marker MAP-2 (red). Right: Cells immunostained for δ-adaptin (green) and TH (red), with area enlarged as indicated. Scale bars = 50 μm. **(B)** AGAP1, ubiquitous AP3μ3A, neuron-specific AP3β3B and the synaptic vesicle marker synaptophysin were detected by immunoblot in synaptosomes prepared from mouse striatum. H, homogenate; S1, supernatant 1 fraction; P1, pellet 1 fraction; P2', synaptosome fraction. Protein content of each fraction was equalized before SDS-PAGE separation.

6.3.3 M5 receptor activation potentiates stimulated dopamine release from striatal synaptosomes

In order to confirm previous reports of a dopamine release-potentiating function of M5 receptors localized to presynaptic dopaminergic terminals, neurotransmitter release experiments were performed in collaboration with Dr. Hugh Hemmings (Weill Cornell Medical School, New York). Synaptosomes isolated from the striata of M5 *wt/wt* or M5 -/- animals were loaded with [3H]dopamine and [14C]glutamate, and stimulated release of neurotransmitter was measured in a superfusion device. Incubation of striatal synaptosomes with the muscarinic receptor agonist oxotremorine-M (oxo-M) significantly potentiated the K^+-stimulated release of [3H]dopamine from wild-type, but not M5 -/- animals (figure 6.3A). Oxo-M treatment did not alter the magnitude of [14C]glutamate release in either M5 *wt/wt* or *-/-* animals (figure 6.3B). Thus, activation of presynaptic M5 muscarinic receptors potentiated stimulated dopamine release in a neurotransmitter-specific manner, confirming previous studies performed in wild-type and M5 -/- mouse striatal slices (Yamada et al., 2001a) and in rat striatal synaptosomes (Martire et al., 2007).

6.3.4 Fast scan cyclic voltammetric studies of striatal dopamine release

Although the neurotransmitter release studies described above positively identified presynaptic M5 as a dopamine release-modulating receptor, the relatively low (≥ 2 minute) temporal resolution and *in vitro* nature of synaptosome superfusion limits the utility of this experimental system to the study of trafficking-

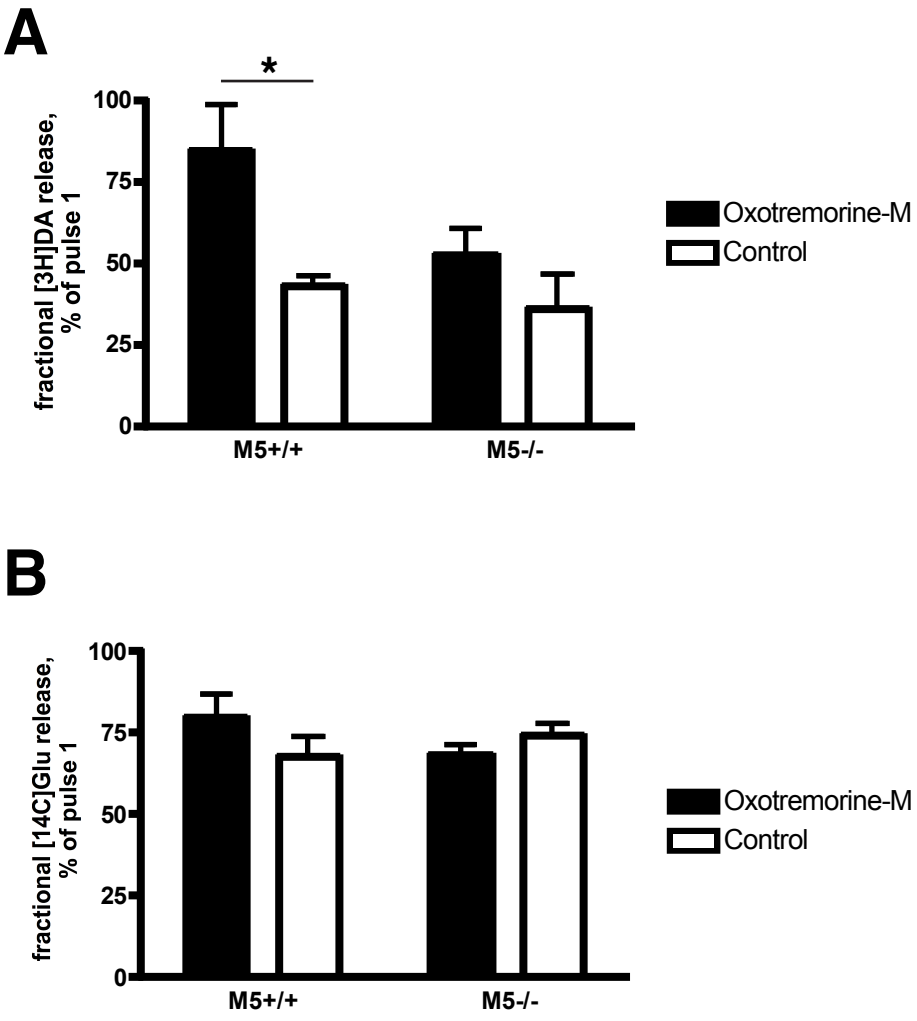

Figure 6.3 Activation of M5 receptors potentiates dopamine release from mouse striatum synaptosomes. Striatal synaptosomes prepared from mice of indicated genotypes and were simultaneously loaded with [3H]dopamine and [14C]glutamate. K^+-stimulated neurotransmitter outflow was measured in the presence and absence of oxotremorine-M. (*): (A)(*): $P < 0.05$, Bonferroni post-test / two-way ANOVA $P = 0.06$.

dependent functions of M5. To overcome this, we collaborated with Dr. David Sulzer (Columbia University, New York) to perform fast scan cyclic voltammetric (CV) recordings of stimulated dopamine release from acutely prepared mouse striatal slices. We first compared dopamine release magnitude after electrical stimulation in M5 -/- and wild-type mouse dorsolateral striatum, an area primarily innervated by nigrostriatal dopaminergic neurons projecting from the SNc. An approximately 40% reduction in the extracellular concentration of released dopamine was observed in M5 -/- mice as compared to wild-type (figure 6.4A). Next, we performed experiments in which striatal dopaminergic terminals were repeatedly electrically stimulated before and after the addition of the non-selective muscarinic receptor agonist oxo-M to the perfusion buffer. In contrast to our observations in superfused synaptosomes, oxo-M rapidly and strongly decreased the concentration of dopamine released after electrical stimulation in both wild-type and M5 -/- slices. However, this effect was larger in magnitude for M5 -/- as compared to wild-type mouse striata, consistent with a release-potentiating function of M5 receptors (figure 6.4B).

Next, we examined the role of AGAP1 interaction and AP-3 in the dopamine release-potentiating function of M5. We first used striatal slices from *M5Δ* mice to model M5 recycling dysfunction through AGAP1 interaction loss-of-function. Extracellular concentrations of dopamine released after electrical stimulation were decreased in M5 Δ/Δ striata compared to wild-type controls, with a magnitude comparable to that seen in M5 -/- animals (figure 6.4A). However, we observed no difference in magnitude or pattern of stimulated dopamine

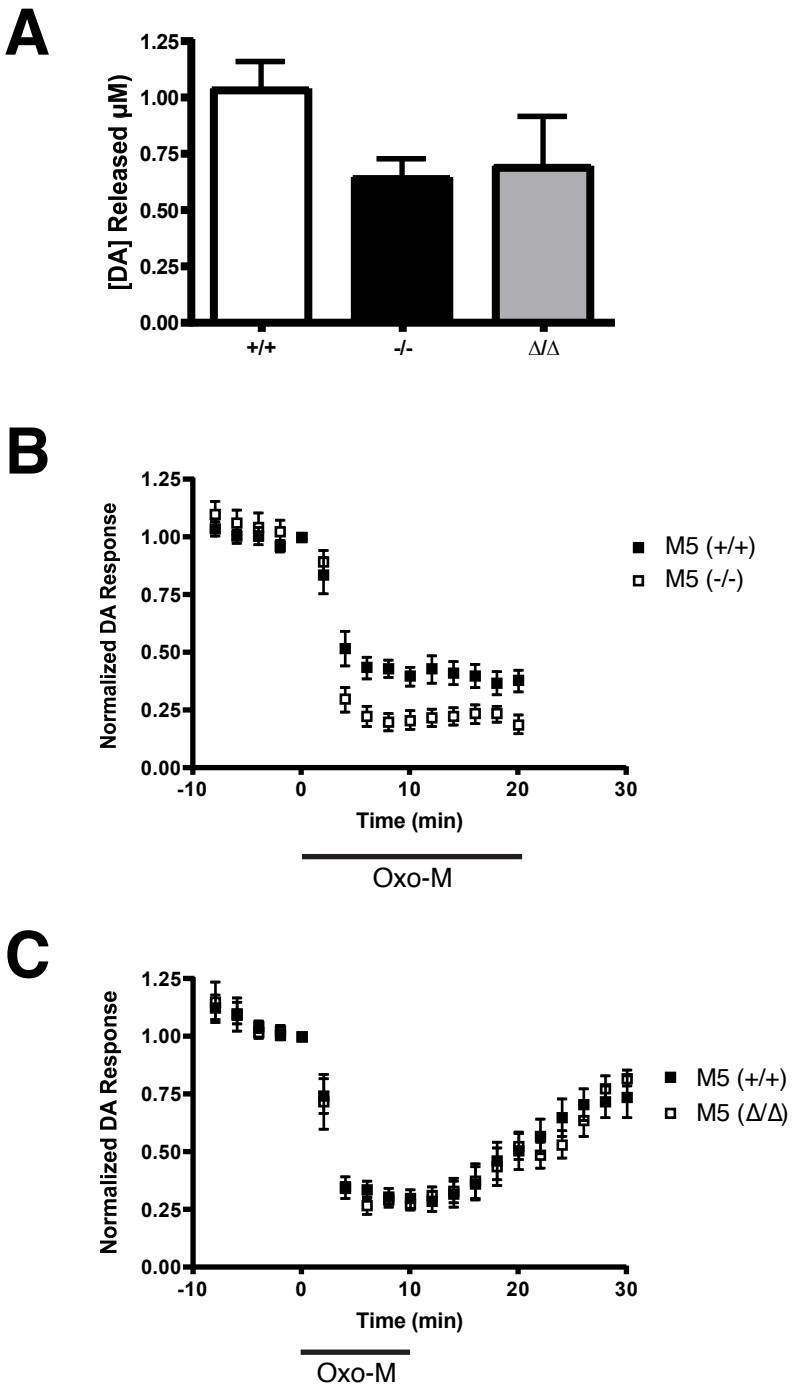

Figure 6.4 Analysis of dopamine release in M5 -/- and M5 Δ/Δ animals by fast-scan cyclic voltammetry. **(A)** Measurement of dopamine release evoked from single electrical stimuli in striatal slices prepared from mice of indicated genotypes. **(B)** and **(C)** Evoked dopamine release from M5 +/+, -/- and Δ/Δ striata was measured at two minute intervals after addition of 10μM oxotremorine-M (oxo-M) to the perfusion bath where indicated. In (C), oxo-M treatment is followed by a 20-minute washout period. Data are normalized to release at time=0.

release inhibition between M5 Δ/Δ and wild-type striata after either ten minutes of oxo-M administration or subsequent washout (figure 6.4C). We next examined the suitability of the mixed genetic background, *Ap3d1*-null mutant *mocha* (*mh*) mouse as a model for neuronal AP-3 dysfunction. Immunoblot analysis of whole-brain lysate from *Ap3d1 wt/wt, wt/mh, and mh/mh* mice confirmed the absence of both ubiquitous and brain-specific AP-3 subunits in *mh/mh* animals, with decreased AP-3A and AP-3B subunit abundance apparent in *wt/mh* heterozygotes as compared to *Ap3d1 wt/wt* or C57BL/6 controls. AGAP1 protein levels were not affected by *Ap3d1* genotype, however (figure 6.5A). We observed no difference in the ability of oxo-M to inhibit stimulated striatal dopamine release between *Ap3d1 mh/mh* and *mh/wt* heterozygote mice, although the overall degree of oxo-M inhibition was larger than that observed in C57BL/6N background mice (figure 6.5B). Taken together, these preliminary data suggest a decreased steady-state activity of M5Δ receptors as compared to M5 wild-type, but do not support the involvement of either AGAP1 interaction or AP-3 activity in the dynamic regulation of presynaptic M5 function.

6.4 Discussion

The experiments described in this chapter examined muscarinic receptor modulation of dopamine release as a functional readout of M5 receptor activity. We confirmed a presynaptic function of the M5 muscarinic acetylcholine receptor in the potentiation of stimulated dopamine release through superfusion of nerve terminal isolates (synaptosomes) derived from wild-type and M5 -/- mice. By

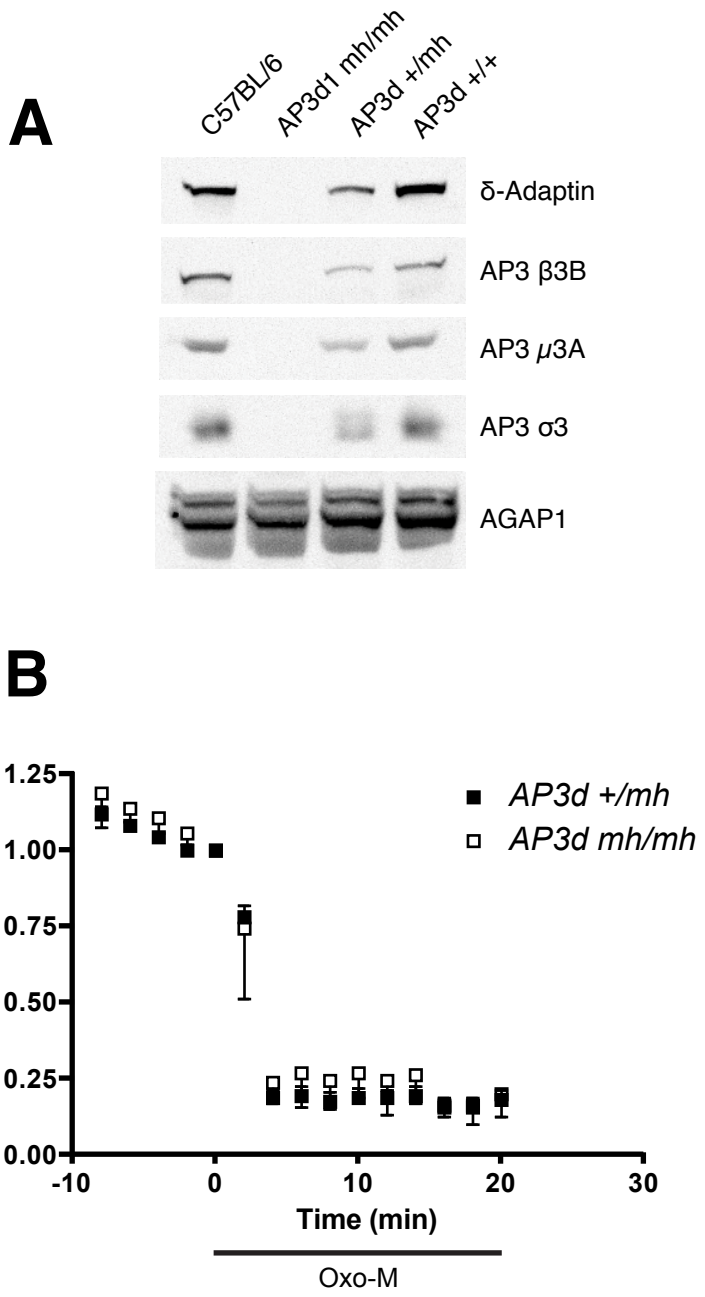

Figure 6.5 Analysis of dopamine release in *mocha* mice by fast-scan cyclic voltammetry. **(A)** Immunoblot detection of AP-3 subunits and AGAP1 from mouse brain lysates of indicated genotypes. **(B)** Evoked dopamine release from mocha (*Ap3d1 mh/mh*) or heterozygous control (*+/mh*) mouse striatum was measured at two minute intervals after addition of 10μM oxotremorine-M (oxo-M) to the perfusion bath where indicated. Data are normalized to release at time=0.

examining this phenomenon in striatal slices with the quantitative and temporally sensitive CV method, we determined that elimination of M5 receptors 1) decreased the concentration of dopamine released by electrical stimulation, and 2) increased the degree to which a saturating concentration of the non-selective muscarinic agonist oxo-M depressed evoked dopamine release. These novel observations are consistent with a presynaptic release-potentiating function of M5, and indicate that this potentiation occurs within an overall context of MR-mediated inhibition of dopamine release.

Our subsequent experiments in the CV system aimed to determine the effect of the AGAP1 domain-of-interaction deletion and the absence of AP-3 on the identified M5-mediated dopamine release effect. Although the results described have not been finalized, a number of trends are clear. Stimulated dopamine release is decreased in the M5 Δ/Δ mouse compared to wild-type, suggesting that M5Δ receptor signaling efficacy is down-regulated. However, oxo-M treatment did not differentially attenuate stimulated dopamine release in M5 Δ/Δ and wild-type mice, nor was desensitization-like rundown of dopamine release potentiation observed for Δ/Δ. Similarly, we observed no difference between *mocha* mutants (*mh/mh*) and heterozygous controls (*mh/wt*) in the oxo-M treatment experiment. In the latter case, we chose to use *mh/wt* controls, as the *Ap3d1*^{wt} allele is maintained in repulsion to the recessive *grizzled* (*gr*) mutation in this strain. Homozygous *gr/gr* animals are sub-viable, and the genetic mechanism resulting in the *grizzled* phenotype has not been determined (Burwinkel et al., 1998). We are currently examining evoked and oxo-M

modulated dopamine release for animals of all genotypes in the *mocha* strain (*mh/mh, mh/wt*, and *wt/wt*). However, interpretation of these dopamine release data may be complicated by the generalized dysfunction of nerve terminals in *Ap3d1 -/-* animals (Newell-Litwa et al., 2007). In addition, examination of oxo-M-induced [3H]dopamine outflow from synaptosomes prepared from M5 Δ/Δ striata may lend further support for our model of down-regulation of M5Δ receptors *in vivo*.

While our preliminary data do not support a role of either AGAP1 interaction or AP-3 in the short-term maintenance of M5 sensitivity under sustained agonist stimulation, the evoked release of dopamine was apparently lower in animals expressing the M5Δ receptor. If these results are confirmed in further experimental replicates, how do we reconcile the seemingly M5 -/- -like evoked release and +/+ -like oxo-M stimulated release results observed in M5 Δ/Δ striata? Based on our observation that long-term agonist stimulation of M5 receptors expressed in cultured neurons leads to significant down-regulation of M5Δ, but not M5 wild-type, receptors, we propose the following mechanism: Under normal conditions, dopaminergic terminal M5 receptors receive constant ACh input from the highly arborized, tonically active giant aspiny cholinergic interneurons. A slow, AGAP1-dependent recycling mechanism is required for the maintenance of cell-surface M5 receptor density under this constant stimulation condition. In the absence of AGAP1 interaction, activated M5 receptors fail to recycle, leading to long term down-regulation of plasma membrane receptors. In our evoked dopamine release experiments, a moderate striatal ACh tone results

in partial receptor occupancy and stimulation; the greater surface density of M5 wild-type as compared to M5Δ receptors leads to an increase in $G\alpha_q$-stimulated PIP_2 hydrolysis and greater KCNQ2/3 channel inhibition, resulting in enhanced membrane depolarization and an increase in the magnitude of dopamine release detected. In the oxo-M stimulation experiments, however, the agonist was applied at a high concentration, leading to saturation of the $G\alpha_q$-PIP_2-KCNQ2/3 signaling pathway even at the low M5 surface receptor density hypothesized to exist in the M5 Δ/Δ mouse. Further complicating interpretation of the latter experiment was the fact that muscarinic receptor agonist application is expected to decrease tonic ACh release through activation of cholinergic interneuron M4 autoreceptors, which may in turn influence the activity of nicotinic ACh receptors present on dopaminergic terminals. Confirmation of our proposed model mechanism awaits further experimental replicates; in addition, the use of muscarinic and/or nicotinic antagonists in the electrically-evoked dopamine release experiments could provide evidence supporting a role of M5 receptor density in the observed M5 Δ/Δ phenotype.

7 CONCLUSIONS AND FUTURE DIRECTIONS

Muscarinic receptors play an essential role in the regulation of mammalian physiology. Nearly every tissue in the body depends on the regulated transduction of cholinergic signals by a combination of muscarinic receptors for normal function. In the brain, mediation of cholinergic neurotransmission by muscarinic receptors is required for such basic processes as attention, arousal, movement, motivation, learning and memory, the disruption of which is implicated in the pathology of a number of currently intractable diseases. However, the ubiquity of MRs, their overlapping mechanisms of signal transduction, and their pharmacological similarity have greatly hindered progress towards understanding the cell- and subtype-specific function and regulation of these receptors. Indeed, development of compounds or techniques capable of identifying or modulating the activity of individual muscarinic receptor subtypes in isolated populations of cells would be of great use both scientifically and clinically.

The function of GPCRs depends critically on temporally and spatially coordinated protein-protein interactions between cytoplasmic receptor domains and signal-transducing and/or regulatory molecules. In the muscarinic receptors, one of these cytoplasmic regions, the third intracellular loop, is exceptionally large and divergent in sequence across the five MR subtypes. Although some functions have been assigned to the MR i3 loops, the phylogenetic sequence conservation of this region implies the presence of critical protein interaction domains that have yet to be identified. In an effort to uncover such molecules,

we performed yeast two-hybrid screens using as baits the five muscarinic receptor i3 loop domains. We isolated three potential muscarinic receptor interacting proteins, AGAP1, SNX20, and UHRF1BP1L, on which biochemical protein-protein interaction analysis was performed with the intention of identifying a single candidate for subsequent investigation. We chose to study the M5i3 binding protein AGAP1, as we observed clear, domain-delineated interaction between M5 and AGAP1 *in vitro*, and since published functional characterizations of this Arf GAP protein suggested a potential role in receptor trafficking.

The M5 muscarinic receptor is the least-expressed MR in mammals, and its molecular biology and regulation have been little studied. Thus, a number of our basic findings on the expression and trafficking patterns of this receptor were novel. For instance, we demonstrate that exogenously expressed M5 receptors undergo endocytic recycling in HEK-293T cells, with a time course consistent with trafficking through the “slow” endocytic recycling compartment-dependent pathway (Grant and Donaldson, 2009). We also show that M5 receptors expressed in primary cultured hippocampal neurons distribute uniformly in the plasma membrane and are not excluded from either the somatodendritic or axonal compartments. On the functional level, we confirmed a dopamine release-potentiating activity of M5 receptors localized to nigrostriatal and mesolimbic neuron terminals. Although this presynaptic modulatory function was previously examined in [3H]dopamine release experiments performed on rat striatum synaptosomes and both wild-type and M5 -/- mouse striatal slices (Yamada et al., 2001a; Martire et al., 2007), our study is the first to apply the fast

scan cyclic voltammetry method to the examination of M5-specific modulation of endogenous dopamine release in mouse striatum.

Of greatest overall significance, however, is our demonstration of a neuron-specific trafficking function for the AGAP1-M5 interaction. Our results demonstrate that in the primary cultured rat neuron exogenous expression system, interaction with AGAP1 is required for efficient endocytic recycling of M5 receptors after agonist-stimulated endocytosis. In non-neuronal cells, AGAP1 was previously demonstrated to regulate the trafficking of lysosomally-targeted integral membrane proteins by virtue of its ability to bind to the AP-3 adaptor protein complex (Nie et al., 2003). We found that subunits of both the ubiquitously expressed AP-3A and neuron-specific AP-3B complexes associated with the M5 i3 loop in an AGAP1-dependent manner, and that the endocytic recycling of M5 in neurons was sensitive to depletion of AP-3B. The AP-3A complex has been shown to regulate the endocytic trafficking of membrane proteins to lysosomes and lysosome-like organelles, while in neurons the AP-3B complex is known to mediate the formation of a subset of synaptic vesicles, and is required for the targeting of certain membrane proteins to the nerve terminal (Kantheti et al., 1998; Blumstein et al., 2001; Salazar et al., 2004b). To our knowledge, however, neither AGAP1, AP-3A nor AP-3B have been implicated in the mechanism of endocytic recycling, although the AGAP-like protein ACAP1 was found to promote the recycling of internalized transferrin receptors (Dai et al., 2004). Our observation of AGAP1- and AP-3-dependent M5 receptor recycling is therefore indicative of a previously undescribed GPCR trafficking

pathway. In addition, our results strongly suggest that the mechanism of M5 recycling in neurons relies upon a protein-protein binding event between the M5 i3 loop and an AGAP1-AP-3B complex. Thus, AGAP1 may possess target-recognition properties in addition to its characterized Arf1 regulatory function, which further suggests that members of the AP-3 holocomplex (such as AGAP1 and BLOC-1) may function in the recognition of sorting signal sequences to a greater degree than previously recognized.

Further characterization of the AGAP1-mediated recycling of M5 receptors may reveal sorting signals or regulatory mechanisms important for the function of other classes of GPCRs. We identified a 23-amino acid region in the i3 loop of M5 that was required for AGAP1 interaction and efficient endocytic recycling in neurons. We also identified a series of residues in this i3 loop domain of interaction whose mutation eliminated or reduced AGAP1 binding activity. The sequence of these critical residues resembled, but did not exactly conform to recognized tyrosine- and dileucine-based sorting signals commonly present on GPCR i3 loop or C-terminal tail regions (Bonifacino and Traub, 2003). To date, relatively few endocytic targeting motifs have been identified; thus, the precise identification of an AGAP1 binding motif would expand our understanding of the structural determinants of GPCR recycling, and could help identify other GPCRs whose endocytic traffic is AGAP1-dependent. In addition, a deeper mechanistic understanding of AGAP1 / AP-3-mediated M5 recycling could potentially reveal points at which this putative trafficking pathway is regulated. The targeting of endocytosed GPCRs to the degradative or recycling pathways plays a critical

role in determining the effect of sustained stimulation on surface receptor density, and in turn the magnitude of second messenger responses to neurotransmitters. An emerging model of neuronal plasticity implicates regulation of glutamate channel trafficking as a key mechanism of signal “gain”-tuning, by which a neuron’s up- or down-regulation of surface receptor levels acts to alter its response to a given synaptic input (Turrigiano, 2008). An analogous mechanism has been shown to tune GPCR signaling responses in neurons and other cells, the regulation of which may occur at the level of GPCR targeting sequence recognition (Hanyaloglu and von Zastrow, 2008). For example, activity-induced receptor ubiquitination was shown to shift targeting of a GPCR from the recycling to the degradative pathways (Shenoy et al., 2001) and phosphorylation of the AGAP1-like molecule ACAP1 is required for its binding to, and its recycling pathway targeting of β-Integrin (Li et al., 2005). Continuing biochemical and cell biological studies of the M5 - AGAP1 interaction may shed light upon such post-translational modifications regulating M5 trafficking.

The study of M5 function *in vivo* is complicated by the receptor’s low abundance relative to other muscarinic receptors and the lack of pharmacological tools appropriate for the isolation of subtype-specific signaling events. In order to better understand the physiological consequences of AGAP1-dependent M5 receptor recycling, we generated an i3 loop domain-of-interaction mutant (M5Δ) mouse. M5 is the only muscarinic receptor detectably expressed in midbrain dopaminergic neurons, in which it mediates the dopamine release-potentiating activity of ACh (along with ionotropic nicotinic ACh receptors) (Forster et al.,

2002). From terminals of these neurons present in striatal slices, we detected a decrease in the magnitude of evoked dopamine release in mice expressing M5Δ receptors as compared to wild-type. As we observed chronic agonist treatment to result in surface density down-regulation of M5Δ, but not M5 wild-type receptors *in vitro*, we hypothesized that abrogation of AGAP1 / AP-3-mediated endocytic recycling of M5 results in down-regulation of M5 receptor signaling at striatal dopaminergic terminals *in vivo*. If these data are indeed confirmed by additional replicates, our model predicts an important role for the AGAP1-M5 interaction in the maintenance of tonic basal ganglia function. The interaction between cholinergic and dopaminergic activity in the striatum influences the activity and plasticity of the medium spiny output neurons, and is in turn required for proper coordination of motivated locomotor activity (Pisani et al., 2007). As the giant aspiny cholinergic interneurons provide a constant ACh tone in the striatum, an efficient endocytic recycling mechanism may be required for the maintenance of M5 signaling efficacy at the presynaptic dopaminergic terminal. Our experiments examined the release-modulating functions of dopaminergic nerve terminal receptors. However, M5 receptors localized to somatodendritic compartments of midbrain dopaminergic neurons also function to stimulate dopamine release (Yeomans et al., 2001; Miller and Blaha, 2005). Indeed, Ch5/ Ch6 cholinergic afferent-stimulated dopamine release from VTA neurons is characteristically prolonged in duration, suggesting that M5 endocytic recycling may play a role in sustaining sensitivity to ACh (Forster et al., 2002). *In vivo* chronamperometric measurements of dopamine release in the M5Δ mouse could

reveal AGAP1 interaction-dependent postsynaptic functions of M5, as could electrophysiological or Ca^{2+} imaging studies of isolated dopaminergic neurons.

In the process of examining the functional role of the putative AGAP1-M5 interaction, we developed novel technical approaches whose application extends beyond the present project. First, the use of primary cultured rat neurons as an expression system for the analysis of exogenously-expressed receptors by radioligand binding has, to our knowledge, not been described. Such a system may prove useful for experiments involving brain-expressed receptors, as many GPCRs are regulated in a cell type-specific manner, and the more commonly utilized tissue culture cell systems may not adequately model neuronal physiology. We also describe in this report a selection-based method for the enrichment of shRNA-expressing primary neurons. For some targeted proteins, we were able to achieve knockdown efficiencies of near 100%, which is a considerable improvement upon previously reported techniques (Zeitelhofer et al., 2007). We have recently developed cell-penetrating peptides targeting the M5i3 domain of interaction with AGAP1, with the aim of using these molecules *in vitro* and *in vivo* to acutely inhibit binding of AGAP1 to M5. In combination with a recently described M5 receptor positive allosteric modulator with >30-fold selectivity over the other four muscarinic receptor subtypes (Bridges et al., 2009), such tools may greatly facilitate the investigation of M5-specific and AGAP1-dependent physiology.

The dysfunction of both M5 receptors and the AP-3 complex have been linked to the pathophysiology of schizophrenia. Schizophrenia is associated with

increased activity of the mesolimbic dopaminergic pathway, and neuroleptic drugs used to treat the disorder typically target the D2 dopamine receptor. The M5 -/- mouse displays abnormalities in schizophrenia-related sensorimotor behaviors, and is hyposensitive to psychostimulants, a condition indicative of a reduction in striatal dopamine levels and consistent with a release-potentiating effect of VTA M5 receptors (Wang et al., 2004; Thomsen et al., 2005; Thomsen et al., 2007). Alterations in synaptic terminal morphology and function, including decreased abundance of the AP-3 associated BLOC-1 protein Dysbindin, have been observed in both schizophrenic humans and in the AP-3 null *mocha* mouse (Talbot et al., 2004; Harrison and Weinberger, 2005). In addition, genetic linkage studies have implicated variations of the M5 (*Chrm5*) and Dysbindin (*Dtnbp1*) genes as conferring susceptibility to schizophrenia, the former in combination with the dopaminergic neuron-expressed α7 nicotinic acetylcholine receptor (*Chrna7*) gene (Schwab et al., 2003; De Luca et al., 2004). While the function of AGAP1 had not been previously associated with the pathology of schizophrenia, we observed binding of Dysbindin to the M5 i3 loop (presumably through an indirect AGAP1/AP-3 interaction), and our data suggest a dopamine release-related functional link between M5 and an AGAP1/AP-3 trafficking protein complex. Intriguingly, a recent genome-wide association study of common variants linked with schizophrenia susceptibility in populations of European ancestry identified the *AGAP1* gene as the strongest single locus association, though below the study's significance threshold ($P<5x10^{-8}$) (Shi et al., 2009). Given these observations, further studies of the relationship between the M5 /

AGAP1 interaction and schizophrenia are warranted, including 1) direct examination of the role of Dysbindin in M5 trafficking; 2) investigation of the dopamine release characteristics of mesolimbic tract terminals in the medioventral striatum of M5Δ mice; 3) behavioral analyses of M5Δ mice; and 4) determination of whether variations in the *Chrm5*, *Dtnbp1*, and *AGAP1* genes interact to confer schizophrenia risk.

8 MATERIALS AND METHODS

8.1 Rodent Strains

All procedures involving animals were performed in accordance with the National Institutes of Health Guide for the Care and Use of Laboratory Animals and were approved by the Rockefeller University Institutional Animal Care and Use Committee. Female adult (3-6 month old) timed pregnant Sprague-Dawley rats were obtained from Charles River Labs or Taconic Labs. Breeding pairs of C57Bl/6N mice were obtained from Charles River, and were bred in-house. The $M5^{-/-}$ strain was a kind gift from Jürgen Wess (National Institute of Diabetes and Digestive and Kidney Disease, Bethesda MD), generated as described (Yamada et al., 2001a). The $M5^{-/-}$ strain was extensively backcrossed (>10 generations) onto the C57Bl/6N background before receipt; mice were maintained as -/- homozygotes, and heterozygote matings were performed when necessary for generation of wild-type littermates. STOCK *gr* +/+ *Ap3d1*^{mh}/J mice carrying the *mocha* allele (*mh*), a spontaneous null mutation of the *Ap3d1* gene (Lane and Deol, 1974; Kantheti et al., 1998), were obtained from the Jackson Laboratory. In this strain, the *Ap3d1mh* allele is maintained on a mixed background in repulsion to the pigmentation mutant *gr* allele. Mice were maintained as heterozygotes, as *mh* homozygotes were observed to be infertile. The *Chrm5*$^{\Delta/\Delta}$ strain was generated and maintained as described below.

8.2 Genotyping of Mice

Tail biopsies (0.5mm) of 3-4 week old weanling mice were solubilized overnight at 55°C in 130μl DirectPCR tail lysis reagent containing 0.75mg/ml proteinase-K (Viagen Biotech). Proteinase K was deactivated at 85°C for 45 minutes, and crude lysates (0.6μl) were used directly as template DNA for PCR reactions (12μl). For PCR genotyping of the $M5^-$ allele (in which the Neo selection cassette was still present (Yamada et al., 2001a)) a single PCR reaction (annealing temp. 55°C) included a set of 3 primers: a Neo-specific forward primer (5'-TGG ATG TGG AAT GTG TGC GAG G), M5wt forward (5'-TCC GTC ATG ACC ATA CTC TA), and an M5 reverse primer (5'-CCC GTT GTT GAG GTG CTT CTA C) in a region of the M5 gene 3' to the NEO disruption. For PCR genotyping of the $M5^{\Delta}$ allele, forward (5'-AAG CCA AGG CCA CTG ACC CTG TCT TTC A) and reverse (5'-CCA GGC CTT TTG TTG AAG GGT CTT TGG ACA) primers flanking the deleted region were used with a 61°C annealing step. PCR products were resolved by electrophoresis through a 2.5% agarose gel and detected by UV illumination in the presence of ethidium bromide. Direct sequencing of M5wt and M5Δ loci was performed on 2 purified PCR products (QIAquick PCR purification kit, Qiagen) spanning the M5 coding sequence amplified from tail DNA prepared as described above. Forward (5'-AGA GGG GAG GTA GCT CCA AAC AGA GAG TAG) and reverse (5'-AGT TGG TAA CCT GCT CAG CCT TTT CCC AGT) primer pairs for the 5' product, and forward (5'-TGG CAG AAG TCA AGA AGA GAA AAC CGG CTC) and reverse (5'-GGC AGA TGA CAT TCC TTT AAC AAG CAA ACC) primer pairs for the 3' product were

amplified with the Expand High Fidelity PCR System (Roche) according to the manufacturer's protocol, with 60.4°C annealing steps. *Mocha* (*+ Ap3d1^{mh} / + Ap3d1^{mh}*), *grizzled* (*gr + / gr +*) and heterozygote (*+ Ap3d1^{mh} / gr +*) mice were identified by coat color phenotype.

8.3 Generation of the M5*Δ369-386* Mutant Knock-in Mouse

Mutant mice carrying an AGAP1-domain-of-interaction deletion mutation in the *Chrm5* gene ("M5Δ") were generated by a homology-based "knock-in" strategy by Ozgene, Inc. Briefly, PCR cloning from C57Bl/6 genomic DNA was used to generate a targeting vector containing a PKG promoter-driven neomycin resistance cassette (Neo) flanked by loxP sites , and 5' and 3' homology arms used to target homologous recombination of the construct to the endogenous M5 locus. The 5' homology arm contained the single M5 exon, in which the region coding for residues 369-386 was deleted by PCR mutagenesis. In order to facilitate screening of target clones, an SphI restriction site was engineered following the 5' LoxP sequence, and KpnI and BglII sites engineered following the 3' LoxP sequence. C57Bl/6-derived ES cells were electroporated with the linearized targeting vector, and neomycin-resistant colonies were selected with G418. Resistant clones were screened for proper homologous recombination by Southern blot using a Neo probe with EcoRV digestion, and probes external to the 5' and 3' targeting regions derived by PCR from C57Bl/6 genomic DNA: 5' probe (SphI digestion), 5'-CTT TAG AAG GAA TGG TTT CAG GGC (forward), 5'-CAT ACC TGG ATG GAA GGA CAT GG (reverse); 3' probe (KpnI digestion), 5'-

CCT TAT TAG CAC TTG TCT GCT TCC G (forward), 5'-AGG CTA TGT AGG TAG GGA GAT GGC (reverse). Integration of the mutant M5$^{\Delta}$ locus was confirmed in targeted ES clones by sequencing, and clones were injected into C57BL/6J-*Tyr^{cBrd}* blastocysts and implanted into pseudopregnant females. Strongly chimeric male mice were crossed to transgenic C57Bl/6-Cre recombinase females, and offspring were tested by Southern blot for transmission of the M5$^{\Delta}$ allele (with 5' and 3' probes as described above) and for excision of the Neo cassette with BglII digestion using a probe directly 5' to the remaining LoxP site (PCR primers for probe were 5'-TGT TAC GCT CTC TGC AAC AGA ACC (forward), 5'-TAT CTG GAG GTG CAA CTG GCT TAC (reverse)). Males carrying the M5$^{\Delta/\Delta Neo}$ allele were crossed to C57Bl/6 females, and offspring of genotype M5$^{\Delta/\Delta Neo}$ / ΔCre were selected for breeding.

8.4 Constructs

The following expression vectors were used: for mammalian expression, pcDNA 3.1(+) myc/His (Invitrogen), pEGFP-N3 and -C2 (BD Biosciences Clontech), and pAAV-MCS (Stratagene); for yeast expression, pACTII, pAS2ΔΔ and pLEX9 (Fromont-Racine et al., 1997); for bacterial expression, pGEX-4T and pGEX-5X (Amersham / GE Life Sciences). For subcloning and/or TA cloning, pCR Zero Blunt and pCR II Topo (Invitrogen) vectors were used, the latter employing Taq polymerase for PCR amplification, and ligated according to the manufacturer's protocol. The following plasmids were kind gifts, and were used as templates for PCR cloning into appropriate expression vectors: pRSET-B-

mCherry (R. Tsien), pCD-hM1,2,& 3 (E. Hulme), pcDNA3.1(-)-rM4 and pCD2-rM2 (T. Bonner).

Plasmid constructs were prepared using standard molecular cloning techniques. PCR amplification was performed with Accuprime Pfx polymerase (Invitrogen), and ligations with the Rapid DNA Ligation Kit (Roche). For amplification of protein coding sequences from mouse, rat or human cDNA libraries, a 2-step nested PCR approach was used to generate PCR products with 5' and 3' restriction sites, allowing direct cloning into expression vectors (primer sets are summarized in table 9.5). Most mammalian expression constructs included a Kozak translation initiation sequence (5'-GCC-ACC-**ATG**-G-3') engineered into the coding sequence start position. mCherry N- and C-terminal fusion mammalian expression vectors were generated by PCR amplification of the mCherry coding sequence and cloning into the XhoI PspOMI or Asp718I and HindIII sites of pcDNA3.1(+) A, respectively. C-myc epitope tags and GFP / mCherry fusions were created by in-frame cloning of cDNA PCR products into appropriate vectors, with stop / start codons omitted as required. N- or C-terminal HA or FLAG epitope tags were introduced by appending PCR primers (HA, 5'- TAT CCA TAT GAC GTC CCA GAC TAT GCC; FLAG, 5'- GAT TAC AAG GAT GAC GAC GAT AAG). Short (<75nt) coding sequences were cloned by ligation of oligo duplexes containing 5' and 3' overhangs into complimentary restriction sites. Sequences of all cloned fragments derived by PCR or oligo duplex ligation were confirmed by sequencing.

Point mutations were generated by site-directed mutagenesis from plasmid DNA template using the Quick Change kit (Stratagene), DpnI digestion of template DNA, and primer sets summarized in table 9.4. Deletion mutants and internal HA tags were generated by amplification of appropriate 5‘ and 3‘ PCR products containing, respectively, complimentary 3‘ and 5‘ sites for the 3’ distal cutter BbsI, and subsequent 3-way ligation into expression vectors. Point- or deletion- mutated regions were validated by sequencing, and restriction fragments containing the desired mutations subcloned into the parent plasmid. Truncation mutants for Y2H domain-of-interaction mapping were generated by PCR from full-length template and cloned into pAS2ΔΔ or pACT2.

Short hairpin RNAs (shRNAs; 19nt) targeting rat AGAP1, AP3β3B, and δ-Adaptin (or non-targeting negative control) were designed using Oligoengine 2 software. Oligonucleotides were annealed and ligated into the BglII and XhoI sites of pSuper.puro (Oligoengine) according to the manufacturer’s protocol. Transcribed shRNAs included a hairpin loop sequence of 5’-UUC AAG AGA, and yielded cleaved dsRNA products of 19nt with 3’ UU overhangs. At least 3 shRNA constructs for each target were created, and validated for target knockdown by immunoblot before use in functional experiments. Targeted sequences used for this study were 5’-ACC CTA GAC GTG TCT CTC C (AGAP1), 5’-AAC GCA TCG ACC TGA TTC A (AP3β3B), GAG GAA ATG AAG ACC ACG C (δ-Adaptin), and 5’-GTT CCG AAC ACA CGC ACA A (non-targeting control).

8.5 RT-PCR

Wild-type, $M5^{-/-}$, and $M5^{\Delta/\Delta}$ mice were sacrificed by CO_2 inhalation, and ventral midbrains were dissected and snap-frozen in LN_2. Tissue was homogenized in 0.6ml TRIzol (Invitrogen) and total RNA extracted and EtOH-precipitated according to the manufacturer's protocol. RNA pellets were dissolved in 45μl nuclease-free ddH_20 and treated with 2U TURBO DNase (Ambion) at 37°C for 30 minutes. DNase was deactivated and RNA isolated by TRIzol extraction / EtOH precipitation, and RNA pellets dissolved in 20μl ddH_20. RNA content was quantified by 260nm absorbance with a Nanodrop spectrophotometer (Thermo Scientific), and 2μg total RNA was denatured and reverse-transcribed with the High Capacity RNA-to-cDNA kit (Applied Biosystems) according to the manufacturer's protocol. Negative control reactions that omitted reverse transcriptase enzyme were performed in parallel. 1μl reverse-transcribed cDNA (or negative controls) was used as template for a PCR reaction performed exactly as described for the genotyping of M5Δ animals.

8.6 Yeast Methods

Saccharomyces cerevisiae haploid strains CG1945, Y187 and L40 were obtained from BD Clontech, and used as described below (genotypes are listed in table 9.7). The bait plasmid pAS2ΔΔ and the prey plasmid pACTIIst were derived from pAS2 and pACTII (BD Clontech), respectively, the former by deletion of the CYH2 gene and HA fusion epitope (Fromont-Racine et al., 1997). The pLEX9 bait plasmid was derived from pBTM116 (Vojtek et al., 1993).

For transformation of yeast with plasmid DNA, cultures were grown in YPD medium at 30°C until log-growth phase (OD_{600} = 0.5-0.8). Cells were collected by centrifugation (2000g, 10 minutes), washed with ddH_20, centrifuged again, and washed in TE-LiOAc (10mM tris, pH=7.5, 1mM EDTA, 100mM LiOAc). Cells were centrifuged and resuspended in TE-LiOAc containing 45% polyethylene glycol, 40μg heat-denatured herring testes carrier DNA, and 1μg plasmid DNA. The transformation mixtures were incubated at 30°C for 45 minutes, heat shocked at 42°C for 15 minutes, and the cells were collected by centrifugation. After a final ddH_20 wash and centrifugation, cells were plated on YNB-agar plates supplemented with appropriate selection mixtures: For pAS2ΔΔ and pLEX9 contructs, CSM-Trp; for pACTII contructs, CSM-Leu; for co-transformation, CSM-Trp-Leu. Yeast plates were incubated at 30°C for 3 days before assay or isolation of clonal inoculum.

β-Galactosidase activity in yeast was determined by an X-Gal lift assay. Yeast colonies were transfered from agar plates to Hybond-C membranes (Amersham / GE Healthcare). Membranes were subjected to 2 freeze-thaw cycles in LN_2 to lyse yeast cells, and were then transferred to filter paper saturated with Z-buffer (60mM Na_2HPO_4, 60mM NaH_2PO_4, 10mM KCl, 1mM $MgSO_4$, pH=7.0) containing 0.35% (v/v) β-mercaptoethanol, 1.67% (v/v) DMF and 0.33 mg/ml X-Gal. Filters were incubated in sealed containers at 37°C for indicated intervals, and X-Gal chromogen development was fixed by incubation of filters in 1M Na_2CO_3 for 1 minute, followed by a 1 minute rinse in ddH_2O.

Yeast two-hybrid (Y2H) screens were performed using a mating protocol as previously described (Fromont-Racine et al., 1997; Flajolet et al., 2000). Y187 yeast was transformed as described above with pACTIIst or pACTII cDNA libraries (rat and human, respectively), in which cDNAs were cloned-in frame with the Gal4 AD. For each library, 20 million transformant colonies were collected, pooled in YPD, and frozen in aliquots at -80°C. Rat or human MR i3 loops were cloned into pAS2ΔΔ or pLex9 vectors in-frame with the Gal4 or LexA DNA BD, respectively, and transformed into the CG1945 or L40 strains, respectively. For each screen, transformed bait strains were cultured to log growth in YNB + CSM-Trp, and then mixed with a single thawed vial of the appropriate prey library strain. Yeast were plated onto YPD-agar plates, and mating was allowed to proceed for 4.5 hours at 30°C. Yeast was then collected in ddH_20 and distributed to 40 YNB-agar +CSM-Trp-Leu-His plates. A small amount of each screen was reserved for plating on control YNB-agar+CSM plates: -Trp, total bait CFUs; -Leu, total prey CFUs; and -Trp-Leu, total diploids (measuring mating efficiency). Screen plates were incubated at 30°C for 3-4 days, until interaction-positive diploid colonies were observed on the *His* -selective media. [His+] colonies were counted, and then assayed for activation of the *LacZ* reporter by X-Gal overlay: 10ml of warm liquid X-Gal mixture (0.5% (w//v) agar, 0.1% (w/v) SDS, 6% (v/v) DMF, 0.04% (w/v) X-Gal was poured on each of the screen plates, allowed to solidify, and incubated at 30°C for 30 minutes to 18 hours (depending on speed of color development). Blue colonies were then streaked onto -Trp-Leu-His plates, grown for 3 days at 30°C, and β-Galactosidase activity was confirmed by

lift assay as described above. Yeast cells from [His+][LacZ+] clones were collected, lysed by heat and mechanical disruption, and cDNA library fragments from pACTII plasmid DNA were amplified by PCR with the primer set 5'-CGC GTT TGG AAT CAC TAC AGG GAT G (forward) and 5'-GAA ATT GAG ATG GTG CAC GAT GCA C (reverse). PCR products were sequenced and analyzed by BLAST. Clones with in-frame ORF sequences were cultured for 3 passages in liquid YNB+CSM-Trp media, yeast was collected at log-phase growth by centrifugation, extracts were prepared by heat and mechanical disruption of cells, and DNA purified by NH_4OAc precipitation. Rescued prey plasmid was transformed into *E. coli*, amplified, and purified with standard techniques.

8.7 Mammalian Cell Culture and Transfection

Mammalian tissue culture cell lines unavailable from Greengard Lab cryopreserved stocks were obtained from the American Type Culture Collection. Cells were maintained in a humidified 5% CO_2 atmosphere incubator, passaged by trypsinization (0.25% [w/v] trypsin, 1mM EDTA in HBSS [Invitrogen]) every 3-4 days, and were cultured in the following media: HEK-293T, COS7 and A2058, 10% (v/v) in DMEM; CHO, 10% FBS in F12K; NIH-3T3, 10% BCS in DMEM; RIN-m5f, 10% FBS in RPMI-1640. Cells were transfected with plasmid DNA according to the manufacturer's protocols using Lipofectamine 2000 (Invitrogen) for NIH-3T3 and RIN-m5f cells, or Fugene6 (Roche) for all other cell lines. Lipofectamine 2000 was used for transfection of siRNA (Stealth; Invitrogen) in all cell lines, with the medium GC Stealth control duplex (Invitrogen) used for

negative controls. Stable transfection of neomycin resistance-containing plasmids in CHO or HEK-293T cells was achieved by selection with 1mg/ml G-418 (Invitrogen) 72 hours after transfection. After die-off was complete (approximately 10 days), G-418 was reduced to a maintenance concentration of 100μg/ml, and individual clones were selected for growth by dilution plating and subsequent cloning ring isolation.

8.8 Rat Hippocampal Neuron Primary Culture and Transfection

The culture of embryonic rat hippocampal neurons was performed essentially as described (Goslin et al., 1998). Hippocampi from embryonic day 18-19 Sprague-Dawley rat embryos were dissected into 4°C Ca^{+2} / Mg^{+2} -free HBSS. The collected tissue was dissociated in 0.25% (w/v) trypsin / 1mM EDTA / HBSS at 37°C for 30 minutes. Hippocampi were rinsed twice in plating media (Neurobasal medium [Invitrogen] containing 10% (v/v) FBS and 0.5mM L-glutamine), dissociated by trituration with a fire-polished Pasteur pipette, strained through a 40μm filter, and collected by centrifugation. Cells were counted and plated (at 10,000 cells / cm^2 or 50,000 cells / cm^2 for transfection experiments) in plating media on either poly-L-Lysine -coated glass coverslips (BD Biosciences) or poly-L-Lysine (PLL) -coated glass-bottomed dishes (Mattek) that had been re-coated with 1mg/ml PLL. Cells were cultured in 24-well dishes at 37°C in a humidified 5% CO_2 tissue culture incubator. After 24 hours, plating media was replaced with NBM complete media (Neurobasal medium containing 2% B27 and 1% N2 supplements [Invitrogen], 0.5mM L-glutamine, and 10μM

5-fluorodeoxyuridine [FDU]). Subsequently, 50% of the media was changed every 5-6 days.

Mature hippocampal neurons (DIV 10-13) were transfected according to a modified calcium phosphate method (Jiang and Chen, 2006) using a commercial transfection kit (Invitrogen). Growth media was reserved and replaced with new NBM complete. Plasmid DNA (1μg) combined with $CaCl_2$ was added slowly to 2x HBS, mixed gently, and incubated for 15-20 minutes. Precipitates were added to coverslips or glass-bottomed dishes, and neurons were incubated for 2.5 hours. Media was then removed and replaced with NBM complete previously equilibrated in a 10% CO_2 incubator, after which dishes were immediately returned to the 5% CO_2 incubator. After 30 minutes, precipitates were observed to be largely dissolved and the acidulated media had returned to normal pH; media was then replaced with reserved NBM complete. Experiments were performed on neurons 24 hours after transfection.

8.9 Rat Cortico-hippocampal Culture and Nucleofection

Rat embryonic cortico-hippocampal tissue was dissected, trypsinized, and dissociated as described above, except that trypsinization proceeded for 1 hour, and 10% (v/v) FBS in DMEM was used as plating media. Cells were centrifuged, and media was aspirated and replaced with 100μl supplemented rat neuron nucleofection solution (Amaxa) per 5 million cells, according to the manufacturer's protocol. DNA (either 3μg receptor-coding plasmid, or 2μg each receptor-coding and shRNA-coding) along with 100μl cell suspension was added

to an amaxa cuvette and electroporated with program O-03. Cells were immediately removed to FBS/DMEM, and plated in 24-well dishes pre-coated with 0.1mg/ml PLL. Plating density was 1 million cells / well for shRNA experiments, and 800,000 cells / well for all other experiments. After 24 hours, media was removed and replaced with NBM complete. For shRNA experiments, NBM complete was supplemented with 1μg/ml puromycin. Cultures were maintained for up to 14 days, with 50% media changes (NBM complete) performed every 3 days.

8.10 Mouse Midbrain Dopaminergic Neuron Culture

Mouse midbrain dopaminergic cultures were prepared according to the method of Sulzer (Rayport et al., 1992) with modifications (Brewer and Torricelli, 2007). One to three- day old mouse pups were euthanized by CO_2, and sterilized by immersion in 70% EtOH. Brains were removed to ice-cold HABG media (Hibernate-A media (BrainBits LLC) supplemented with 2% B27 and 0.5mM L-glutamine), meninges were removed, and ventral midbrains were dissected and chopped. Tissue was rinsed in Hibernate-A -Ca^{+2} (BrainBits LLC), and then digested with 34 units / ml papain (Worthington) in Hibernate-A -Ca^{+2} containing 0.5mM kynurenic acid (Sigma) with stirring for 1.5h at 37°C. The digested tissue was then rinsed twice in HABG, and dissociated by 3 rounds of trituration with a fire-polished Pasteur pipette followed by straining through a 40μm filter. Cells were collected by centrifugation and resuspended in DAergic media (Neurobasal-A [Invitrogen] containing 2% B27, 0.5mM L-Glutamine,

0.5mM kynurenic acid, 1mM HCl, and 1% (v/v) heat-inactivated FBS). Viable cells were indicated by trypan blue dye exclusion, counted, and cells were plated on PLL -coated glass coverslips at a density of 100,000 cells / coverslip. 24 hours after plating, coverslips were moved to new DAergic media containing 10ng/ml GDNF (Millipore). One to two days later (or when glia were observed to be nearly confluent), 10μM FDU was added; 50% media changes were performed every 3 days thereafter.

8.11 Immunoblotting and Sample Preparation

Rodent brain lysates were prepared in RIPA buffer (PBS, pH=7.4, 1% (v/v) Triton X-100, 0.5% (w/v) sodium deoxycholate, 0.1%(w/v) SDS, 1% (v/v) protease inhibitor cocktail III (Calbiochem), 0.5mM PMSF) including phosphatase inhibitors (50mM NaF, 200μM Na_3VO_4, 2mM EDTA, 5mM $Na_4P_2O_7$) by homogenization in a Potter-Elvehjem tissue grinder, incubation at 4°C for 1 hour, and centrifugation at 20,000xg for 30 minutes (pellets were discarded). Lysates from other tissues were prepared as indicated. When required, protein content was determined with a bicinchoninic acid (BCA) assay kit (Pierce / Thermo Scientific). Samples were resuspended in 1x LDS buffer (Invitrogen) containing 100mM DTT and incubated at 70°C for 10 minutes. Samples to be blotted for muscarinic receptors were incubated at 24°C for 1 hour, as heating led to aggregation of receptor protein. Reduced samples were loaded onto NuPage Bis-Tris 4-12% polyacrylamide gels (Invitrogen), separated by SDS-PAGE, and electro-transferred to nitrocellulose membranes. To visualize transferred

proteins, membranes were rinsed in ddH_2O, incubated in 0.5% ponceau red / 5% HOAc for 1 minute, rinsed in ddH_2O, and scanned. For visualization by enhanced chemiluminescence (ECL), membranes were blocked either 1h at 24°C or overnight at 4°C in PBST (0.1% Tween-20 in PBS, pH=7.4) containing 5% nonfat dry milk (w/v). Membranes were then incubated with primary antibodies (see table 8.2) diluted in blocking buffer for either 1 hour at 24°C or overnight at 4°C, followed by 4 washes with PBST. Appropriate horseradish peroxidase-conjugated secondary antibodies (Jackson ImmunoResearch) were diluted in PBST (1:10,000) and incubated with membranes for 1h at 24°C, followed by 4 washes in PBST and a final rinse in PBS. Immunoreactive signals were detected by ECL (Perkin Elmer) and exposure to BioMax XAR film (Kodak). For ECL detection of M3-phospho-S577, 3% (w/v) BSA / 0.1% (v/v) Tween-20 / TBS (pH=8.0) was used for blocking and dilution of primary antibody. For detection by infrared fluorescence, membranes were blocked in Odyssey blocking buffer (Li-Cor Biosciences) for 1 hour at 24°C, followed by overnight incubation at 4°C with antibodies diluted in Odyssey blocking buffer containing 0.1% Tween-20. After washing, blots were incubated 45 minutes with IR-dye conjugated secondary antibodies diluted in Odyssey blocking buffer / 0.1% Tween-20. Membranes were then washed and visualized by scanning on an Odyssey infrared imager (Li-Cor Biosciences) for fluorescent emission at 680 and 800 nm.

8.12 Coomassie Staining

Samples were prepared and separated by SDS-PAGE as for immunoblotting. Gels were either stained 1 hour in 40% (v/v) MeOH / 10% (v/v) HOAc / 0.25% (w/v) Coomassie R-250, followed by overnight destaining in 40% MeOH / 10% HOAc, or rinsed 3 times in ddH_2O, followed by 1 hour staining in SimplyBlue SafeStain (Invitrogen) followed by overnight destaining in ddH_2O.

8.13 Immunofluorescence Staining

Cells grown on glass coverslips were rinsed and fixed either in 4% (w/v) paraformaldehyde / 4% (w/v) sucrose in PBS (pH=7.4) for 30 minutes at 24°C , or with -20°C MeOH for 2.5 minutes, followed by rinsing in PBS. In some cases, cells were pre-extracted before fixation with 0.03% saponin in cytosolic buffer (25mM HEPES-KOH, pH=7.4, 25mM KCl, 2.5mM Mg acetate, 5mM EGTA, 150mM K-glutamate) for 30 seconds at 37°C, rinsed at 37°C with intracellular buffer, and fixed for 30 minutes at 24°C with 4% (w/v) paraformaldehyde in cytosolic buffer (Morris and Cooper, 2001). Fixed cells were permeabilized with 0.25% (v/v) Triton X-100 in PBS for 10 minutes, rinsed in PBS, and blocked for 30 minutes in antibody diluent (2% [w/v] BSA, 0.05% (v/v) Triton X-100, 0.02% NaN_3 in PBS), followed by incubation with primary antibodies diluted in antibody diluent for either 1.5 hours (24°C) or overnight (4°C) in a humidified chamber (table 8.1). Coverslips were washed 4 times in PBS containing 0.05% (v/v) Triton X-100, and were incubated with appropriate fluorescent dye - conjugated secondary antibodies diluted in antibody diluent for 45 minutes at 24°C. After

washing, coverslips were mounted in Fluoromount-G (Southern Biotech) and imaged with a LSM510 confocal system (Zeiss Microimaging) using either 40x 1.3NA or 100x 1.4NA oil objectives. In some cases, staining was limited to extracellular epitopes by eliminating the permeabilization step and excluding all detergents from the staining procedure.

8.14 Live Imaging of Primary Cultured Hippocampal Neurons

Primary cultures of embryonic rat hippocampal neurons were prepared as described above, and plated on glass-bottom tissue culture dishes (MatTek). DIV 10-13 cultures were transfected with GFP- and/or mCherry- tagged expression constructs by the calcium phosphate method. Twenty four hours after transfection, media was replaced with imaging buffer (Hibernate-E low fluorescence [BrainBits LLC], 2% B27, 0.5mM L-glutamine) and pre-incubated 30 minutes at 37°C in an ambient CO_2 incubator. Cells were imaged at 37°C with a Axiovert 200M microscope (Zeiss Microimaging) equipped with an UltraView spinning disk confocal head (Perkin Elmer), EMCCD camera (Hamamatsu), piezo-actuated specimen stage (Prior Scientific) and 100X 1.46NA α-Plan-Apochromat objective (Carl Zeiss Microimaging). CCh (1mM) was added to the imaging buffer as indicated. Near-simultaneous GFP and mCherry emission was detected with a FITC / Texas Red filter set, respectively, and acquired and analyzed using Metamorph software (Molecular Devices).

8.15 Production of Recombinant GST-fusion Protein

Desired cDNA fragments were cloned into pGEX 4T or 5X vectors in-frame with the glutathione-S-transferase (GST) coding sequence (under transcriptional control from the *Lac* operon) as described above, and transformed into the *E. coli* strain BL21(DE3)pLysS. Cultures were grown at 37°C in Luria-Bertani media until log-phase, induced with 1mM of the allolactose analogue IPTG, and incubated at 24°C for 3 hours. Bacteria were collected by centrifugation, and lysed by a freeze-thaw cycle in LN_2 followed by incubation at 4°C in lysis buffer (PBS, pH=7.4, 1% (v/v) Triton X-100, 1mM DTT, 1% (v/v) protease inhibitor cocktail III (Calbiochem), 0.5mM PMSF, 1 mg/ml lysozyme). The lysate was sonicated to disrupt genomic DNA, and was then cleared by centrifugation at 20,000g for 30 minutes. Recombinant GST-fusion proteins were then purified by batch affinity chromatography using Glutathione Sepharose 4B (Amersham / GE Life Sciences) at 4°C for 12 hours. The affinity matrix was then washed 3 times in lysis buffer with decreasing detergent concentrations (0.5%, 0.1%, 0%), and then stored at -20°C in 1:1 (v/v) PBS:glycerol. Purity, integrity, and concentration of recombinant GST proteins were analyzed by SDS-PAGE and coomassie staining as described above (with standardized BSA included as necessary for quantification).

8.16 GST Pulldown Assay

For pulldown of exogenously expressed proteins, COS-7 or HEK-293 cells were transfected with c-myc -tagged protein expression plasmids as indicated.

48 hours later, cells were lysed for 1 hour at 4°C in L-100 buffer (PBS, pH=7.4, 100mM KCl, 0.5% (v/v) Triton X-100, 1mM DTT, 1% (v/v) protease inhibitor cocktail III (Calbiochem), 0.5mM PMSF). Lysates were cleared by centrifugation, a sample was reserved ("input"), and remaining lysate (1ml) was incubated with 5μg glutathione sepharose-bound GST fusion proteins overnight at 4°C. Alternatively, [35S]methionine-labeled proteins were prepared from cDNA templates using the TNT quick coupled transcription-translation kit as described for the phospholipid binding assay, and labeled proteins were diluted in L-100 buffer and incubated with sepharose-bound GST proteins as described above. The affinity matrix was washed 3 times for 5 minutes at 4°C with respective lysis buffers, and bound proteins were eluted in 2X LDS loading buffer / 100mM DTT. Eluted and input samples were processed for immunoblotting as described above, with GST fusion protein content verified by ponceau staining, and bound proteins detected by anti-HA 3F10, rabbit anti-GFP, or anti-c-myc 9E10 primary antibodies as indicated.

For pulldown of endogenously expressed proteins from rodent brain lysates, whole mouse or rat brains were homogenized in L-100 buffer containing 0.1% (v/v) Triton X-100 with a Potter-Elvehjem tissue grinder and incubated at 4°C for 1 hour. Lysates were cleared by centrifugation at 20,000g for 30 minutes, Triton X-100 concentration was adjusted to 0.5% (v/v), and GST-pulldown experiments were performed as described above, except using 40μg GST fusion proteins per 1ml lysate, performing 2 washes, and using indicated primary antibodies against endogenous rodent brain proteins as indicated.

8.17 Co-Immunoprecipitation

For co-immunoprecipitation of proteins with muscarinic receptors, tissue culture cells (HEK-293T, COS-7, CHO) or primary cultured rat cortico-hippocampal neurons were transfected / nucleofected with expression vectors for GFP- or HA- tagged MRs with or without co-transfection / co-nucleofection of myc-tagged putative interacting protein expression plasmids as indicated. Cells were treated with CCh as indicated, and were lysed on ice in Co-IP buffer (50mM Tris-HCl, pH=8.0, 50mM NaF, 200μM Na3VO4, 1% (v/v) protease inhibitor cocktail III (Calbiochem), 0.5mM PMSF) including either 0.86% (w/v) digitonin / 0.17% (w/v) Na Cholate, 1% (w/v) CHAPSO, or 0.5% (w/v) Triton X-100. For cross-linking experiments, cells were rinsed twice in PBS, incubated with 0.2 mg/ml of the disulfide-cleavable bifunctional crosslinker Dithiobis[succiniminyl propionate] (DSP) (Pierce / Thermo Scientific) for 20 minutes at 24°C, washed/quenched for 15 minutes in TBS, and solubilized in RIPA buffer. Lysates were cleared by centrifugation, an aliquot was reserved ("input"), and lysates were incubated with anti-GFP antibodies (1:500 rabbit polyclonal ab290 (Abcam); mouse monoclonal (19C8 10.2ul 19F7 3.4ul) (M. Heiman)) or 20ul HA.11-agarose slurry (Covance) for 3 hours at 4°C. GFP immunocomplexes were precipitated by incubation with protein A- (Amersham / GE Life Sciences) or protein A/G- (Pierce / Thermo Scientific) sepharose for 2 hours at 4°C, all resins were washed 3 times in respective lysis buffer (or 0.1% (w/v) digitonin), and proteins eluted by incubation at room temperature with LDS loading buffer / DTT

as described above. Samples were analyzed by immunoblotting for immuno- and co-immuno- precipitated proteins as described above.

Co-immunoprecipitation of AP-3 components with myc-tagged AGAP1 was performed as previously described (Nie et al., 2003). Briefly, NIH-3T3 cells transfected with expression plasmids encoding full length or truncated AGAP1-myc were lysed in 3T3 buffer (25mM tris, pH=8.0, 100mM NaCl, 1% (v/v) Triton X-100, 10% (v/v) glycerol, 1% (v/v) protease inhibitor cocktail III (Calbiochem), 0.5mM PMSF) with 3 freeze-thaw cycles in LN_2. Lysates were cleared by centrifugation, and then incubated with 20μl / ml anti-myc 9E10 agarose (Covance) for 14 hours at 4°C. The affinity matrix was washed 3 times with 3T3 buffer, proteins were eluted with LDS sample buffer / DTT at 70°C, and samples analyzed by immunoblotting as described above.

8.18 Subcellular Fractionation Experiments

Subcellular fractionation of cultured primary neurons by glycerol velocity gradient centrifugation was performed essentially as described (West et al., 1997b). Rat cortico-hippocampal neurons (25 million cells) were nucleofected with indicated M5 expression plasmids, plated in PLL-coated 100mm dishes, and cultured as described above for 14 days. A 7-step 5-30% (v/v) gradient of glycerol in SV buffer (10mM HEPES pH=7.4, 150mM NaCl, 1mM EGTA, 1mM $MgCl_2$) was prepared and allowed to diffuse at 24°C for 2 hours during membrane preparation. Cells were treated with 0.1mM CCh for 1 hour, washed once in SV buffer, collected in SV buffer, and pelleted by centrifugation at 5500g

for 5 minutes. Pellets were resuspended in ice-cold ddH_20, homogenized with 12 strokes of a teflon-glass homogenizer at 500 rpm, adjusted to 1X SV buffer, and centrifuged at 1000g for 5 minutes. The supernatant was collected, supplemented with 1% (v/v) Protease Inhibitor Cocktail III (Calbiochem) and 0.5mM PMSF, loaded on top of the previously prepared glycerol gradient, and was ultracentrifuged for 66 minutes at 48,000 rpm in a sw50.1 rotor (Beckman Coulter). Fractions (8) were unloaded from the top of the gradient. For immunoblot analysis, fraction volume was adjusted to 1.3ml with SV buffer, fractions were ultracentrifuged for 2 hours at 150,000g, pellets were solubilized in LDS sample buffer / 100mM DTT, and samples were processed as described above. For analysis of M5 content by radioligand binding, fractions (250μl) were diluted to a total volume of 500μl with SV buffer, and incubated with 1nM [3H]3-quinuclidinyl benzilate (Perkin Elmer) for 1 hour at 37°C. Non-specific binding was determined in the presence of 1μM atropine. Samples were collected by vacuum filtration on GF/B glass fiber filters (Whatman) presoaked 1 hour in 0.05% (w/v) polyethylenimine. Filters were rapidly washed with 5ml ice-cold SV buffer, dried, and bound radioactivity determined by liquid scintillation spectrometry.

Analysis of M5 transport to lysosomes was performed by self-forming Percoll density gradient centrifugation essentially as described (Schaub et al., 2005). Rat cortico-hippocampal neurons (15 million cells) were nucleofected with M5wt-GFP and M5Δ-GFP and cultured for 19 days as described. Cells were treated with 1mM CCh in the presence of the lysosomal protease inhibitor

leupeptin (Sigma; 100μM) for 4.5 hours. Cells were collected in HB (250mM sucrose, 1mM EDTA) and homogenized by 12 passes through a 1-ml syringe attached to a 25-gauge needle. Homogenates were adjusted to 1.7ml with HB and centrifuged for 10 minutes at 370g. The post-nuclear supernatant was loaded on top of 8.5ml 17.5% (w/v) Percoll (sigma) / 1X HB, underlayered with 1.2ml 10X HB, and centrifuged for 30 minutes at 26,500g in an SS-34 rotor (Sorvall / Thermo Scientific). Nine 1.2ml fractions were collected from the top of the gradient, and fractions were ultracentrifuged at 200,000g for 30 minutes. Membrane layers were collected, solubilized in 1X LDS/DTT, and analyzed by immunoblotting as described above.

Fractionation of rat brain homogenate by density gradient using the iso-osmotic centrifugation medium iodixanol was performed generally as described (Lee et al., 2003). 1/2 of an adult female rat brain was homogenized in HM (0.25M sucrose, 20mM tris, pH=7.4, 1mM EDTA, 1mM EGTA) with a tight-pestle dounce homogenizer (20 strokes) followed by passage through 20- and 25-gauge needles (20 and 10 times, respectively). Homogenates were centrifuged for 10 minutes at 500g, and then the post-nuclear supernatant adjusted to 25% (w/v) iodixanol (OptiPrep; Axis-Shield) / 1X HB and overlayered with an iodixanol / 1X HB step gradient (20, 18.5, 16.5, 14.5, 12.5, 10.5, 8.5, 6.5, 5% (w/v)). Gradients were centrifuged at 27,000 RPM for 20 hours at 4°C in an SW41 rotor (Beckman Coulter), and 26 fractions collected from the top. Fractions were solubilized in LDS sample buffer / DTT and analyzed by immunoblot as described above.

8.19 [N-methyl-3H]-Scopolamine Radioligand Binding Assay

For experiments in tissue culture cells, cells were plated in 12- or 24-well dishes pre-coated with PLL. For transient plasmid transfection or siRNA experiments, cells were transfected 24 hours after plating with expression plasmids or siRNA duplexes as described above. Forty eight hours after transfection, cells were treated as indicated, transferred to ice, and washed once in ice-cold HEPES-HBSS (118 mM NaCl, 5mM KCl, 1mM CaCl2, 1mM MgCl2, 5mM Glucose, 15mM HEPES, pH=7.4). Cells were incubated for 3 hours at 4°C in HHBS containing 1nM of the cell-impermeant MR antagonist [N-methyl-3H]-scopolamine ([3H]NMS; Perkin Elmer). For heterologous competition binding experiments, various concentrations of unlabeled drugs were added. Non-specific binding was determined by addition of 10μM benztropine mesylate (Sigma). Binding was terminated by aspiration and 3 rapid washes with ice-cold HEPES-HBSS. Cells were solubilized overnight in 0.1% SDS, lysates were removed to vials containing 5ml scintillation cocktail (Ready-Safe, Beckman Coulter) and total radioactivity measured by liquid scintillation spectrometry. Assays were performed in triplicate, with specific binding determined by subtraction of NSB from all values. Non-linear regression analysis of competition binding data was performed with curve-fitting software (GraphPad Prism). When indicated, cell lysates were collected in RIPA buffer and stored at -20°C.

For radioligand binding experiments in primary cultured rat neurons, mature cultures (DIV 12-13) were assayed essentially as described above.

Neurons were nucleofected before plating with expression and/or shRNA plasmids as indicated. Heterologous [3H]NMS competition binding pilot experiments examining IC50 values of the muscarinic antagonist AF-DX 384 (Tocris) in control-, M5wt-, and M5Δ- nucleofected cultures were performed as described above. Thereafter, all M5 [3H]NMS binding experiments were performed in the presence of 5μM AF-DX 384. M5-specific [3H]NMS binding was defined by subtracting control (empty vector) values from those of M5wt- or M5Δ- nucleofected wells. All assays were performed in triplicate.

8.20 Muscarinic Receptor Internalization and Recycling Assays

For experiments in tissue culture cells, cells were pre-incubated 2 hours in growth media containing 10μg/ml cycloheximide (CHX) in order to arrest synthesis of receptor proteins. CHX was included in all washes and incubations thereafter. To induce receptor endocytosis, the non-hydrolyzable acetylcholine analogue carbachol (CCh) (100μM) was added, and cells were incubated for various times. To measure recycling of internalized muscarinic receptors, CCh-treated cells were rinsed 3 times in 37°C Ca^{2+}- and Mg^{2+}- free HBSS, and then incubated in CCh-free growth media for various times. At the end of the treatment period, cells not subjected to recycling conditions were rinsed 3 times in 37°C HBSS, all wells were washed with ice-cold HEPES-HBSS, and cells were assayed for surface muscarinic receptor binding with [3H]NMS as described above.

For experiments in primary cultured neurons, growth media was replaced with HABG (pH=7.3) and cells were pre-incubated 1 hour at 37°C in an ambient-CO_2 incubator. For Brefeldin-A (BFA) inhibition experiments, cells were pre-incubated 2 hours in HABG with (5μM) BFA or EtOH solvent only; BFA / EtOH was also present in all subsequent washes and incubations. Internalization was induced by incubation with 100μM CCh for 30 minutes. Recycling of internalized receptors was induced by washing 3 times with with 37°C MOPS rinse buffer (10mM MOPS, pH=7.3, 90mM NaCl, 1.8 mM $CaCl_2$, 5.4 mM KCl, 0.8mM $MgCl_2$, 0.9mM $NaHCO_3$, 0.9mM NaH_2PO_4, 25mM glucose) and incubation for 1 hour in new HABG. Control- and non-recycled- wells were rinsed 3 times with MOPS rinse buffer, all cells were washed with ice-cold HEPES-HBSS, and surface [3H]-NMS binding was performed as described above. For K+ depolarization treatments, cells were treated with depolarization buffer (10mM MOPS, pH=7.3, 45mM KCl, 50.4mM NaCl, 0.8mM $MgCl_2$, 0.9mM $NaHCO_3$, 0.9 mM NaH_2PO_4, 25mM glucose) for 1 or 5 minutes, with or without standard media washout as indicated.

8.21 Mouse Cerebral Vasculature Isolation and Radioligand Binding

Microvessels from wild-type, $M5^{\Delta/\Delta}$ and $M5^{-/-}$ mouse brains were isolated according to a published protocol (Jung and Levy, 2005). Two mice from each genotype were sacrificed by CO_2 inhalation, and pooled brains were minced in ice-cold DMEM / 20mM HEPES (pH=7.5). Tissue was collected by centrifugation (5 minutes, 500g) and digested in 0.05% collagenase/dispase (Roche) in PBS for

30 minutes at 37°C. The digestions were stopped by addition of 1mM EDTA, and tissue was collected by centrifugation (10 minutes, 1000g) and resuspended in DMEM / HEPES containing 17% dextran (molecular weight 60,000-90,000 daltons; Sigma). Tissue suspensions were centrifuged for 30 minutes at 10,000g, and blood vessel-containing pellets were collected, resuspended in 4°C THM buffer (50mM Tris-HCl, pH=7.4, 2mM $MgCl_2$) and re-centrifuged at 10,000g for 15 minutes. Pellets were resuspended in 2.5ml THM, homogenized with a Polytron device (Kinematica GmbH), and total protein measured by BCA assay. Vessel homogenates were adjusted for equal protein content, and incubated in triplicate with 1nM [3H]NMS at 4°C for 3 hours. Non-specific binding was defined by the addition of 10μM benztropine mesylate. Binding was terminated by centrifugation at 10,000g for 5 minutes at 4°C. The supernatant was aspirated, tubes rapidly washed with 1.5ml ice-cold THM buffer, and pellets incubated in 0.1% SDS overnight. [3H] content in solubilized pellets was measured by liquid scintillation spectrometry, and specific [3H]NMS binding determined by subtraction of non-specific DPM values from total binding.

8.22 MAP Kinase Activation Assay

HEK-293T cells transfected with MR-coding constructs were grown to confluence in 24-well dishes and pretreated 30 minutes in serum-free Opti-Mem (Invitrogen). Cells were treated with various concentrations of CCh for 10 minutes, rinsed once in ice-cold PBS, and lysed in phospho-triton buffer (PBS pH=7.4, 0.5% Triton X-100, 2mM EDTA, 200μM Na_3VO_4, 50mM NaF, 5mM

$Na_4P_2O_7$, 1% (v/v) protease inhibitor cocktail III (Calbiochem), 0.5mM PMSF) at 4°C for 1 hour. Lysates were cleared by centrifugation at 10,000g for 15 minutes and processed for immunoblotting as described above. Total and phosphorylated (pT202 / pY204) forms of p44/42 MAP kinase were detected by Odyssey imaging (Li-Cor) with indicated antibodies.

8.23 Inositol Monophosphate Accumulation Assay

Activation of PLC-β by $G\alpha_q$-coupled MRs was monitored via the accumulation of the D-*myo*-inositol 1,4,5 triphosphate metabolite inositol monophosphate (IP1) in the presence of the inositol monophosphatase inhibitor LiCl (Trinquet et al., 2006). HEK-293T cells plated on poly-L-lysine -coated 24-dishes were transfected with MR expression plasmids (0.25μg/well). Forty eight hours later, growth media was replaced with IP-One stimulation buffer (10mM HEPES , pH=7.4, 1mM CaCl2, 0.5mM MgCl2, 4.2mM KCl, 146 mM NaCl, 5.5 mM glucose, 50mM LiCl) containing various concentrations of carbachol. After 1 hour of incubation at 37°C, cells were lysed and assayed for IP1 content with the IP-One ELISA kit (Cisbio) according to the manufacturer's protocol. Unknown IP1 values were interpolated from a standard curve, and EC50 values for CCh determined by curve-fitting to a dose-response model with nonlinear regression software (GraphPad Prism).

8.24 Fluo-3 Calcium Assays

Fluorometric measurement of intracellular Ca^{2+} concentration was performed essentially as described (Cypess et al., 1999). CHO cells transfected with MR expression plasmids 48 hours previously were harvested in PBS and incubated at 37°C for 1 hour. Cells were collected by centrifugation at 2000g for 2 minutes, and washed 3 times in EBSSH-P (26mM HEPES, pH=7.4, 125mM NaCl, 5mM KCl, 1mM $MgSO_4$, 1mM NaH_2PO_4, 5.6mM glucose, 2mM $CaCl_2$, 0.1% (w/v) BSA, 2.5mM probenecid (Invitrogen)). Cells were resuspended in EBSSH-P and loaded with 2μM of the cell-permeant fluorescent Ca^{2+} indicator Fluo-3/AM (Invitrogen) for 1 hour at 24°C. Cells were washed once in EBSSH-P, and pre-treated with 100μM CCh for 30 minutes when indicated. Cells were washed twice more, resuspended in 1.5ml EBSSH-P, and Fluo-3 fluorescence (excitation = 505nm, emission = 525nm) was monitored with a F-2000 fluorescence spectrophotometer (Hitachi) with constant stirring. MR stimulation with 100μM CCh was performed after baseline fluorescence values had been established (1 minute or greater). At the end of recordings, fluorescence maxima and minima (E_{max} and E_{min}) were determined by cell lysis (.07% (v/v) Triton X-100) and Ca^{2+} chelation (5mM EGTA, 37.5mM Tris, pH=8.7), respectively. Fluorescence emission at each 0.1 second time point was normalized to E_{max} and E_{min} and data were plotted as F/F_0 ratios.

8.25 *In situ* Hybridization

15μm thick coronal and sagittal sections of fresh-frozen C57Bl/6 wild-type mouse brain were mounted on slides, fixed in 4% paraformaldehyde for 10 minutes, rinsed in PBS, acetylated with acetic anhydride in triethanolamine buffer for 10 minutes, rinsed in PBS, dehydrated in ascending concentrations of EtOH, and dried. A 772-bp region of the AGAP1 3' UTR was amplified from a mouse brain cDNA library by PCR (forward 5'-AAG TTG CAA CCA CCA CGT GAG TCC CTC AGT TCC CTC, reverse 5'-CCA AGT AAG GGG ACT GAA GTC AAA TAA TAC CCA GC) and cloned into pCRII. The plasmid was linearized and used as template to prepare [33P]-labeled riboprobe using a Maxiscript kit (Ambion) and either T7 (sense) or SP6 (antisense) RNA polymerase. Riboprobes were column purified (NucAway, Ambion), and prepared slides were hybridized for 17 hours at 60°C with $1x10^6$ Ci of probe in hybridization buffer (50% (v/v) formamide, 0.6M NaCl, 50μg/ml salmon sperm DNA, 1X Denhardt's solution (Invitrogen), 10% (w/v) dextran sulfate, 250μg/ml tRNA, 100mM Tris-Cl pH=8, 2mM EDTA). Slides were washed 3 times for 5 minutes with 2X SSC (30mM Na citrate, pH=7.0, 300mM NaCl) and treated for 1 hour at 37°C with RNase A (2μg/ml). Slides were rinsed twice in ddH_2O, washed once in 2X SSC for 20 minutes, washed once each in 0.5X and 0.2X SSC at 50°C for 30 minutes, dehydrated in ascending concentrations of EtOH, dried, and exposed to Kodak MR film at -80°C.

8.26 Northern Blotting

For the mAGAP1 Northern blot, antisense [33P]-labeled riboprobe to the AGAP1 3'-UTR was synthesized and purified as described for *in situ* hybridization. A mouse Multiple Tissue Northern blot (BD Biosciences) was pre-hybridized in Ultrahyb buffer (Ambion) for 30 minutes at 68°C, and then hybridized with $8x10^6$ Ci probe in 8ml Ultrahyb at 68°C overnight. The blot was washed twice for 5 minutes at 68°C in 2X SSC / 0.1% (w/v) SDS, washed twice for 15 minutes at 68°C with 0.1X SSC / 0.1% SDS, and was then exposed to Biomax XAR film (Kodak).

8.27 Phospholipid Binding Assay

The TNT T7 Quick coupled transcription/translation system (Promega) was used to synthesize *in vitro* [35S]methionine-labeled full-length and truncated AGAP1 proteins from AGAP1 cDNAs (full-length and 552-861 truncation mutant) cloned in the T7 promoter-containing pcDNA3.1 vector. Reactions were incubated at 30°C for 2 hours, and product synthesis was confirmed by autoradiography: One μl of reaction mixture was separated by SDS-PAGE as described above, and the gel was fixed for 30 minutes in 40% MeOH / 10% HOAc / 3% glycerol. The gel was dried and imaged by storage phosphor autoradiography with a Storm scanner (GE Life Sciences) after overnight exposure. Phospholipid dot-blot arrays (PIP strips; Echelon Biosciences) were blocked 1 hour at 24°C in PIP blocking buffer (TBS pH=8, 3% (w/v) fatty acid-free BSA, 0.1% (v/v) Tween-20). Arrays were incubated with remaining

[35S]methionine-labeled proteins in PIP blocking buffer for 3 hours, washed 6 times for 5 minutes in PIP blocking buffer, dried, and imaged by storage phosphor autoradiography.

8.28 Superfused Mouse Striatal Synaptosome Neurotransmitter Release

Experiments measuring stimulated release of [3H]dopamine from striatal synaptosomes were performed according to previously described protocols (Yamada et al., 2001a; Westphalen and Hemmings, 2003; Martire et al., 2007) in collaboration with Dr. Hugh Hemmings (Weill Cornell Medical School, New York NY). Mice were sacrificed by cervical dislocation, and striata rapidly dissected on ice. Striatal tissue was homogenized in 0.32M sucrose with a motor-driven teflon-glass homogenizer (500rpm, 10 strokes, 4°C). The homogenate was centrifuged at 4,000g for 2 minutes, the resulting supernatant layered on top of 0.8M sucrose, and was re-centrifuged at 36,000g for 30 minutes. The resulting pellet, containing demyelinated nerve terminals (synaptosomes), was resuspended in ice-cold 0.32M sucrose. Synaptosomes were suspended in Krebs-HEPES buffer (20mM HEPES, pH=7.4, 140mM NaCl, 5mM KCl, 1mM $MgCl_2$, 1.2mM Na_2HPO_4, 5mM $NaHCO_3$, 10mM glucose) containing 10μM pargyline and 500nM desipramine, and were loaded with [14C]glutamate (Perkin Elmer) for 45 minutes and with [3H]dopamine (Perkin Elmer) for 15 minutes at 35°C. [3H]/[14C]-Loaded synaptosomes were centrifuged at 20,000g for 10 minutes, resuspended in 0.32M sucrose, loaded into superfusion chambers (Brandel) capped with GF/B glass fiber filters (Whatman), and superfused with

superfusion buffer (Krebs-HEPES, 2mM $CaCl_2$, 20μM pargyline) at 37°C with a modified Brandel SF12 superfusion apparatus (Westphalen and Hemmings, 2003) operating at a flow rate of 0.25ml/min and collecting fractions at 2-minute intervals. After a 30-minute equilibration period, neurotransmitter release was stimulated with a 2-minute pulse of superfusion buffer containing 15mM KCl. After an additional 12 minute interval with standard (5mM KCl) superfusion buffer, a second 2-minute pulse of superfusion buffer containing either 15mM KCl or 15mM KCl + 100μM oxotremorine-M (Tocris) was applied. At the end of the experiment, synaptosomes were lysed with 0.2M perchloric acid. [3H]Dopamine and [14C]glutamate were quantified in collected fractions (including synaptosomal lysate) added to Biosafe II scintillation cocktail (Research Products International) using liquid scintillation spectrometry with dual isotope quench correction.

Raw data were converted to fractional release values (CPM [3H]dopamine or [14C]glutamate released as a % of total remaining labeled neurotransmitter at the start of fraction collection) and plotted against fraction collection time. Basal release curves were interpolated from pre-, inter-, and post K^+ stimulation pulse periods, and used to calculate the cumulative fractional release above baseline after the 2 stimulation pulses.

8.29 Fast Scan Cyclic Voltammetry

Fast scan cyclic voltammetric measurement of dopamine release was performed in the laboratory of Dr. David Sulzer (Columbia University, New York

NY) according to previously published protocols (Zhang and Sulzer, 2003). For the preparation of acute striatal slices, mice were sacrificed by cervical dislocation, decapitated, and brains were washed in ice-cold oxygenated artificial cerebrospinal fluid (aCSF in mM: 119 NaCl, 2.5 KCl, 23.8 $NaHCO_3$, 2.4 $CaCl_2$, 1.2 $MgCl_2$, 1.2 NaH_2PO_4, 10 glucose, and saturated with 95% O_2 / 5 % CO_2). Striatal brain slices were cut on a vibratome at 250μm thickness from the second to fourth frontal slice of caudate–putamen (bregma, +1.54 mm to +0.62 mm) (Franklin and Paxinos, 1997). Slices were allowed to recover for 1.5 hr in a holding chamber in aCSF at room temperature.

For cyclic voltammetry recordings, striatal slices were placed in a recording chamber and superfused (~1 ml/min) with aCSF at ~30 °C. Disk carbon fiber electrodes of 5μm in diameter with a freshly cut surface were placed close to corpus callosum in the dorsal striatum (laterodorsal to dorsal section). Consistent insertion of the recording electrode into the tissue was achieved by using geometrical feature of the stimulating electrode and changes in basal currents associated to transition from solution to tissue. For cyclic voltammetry (CV), triangular voltage waves (+450 to +800 mV at 294 V/s vs Ag/AgCl, every 100 ms) were generated using Igor's application (Data Acquisition) created by Eugene V. Mosharov (Igor v5.0; WaveMetrics, Inc., www.wavemetrics.com),and were applied to the recording electrode using an ITC-18 analog–digital interface (HEKA Instruments Inc., Bellmore, NY)and the Axopatch 200B amplifier (Molecular Devices, Burlingame, CA). Striatal slices were electrically stimulated with a bipolar stimulating electrode using an Iso-Flex stimulus isolator triggered

by a Master-8 pulse generator (A.M.P.I., Jerusalem, Israel). Currents were recorded with an Axopatch 200B amplifier with a low-pass Bessel Filter setting at 10 kHz, digitized at 25 kHz, and acquired with the Igor's application. DA signals were identified by background-subtracted cyclic voltammograms, and DA peak currents were determined using an IGOR's application (Quanta Analysis) created by E. Mosharov (www.sulzerlab.org/download.html). Recording electrodes were calibrated before and after each experiment to determine the concentration of dopamine released by each stimulus. Eight prepulses were delivered every two minutes before each experiment to achieve constant dopamine release. For oxotremorine-M (Oxo-M) incubations, a single stimulus was applied every two minutes. Four prepulses were used as preincubation controls. Oxo-M was either applied for ten pulses (20 minutes), or for five pulses (10 minutes) followed by a ten pulse (20 minute) washout with aCSF.

Table 9.1 Immunocytochemistry antibody list

antigen (Ab name)	source	host	dilution - IF
adaptin δ (SA4)	DSHB (A. Peden)	mouse	1:100
c-myc (ab9106)	Abcam	rabbit	1:200
c-myc (9E10)	Covance	mouse	1:500
EEA1 (610456)	BD Transduction Labs	mouse	1:500
GFP (ab6556)	Abcam	rabbit	1:10000
GFP (ab13970)	Abcam	chicken	1:2000
HA (3F10)	Roche	rat	1:50
HA (HA.11)	Covance	mouse	1:100
KIAA0701 (ab26176)	Abcam	chicken	1:500
MAP-2 (AB5622)	Chemicon	rabbit	1:1000
rab5 (108011)	Synaptic Systems	mouse	1:150
rab7 (ab50533)	Abcam	mouse	1:150
synapsin I (ab8)	Abcam	rabbit	1:500
transferrin receptor	Zymed	mouse	1:500
tyrosine hydroxylase	Abcam	mouse	1:250
tyrosine hydroxylase	Chemicon	rabbit	1:1000

Table 9.2 Immunoblotting antibody list

antigen (antibody)	source	host	dliution - IB
β-actin (AC-15)	Abcam	mouse	1:10000
adaptin α (610501)	BD Transduction Labs	mouse	1:1000
adaptin β2 (610381)	BD Transduction Labs	mouse	1:10000
adaptin γ (610385)	BD Transduction Labs	mouse	1:5000
adaptin δ (SA4)	DSHB (A. Peden)	mouse	1:1000
Adaptin σ3A (611272)	BD Transduction Labs	mouse	1:250
rAGAP1 (AS625)	S. Meurer	rabbit	1:1000
c-myc (9E10)	Covance	mouse	1:1000
EEA1 (610456)	BD Transduction Labs	mouse	1:2500
GAL4 AD (345765)	Calbiochem	mouse	1:500
GAL4 DNA-BD (5399)	Clontech	mouse	1:4000
GFP (ab6556)	Abcam	rabbit	1:5000
HA (3F10)	Roche	rat	1:500
HA (HA.11)	Covance	mouse	1:1000
KIAA0701 (ab26176)	Abcam	chicken	1:2000
M3 pS577 (RU1653)	(affinity purified)	rabbit	1:1000
Na+, K+ ATPase β2 (610914)	BD Transduction Labs	mouse	1:500
β-NAP (610892)	BD Transduction Labs	mouse	1:500
p44/42 MAPK (9102)	Cell Signalling	rabbit	1:1000
Phospho-p44/42 MAPK (9106)	Cell Signalling	mouse	1:1000
p47A (610890)	BD Transduction Labs	mouse	1:250
rab5 (610281)	BD Transduction Labs	mouse	1:250
synaptophysin (611880)	BD Transduction Labs	mouse	1:20000

Table 9.3 RNA and DNA oligos used for siRNA transfection and construction of shRNA plasmids

oligo	sequence
hAGAP1 1 +	CCGUGCACAUCAGCCAGACAAGUAA
hAGAP1 1 -	UUACUUGUCUGGCUGAUGUGCACGG
hAGAP1 2 +	GGUGGGAGUUUAAGCGACUAUUCCU
hAGAP1 2-	AGGAAUAGUCGCUUAAACUCCCACC
hAGAP1 3 +	GCGUGCUGACCUAUCAUCCCAGUUU
hAGAP1 3 -	AAACUGGGAUGAUAGGUCAGCACGC
shRNA ctl +	GATCCCCGTTCCGAACACACGCACAATTCAAGAGATTGTG CGTGTGTTCGGAACTTTTTC
shRNA ctl -	TCGAGAAAAAGTTCCGAACACACGCACAATCTCTTGAATT GTGCGTGTGTTCGGAACGGG
rAP3b2 1374 +	GATCCCCATTCCAGACCTACATTCGCTTCAAGAGAGCGAA TGTAGGTCTGGAATTTTTTC
rAP3b2 1374 -	TCGAGAAAAAATTCCAGACCTACATTCGCTCTCTTGAAGC GAATGTAGGTCTGGAATGGG
rAP3b2 1611 +	GATCCCCAGACAACATCCAGGTACCCTTCAAGAGAGGGTA CCTGGATGTTGTCTTTTTTC
rAP3b2 1611 -	TCGAGAAAAAAGACAACATCCAGGTACCCTCTCTTGAAGG GTACCTGGATGTTGTCTGGG
rAP3b2 770 +	GATCCCCAACGCATCGACCTGATTCATTCAAGAGATGAATC AGGTCGATGCGTTTTTTTC
rAP3b2 770 -	TCGAGAAAAAAACGCATCGACCTGATTCATCTCTTGAATGA ATCAGGTCGATGCGTTGGG
rAGAP1 2680 +	GATCCCCGACGCCATAAGTTCCACCATTCAAGAGATGGTG GAACTTATGGCGTCTTTTTC
rAGAP1 2680 -	TCGAGAAAAAGACGCCATAAGTTCCACCATCTCTTGAATG GTGGAACTTATGGCGTCGGG
rAGAP1 135 +	GATCCCCCGTGAGTCTCTCAGTTCCCTTCAAGAGAGGGAA CTGAGAGACTCACGTTTTTC
rAGAP1 135 -	TCGAGAAAAACGTGAGTCTCTCAGTTCCCTCTCTTGAAGG GAACTGAGAGACTCACGGGG
rAGAP1 2059 +	GATCCCCACCCTAGACGTGTCTCTCCTTCAAGAGAGGAGA GACACGTCTAGGGTTTTTTC
rAGAP1 2059 -	TCGAGAAAAAACCCTAGACGTGTCTCTCCTCTCTTGAAGG AGAGACACGTCTAGGGTGGG
rAp3d1 3582 +	GATCCCCCACCTATCGTGACGAGCTGTTCAAGAGACAGCT CGTCACGATAGGTGTTTTTC
rAp3d1 3582 -	TCGAGAAAAACACCTATCGTGACGAGCTGTCTCTTGAACA GCTCGTCACGATAGGTGGGG
rAp3d1 3288 +	GATCCCCTCGTACCTGATCACCACCCTTCAAGAGAGGGTG GTGATCAGGTACGATTTTTC
rAp3d1 3288 -	TCGAGAAAAATCGTACCTGATCACCACCCTCTCTTGAAGG GTGGTGATCAGGTACGAGGG
rAp3d1 1169 +	GATCCCCGAGGAAATGAAGACCACGCTTCAAGAGAGCGT GGTCTTCATTTCCTCTTTTTC
rAp3d1 1169 -	TCGAGAAAAAGAGGAAATGAAGACCACGCTCTCTTGAAGC GTGGTCTTCATTTCCTCGGG

Table 9.4 PCR mutagenesis primers

primer	sequence
rAGAP1 S600A +	CAGCCTGCAGTCCTGTGAGGCCAGCAAGAATAAGTCCCG
rAGAP1 S600A -	CGGGACTTATTCTTGCTGGCCTCACAGGACTGCAGGCTG
rAGAP1 S605A +	GAGAGCAGCAAGAATAAGGCCCGACTCACCAGCCAGAGC
rAGAP1 S605A -	GCTCTGGCTGGTGAGTCGGGCCTTATTCTTGCTGCTCTC
rAGAP1 T608A +	CAAGAATAAGTCCCGACTCGCCAGCCAGAGCGAAGCCATG
rAGAP1 T608A -	CATGGCTTCGCTCTGGCTGGCGAGTCGGGACTTATTCTTG
rAGAP1 S609A +	GAATAAGTCCCGACTCACCGCCCAGAGCGAAGCCATGGC
rAGAP1 S609A -	GCCATGGCTTCGCTCTGGGCGGTGAGTCGGGACTTATTC
rM5 K371A S372A +	GCTGCTCACAGACTCGCGGCTCAGAAGTGTGTTGCC
rM5 K371A S372A -	GGCAACACACTTCTGAGCCGCGAGTCTGTGAGCAGC
rM5 K374A C375A +	CTCACAGACTCAAGAGTCAGGCGGCTGTTGCCTATAAGTT CCG
rM5 K374A C375A -	CGGAACTTATAGGCAACAGCCGCCTGACTCTTGAGTCTGT GAG
rM5 Y378A K379A F380A +	CAGAAGTGTGTTGCCGCTGCGGCCCGATTGGTGGTAAAAG
rM5 Y378A K379A F380A -	CTTTTACCACCAATCGGGCCGCAGCGGCAACACACTTCTG
rM5 K371A K374A +	GCTGCTCACAGACTCGCGAGTCAGGCGTGTGTTGCCTATA AG
rM5 K371A K374A -	CTTATAGGCAACACACGCCTGACTCGCGAGTCTGTGAGCA GC
rM5 K379A K385A +	GAAGTGTGTTGCCTATGCGTTCCGATTGGTGGTAGCAGCC GATGGGACCCAGG
rM5 K379A K385A -	CCTGGGTCCCATCGGCTGCTACCACCAATCGGAACGCATA GGCAACACACTTC
rM5 L382A V383A +	GTTGCCTATAAGTTCCGAGCGGCGGTAAAAGCCGATGGGA CC
rM5 L382A V383A -	GGTCCCATCGGCTTTTACCGCCGCTCGGAACTTATAGGCA AC
rM5 deletion mutant BbsI -	ATATGAAGACCTGTGAGCAGCAGCTGGAGA
rM5 deletion mutant BbsI +	ATATGAAGACGCTCACGATGGGACCCAGGAGACTAACAAT GGC
rM5 HA 1 HindIII +	ATATAAGCTTACCACCATGGAAGGGGAGTCTTACAATGAA
rM5 HA 1 BbsI -	ATATGAAGACTGGGACGTCATATGGATATCCATGGCGTTCC AAAGCCTGGTGATTTAC
rM5 HA 2 BbsI +	ATATGAAGACACGTCCCAGACTATGCCCTGTGGGAAGTCAT TACTATTGCAGTTGTG
rM5 HA 2 Xho -	ATATCTCGAGTCAGGGTAGCTTGCTGTTTCCTTGCCAATAC AA
rM5 e2 HA 1 EcoRI +	ATATGAATTCACCACCATGGAAGGGGAGTCTTACA
rM5 e2 HA 1 Bbs -	ATATGAAGACTGGGACGTCATATGGATAGAGGAACTGGATC TGGCACTCATCA
rM5 e2 HA 2 Bbs +	ATATGAAGACACGTCCCAGACTATGCCTCTGAACCCACCAT CACTTTTGGGACTGCCATTGCT
rM3 C-tail T549A +	CCCCGAATTCAACAAAGCATTCAGAACCACCTTC
rM3 C-tail T549A -	GAAGGTGGTTCTGAATGCTTTGTTGAATTCGGGG
rM3 C-tail T552A +	CAACAAAACATTCAGAGCCACCTTCAAGACGCTC
rM3 C-tail T552A -	GAGCGTCTTGAAGGTGGCTCTGAATGTTTTGTTG
rM3 C-tail T553A +	CAAAACATTCAGAACCGCCTTCAAGACGCTCCTC

primer	sequence
rM3 C-tail T553A -	GAGGAGCGTCTTGAAGGCGGTTCTGAATGTTTTG
rM3 C-tail T556A +	CAGAACCACCTTCAAGGCGCTCCTCTTGTGCCAG
rM3 C-tail T556A -	CTGGCACAAGAGGAGCGCCTTGAAGGTGGTTCTG
rM3 C-tail S577A +	GTACCAGCAGAGACAGGCGGTCATTTTTCACAAG
rM3 C-tail S577A -	CTTGTGAAAAATGACCGCCTGTCTCTGCTGGTAC
rM3 C-tail S577D +	GTACCAGCAGAGACAGGATGTCATTTTTCACAAG
rM3 C-tail S577D -	CTTGTGAAAAATGACATCCTGTCTCTGCTGGTAC
rM3 C-tail S577E +	GTACCAGCAGAGACAGGAGGTCATTTTTCACAAG
rM3 C-tail S577E -	CTTGTGAAAAATGACCTCCTGTCTCTGCTGGTAC

Table 9.5 PCR Primers for cloning from cDNA libraries

primer	sequence
rM1 XhoI +	ATATCTCGAGGCCACCATGAACACCTCAGTGCCCCCTGCT GTCAGTCCCAACAT
rM1 no stop HindIII -	ATATAAGCTTCGCATTGGCGGGAGGGGGTGCGGTGCACAG AGCCAG
rM1 FLAG HindIII +	ATATATAAGCTTATGGATTACAAGGATGACGACGATAAGAAC ACCTCAGTGCCCCCTGC
rM1 XhoI -	ATATATCTCGAGTTAGCATTGGCGGGAGGGGGTGCGGTGC AC
rM2 outer +	GGCCACTTGACTACTGAACACAAAA
rM2 outer -	TCACCGTGTAGCGCCTATGTTCTTG
rM2 + xhoI	ATATCTCGAGACCACCATGAATAACTCAACAAAC
rM2 Hind III- no stop	TATAAAGCTTCCCGTGTAGCGCCTAT
rM2 FLAG Hind III +	ATATAAGCTTACCATGGATTACAAGGATGACGACGATAAGAA TAACTCAACAAACTCC
rM2 XhoI -	ATATCTCGAGTCACCGTGTAGCGCCTATGTTCTTGTAATG
rM3 outer +	ATGACCTTGCACAGTAACAGTACAA
rM3 outer -	TCCTTGAAGGACAGAGGTAGAGTAG
rM3 Asp718 I +	ATATGGTACCGCCACCATGACCTTGCACAGTAACAGTACAA CCTCGCCTTTGTT
rM3 N-term HA EcoRI +	ATATGAATTCGCCACCATGTATCCATATGACGTCCCAGACTA TGCCACCTTGCACAGTAACAGTACAACC
rM3 FLAG Asp718 +	ATATGGTACCATGGATTACAAGGATGACGACGATAAGACCT TGCACAGTAACAGT
rM3 PspOM I -	ATATGGGCCCCTACAAGGCCTGCTCCGGCACTCGCTTGTG
rM3 no stop PspOM I -	ATATGGGCCCATCAAGGCCTGCTCCGGCACTCGCTTGTGA AAAATGA
rM4 HindIII +	ATATAAGCTTGCCACCATGGCCAACTTCACGCCTGTCAATG GCAGCTCAGCCAA
rM4 no stop EcoR I -	ATATGAATTCTCCCTGGCTGTGCCGATGTTCCGATACTGGC ACAGCA
rM4 EcoRI -	ATATATGAATTCCTACCTGGCTGTGCCGATGTTCCGATACTG
rM4 FLAG HindIII +	ATATATAAGCTTATGGATTACAAGGATGACGACGATAAGGCC AACTTCACGCCTGTCAA
rM4 EcoRI -	ATATATGAATTCCTACCTGGCTGTGCCGATGTTCCGATACTG
rM5 outer +	ATGGAAGGGGAGTCTTACAATGAAAGC

primer	sequence
rM5 outer -	GGGTAGCTTGCTGTTTCCTTGCCAA
rM5 XhoI +	ATATCTCGAGACCACCATGGAAGGGGAGTCTTACAATGA
rM5 HindIII - no stop	ATATAAGCTTGGGGTAGCTTGCTGTTTCCTT
rM5 N-term HA EcoR I +	ATATGAATTCACCACCATGTATCCATATGACGTCCCAGACTA TGCCGAAGGGGAGTCTTACAATGAAA
rM5 N-term HA Xho I -	ATATCTCGAGTCAGGGTAGCTTGC
rM5 FLAG HindIII +	ATATAAGCTTACCATGGATTACAAGGATGACGACGATAAGGA AGGGGAGTCTTACAAT
rM5 XhoI -	ATATCTCGAGTCAGGGTAGCTTGCTGTTTCCTTGCCAATA
rM1 c-tail EcoRI +	ATATGAATTCAACAAAGCCTTCCGGGACACG
rM1 c-tail XhoI -	ATATCTCGAGTTAGCATTGGCGGGAGGGGG
rM2 c-tail EcoRI linker +	AATTCAATGCCACCTTCAAAAAGACTTTTAAGCACCTCCTC ATGTGTCATTACAAGAACATAGGCGCTACACGGTGAC
rM2 c-tail XhoI linker -	TCGAGTCACCGTGTAGCGCCTATGTTCTTGTAATGACACAT GAGGAGGTGCTTAAAAGTCTTTTTGAAGGTGGCATTG
rM3 c-tail EcoRI +	ATATGAATTCAACAAAACATTCAGAACCACCTTCAAGACG
rM3 c-tail XhoI -	ATATCTCGAGCTACAAGGCCTGCTCCGGCA
rM4 c-tail EcoRI linker +	AATTCAATGCCACTTTCAAAAAGACCTTCCGGCACCTTTTG CTGTGCCAGTATCGGAACATCGGCACAGCCAGGTAGC
rM4 c-tail XhoI linker -	TCGAGCTACCTGGCTGTGCCGATGTTCCGATACTGGCACA GCAAAAGGTGCCGGAAGGTCTTTTTGAAAGTGGCATTG
rM5 c-tail EcoRI +	ATATGAATTCAACAGAACTTTCAGGAAAACC
rM5 c-tail XhoI -	ATATCTCGAGTCAGGGTAGCTTGCTGTTTC
rNRBP2 5', Bgl II, pACT in-frame	ATATATAGATCTTAGCGGCCCCGGAGCCGGCGCC
rNRBP2 3' Bgl II w/ stop	ATATATAGATCTCTACGCTTGTGTCCCACGGTACTTG
rNRBP2 5' w/UTR, HindIII	ATATATAAGCTTCGAGCCATGGCGGCCCCGGAGCCG
rNRBP2 internal EcoR I -	TTGTGGGCTGAGGGTCGGCGGGCAGGGTCC
rAGAP1 + outer	TTTTTTTAGCGCCTCCTCGG
rAGAP1 - outer	TTCCACCTGGAAGAGGGAGG
rAGAP1 + inner EcoRI	ATATATGAATTCTGCACCATGAACTACCAGCAGCAGCTGGC CAACTCGGC
rAGAP1 - inner XhoI	ATATATCTCGAGGATGACACTGGGCGCCCTCCCGCTACTGT TGTTCCTGC
rSNX20 outer +	GCTGCATTTAGAAGGCACCC
rSNX20 outer -	ACTGTCTGCGCAGCCTGGAT
rSNX20 inner EcoRI +	ATATATGAATTCGCCGCCATGGCAAGTCCACAGCATCCTGG GGGCCCTGG
rSNX20 inner XhoI -	ATATATCTCGAGGGACAGATACTCCCGCACGGTGAGCTCCT TCAGGGTGG
mAP3b2 outer +	TTCCTCGACCAAAGCCCAACCCGGCCGCTCAGCCACCCC TCAGCGCAGATCCATGT
mAP3b2 outer -	GAGGCGAGGGGGAGAGATCTGTGAGCAGATGTCAC
mAP3b2 inner XhoI +	ATATCTCGAGTTCGGCCGCTCCGGCCTACAGCGAAGACAA GGG
mAP3b2 inner PspOMI -	ATATGGGCCCTCACTGGGTCAGAGCCTGAATCACATCCTT
mAP3b1 outer +	TTGGTTCGGTGTCCTCCGAACGCCAGCCATCCGTAGA
mAP3b1 outer -	GCCAGATTCTGAAGTCCAGATGTAAGCAGG

primer	sequence
mAP3b1 inner no start EcoRI +	ATATGAATTCTTCTAGCAACAGTTTCGCCTACAACGAGCAG TCGGGA
mAP3b1 inner PspOM I -	ATATGGGCCCTTACCCCTGGGACAGGACAGGCTTCAGCTC
rKIAA0701 outer +	AGTCTCTCCCGAGAGTGAGCTCTCCGGCGCCTCTCCT
rKIAA0701 outer -	GGTCTGGAACAGCCACACTTTACCACACGC
rKIAA0701 inner +	ATATGGTACCGGCACCATGGCTGGGATCATTAAGAAACAG
rKIAA0701 inner no stop -	ATATGGGCCCCGGCCGCTGCAGCTGGCCCAGGGCCAGCC T
mCherry PspOMI +	ATATGGGCCCATGGTGAGCAAGGGCGAGGAGGATAACATG GCCATC
mCherry NotI -	ATATGCGGCCGCTGCTTGTACAGCTCGTCCATGCCGCCGG TGGAGTGGC

Table 9.6 PCR primers for cloning of Y2H constructs

primer	sequence
rM1 i3 loop BamHI +	ATATGGATCCTGCGCATCTACCGGGAGACAGAAA
rM1 i3 loop SalI -	ATATGTCGACTCAGGTCCGAGCTGCCTTCTTCTCC
rM2 i3 loop NcoI +	ATATCCATGGCGCATATATCCCGGGCAAGCAAGA
rM2 i3 loop BamHI -	ATATGGATCCTCATGTCCTGGTCACTTTCTTTTCC
rM3 i3 loop NcoI +	ATATCCATGGCGAGGATCTATAAGGAAACTGAGA
rM3 i3 loop BamHI -	ATATGGATCCTCACGTCTGGGCGGCCTTCTTCTCC
rM4 i3 loop NcoI +	ATATCCATGGCGCACATCTCACTGGCCAGCCGCA
rM4 i3 loop BamHI -	ATATGGATCCTCATGTCCGAGTCACTTTGCGCTCC
rM5 i3 loop NcoI +	ATATCCATGGCGCGGATCTACCGGGAGACAGAGA
rM5 i3 loop SalI -	ATATGTCGACTCAGGTCTGAGCCGCTTTCCTCTCT
hM2 i3 loop NcoI +	ATATCCATGGCGCACATATCCCGAGCCAGCAAGA
hM2 i3 loop SalI -	ATATGTCGACTCATGTCCTGGTGACTTTCTTTTCC
hM3 i3 loop NcoI +	ATATCCATGGCGAGGATCTATAAGGAAACTGAAA
hM3 i3 loop BamHI -	ATATGGATCCTCAGGTCTGGGCCGCTTTCTTCTCC
hM5 i3 loop NcoI +	ATATCCATGGCGCGAATCTACCGGGAAACAGAGA
hM5 i3 loop BamHI -	ATATGGATCCTCATGTCTGGGCTGCTTTCCTCTCT
rM5i3 (1) NcoI +	ATATCCATGGGACGGATCTACCGGGAGACAGAGAAG
rM5i3 (91) BamHI -	ATATGGATCCTCAGCTGCTACAGGTAGTAACCT
rM5i3 (73) NcoI +	ATATCCATGGGAGCCACTGACCTAAGTGCTGA
rM5i3 (162) BamHI -	ATATGGATCCTCAACACTTCTGACTCTTGAGTC
rM5i3 (141) NcoI +	ATATCCATGGGAGACTATGACACTCCCAAATAC
rM5i3 (229) SalI -	ATATGTCGACTCAGGTCTGAGCCGCTTTCCTCT
rM5i3 (18) NcoI +	ATATCCATGGGAGGTTCTGATTCTGTGGCAGA
rM5i3 (220) SalI -	ATATGTCGACTCACAGAACCATTCTCTTTCGTT
rM5i3 (210) SalI -	ATATGTCGACTCAATGACTGAGGTTGGGATCCG
rM5i3 (200) SalI -	ATATGTCGACTCATGAAGGGTCTTTGGACACTG
rM5i3 (190) SalI -	ATATGTCGACTCAGGGCATGATTTTCACCTTTC
rM5i3 (180) SalI -	ATATGTCGACTCAGTTAGTCTCCTGGGTCCCAT
rM5i3 (170) SalI -	ATATGTCGACTCACACCAATCGGAACTTATAGG
rM5i3 (173) SalI -	ATATGTCGACTCAGGCTTTTACCACCAATCGGA
rM5i3 (146) NcoI +	ATATCCATGGGAAAATACTTTCTGTCTCCAGC
rM5i3 (151) NcoI +	ATATCCATGGGACCAGCTGCTGCTCACAGACT

primer	sequence
rM5i3 (156) NcoI +	ATATCCATGGGAAGACTCAAGAGTCAGAAGTG
rM5i3 (161-180) NcoI + linker	CATGGGAAAGTGTGTTGCCTATAAGTTCCGATTGGTGGTAA AAGCCGATGGGACCCAGGAGACTAACTGAG
rM5i3 (161-180) SalI - linker	TCGACTCAGTTAGTCTCCTGGGTCCCATCGGCTTTTACCAC CAATCGGAACTTATAGGCAACACACTTTCC
rM5i3 (166-180) NcoI + linker	CATGGGAAAGTTCCGATTGGTGGTAAAAGCCGATGGGACC CAGGAGACTAACTGAG
rM5i3 (166-180) SalI - linker	TCGACTCAGTTAGTCTCCTGGGTCCCATCGGCTTTTACCAC CAATCGGAACTTTCC
rM2 i3 (5) EcoRI +	ATATGAATTCGCAAGCAAGAGTAGAATAAAGAAGGAAAAGA AGGAACCTGTGG
rM2 i3 (30) EcoRI +	ATATGAATTCGGAAGAATTGTAAAGCCAAACAATAACAATAT GCCTGGTGGTGATGG
rM2 i3 (60) EcoRI +	ATATGAATTCGACGGCGTGACTGAAAACTGTGTTCAGGGG GAGGAGAAAGA
rM2 i3 (90) EcoRI +	ATATGAATTCGATGATGAGATAACCCAGGATGAAAACACAG TTTCCACTTCGCTG
rM2 i3 (120) EcoRI +	ATATGAATTCGTCACCAAGGCCCAAAAGGGTGATGTGTGC ACCCCAACGAGTACC
rM2 i3 (150) EcoRI +	ATATGAATTCCAGAACATTGTAGCCCGCAAAATCGTGAAGA TGACCAAG
rAGAP1 (520) BamHI +	ATATGGATCCAGCTCGACCCACCCC
rAGAP1 (591) XhoI -	ATATCTCGAGTCAGATCTGGCTCTCGAT
rAGAP1 (552) BamHI +	ATATGGATCCCTGAAGAGCAAGAAGA
rAGAP1 (645) XhoI -	ATATCTCGAGTCAGGCTCCCAAGTTCAA
rAGAP1 (592-611) BamHI + linker	GATCCTAGCCAGCCTGCAGTCCTGTGAGAGCAGCAAGAAT AAGTCCCGACTCACCAGCCAGAGCTGAC
rAGAP1 (592-611) XhoI - linker	TCGAGTCAGCTCTGGCTGGTGAGTCGGGACTTATTCTTGC TGCTCTCACAGGACTGCAGGCTGGCTAG
rAGAP1 (602-621) BamHI + linker	GATCCTAAAGAATAAGTCCCGACTCACCAGCCAGAGCGAA GCCATGGCACTGCAGTCAATCCGTAACTGAC
rAGAP1 (602-621) XhoI - linker	TCGAGTCAGTTACGGATTGACTGCAGTGCCATGGCTTCGC TCTGGCTGGTGAGTCGGGACTTATTCTTTAG
rAGAP1 (612-631) BamHI + linker	GATCCTAGAAGCCATGGCACTGCAGTCAATCCGTAACATGA GAGGGAACTCGCACTGCGTGGACTGTTGAC
rAGAP1 (612-631) XhoI - linker	TCGAGTCAACAGTCCACGCAGTGCGAGTTCCCTCTCATGT TACGGATTGACTGCAGTGCCATGGCTTCTAG
rAGAP1 (622-641) BamHI + linker	GATCCTAAACATGAGAGGGAACTCGCACTGCGTGGACTGT GACACCCAGAACCCCAACTGGGCCAGTTGAC
rAGAP1 (622-641) XhoI - linker	TCGAGTCAACTGGCCCAGTTGGGGTTCTGGGTGTCACAG TCCACGCAGTGCGAGTTCCCTCTCATGTTTAG
rAGAP1 (552) BamHI +	ATATGGATCCCTGAAGAGCAAGAAGAAAACTTG
rAGAP1 (600) XhoI -	ATATCTCGAGTCAGCTCTCACAGGACTGCAGGC
rAGAP1 (596) BamHI +	ATATGGATCCAGTCCTGTGAGAGCAGCAAG
rAGAP1 (645) XhoI -	ATATCTCGAGTCAGGCTCCCAAGTTCAAACTGG
rAGAP1 (609)XhoI -	ATATCTCGAGTCAGCTGGTGAGTCGGGACTTAT
rAGAP1 (618) XhoI -	ATATCTCGAGTCATGACTGCAGTGCCATGGCTT
rAGAP1 (627) XhoI -	ATATCTCGAGTCAGTGCGAGTTCCCTCTCATGT
rAGAP1 (636) XhoI -	ATATCTCGAGTCAGGGGTTCTGGGTGTCACAGT
rAGAP1 (560) BamHI +	ATATGGATCCTGTTTATCATTGTGTCCCTCAC

primer	sequence
rAGAP1 (568) BamHI +	ATATGGATCCTGCAGACGTGGCACTTTGAAGC
rAGAP1 (576) BamHI +	ATATGGATCCTGACATACGAGGAGCGAGACGC
rAGAP1 (584) BamHI +	ATATGGATCCTGGTCCAAGCCATCGAGAGCCA
rAGAP1 (614-861) Hind III +	ATATAAGCTTGCCACCATGGCACTGCAGTCAATCCGTAACA TGAGAGGGAACTC
rAGAP1 (1-613) XhoI -	ATATCTCGAGGGCTTCGCTCTGGCTGGTGAGTCGGGACTT
rSNX20 (2) EcoRI +	ATATGAATTCTAGCAAGTCCACAGCATCCTGGGGGCCCTG GCTGG
rSNX20 (313) XhoI -	ATATCTCGAGTCAGGACAGATACTCCCGCACGGTGAGC
rSNX20 (2-156) XhoI -	ATATCTCGAGTCACAGGCGCCGTTCGCAGATGGTCTCG
rSNX20 (78) EcoRI +	ATATGAATTCTAGCCTCAGCCAGAATCGAGGAGAGGAAAGT CTC
rSNX20 (234) XhoI-	ATATCTCGAGTCACAGGCACACGAGCATGGCGCAGAGA
rSNX20 (157) EcoRI +	ATATGAATTCTAGAGCTGCGCGAGTACCTGCGGCTGC
rSNX20 (87) EcoRI +	ATATGAATTCTAGTCTCCAAGTTTGTGATGTACCAGGTCGT GGT
rSNX20 (97) EcoRI +	ATATGAATTCTAGTCATCCAGACTGGGAGCTTCGACAGC
rSNX20 (107) EcoRI +	ATATGAATTCTAAAGGCTGTGGTGGAGCGGCGCTACT
rSNX20 (117) EcoRI +	ATATGAATTCTATTCGAGAGGCTGCAGAGGGCCCTCC
rSNX20 (127) EcoRI +	ATATGAATTCTACGCTTCGGGCCGGAGCTGGAGGACG
rSNX20 (137) EcoRI +	ATATGAATTCTATTCCCGCGGAAGCGCCTGACCGGGA
rSNX20 (147) EcoRI +	ATATGAATTCTATCGGCCGAGACCATCTGCGAACGGC
rNRBP2 (79) BamHI +	ATATGGATCCTTGCGGCCCCGGAGCCGGCGCCGAGGAGA G
rNRBP2 (491) XhoI -	ATATCTCGAGTCACGCTTGTGTCCC
rNRBP2 (395) BamHI +	ATATGGATCCTGTTGGCCCCACCCC
rNRBP2 (453) XhoI -	ATATCTCGAGTCAGGTCAGCTGCCGATG
rNRBP2 (442) BamHI +	ATATGGATCCTTTTGGTGCTTGAGG
rKIAA0701 (1469) XhoI -	ATATCTCGAGTCAGGGCCCCGGCCGCTGCAGCTGGCCCA GGGC
rKIAA0701 (1117) EcoRI +	ATATGAATTCTACTGGACAGCGTGGGATTCGAAGAGCAGCT G
rKIAA0701 (1188) EcoRI +	ATATGAATTCTAATGTCGGTCGTGGTGTTTAAAATCATTGGT GTTAGTGG
rKIAA0701 (1258) EcoRI +	ATATGAATTCTAGAAAGTGGGCCAGGTGCTGTCGTACACTC T
rKIAA0701 (1328) EcoRI +	ATATGAATTCTAGGTAGCACAGTGTCCCTCCAGCCAAGTCC C
rKIAA0701 (1399) EcoRI +	ATATGAATTCTAACGAGCCCAGAGGTTCCTTTGCCTTCACA G
rCentg1 (1095-1186) outer +	TTCTGCTGCTTCTGGCCCACGCGCGACATG
rCentg1 (1095-1186) outer -	AATGGTCCACCCGGTGTAGTCGTGCCTGGCC
rCentg1 (1095-1186) inner BamHI +	ATATGGATCCCTCGCCCACGTTGTTATTACACAGCTGCTG
rCentg1 (1095-1186) inner XhoI -	ATATCTCGAGCTATACCAGCGCGATCGTGGTGTCCACGCG
rCentg3 (1299-1377) outer +	GGGTCCAAGGAGGAGGTGAACGAGACCTACGGGGATGG
rCentg3 (1299-1377) outer -	TTCATCCCTGCGCCCTCGTCACCCCTCTTCTCTGCACCCC TGCT

primer	sequence
rCentg3 (1299-1377) inner BamHI +	ATATGGATCCGCCAACGTCGTTTTCACACAGCTGCTCATC
rCentg3 (1299-1377) inner XhoI -	ATATCTCGAGTCATAGGATACTAGGGCTGCGGTGCAGTTC
hCtglf1 outer +	ATGGGGAACATACTGACCTGTCGTGTGCAC
hCtglf1 outer -	CAGATACTACACGCACTCGTCGGGGCAGCC
hCtglf1 (379-437) BamHI +	ATATGGATCCGACACCTAAAGAAGAAAAGCACCAACAACTT TATGATTGTGTCTGCCACTGGC
hCtglf1 (379-437) XhoI -	ATATCTCGAGTCAGCTGGTCAGCTGGGACTTGCTTTTACTG CTCTCGC
rDynlt1 (2-113) BamHI +	ATATGGATCCTAGAAGACTTCCAGGCCTCCGAGGAGACTG CATTTGT
rDynlt1 (2-113) XhoI -	ATATCTCGAGTCAGATGGACAGTCCGAAGGCACTGACGAT GCAGT

Table 9.7 Genotypes of yeast strains

strain	genotype	reference
CG1945	*MATa, ura3, his3, ade2, lys2, trp1, leu2, 112, gal4-542, gal80-538, cyh^{r}2, LYS::GAL1*$_{UAS}$*-GAL1*$_{TATA}$*-HIS3, URA3::GAL4*$_{17\text{-}mers(x3)}$*-CYC1*$_{TATA}$*-lacZ*	(Feilotter et al., 1994)
Y187	*MATα, ura3, his3, ade2, trp1, leu2, 112, gal4Δ, met$^-$, gal80Δ, URA3::GAL1*$_{UAS}$*-GAL1*$_{TATA}$*-lacZ*	(Harper et al., 1993)
L40	*MATa, trp1, leu2, his3, LYS2::lexA-HIS3, URA3::lexA-LacZ*	(Vojtek et al., 1993)

9 REFERENCES

Abdul-Ghani, M., Hartman, K. L. and Ngsee, J. K. (2005). Abstrakt interacts with and regulates the expression of sorting nexin-2. J Cell Physiol *204*, 210-8.

Achour, L., Labbe-Jullie, C., Scott, M. G. and Marullo, S. (2008). An escort for GPCRs: implications for regulation of receptor density at the cell surface. Trends Pharmacol Sci *29*, 528-35.

Araya, R., Noguchi, T., Yuhki, M., Kitamura, N., Higuchi, M., Saido, T. C., Seki, K., Itohara, S., Kawano, M., Tanemura, K., Takashima, A., Yamada, K., Kondoh, Y., Kanno, I., Wess, J. and Yamada, M. (2006). Loss of M5 muscarinic acetylcholine receptors leads to cerebrovascular and neuronal abnormalities and cognitive deficits in mice. Neurobiol Dis *24*, 334-44.

Auld, D. S., Kornecook, T. J., Bastianetto, S. and Quirion, R. (2002). Alzheimer's disease and the basal forebrain cholinergic system: relations to beta-amyloid peptides, cognition, and treatment strategies. Prog Neurobiol *68*, 209-45.

Badtke, M. P., Cao, F. and Tavis, J. E. (2006). Combining genetic and biochemical approaches to identify functional molecular contact points. Biol Proced Online *8*, 77-86.

Barembaum, M., Moreno, T. A., LaBonne, C., Sechrist, J. and Bronner-Fraser, M. (2000). Noelin-1 is a secreted glycoprotein involved in generation of the neural crest. Nat Cell Biol *2*, 219-25.

Basile, A. S., Fedorova, I., Zapata, A., Liu, X., Shippenberg, T., Duttaroy, A., Yamada, M. and Wess, J. (2002). Deletion of the M5 muscarinic acetylcholine receptor attenuates morphine reinforcement and withdrawal but not morphine analgesia. Proc Natl Acad Sci U S A *99*, 11452-7.

Becamel, C., Alonso, G., Galeotti, N., Demey, E., Jouin, P., Ullmer, C., Dumuis, A., Bockaert, J. and Marin, P. (2002). Synaptic multiprotein complexes associated with 5-HT(2C) receptors: a proteomic approach. EMBO J *21*, 2332-42.

Bendixen, C., Gangloff, S. and Rothstein, R. (1994). A yeast mating-selection scheme for detection of protein-protein interactions. Nucleic Acids Res *22*, 1778-9.

Berkeley, J. L., Gomeza, J., Wess, J., Hamilton, S. E., Nathanson, N. M. and Levey, A. I. (2001). M1 muscarinic acetylcholine receptors activate extracellular signal-regulated kinase in CA1 pyramidal neurons in mouse hippocampal slices. Mol Cell Neurosci *18*, 512-24.

Bermak, J. C., Li, M., Bullock, C. and Zhou, Q. Y. (2001). Regulation of transport of the dopamine D1 receptor by a new membrane-associated ER protein. Nat Cell Biol *3*, 492-8.

Bernstein, L. S., Ramineni, S., Hague, C., Cladman, W., Chidiac, P., Levey, A. I. and Hepler, J. R. (2004). RGS2 binds directly and selectively to the M1 muscarinic acetylcholine receptor third intracellular loop to modulate Gq/11alpha signaling. J Biol Chem *279*, 21248-56.

Bhoumik, A., Singha, N., O'Connell, M. J. and Ronai, Z. A. (2008). Regulation of TIP60 by ATF2 modulates ATM activation. J Biol Chem *283*, 17605-14.

Bluml, K., Mutschler, E. and Wess, J. (1994). Insertion mutagenesis as a tool to predict the secondary structure of a muscarinic receptor domain determining specificity of G-protein coupling. Proc Natl Acad Sci U S A *91*, 7980-4.

Blumstein, J., Faundez, V., Nakatsu, F., Saito, T., Ohno, H. and Kelly, R. B. (2001). The neuronal form of adaptor protein-3 is required for synaptic vesicle formation from endosomes. J Neurosci *21*, 8034-42.

Boeuf, J., Trigo, J. M., Moreau, P. H., Lecourtier, L., Vogel, E., Cassel, J. C., Mathis, C., Klosen, P., Maldonado, R. and Simonin, F. (2009). Attenuated behavioural responses to acute and chronic cocaine in GASP-1-deficient mice. Eur J Neurosci *30*, 860-8.

Bonifacino, J. S. and Dell'Angelica, E. C. (1999). Molecular bases for the recognition of tyrosine-based sorting signals. J Cell Biol *145*, 923-6.

Bonifacino, J. S. and Traub, L. M. (2003). Signals for sorting of transmembrane proteins to endosomes and lysosomes. Annu Rev Biochem *72*, 395-447.

Bonner, T. I., Buckley, N. J., Young, A. C. and Brann, M. R. (1987). Identification of a family of muscarinic acetylcholine receptor genes. Science *237*, 527-32.

Brady, A. E., Wang, Q., Colbran, R. J., Allen, P. B., Greengard, P. and Limbird, L. E. (2003). Spinophilin stabilizes cell surface expression of alpha 2B-adrenergic receptors. J Biol Chem *278*, 32405-12.

Brent, R. and Ptashne, M. (1985). A eukaryotic transcriptional activator bearing the DNA specificity of a prokaryotic repressor. Cell *43*, 729-36.

Brewer, G. J. and Torricelli, J. R. (2007). Isolation and culture of adult neurons and neurospheres. Nat Protoc *2*, 1490-8.

Bridges, T. M., Marlo, J. E., Niswender, C. M., Jones, C. K., Jadhav, S. B., Gentry, P. R., Plumley, H. C., Weaver, C. D., Conn, P. J. and Lindsley, C. W. (2009). Discovery of the first highly M5-preferring muscarinic acetylcholine receptor ligand, an M5 positive allosteric modulator derived from a series of 5-trifluoromethoxy N-benzyl isatins. J Med Chem *52*, 3445-8.

Bronner, C., Achour, M., Arima, Y., Chataigneau, T., Saya, H. and Schini-Kerth, V. B. (2007). The UHRF family: oncogenes that are drugable targets for cancer therapy in the near future? Pharmacol Ther *115*, 419-34.

Budd, D. C., McDonald, J. E. and Tobin, A. B. (2000). Phosphorylation and regulation of a Gq/11-coupled receptor by casein kinase 1alpha. J Biol Chem *275*, 19667-75.

Burwinkel, B., Miglierini, G., Jenne, D. E., Gilbert, D. J., Copeland, N. G., Jenkins, N. A., Ring, H. Z., Francke, U. and Kilimann, M. W. (1998). Structure of the human paralemmin gene (PALM), mapping to human chromosome 19p13.3 and mouse chromosome 10, and exclusion of coding mutations in grizzled, mocha, jittery, and hesitant mice. Genomics *49*, 462-6.

Bymaster, F. P., McKinzie, D. L., Felder, C. C. and Wess, J. (2003). Use of M1-M5 muscarinic receptor knockout mice as novel tools to delineate the physiological roles of the muscarinic cholinergic system. Neurochem Res *28*, 437-42.

Caccamo, A., Oddo, S., Billings, L. M., Green, K. N., Martinez-Coria, H., Fisher, A. and LaFerla, F. M. (2006). M1 receptors play a central role in modulating AD-like pathology in transgenic mice. Neuron *49*, 671-82.

Cachero, T. G., Morielli, A. D. and Peralta, E. G. (1998). The small GTP-binding protein RhoA regulates a delayed rectifier potassium channel. Cell *93*, 1077-85.

Calabresi, P., Centonze, D., Gubellini, P., Pisani, A. and Bernardi, G. (2000). Acetylcholine-mediated modulation of striatal function. Trends Neurosci *23*, 120-6.

Canfield, W. M., Johnson, K. F., Ye, R. D., Gregory, W. and Kornfeld, S. (1991). Localization of the signal for rapid internalization of the bovine cation-independent mannose 6-phosphate/insulin-like growth factor-II receptor to amino acids 24-29 of the cytoplasmic tail. J Biol Chem *266*, 5682-8.

Cao, T. T., Deacon, H. W., Reczek, D., Bretscher, A. and von Zastrow, M. (1999). A kinase-regulated PDZ-domain interaction controls endocytic sorting of the beta2-adrenergic receptor. Nature *401*, 286-90.

Carlson, A. and Bok, D. (1992). Promotion of the release of 11-cis-retinal from cultured retinal pigment epithelium by interphotoreceptor retinoid-binding protein. Biochemistry *31*, 9056-62.

Chen, C., Li, J. G., Chen, Y., Huang, P., Wang, Y. and Liu-Chen, L. Y. (2006). GEC1 interacts with the kappa opioid receptor and enhances expression of the receptor. J Biol Chem *281*, 7983-93.

Cheng, K., Samimi, R., Xie, G., Shant, J., Drachenberg, C., Wade, M., Davis, R. J., Nomikos, G. and Raufman, J. P. (2008). Acetylcholine release by human colon cancer cells mediates autocrine stimulation of cell proliferation. Am J Physiol Gastrointest Liver Physiol *295*, G591-7.

Chernyavsky, A. I., Arredondo, J., Wess, J., Karlsson, E. and Grando, S. A. (2004). Novel signaling pathways mediating reciprocal control of keratinocyte migration and wound epithelialization through M3 and M4 muscarinic receptors. J Cell Biol *166*, 261-72.

Chien, C. T., Bartel, P. L., Sternglanz, R. and Fields, S. (1991). The two-hybrid system: a method to identify and clone genes for proteins that interact with a protein of interest. Proc Natl Acad Sci U S A *88*, 9578-82.

Coleman, M. L., Sahai, E. A., Yeo, M., Bosch, M., Dewar, A. and Olson, M. F. (2001). Membrane blebbing during apoptosis results from caspase-mediated activation of ROCK I. Nat Cell Biol *3*, 339-45.

Cullen, P. J. (2008). Endosomal sorting and signalling: an emerging role for sorting nexins. Nat Rev Mol Cell Biol *9*, 574-82.

Curran, T. and Franza, B. R., Jr. (1988). Fos and Jun: the AP-1 connection. Cell *55*, 395-7.

Cypess, A. M., Unson, C. G., Wu, C. R. and Sakmar, T. P. (1999). Two cytoplasmic loops of the glucagon receptor are required to elevate cAMP or intracellular calcium. J Biol Chem *274*, 19455-64.

D'Souza-Schorey, C. and Chavrier, P. (2006). ARF proteins: roles in membrane traffic and beyond. Nat Rev Mol Cell Biol *7*, 347-58.

Daaka, Y., Luttrell, L. M. and Lefkowitz, R. J. (1997). Switching of the coupling of the beta2-adrenergic receptor to different G proteins by protein kinase A. Nature *390*, 88-91.

Dagher, M. C. and Filhol-Cochet, O. (1997). Making hybrids of two-hybrid systems. Biotechniques *22*, 916-8, 920-2.

Dai, J., Li, J., Bos, E., Porcionatto, M., Premont, R. T., Bourgoin, S., Peters, P. J. and Hsu, V. W. (2004). ACAP1 promotes endocytic recycling by recognizing recycling sorting signals. Dev Cell *7*, 771-6.

Dajas-Bailador, F. and Wonnacott, S. (2004). Nicotinic acetylcholine receptors and the regulation of neuronal signalling. Trends Pharmacol Sci *25*, 317-24.

Danglot, L. and Galli, T. (2007). What is the function of neuronal AP-3? Biol Cell *99*, 349-61.

Daulat, A. M., Maurice, P., Froment, C., Guillaume, J. L., Broussard, C., Monsarrat, B., Delagrange, P. and Jockers, R. (2007). Purification and identification of G protein-coupled receptor protein complexes under native conditions. Mol Cell Proteomics *6*, 835-44.

Daulat, A. M., Maurice, P. and Jockers, R. (2009). Recent methodological advances in the discovery of GPCR-associated protein complexes. Trends Pharmacol Sci *30*, 72-8.

De Luca, V., Wang, H., Squassina, A., Wong, G. W., Yeomans, J. and Kennedy, J. L. (2004). Linkage of M5 muscarinic and alpha7-nicotinic receptor genes on 15q13 to schizophrenia. Neuropsychobiology *50*, 124-7.

Delaney, K. A., Murph, M. M., Brown, L. M. and Radhakrishna, H. (2002). Transfer of M2 muscarinic acetylcholine receptors to clathrin-derived early endosomes following clathrin-independent endocytosis. J Biol Chem *277*, 33439-46.

Dell'Angelica, E. C., Klumperman, J., Stoorvogel, W. and Bonifacino, J. S. (1998). Association of the AP-3 adaptor complex with clathrin. Science *280*, 431-4.

Dell'Angelica, E. C., Ohno, H., Ooi, C. E., Rabinovich, E., Roche, K. W. and Bonifacino, J. S. (1997). AP-3: an adaptor-like protein complex with ubiquitous expression. EMBO J *16*, 917-28.

Dell'Angelica, E. C., Shotelersuk, V., Aguilar, R. C., Gahl, W. A. and Bonifacino, J. S. (1999). Altered trafficking of lysosomal proteins in Hermansky-Pudlak syndrome due to mutations in the beta 3A subunit of the AP-3 adaptor. Mol Cell *3*, 11-21.

Dessy, C., Kelly, R. A., Balligand, J. L. and Feron, O. (2000). Dynamin mediates caveolar sequestration of muscarinic cholinergic receptors and alteration in NO signaling. EMBO J *19*, 4272-80.

Dolphin, A. C. (2003). G protein modulation of voltage-gated calcium channels. Pharmacol Rev *55*, 607-27.

Domon, B. and Aebersold, R. (2006). Mass spectrometry and protein analysis. Science *312*, 212-7.

Donaldson, J. G., Finazzi, D. and Klausner, R. D. (1992). Brefeldin A inhibits Golgi membrane-catalysed exchange of guanine nucleotide onto ARF protein. Nature *360*, 350-2.

Dong, C. and Wu, G. (2006). Regulation of anterograde transport of alpha2-adrenergic receptors by the N termini at multiple intracellular compartments. J Biol Chem *281*, 38543-54.

Dorje, F., Wess, J., Lambrecht, G., Tacke, R., Mutschler, E. and Brann, M. R. (1991). Antagonist binding profiles of five cloned human muscarinic receptor subtypes. J Pharmacol Exp Ther *256*, 727-33.

Durfee, T., Becherer, K., Chen, P. L., Yeh, S. H., Yang, Y., Kilburn, A. E., Lee, W. H. and Elledge, S. J. (1993). The retinoblastoma protein associates with the protein phosphatase type 1 catalytic subunit. Genes Dev *7*, 555-69.

Earnshaw, W. C., Sullivan, K. F., Machlin, P. S., Cooke, C. A., Kaiser, D. A., Pollard, T. D., Rothfield, N. F. and Cleveland, D. W. (1987). Molecular cloning of

cDNA for CENP-B, the major human centromere autoantigen. J Cell Biol *104*, 817-29.

Fam, S. R., Paquet, M., Castleberry, A. M., Oller, H., Lee, C. J., Traynelis, S. F., Smith, Y., Yun, C. C. and Hall, R. A. (2005). P2Y1 receptor signaling is controlled by interaction with the PDZ scaffold NHERF-2. Proc Natl Acad Sci U S A *102*, 8042-7.

Farr, C. D., Gafken, P. R., Norbeck, A. D., Doneanu, C. E., Stapels, M. D., Barofsky, D. F., Minami, M. and Saugstad, J. A. (2004). Proteomic analysis of native metabotropic glutamate receptor 5 protein complexes reveals novel molecular constituents. J Neurochem *91*, 438-50.

Faundez, V., Horng, J. T. and Kelly, R. B. (1998). A function for the AP3 coat complex in synaptic vesicle formation from endosomes. Cell *93*, 423-32.

Feilotter, H. E., Hannon, G. J., Ruddell, C. J. and Beach, D. (1994). Construction of an improved host strain for two hybrid screening. Nucleic Acids Res *22*, 1502-3.

Feng, L., Seymour, A. B., Jiang, S., To, A., Peden, A. A., Novak, E. K., Zhen, L., Rusiniak, M. E., Eicher, E. M., Robinson, M. S., Gorin, M. B. and Swank, R. T. (1999). The beta3A subunit gene (Ap3b1) of the AP-3 adaptor complex is altered in the mouse hypopigmentation mutant pearl, a model for Hermansky-Pudlak syndrome and night blindness. Hum Mol Genet *8*, 323-30.

Fibiger, H. C., Damsma, G. and Day, J. C. (1991). Behavioral pharmacology and biochemistry of central cholinergic neurotransmission. Adv Exp Med Biol *295*, 399-414.

Fields, S. and Song, O. (1989). A novel genetic system to detect protein-protein interactions. Nature *340*, 245-6.

Fiorillo, C. D. and Williams, J. T. (2000). Cholinergic inhibition of ventral midbrain dopamine neurons. J Neurosci *20*, 7855-60.

Fisahn, A., Yamada, M., Duttaroy, A., Gan, J. W., Deng, C. X., McBain, C. J. and Wess, J. (2002). Muscarinic induction of hippocampal gamma oscillations requires coupling of the M1 receptor to two mixed cation currents. Neuron *33*, 615-24.

Flajolet, M., Rotondo, G., Daviet, L., Bergametti, F., Inchauspe, G., Tiollais, P., Transy, C. and Legrain, P. (2000). A genomic approach of the hepatitis C virus generates a protein interaction map. Gene *242*, 369-79.

Flajolet, M., Wang, Z., Futter, M., Shen, W., Nuangchamnong, N., Bendor, J., Wallach, I., Nairn, A. C., Surmeier, D. J. and Greengard, P. (2008). FGF acts as a co-transmitter through adenosine A(2A) receptor to regulate synaptic plasticity. Nat Neurosci *11*, 1402-9.

Foord, S. M., Bonner, T. I., Neubig, R. R., Rosser, E. M., Pin, J. P., Davenport, A. P., Spedding, M. and Harmar, A. J. (2005). International Union of Pharmacology. XLVI. G protein-coupled receptor list. Pharmacol Rev *57*, 279-88.

Forster, G. L., Yeomans, J. S., Takeuchi, J. and Blaha, C. D. (2002). M5 muscarinic receptors are required for prolonged accumbal dopamine release after electrical stimulation of the pons in mice. J Neurosci *22*, RC190.

Frank, S. R., Parisi, T., Taubert, S., Fernandez, P., Fuchs, M., Chan, H. M., Livingston, D. M. and Amati, B. (2003). MYC recruits the TIP60 histone acetyltransferase complex to chromatin. EMBO Rep *4*, 575-80.

Fredriksson, R., Lagerstrom, M. C., Lundin, L. G. and Schioth, H. B. (2003). The G-protein-coupled receptors in the human genome form five main families. Phylogenetic analysis, paralogon groups, and fingerprints. Mol Pharmacol *63*, 1256-72.

Fromont-Racine, M., Rain, J. C. and Legrain, P. (1997). Toward a functional analysis of the yeast genome through exhaustive two-hybrid screens. Nat Genet *16*, 277-82.

Funayama, T., Mashima, Y., Ohtake, Y., Ishikawa, K., Fuse, N., Yasuda, N., Fukuchi, T., Murakami, A., Hotta, Y. and Shimada, N. (2006). SNPs and interaction analyses of noelin 2, myocilin, and optineurin genes in Japanese patients with open-angle glaucoma. Invest Ophthalmol Vis Sci *47*, 5368-75.

Gainetdinov, R. R., Premont, R. T., Bohn, L. M., Lefkowitz, R. J. and Caron, M. G. (2004). Desensitization of G protein-coupled receptors and neuronal functions. Annu Rev Neurosci *27*, 107-44.

Gartner, A., Collin, L. and Lalli, G. (2006). Nucleofection of primary neurons. Methods Enzymol *406*, 374-88.

Gautam, D., Han, S. J., Hamdan, F. F., Jeon, J., Li, B., Li, J. H., Cui, Y., Mears, D., Lu, H., Deng, C., Heard, T. and Wess, J. (2006). A critical role for beta cell M3 muscarinic acetylcholine receptors in regulating insulin release and blood glucose homeostasis in vivo. Cell Metab *3*, 449-61.

Gautam, D., Jeon, J., Starost, M. F., Han, S. J., Hamdan, F. F., Cui, Y., Parlow, A. F., Gavrilova, O., Szalayova, I., Mezey, E. and Wess, J. (2009). Neuronal M3 muscarinic acetylcholine receptors are essential for somatotroph proliferation and normal somatic growth. Proc Natl Acad Sci U S A *106*, 6398-403.

Gingras, A. C., Gstaiger, M., Raught, B. and Aebersold, R. (2007). Analysis of protein complexes using mass spectrometry. Nat Rev Mol Cell Biol *8*, 645-54.

Godi, A., Di Campli, A., Konstantakopoulos, A., Di Tullio, G., Alessi, D. R., Kular, G. S., Daniele, T., Marra, P., Lucocq, J. M. and De Matteis, M. A. (2004). FAPPs control Golgi-to-cell-surface membrane traffic by binding to ARF and PtdIns(4)P. Nat Cell Biol *6*, 393-404.

Goldman, P. S. and Nathanson, N. M. (1994). Differential role of the carboxyl-terminal tyrosine in down-regulation and sequestration of the m2 muscarinic acetylcholine receptor. J Biol Chem *269*, 15640-5.

Gomeza, J., Shannon, H., Kostenis, E., Felder, C., Zhang, L., Brodkin, J., Grinberg, A., Sheng, H. and Wess, J. (1999a). Pronounced pharmacologic deficits in M2 muscarinic acetylcholine receptor knockout mice. Proc Natl Acad Sci U S A *96*, 1692-7.

Gomeza, J., Zhang, L., Kostenis, E., Felder, C., Bymaster, F., Brodkin, J., Shannon, H., Xia, B., Deng, C. and Wess, J. (1999b). Enhancement of D1 dopamine receptor-mediated locomotor stimulation in M(4) muscarinic acetylcholine receptor knockout mice. Proc Natl Acad Sci U S A *96*, 10483-8.

Gomeza, J., Zhang, L., Kostenis, E., Felder, C. C., Bymaster, F. P., Brodkin, J., Shannon, H., Xia, B., Duttaroy, A., Deng, C. X. and Wess, J. (2001). Generation and pharmacological analysis of M2 and M4 muscarinic receptor knockout mice. Life Sci *68*, 2457-66.

Gonzalez-Fernandez, F. (2003). Interphotoreceptor retinoid-binding protein--an old gene for new eyes. Vision Res *43*, 3021-36.

Gorrini, C., Squatrito, M., Luise, C., Syed, N., Perna, D., Wark, L., Martinato, F., Sardella, D., Verrecchia, A., Bennett, S., Confalonieri, S., Cesaroni, M., Marchesi, F., Gasco, M., Scanziani, E., Capra, M., Mai, S., Nuciforo, P., Crook, T., Lough, J.

and Amati, B. (2007). Tip60 is a haplo-insufficient tumour suppressor required for an oncogene-induced DNA damage response. Nature *448*, 1063-7.

Goslin, K., Asmussen, H. and Banker, G. (1998). Rat hippocampal neurons in low-density culture. Culturing Nerve Cells. G. Banker and K. Goslin. Cambridge, MA, MIT Press, 339-370.

Grant, B. D. and Donaldson, J. G. (2009). Pathways and mechanisms of endocytic recycling. Nat Rev Mol Cell Biol *10*, 597-608.

Greengard, P. (2001). The neurobiology of slow synaptic transmission. Science *294*, 1024-30.

Gronier, B. and Rasmussen, K. (1998). Activation of midbrain presumed dopaminergic neurones by muscarinic cholinergic receptors: an in vivo electrophysiological study in the rat. Br J Pharmacol *124*, 455-64.

Gulledge, A. T., Bucci, D. J., Zhang, S. S., Matsui, M. and Yeh, H. H. (2009). M1 receptors mediate cholinergic modulation of excitability in neocortical pyramidal neurons. J Neurosci *29*, 9888-902.

Gurevich, V. V. and Gurevich, E. V. (2008). How and why do GPCRs dimerize? Trends Pharmacol Sci *29*, 234-40.

Gyuris, J., Golemis, E., Chertkov, H. and Brent, R. (1993). Cdi1, a human G1 and S phase protein phosphatase that associates with Cdk2. Cell *75*, 791-803.

Haga, K. and Haga, T. (1985). Purification of the muscarinic acetylcholine receptor from porcine brain. J Biol Chem *260*, 7927-35.

Hall, R. A. (2004). Studying protein-protein interactions via blot overlay or Far Western blot. Methods Mol Biol *261*, 167-74.

Hall, R. A. (2005). Co-Immunoprecipitation as a strategy to evaluate receptor-receptor or receptor-protein interactions. G Protein-Coupled Receptor-Protein Interactions. S. R. George and B. F. O'Dowd. Hoboken, NJ, John Wiley & Sons, 165-178.

Hamilton, S. E., Loose, M. D., Qi, M., Levey, A. I., Hille, B., McKnight, G. S., Idzerda, R. L. and Nathanson, N. M. (1997). Disruption of the m1 receptor gene ablates muscarinic receptor-dependent M current regulation and seizure activity in mice. Proc Natl Acad Sci U S A *94*, 13311-6.

Hanyaloglu, A. C. and von Zastrow, M. (2008). Regulation of GPCRs by endocytic membrane trafficking and its potential implications. Annu Rev Pharmacol Toxicol *48*, 537-68.

Harper, J. W., Adami, G. R., Wei, N., Keyomarsi, K. and Elledge, S. J. (1993). The p21 Cdk-interacting protein Cip1 is a potent inhibitor of G1 cyclin-dependent kinases. Cell *75*, 805-16.

Harrison, P. J. and Weinberger, D. R. (2005). Schizophrenia genes, gene expression, and neuropathology: on the matter of their convergence. Mol Psychiatry *10*, 40-68; image 5.

Hashimoto, H., Horton, J. R., Zhang, X., Bostick, M., Jacobsen, S. E. and Cheng, X. (2008a). The SRA domain of UHRF1 flips 5-methylcytosine out of the DNA helix. Nature *455*, 826-9.

Hashimoto, Y., Morisawa, K., Saito, H., Jojima, E., Yoshida, N. and Haga, T. (2008b). Muscarinic M4 receptor recycling requires a motif in the third intracellular loop. J Pharmacol Exp Ther *325*, 947-53.

Hepler, J. R. (1999). Emerging roles for RGS proteins in cell signalling. Trends Pharmacol Sci *20*, 376-82.

Heydorn, A., Sondergaard, B. P., Ersboll, B., Holst, B., Nielsen, F. C., Haft, C. R., Whistler, J. and Schwartz, T. W. (2004). A library of 7TM receptor C-terminal tails. Interactions with the proposed post-endocytic sorting proteins ERM-binding phosphoprotein 50 (EBP50), N-ethylmaleimide-sensitive factor (NSF), sorting nexin 1 (SNX1), and G protein-coupled receptor-associated sorting protein (GASP). J Biol Chem *279*, 54291-303.

Hope, I. A. and Struhl, K. (1986). Functional dissection of a eukaryotic transcriptional activator protein, GCN4 of yeast. Cell *46*, 885-94.

Hsu, L. J., Schultz, L., Hong, Q., Van Moer, K., Heath, J., Li, M. Y., Lai, F. J., Lin, S. R., Lee, M. H., Lo, C. P., Lin, Y. S., Chen, S. T. and Chang, N. S. (2009). Transforming growth factor beta1 signaling via interaction with cell surface Hyal-2 and recruitment of WWOX/WOX1. J Biol Chem *284*, 16049-59.

Hu, L. A., Tang, Y., Miller, W. E., Cong, M., Lau, A. G., Lefkowitz, R. J. and Hall, R. A. (2000). beta 1-adrenergic receptor association with PSD-95. Inhibition of receptor internalization and facilitation of beta 1-adrenergic receptor interaction with N-methyl-D-aspartate receptors. J Biol Chem *275*, 38659-66.

Huizing, M., Sarangarajan, R., Strovel, E., Zhao, Y., Gahl, W. A. and Boissy, R. E. (2001). AP-3 mediates tyrosinase but not TRP-1 trafficking in human melanocytes. Mol Biol Cell *12*, 2075-85.

Iida, S., Seto, M., Yamamoto, K., Komatsu, H., Tojo, A., Asano, S., Kamada, N., Ariyoshi, Y., Takahashi, T. and Ueda, R. (1993). MLLT3 gene on 9p22 involved in t(9;11) leukemia encodes a serine/proline rich protein homologous to MLLT1 on 19p13. Oncogene *8*, 3085-92.

Ito, Y., Oyunzul, L., Seki, M., Fujino Oki, T., Matsui, M. and Yamada, S. (2009). Quantitative analysis of the loss of muscarinic receptors in various peripheral tissues in M1-M5 receptor single knockout mice. Br J Pharmacol *156*, 1147-53.

Jackson, T. R., Kearns, B. G. and Theibert, A. B. (2000). Cytohesins and centaurins: mediators of PI 3-kinase-regulated Arf signaling. Trends Biochem Sci *25*, 489-95.

Janvier, K., Kato, Y., Boehm, M., Rose, J. R., Martina, J. A., Kim, B. Y., Venkatesan, S. and Bonifacino, J. S. (2003). Recognition of dileucine-based sorting signals from HIV-1 Nef and LIMP-II by the AP-1 gamma-sigma1 and AP-3 delta-sigma3 hemicomplexes. J Cell Biol *163*, 1281-90.

Jiang, M. and Chen, G. (2006). High Ca2+-phosphate transfection efficiency in low-density neuronal cultures. Nat Protoc *1*, 695-700.

Jin, M., Li, S., Nusinowitz, S., Lloyd, M., Hu, J., Radu, R. A., Bok, D. and Travis, G. H. (2009). The role of interphotoreceptor retinoid-binding protein on the translocation of visual retinoids and function of cone photoreceptors. J Neurosci *29*, 1486-95.

Johnson, K. F. and Kornfeld, S. (1992). A His-Leu-Leu sequence near the carboxyl terminus of the cytoplasmic domain of the cation-dependent mannose 6-phosphate receptor is necessary for the lysosomal enzyme sorting function. J Biol Chem *267*, 17110-5.

Jordan, B. A., Trapaidze, N., Gomes, I., Nivarthi, R. and Devi, L. A. (2001). Oligomerization of opioid receptors with beta 2-adrenergic receptors: a role in trafficking and mitogen-activated protein kinase activation. Proc Natl Acad Sci U S A *98*, 343-8.

Jositsch, G., Papadakis, T., Haberberger, R. V., Wolff, M., Wess, J. and Kummer, W. (2009). Suitability of muscarinic acetylcholine receptor antibodies for

immunohistochemistry evaluated on tissue sections of receptor gene-deficient mice. Naunyn Schmiedebergs Arch Pharmacol *379*, 389-95.

Jung, S. S. and Levy, E. (2005). Murine cerebrovascular cells as a cell culture model for cerebral amyloid angiopathy: isolation of smooth muscle and endothelial cells from mouse brain. Methods Mol Biol *299*, 211-9.

Kahn, R. A., Bruford, E., Inoue, H., Logsdon, J. M., Jr., Nie, Z., Premont, R. T., Randazzo, P. A., Satake, M., Theibert, A. B., Zapp, M. L. and Cassel, D. (2008). Consensus nomenclature for the human ArfGAP domain-containing proteins. J Cell Biol *182*, 1039-44.

Kaneko, T., Li, L. and Li, S. S. (2008). The SH3 domain--a family of versatile peptide- and protein-recognition module. Front Biosci *13*, 4938-52.

Kantheti, P., Qiao, X., Diaz, M. E., Peden, A. A., Meyer, G. E., Carskadon, S. L., Kapfhamer, D., Sufalko, D., Robinson, M. S., Noebels, J. L. and Burmeister, M. (1998). Mutation in AP-3 delta in the mocha mouse links endosomal transport to storage deficiency in platelets, melanosomes, and synaptic vesicles. Neuron *21*, 111-22.

Kaupmann, K., Malitschek, B., Schuler, V., Heid, J., Froestl, W., Beck, P., Mosbacher, J., Bischoff, S., Kulik, A., Shigemoto, R., Karschin, A. and Bettler, B. (1998). GABA(B)-receptor subtypes assemble into functional heteromeric complexes. Nature *396*, 683-7.

Keegan, L., Gill, G. and Ptashne, M. (1986). Separation of DNA binding from the transcription-activating function of a eukaryotic regulatory protein. Science *231*, 699-704.

Kim, E. and Sheng, M. (2004). PDZ domain proteins of synapses. Nat Rev Neurosci *5*, 771-81.

Kim, O. J., Ariano, M. A., Namkung, Y., Marinec, P., Kim, E., Han, J. and Sibley, D. R. (2008). D2 dopamine receptor expression and trafficking is regulated through direct interactions with ZIP. J Neurochem *106*, 83-95.

Kohn, E. C., Alessandro, R., Probst, J., Jacobs, W., Brilley, E. and Felder, C. C. (1996). Identification and molecular characterization of a m5 muscarinic receptor in A2058 human melanoma cells. Coupling to inhibition of adenylyl cyclase and stimulation of phospholipase A2. J Biol Chem *271*, 17476-84.

Kornau, H. C., Schenker, L. T., Kennedy, M. B. and Seeburg, P. H. (1995). Domain interaction between NMDA receptor subunits and the postsynaptic density protein PSD-95. Science *269*, 1737-40.

Kostenis, E., Conklin, B. R. and Wess, J. (1997). Molecular basis of receptor/G protein coupling selectivity studied by coexpression of wild type and mutant m2 muscarinic receptors with mutant G alpha(q) subunits. Biochemistry *36*, 1487-95.

Kostenis, E., Zeng, F. Y. and Wess, J. (1999). Structure-function analysis of muscarinic receptors and their associated G proteins. Life Sci *64*, 355-62.

Krudewig, R., Langer, B., Vogler, O., Markschies, N., Erl, M., Jakobs, K. H. and van Koppen, C. J. (2000). Distinct internalization of M2 muscarinic acetylcholine receptors confers selective and long-lasting desensitization of signaling to phospholipase C. J Neurochem *74*, 1721-30.

Kung, L. A. and Snyder, M. (2006). Proteome chips for whole-organism assays. Nat Rev Mol Cell Biol *7*, 617-22.

Kurten, R. C., Cadena, D. L. and Gill, G. N. (1996). Enhanced degradation of EGF receptors by a sorting nexin, SNX1. Science *272*, 1008-10.

Kyttala, A., Yliannala, K., Schu, P., Jalanko, A. and Luzio, J. P. (2005). AP-1 and AP-3 facilitate lysosomal targeting of Batten disease protein CLN3 via its dileucine motif. J Biol Chem *280*, 10277-83.

LaCount, D. J., Vignali, M., Chettier, R., Phansalkar, A., Bell, R., Hesselberth, J. R., Schoenfeld, L. W., Ota, I., Sahasrabudhe, S., Kurschner, C., Fields, S. and Hughes, R. E. (2005). A protein interaction network of the malaria parasite Plasmodium falciparum. Nature *438*, 103-7.

Lane, P. W. and Deol, M. S. (1974). Mocha, a new coat color and behavior mutation on chromosome 10 of the mouse. J Hered *65*, 362-4.

Lawrence, J., Mundell, S. J., Yun, H., Kelly, E. and Venkateswarlu, K. (2005). Centaurin-alpha 1, an ADP-ribosylation factor 6 GTPase activating protein, inhibits beta 2-adrenoceptor internalization. Mol Pharmacol *67*, 1822-8.

Lee, F. J. S. and Liu, F. (2005). GST fusion protein and pull-down strategies to evaluate receptor-receptor or receptor-protein interactions. G Protein-Coupled Receptor-Protein Interactions. S. R. George and B. F. O'Dowd. Hoboken, NJ, John Wiley & Sons, 221-231.

Lee, J. A., Anholt, R. R. and Cole, G. J. (2008). Olfactomedin-2 mediates development of the anterior central nervous system and head structures in zebrafish. Mech Dev *125*, 167-81.

Lee, M. S., Kao, S. C., Lemere, C. A., Xia, W., Tseng, H. C., Zhou, Y., Neve, R., Ahlijanian, M. K. and Tsai, L. H. (2003). APP processing is regulated by cytoplasmic phosphorylation. J Cell Biol *163*, 83-95.

Lefrancois, S., Janvier, K., Boehm, M., Ooi, C. E. and Bonifacino, J. S. (2004). An ear-core interaction regulates the recruitment of the AP-3 complex to membranes. Dev Cell *7*, 619-25.

Lein, E. S., Hawrylycz, M. J., Ao, N., Ayres, M., Bensinger, A., Bernard, A., Boe, A. F., Boguski, M. S., Brockway, K. S., Byrnes, E. J., Chen, L., Chen, T. M., Chin, M. C., Chong, J., Crook, B. E., Czaplinska, A., Dang, C. N., Datta, S., Dee, N. R., Desaki, A. L., Desta, T., Diep, E., Dolbeare, T. A., Donelan, M. J., Dong, H. W., Dougherty, J. G., Duncan, B. J., Ebbert, A. J., Eichele, G., Estin, L. K., Faber, C., Facer, B. A., Fields, R., Fischer, S. R., Fliss, T. P., Frensley, C., Gates, S. N., Glattfelder, K. J., Halverson, K. R., Hart, M. R., Hohmann, J. G., Howell, M. P., Jeung, D. P., Johnson, R. A., Karr, P. T., Kawal, R., Kidney, J. M., Knapik, R. H., Kuan, C. L., Lake, J. H., Laramee, A. R., Larsen, K. D., Lau, C., Lemon, T. A., Liang, A. J., Liu, Y., Luong, L. T., Michaels, J., Morgan, J. J., Morgan, R. J., Mortrud, M. T., Mosqueda, N. F., Ng, L. L., Ng, R., Orta, G. J., Overly, C. C., Pak, T. H., Parry, S. E., Pathak, S. D., Pearson, O. C., Puchalski, R. B., Riley, Z. L., Rockett, H. R., Rowland, S. A., Royall, J. J., Ruiz, M. J., Sarno, N. R., Schaffnit, K., Shapovalova, N. V., Sivisay, T., Slaughterbeck, C. R., Smith, S. C., Smith, K. A., Smith, B. I., Sodt, A. J., Stewart, N. N., Stumpf, K. R., Sunkin, S. M., Sutram, M., Tam, A., Teemer, C. D., Thaller, C., Thompson, C. L., Varnam, L. R., Visel, A., Whitlock, R. M., Wohnoutka, P. E., Wolkey, C. K., Wong, V. Y., Wood, M., Yaylaoglu, M. B., Young, R. C., Youngstrom, B. L., Yuan, X. F., Zhang, B., Zwingman, T. A. and Jones, A. R. (2007). Genome-wide atlas of gene expression in the adult mouse brain. Nature *445*, 168-76.

Lemmon, M. A. (2004). Pleckstrin homology domains: not just for phosphoinositides. Biochem Soc Trans *32*, 707-11.

Letourneur, F. and Klausner, R. D. (1992). A novel di-leucine motif and a tyrosine-based motif independently mediate lysosomal targeting and endocytosis of CD3 chains. Cell *69*, 1143-57.

Li, J., Ballif, B. A., Powelka, A. M., Dai, J., Gygi, S. P. and Hsu, V. W. (2005). Phosphorylation of ACAP1 by Akt regulates the stimulation-dependent recycling of integrin beta1 to control cell migration. Dev Cell *9*, 663-73.

Li, J., Mahajan, A. and Tsai, M. D. (2006). Ankyrin repeat: a unique motif mediating protein-protein interactions. Biochemistry *45*, 15168-78.

Li, S., Armstrong, C. M., Bertin, N., Ge, H., Milstein, S., Boxem, M., Vidalain, P. O., Han, J. D., Chesneau, A., Hao, T., Goldberg, D. S., Li, N., Martinez, M., Rual, J. F., Lamesch, P., Xu, L., Tewari, M., Wong, S. L., Zhang, L. V., Berriz, G. F., Jacotot, L., Vaglio, P., Reboul, J., Hirozane-Kishikawa, T., Li, Q., Gabel, H. W., Elewa, A., Baumgartner, B., Rose, D. J., Yu, H., Bosak, S., Sequerra, R., Fraser, A., Mango, S. E., Saxton, W. M., Strome, S., Van Den Heuvel, S., Piano, F., Vandenhaute, J., Sardet, C., Gerstein, M., Doucette-Stamm, L., Gunsalus, K. C., Harper, J. W., Cusick, M. E., Roth, F. P., Hill, D. E. and Vidal, M. (2004). A map of the interactome network of the metazoan C. elegans. Science *303*, 540-3.

Li, W., Zhang, Q., Oiso, N., Novak, E. K., Gautam, R., O'Brien, E. P., Tinsley, C. L., Blake, D. J., Spritz, R. A., Copeland, N. G., Jenkins, N. A., Amato, D., Roe, B. A., Starcevic, M., Dell'Angelica, E. C., Elliott, R. W., Mishra, V., Kingsmore, S. F., Paylor, R. E. and Swank, R. T. (2003). Hermansky-Pudlak syndrome type 7 (HPS-7) results from mutant dysbindin, a member of the biogenesis of lysosome-related organelles complex 1 (BLOC-1). Nat Genet *35*, 84-9.

Lim, S., Sala, C., Yoon, J., Park, S., Kuroda, S., Sheng, M. and Kim, E. (2001). Sharpin, a novel postsynaptic density protein that directly interacts with the shank family of proteins. Mol Cell Neurosci *17*, 385-97.

Lin, R., Kabbani, N., Binda, A., Canfield, V. and Levenson, R. (2005). Use of the yeast two-hybrid system to detect receptor-protein interactions. G Protein-Coupled Receptor-Protein Interactions. S. R. George and B. F. O'Dowd. Hoboken, NJ, John Wiley & Sons**,** 201-219.

Lin, R., Karpa, K., Kabbani, N., Goldman-Rakic, P. and Levenson, R. (2001). Dopamine D2 and D3 receptors are linked to the actin cytoskeleton via interaction with filamin A. Proc Natl Acad Sci U S A *98*, 5258-63.

Liou, G. I., Bridges, C. D., Fong, S. L., Alvarez, R. A. and Gonzalez-Fernandez, F. (1982). Vitamin A transport between retina and pigment epithelium--an interstitial protein carrying endogenous retinol (interstitial retinol-binding protein). Vision Res *22*, 1457-67.

Liu, L., Zhao, R., Bai, Y., Stanish, L. F., Evans, J. E., Sanderson, M. J., Bonventre, J. V. and Rittenhouse, A. R. (2006). M1 muscarinic receptors inhibit L-type Ca2+ current and M-current by divergent signal transduction cascades. J Neurosci *26*, 11588-98.

Lodowski, D. T., Pitcher, J. A., Capel, W. D., Lefkowitz, R. J. and Tesmer, J. J. (2003). Keeping G proteins at bay: a complex between G protein-coupled receptor kinase 2 and Gbetagamma. Science *300*, 1256-62.

Lohse, M. J., Benovic, J. L., Codina, J., Caron, M. G. and Lefkowitz, R. J. (1990). beta-Arrestin: a protein that regulates beta-adrenergic receptor function. Science *248*, 1547-50.

Luo, J., Busillo, J. M. and Benovic, J. L. (2008). M3 muscarinic acetylcholine receptor-mediated signaling is regulated by distinct mechanisms. Mol Pharmacol *74*, 338-47.

Luttrell, L. M. and Lefkowitz, R. J. (2002). The role of beta-arrestins in the termination and transduction of G-protein-coupled receptor signals. J Cell Sci *115*, 455-65.

Lyssand, J. S., DeFino, M. C., Tang, X. B., Hertz, A. L., Feller, D. B., Wacker, J. L., Adams, M. E. and Hague, C. (2008). Blood pressure is regulated by an alpha1D-adrenergic receptor/dystrophin signalosome. J Biol Chem *283*, 18792-800.

Ma, J. and Ptashne, M. (1988). Converting a eukaryotic transcriptional inhibitor into an activator. Cell *55*, 443-6.

Madziva, M. T., Bai, J., Bhalla, A., Chapman, E. R. and Edwardson, J. M. (2005). Effects of synaptotagmin reveal two distinct mechanisms of agonist-stimulated internalization of the M4 muscarinic acetylcholine receptor. Br J Pharmacol *144*, 761-71.

Maeda, S., Lameh, J., Mallet, W. G., Philip, M., Ramachandran, J. and Sadee, W. (1990). Internalization of the Hm1 muscarinic cholinergic receptor involves the third cytoplasmic loop. FEBS Lett *269*, 386-8.

Mahlknecht, U., Ottmann, O. G. and Hoelzer, D. (2001). Far-Western based protein-protein interaction screening of high-density protein filter arrays. J Biotechnol *88*, 89-94.

Marchese, A., Paing, M. M., Temple, B. R. and Trejo, J. (2008). G protein-coupled receptor sorting to endosomes and lysosomes. Annu Rev Pharmacol Toxicol *48*, 601-29.

Margeta-Mitrovic, M., Jan, Y. N. and Jan, L. Y. (2000). A trafficking checkpoint controls GABA(B) receptor heterodimerization. Neuron *27*, 97-106.

Martinez-Arca, S., Rudge, R., Vacca, M., Raposo, G., Camonis, J., Proux-Gillardeaux, V., Daviet, L., Formstecher, E., Hamburger, A., Filippini, F., D'Esposito, M. and Galli, T. (2003). A dual mechanism controlling the localization and function of exocytic v-SNAREs. Proc Natl Acad Sci U S A *100*, 9011-6.

Martire, M., D'Amico, M., Panza, E., Miceli, F., Viggiano, D., Lavergata, F., Iannotti, F. A., Barrese, V., Preziosi, P., Annunziato, L. and Taglialatela, M. (2007). Involvement of KCNQ2 subunits in [3H]dopamine release triggered by depolarization and pre-synaptic muscarinic receptor activation from rat striatal synaptosomes. J Neurochem *102*, 179-93.

Maudsley, S., Martin, B. and Luttrell, L. M. (2007). G protein-coupled receptor signaling complexity in neuronal tissue: implications for novel therapeutics. Curr Alzheimer Res *4*, 3-19.

Maurice, P., Daulat, A. M., Broussard, C., Mozo, J., Clary, G., Hotellier, F., Chafey, P., Guillaume, J. L., Ferry, G., Boutin, J. A., Delagrange, P., Camoin, L. and Jockers, R. (2008). A generic approach for the purification of signaling complexes that specifically interact with the carboxyl-terminal domain of G protein-coupled receptors. Mol Cell Proteomics *7*, 1556-69.

Maxfield, F. R. and McGraw, T. E. (2004). Endocytic recycling. Nat Rev Mol Cell Biol *5*, 121-32.

McClatchy, D. B., Knudsen, C. R., Clark, B. F., Kahn, R. A., Hall, R. A. and Levey, A. I. (2002). Novel interaction between the M4 muscarinic acetylcholine receptor and elongation factor 1A2. J Biol Chem *277*, 29268-74.

McDonald, P. H., Chow, C. W., Miller, W. E., Laporte, S. A., Field, M. E., Lin, F. T., Davis, R. J. and Lefkowitz, R. J. (2000). Beta-arrestin 2: a receptor-regulated MAPK scaffold for the activation of JNK3. Science *290*, 1574-7.

McGraw, T. E., Pytowski, B., Arzt, J. and Ferrone, C. (1991). Mutagenesis of the human transferrin receptor: two cytoplasmic phenylalanines are required for efficient internalization and a second-site mutation is capable of reverting an internalization-defective phenotype. J Cell Biol *112*, 853-61.

Mesulam, M. M. (2004). The cholinergic innervation of the human cerebral cortex. Prog Brain Res *145*, 67-78.

Meurer, S., Pioch, S., Wagner, K., Muller-Esterl, W. and Gross, S. (2004). AGAP1, a novel binding partner of nitric oxide-sensitive guanylyl cyclase. J Biol Chem *279*, 49346-54.

Miller, A. D. and Blaha, C. D. (2005). Midbrain muscarinic receptor mechanisms underlying regulation of mesoaccumbens and nigrostriatal dopaminergic transmission in the rat. Eur J Neurosci *21*, 1837-46.

Miller, K. A., Sawicka, D., Barsky, D. and Albala, J. S. (2004). Domain mapping of the Rad51 paralog protein complexes. Nucleic Acids Res *32*, 169-78.

Mitchell, R., Robertson, D. N., Holland, P. J., Collins, D., Lutz, E. M. and Johnson, M. S. (2003). ADP-ribosylation factor-dependent phospholipase D activation by the M3 muscarinic receptor. J Biol Chem *278*, 33818-30.

Miyakawa, T., Yamada, M., Duttaroy, A. and Wess, J. (2001). Hyperactivity and intact hippocampus-dependent learning in mice lacking the M1 muscarinic acetylcholine receptor. J Neurosci *21*, 5239-50.

Moreno, T. A. and Bronner-Fraser, M. (2002). Neural expression of mouse Noelin-1/2 and comparison with other vertebrates. Mech Dev *119*, 121-5.

Morris, S. M. and Cooper, J. A. (2001). Disabled-2 colocalizes with the LDLR in clathrin-coated pits and interacts with AP-2. Traffic *2*, 111-23.

Nadler, L. S., Kumar, G. and Nathanson, N. M. (2001). Identification of a basolateral sorting signal for the M3 muscarinic acetylcholine receptor in Madin-Darby canine kidney cells. J Biol Chem *276*, 10539-47.

Nakatsu, F. and Ohno, H. (2003). Adaptor protein complexes as the key regulators of protein sorting in the post-Golgi network. Cell Struct Funct *28*, 419-29.

Nakatsu, F., Okada, M., Mori, F., Kumazawa, N., Iwasa, H., Zhu, G., Kasagi, Y., Kamiya, H., Harada, A., Nishimura, K., Takeuchi, A., Miyazaki, T., Watanabe, M., Yuasa, S., Manabe, T., Wakabayashi, K., Kaneko, S., Saito, T. and Ohno, H. (2004). Defective function of GABA-containing synaptic vesicles in mice lacking the AP-3B clathrin adaptor. J Cell Biol *167*, 293-302.

Nathanson, N. M. (2000). A multiplicity of muscarinic mechanisms: enough signaling pathways to take your breath away. Proc Natl Acad Sci U S A *97*, 6245-7.

Newell-Litwa, K., Seong, E., Burmeister, M. and Faundez, V. (2007). Neuronal and non-neuronal functions of the AP-3 sorting machinery. J Cell Sci *120*, 531-41.

Newman, L. S., McKeever, M. O., Okano, H. J. and Darnell, R. B. (1995). Beta-NAP, a cerebellar degeneration antigen, is a neuron-specific vesicle coat protein. Cell *82*, 773-83.

Nie, Z., Boehm, M., Boja, E. S., Vass, W. C., Bonifacino, J. S., Fales, H. M. and Randazzo, P. A. (2003). Specific regulation of the adaptor protein complex AP-3 by the Arf GAP AGAP1. Dev Cell *5*, 513-21.

Nie, Z., Fei, J., Premont, R. T. and Randazzo, P. A. (2005). The Arf GAPs AGAP1 and AGAP2 distinguish between the adaptor protein complexes AP-1 and AP-3. J Cell Sci *118*, 3555-66.

Nie, Z., Hirsch, D. S., Luo, R., Jian, X., Stauffer, S., Cremesti, A., Andrade, J., Lebowitz, J., Marino, M., Ahvazi, B., Hinshaw, J. E. and Randazzo, P. A. (2006). A BAR domain in the N terminus of the Arf GAP ASAP1 affects membrane structure and trafficking of epidermal growth factor receptor. Curr Biol *16*, 130-9.

Nie, Z. and Randazzo, P. A. (2006). Arf GAPs and membrane traffic. J Cell Sci *119*, 1203-11.

Nie, Z., Stanley, K. T., Stauffer, S., Jacques, K. M., Hirsch, D. S., Takei, J. and Randazzo, P. A. (2002). AGAP1, an endosome-associated, phosphoinositide-dependent ADP-ribosylation factor GTPase-activating protein that affects actin cytoskeleton. J Biol Chem *277*, 48965-75.

Novak, E. K., Hui, S. W. and Swank, R. T. (1984). Platelet storage pool deficiency in mouse pigment mutations associated with seven distinct genetic loci. Blood *63*, 536-44.

Obsilova, V., Silhan, J., Boura, E., Teisinger, J. and Obsil, T. (2008). 14-3-3 proteins: a family of versatile molecular regulators. Physiol Res *57 Suppl 3*, S11-21.

Ohno, H., Aguilar, R. C., Yeh, D., Taura, D., Saito, T. and Bonifacino, J. S. (1998). The medium subunits of adaptor complexes recognize distinct but overlapping sets of tyrosine-based sorting signals. J Biol Chem *273*, 25915-21.

Oki, T., Takagi, Y., Inagaki, S., Taketo, M. M., Manabe, T., Matsui, M. and Yamada, S. (2005). Quantitative analysis of binding parameters of [3H]N-methylscopolamine in central nervous system of muscarinic acetylcholine receptor knockout mice. Brain Res Mol Brain Res *133*, 6-11.

Oksche, A., Boese, G., Horstmeyer, A., Furkert, J., Beyermann, M., Bienert, M. and Rosenthal, W. (2000). Late endosomal/lysosomal targeting and lack of recycling of the ligand-occupied endothelin B receptor. Mol Pharmacol *57*, 1104-13.

Oldham, W. M. and Hamm, H. E. (2008). Heterotrimeric G protein activation by G-protein-coupled receptors. Nat Rev Mol Cell Biol *9*, 60-71.

Ooi, C. E., Dell'Angelica, E. C. and Bonifacino, J. S. (1998). ADP-Ribosylation factor 1 (ARF1) regulates recruitment of the AP-3 adaptor complex to membranes. J Cell Biol *142*, 391-402.

Ooi, C. E., Moreira, J. E., Dell'Angelica, E. C., Poy, G., Wassarman, D. A. and Bonifacino, J. S. (1997). Altered expression of a novel adaptin leads to defective pigment granule biogenesis in the Drosophila eye color mutant garnet. EMBO J *16*, 4508-18.

Pals-Rylaarsdam, R., Gurevich, V. V., Lee, K. B., Ptasienski, J. A., Benovic, J. L. and Hosey, M. M. (1997). Internalization of the m2 muscarinic acetylcholine receptor. Arrestin-independent and -dependent pathways. J Biol Chem *272*, 23682-9.

Parent, A., Laroche, G., Hamelin, E. and Parent, J. L. (2008). RACK1 regulates the cell surface expression of the G protein-coupled receptor for thromboxane A(2). Traffic *9*, 394-407.

Park, M., Penick, E. C., Edwards, J. G., Kauer, J. A. and Ehlers, M. D. (2004). Recycling endosomes supply AMPA receptors for LTP. Science *305*, 1972-5.

Park, M., Salgado, J. M., Ostroff, L., Helton, T. D., Robinson, C. G., Harris, K. M. and Ehlers, M. D. (2006). Plasticity-induced growth of dendritic spines by exocytic trafficking from recycling endosomes. Neuron *52*, 817-30.

Park, P. S. and Wells, J. W. (2003). Monomers and oligomers of the M2 muscarinic cholinergic receptor purified from Sf9 cells. Biochemistry *42*, 12960-71.

Pawson, T. and Nash, P. (2003). Assembly of cell regulatory systems through protein interaction domains. Science *300*, 445-52.

Peden, A. A., Oorschot, V., Hesser, B. A., Austin, C. D., Scheller, R. H. and Klumperman, J. (2004). Localization of the AP-3 adaptor complex defines a novel endosomal exit site for lysosomal membrane proteins. J Cell Biol *164*, 1065-76.

Peden, A. A., Rudge, R. E., Lui, W. W. and Robinson, M. S. (2002). Assembly and function of AP-3 complexes in cells expressing mutant subunits. J Cell Biol *156*, 327-36.

Perez-Burgos, A., Perez-Rosello, T., Salgado, H., Flores-Barrera, E., Prieto, G. A., Figueroa, A., Galarraga, E. and Bargas, J. (2008). Muscarinic M(1) modulation of N and L types of calcium channels is mediated by protein kinase C in neostriatal neurons. Neuroscience *155*, 1079-97.

Peterson, G. L., Toumadje, A., Johnson, W. C., Jr. and Schimerlik, M. I. (1995). Purification of recombinant porcine m2 muscarinic acetylcholine receptor from Chinese hamster ovary cells. Circular dichroism spectra and ligand binding properties. J Biol Chem *270*, 17808-14.

Phizicky, E., Bastiaens, P. I., Zhu, H., Snyder, M. and Fields, S. (2003). Protein analysis on a proteomic scale. Nature *422*, 208-15.

Phizicky, E. M. and Fields, S. (1995). Protein-protein interactions: methods for detection and analysis. Microbiol Rev *59*, 94-123.

Pina, C., May, G., Soneji, S., Hong, D. and Enver, T. (2008). MLLT3 regulates early human erythroid and megakaryocytic cell fate. Cell Stem Cell *2*, 264-73.

Pisani, A., Bernardi, G., Ding, J. and Surmeier, D. J. (2007). Re-emergence of striatal cholinergic interneurons in movement disorders. Trends Neurosci *30*, 545-53.

Popova, J. S. and Rasenick, M. M. (2004). Clathrin-mediated endocytosis of m3 muscarinic receptors. Roles for Gbetagamma and tubulin. J Biol Chem *279*, 30410-8.

Porter, A. C., Bymaster, F. P., DeLapp, N. W., Yamada, M., Wess, J., Hamilton, S. E., Nathanson, N. M. and Felder, C. C. (2002). M1 muscarinic receptor signaling in mouse hippocampus and cortex. Brain Res *944*, 82-9.

Qtaishat, N. M., Wiggert, B. and Pepperberg, D. R. (2005). Interphotoreceptor retinoid-binding protein (IRBP) promotes the release of all-trans retinol from the isolated retina following rhodopsin bleaching illumination. Exp Eye Res *81*, 455-63.

Rapoport, I., Chen, Y. C., Cupers, P., Shoelson, S. E. and Kirchhausen, T. (1998). Dileucine-based sorting signals bind to the beta chain of AP-1 at a site distinct and regulated differently from the tyrosine-based motif-binding site. EMBO J *17*, 2148-55.

Rapoport, I., Miyazaki, M., Boll, W., Duckworth, B., Cantley, L. C., Shoelson, S. and Kirchhausen, T. (1997). Regulatory interactions in the recognition of endocytic sorting signals by AP-2 complexes. EMBO J *16*, 2240-50.

Rasmussen, S. G., Choi, H. J., Rosenbaum, D. M., Kobilka, T. S., Thian, F. S., Edwards, P. C., Burghammer, M., Ratnala, V. R., Sanishvili, R., Fischetti, R. F., Schertler, G. F., Weis, W. I. and Kobilka, B. K. (2007). Crystal structure of the human beta2 adrenergic G-protein-coupled receptor. Nature *450*, 383-7.

Rayport, S., Sulzer, D., Shi, W. X., Sawasdikosol, S., Monaco, J., Batson, D. and Rajendran, G. (1992). Identified postnatal mesolimbic dopamine neurons in culture: morphology and electrophysiology. J Neurosci *12*, 4264-80.

Regard, J. B., Sato, I. T. and Coughlin, S. R. (2008). Anatomical profiling of G protein-coupled receptor expression. Cell *135*, 561-71.

Rong, R., Ahn, J. Y., Huang, H., Nagata, E., Kalman, D., Kapp, J. A., Tu, J., Worley, P. F., Snyder, S. H. and Ye, K. (2003). PI3 kinase enhancer-Homer complex couples mGluRI to PI3 kinase, preventing neuronal apoptosis. Nat Neurosci *6*, 1153-61.

Rosenbaum, D. M., Cherezov, V., Hanson, M. A., Rasmussen, S. G., Thian, F. S., Kobilka, T. S., Choi, H. J., Yao, X. J., Weis, W. I., Stevens, R. C. and Kobilka, B. K. (2007). GPCR engineering yields high-resolution structural insights into beta2-adrenergic receptor function. Science *318*, 1266-73.

Rosenbaum, D. M., Rasmussen, S. G. and Kobilka, B. K. (2009). The structure and function of G-protein-coupled receptors. Nature *459*, 356-63.

Rozenfeld, R. and Devi, L. A. (2008). Regulation of CB1 cannabinoid receptor trafficking by the adaptor protein AP-3. FASEB J *22*, 2311-22.

Ruden, D. M., Ma, J., Li, Y., Wood, K. and Ptashne, M. (1991). Generating yeast transcriptional activators containing no yeast protein sequences. Nature *350*, 250-2.

Ryan, X. P., Alldritt, J., Svenningsson, P., Allen, P. B., Wu, G. Y., Nairn, A. C. and Greengard, P. (2005). The Rho-specific GEF Lfc interacts with neurabin and spinophilin to regulate dendritic spine morphology. Neuron *47*, 85-100.

Salazar, G., Craige, B., Love, R., Kalman, D. and Faundez, V. (2005a). Vglut1 and ZnT3 co-targeting mechanisms regulate vesicular zinc stores in PC12 cells. J Cell Sci *118*, 1911-21.

Salazar, G., Craige, B., Styers, M. L., Newell-Litwa, K. A., Doucette, M. M., Wainer, B. H., Falcon-Perez, J. M., Dell'Angelica, E. C., Peden, A. A., Werner, E. and Faundez, V. (2006). BLOC-1 complex deficiency alters the targeting of adaptor protein complex-3 cargoes. Mol Biol Cell *17*, 4014-26.

Salazar, G., Craige, B., Wainer, B. H., Guo, J., De Camilli, P. and Faundez, V. (2005b). Phosphatidylinositol-4-kinase type II alpha is a component of adaptor protein-3-derived vesicles. Mol Biol Cell *16*, 3692-704.

Salazar, G., Love, R., Styers, M. L., Werner, E., Peden, A., Rodriguez, S., Gearing, M., Wainer, B. H. and Faundez, V. (2004a). AP-3-dependent mechanisms control the targeting of a chloride channel (ClC-3) in neuronal and non-neuronal cells. J Biol Chem *279*, 25430-9.

Salazar, G., Love, R., Werner, E., Doucette, M. M., Cheng, S., Levey, A. and Faundez, V. (2004b). The zinc transporter ZnT3 interacts with AP-3 and it is preferentially targeted to a distinct synaptic vesicle subpopulation. Mol Biol Cell *15*, 575-87.

Salazar, G., Zlatic, S., Craige, B., Peden, A. A., Pohl, J. and Faundez, V. (2009). Hermansky-Pudlak syndrome protein complexes associate with phosphatidylinositol 4-kinase type II alpha in neuronal and non-neuronal cells. J Biol Chem *284*, 1790-802.

Santiago, M. P. and Potter, L. T. (2001). Biotinylated m4-toxin demonstrates more M4 muscarinic receptor protein on direct than indirect striatal projection neurons. Brain Res *894*, 12-20.

Satake, H. and Sakai, T. (2008). Recent advances and perceptions in studies of heterodimerization between G protein-coupled receptors. Protein Pept Lett *15*, 300-8.

Scarselli, M. and Donaldson, J. G. (2009). Constitutive internalization of G protein-coupled receptors and G proteins via clathrin-independent endocytosis. J Biol Chem *284*, 3577-85.

Schaff, U. Y., Shih, H. H., Lorenz, M., Sako, D., Kriz, R., Milarski, K., Bates, B., Tchernychev, B., Shaw, G. D. and Simon, S. I. (2008). SLIC-1/sorting nexin 20: a novel sorting nexin that directs subcellular distribution of PSGL-1. Eur J Immunol *38*, 550-64.

Schaub, B. E., Nair, P. and Rohrer, J. (2005). Analysis of protein transport to lysosomes. Curr Protoc Cell Biol *Chapter 15*, Unit 15 8.

Scheerer, P., Park, J. H., Hildebrand, P. W., Kim, Y. J., Krauss, N., Choe, H. W., Hofmann, K. P. and Ernst, O. P. (2008). Crystal structure of opsin in its G-protein-interacting conformation. Nature *455*, 497-502.

Scheuber, A., Rudge, R., Danglot, L., Raposo, G., Binz, T., Poncer, J. C. and Galli, T. (2006). Loss of AP-3 function affects spontaneous and evoked release at hippocampal mossy fiber synapses. Proc Natl Acad Sci U S A *103*, 16562-7.

Schoeber, J. P., Topala, C. N., Wang, X., Diepens, R. J., Lambers, T. T., Hoenderop, J. G. and Bindels, R. J. (2006). RGS2 inhibits the epithelial Ca2+ channel TRPV6. J Biol Chem *281*, 29669-74.

Schwab, S. G., Knapp, M., Mondabon, S., Hallmayer, J., Borrmann-Hassenbach, M., Albus, M., Lerer, B., Rietschel, M., Trixler, M., Maier, W. and Wildenauer, D. B. (2003). Support for association of schizophrenia with genetic variation in the 6p22.3 gene, dysbindin, in sib-pair families with linkage and in an additional sample of triad families. Am J Hum Genet *72*, 185-90.

Seeger, T., Fedorova, I., Zheng, F., Miyakawa, T., Koustova, E., Gomeza, J., Basile, A. S., Alzheimer, C. and Wess, J. (2004). M2 muscarinic acetylcholine receptor knock-out mice show deficits in behavioral flexibility, working memory, and hippocampal plasticity. J Neurosci *24*, 10117-27.

Seong, E., Wainer, B. H., Hughes, E. D., Saunders, T. L., Burmeister, M. and Faundez, V. (2005). Genetic analysis of the neuronal and ubiquitous AP-3 adaptor complexes reveals divergent functions in brain. Mol Biol Cell *16*, 128-40.

Shaner, N. C., Campbell, R. E., Steinbach, P. A., Giepmans, B. N., Palmer, A. E. and Tsien, R. Y. (2004). Improved monomeric red, orange and yellow fluorescent proteins derived from Discosoma sp. red fluorescent protein. Nat Biotechnol *22*, 1567-72.

Shapiro, M. S., Gomeza, J., Hamilton, S. E., Hille, B., Loose, M. D., Nathanson, N. M., Roche, J. P. and Wess, J. (2001). Identification of subtypes of muscarinic receptors that regulate Ca2+ and K+ channel activity in sympathetic neurons. Life Sci *68*, 2481-7.

Sharif, J., Muto, M., Takebayashi, S., Suetake, I., Iwamatsu, A., Endo, T. A., Shinga, J., Mizutani-Koseki, Y., Toyoda, T., Okamura, K., Tajima, S., Mitsuya, K., Okano, M. and Koseki, H. (2007). The SRA protein Np95 mediates epigenetic inheritance by recruiting Dnmt1 to methylated DNA. Nature *450*, 908-12.

Shenoy, S. K., McDonald, P. H., Kohout, T. A. and Lefkowitz, R. J. (2001). Regulation of receptor fate by ubiquitination of activated beta 2-adrenergic receptor and beta-arrestin. Science *294*, 1307-13.

Shi, J., Levinson, D. F., Duan, J., Sanders, A. R., Zheng, Y., Pe'er, I., Dudbridge, F., Holmans, P. A., Whittemore, A. S., Mowry, B. J., Olincy, A., Amin, F., Cloninger, C. R., Silverman, J. M., Buccola, N. G., Byerley, W. F., Black, D. W., Crowe, R. R., Oksenberg, J. R., Mirel, D. B., Kendler, K. S., Freedman, R. and Gejman, P. V. (2009). Common variants on chromosome 6p22.1 are associated with schizophrenia. Nature.

Siman, R. G. and Klein, W. L. (1983). Differential regulation of muscarinic and nicotinic receptors by cholinergic stimulation in cultured avian retina cells. Brain Res *262*, 99-108.

Simon, M. I., Strathmann, M. P. and Gautam, N. (1991). Diversity of G proteins in signal transduction. Science *252*, 802-8.

Simon, V., Guidry, J., Gettys, T. W., Tobin, A. B. and Lanier, S. M. (2006). The proto-oncogene SET interacts with muscarinic receptors and attenuates receptor signaling. J Biol Chem *281*, 40310-20.

Simonin, F., Karcher, P., Boeuf, J. J., Matifas, A. and Kieffer, B. L. (2004). Identification of a novel family of G protein-coupled receptor associated sorting proteins. J Neurochem *89*, 766-75.

Simpson, F., Peden, A. A., Christopoulou, L. and Robinson, M. S. (1997). Characterization of the adaptor-related protein complex, AP-3. J Cell Biol *137*, 835-45.

Singer-Lahat, D., Liu, J., Wess, J. and Felder, C. C. (1996). The third intracellular domain of the m3 muscarinic receptor determines coupling to calcium influx in transfected Chinese hamster ovary cells. FEBS Lett *386*, 51-4.

Smith, G. P. (1985). Filamentous fusion phage: novel expression vectors that display cloned antigens on the virion surface. Science *228*, 1315-7.

Squatrito, M., Gorrini, C. and Amati, B. (2006). Tip60 in DNA damage response and growth control: many tricks in one HAT. Trends Cell Biol *16*, 433-42.

Stanasila, L., Abuin, L., Diviani, D. and Cotecchia, S. (2006). Ezrin directly interacts with the alpha1b-adrenergic receptor and plays a role in receptor recycling. J Biol Chem *281*, 4354-63.

Stengel, P. W., Gomeza, J., Wess, J. and Cohen, M. L. (2000). M(2) and M(4) receptor knockout mice: muscarinic receptor function in cardiac and smooth muscle in vitro. J Pharmacol Exp Ther *292*, 877-85.

Stenmark, H. (2009). Rab GTPases as coordinators of vesicle traffic. Nat Rev Mol Cell Biol *10*, 513-25.

Stephen, C. W. and Lane, D. P. (1992). Mutant conformation of p53. Precise epitope mapping using a filamentous phage epitope library. J Mol Biol *225*, 577-83.

Stockinger, W., Sailler, B., Strasser, V., Recheis, B., Fasching, D., Kahr, L., Schneider, W. J. and Nimpf, J. (2002). The PX-domain protein SNX17 interacts with members of the LDL receptor family and modulates endocytosis of the LDL receptor. EMBO J *21*, 4259-67.

Stoorvogel, W., Oorschot, V. and Geuze, H. J. (1996). A novel class of clathrin-coated vesicles budding from endosomes. J Cell Biol *132*, 21-33.

Sur, C., Mallorga, P. J., Wittmann, M., Jacobson, M. A., Pascarella, D., Williams, J. B., Brandish, P. E., Pettibone, D. J., Scolnick, E. M. and Conn, P. J. (2003). N-desmethylclozapine, an allosteric agonist at muscarinic 1 receptor, potentiates N-methyl-D-aspartate receptor activity. Proc Natl Acad Sci U S A *100*, 13674-9.

Svenningsson, P., Chergui, K., Rachleff, I., Flajolet, M., Zhang, X., El Yacoubi, M., Vaugeois, J. M., Nomikos, G. G. and Greengard, P. (2006). Alterations in 5-HT1B receptor function by p11 in depression-like states. Science *311*, 77-80.

Svenningsson, P., Nishi, A., Fisone, G., Girault, J. A., Nairn, A. C. and Greengard, P. (2004). DARPP-32: an integrator of neurotransmission. Annu Rev Pharmacol Toxicol *44*, 269-96.

Szekeres, P. G., Koenig, J. A. and Edwardson, J. M. (1998a). Involvement of receptor cycling and receptor reserve in resensitization of muscarinic responses in SH-SY5Y human neuroblastoma cells. J Neurochem *70*, 1694-703.

Szekeres, P. G., Koenig, J. A. and Edwardson, J. M. (1998b). The relationship between agonist intrinsic activity and the rate of endocytosis of muscarinic receptors in a human neuroblastoma cell line. Mol Pharmacol *53*, 759-65.

Tahvanainen, J., Pykalainen, M., Kallonen, T., Lahteenmaki, H., Rasool, O. and Lahesmaa, R. (2006). Enrichment of nucleofected primary human CD4+ T cells: a novel and efficient method for studying gene function and role in human primary T helper cell differentiation. J Immunol Methods *310*, 30-9.

Talbot, K., Eidem, W. L., Tinsley, C. L., Benson, M. A., Thompson, E. W., Smith, R. J., Hahn, C. G., Siegel, S. J., Trojanowski, J. Q., Gur, R. E., Blake, D. J. and Arnold, S. E. (2004). Dysbindin-1 is reduced in intrinsic, glutamatergic terminals of the hippocampal formation in schizophrenia. J Clin Invest *113*, 1353-63.

Tan, C. M., Brady, A. E., Nickols, H. H., Wang, Q. and Limbird, L. E. (2004). Membrane trafficking of G protein-coupled receptors. Annu Rev Pharmacol Toxicol *44*, 559-609.

Taneichi-Kuroda, S., Taya, S., Hikita, T., Fujino, Y. and Kaibuchi, K. (2009). Direct interaction of Dysbindin with the AP-3 complex via its mu subunit. Neurochem Int *54*, 431-8.

Tang, Y., Hu, L. A., Miller, W. E., Ringstad, N., Hall, R. A., Pitcher, J. A., DeCamilli, P. and Lefkowitz, R. J. (1999). Identification of the endophilins (SH3p4/p8/p13) as novel binding partners for the beta1-adrenergic receptor. Proc Natl Acad Sci U S A *96*, 12559-64.

Thomsen, M., Woldbye, D. P., Wortwein, G., Fink-Jensen, A., Wess, J. and Caine, S. B. (2005). Reduced cocaine self-administration in muscarinic M5 acetylcholine receptor-deficient mice. J Neurosci *25*, 8141-9.

Thomsen, M., Wortwein, G., Fink-Jensen, A., Woldbye, D. P., Wess, J. and Caine, S. B. (2007). Decreased prepulse inhibition and increased sensitivity to muscarinic, but not dopaminergic drugs in M5 muscarinic acetylcholine receptor knockout mice. Psychopharmacology (Berl) *192*, 97-110.

Tobin, A. B., Lambert, D. G. and Nahorski, S. R. (1992). Rapid desensitization of muscarinic m3 receptor-stimulated polyphosphoinositide responses. Mol Pharmacol *42*, 1042-8.

Tobin, A. B. and Nahorski, S. R. (1993). Rapid agonist-mediated phosphorylation of m3-muscarinic receptors revealed by immunoprecipitation. J Biol Chem *268*, 9817-23.

Toby, G. G. and Golemis, E. A. (2001). Using the yeast interaction trap and other two-hybrid-based approaches to study protein-protein interactions. Methods *24*, 201-17.

Toews, M. L. (2000). Radioligand-binding assays for G protein-coupled receptor internalization. Regulation of G Protein-Coupled Receptor Function and Expression. New York, NY, Wiley-Liss**,** 199-230.

Tolbert, L. M. and Lameh, J. (1996). Human muscarinic cholinergic receptor Hm1 internalizes via clathrin-coated vesicles. J Biol Chem *271*, 17335-42.

Torrecilla, I., Spragg, E. J., Poulin, B., McWilliams, P. J., Mistry, S. C., Blaukat, A. and Tobin, A. B. (2007). Phosphorylation and regulation of a G protein-coupled receptor by protein kinase CK2. J Cell Biol *177*, 127-37.

Trendelenburg, A. U., Gomeza, J., Klebroff, W., Zhou, H. and Wess, J. (2003). Heterogeneity of presynaptic muscarinic receptors mediating inhibition of sympathetic transmitter release: a study with M2- and M4-receptor-deficient mice. Br J Pharmacol *138*, 469-80.

Triezenberg, S. J., LaMarco, K. L. and McKnight, S. L. (1988). Evidence of DNA: protein interactions that mediate HSV-1 immediate early gene activation by VP16. Genes Dev *2*, 730-42.

Trinquet, E., Fink, M., Bazin, H., Grillet, F., Maurin, F., Bourrier, E., Ansanay, H., Leroy, C., Michaud, A., Durroux, T., Maurel, D., Malhaire, F., Goudet, C., Pin, J. P., Naval, M., Hernout, O., Chretien, F., Chapleur, Y. and Mathis, G. (2006). D-myo-inositol 1-phosphate as a surrogate of D-myo-inositol 1,4,5-tris phosphate to monitor G protein-coupled receptor activation. Anal Biochem *358*, 126-35.

Tsao, P. and von Zastrow, M. (2000). Downregulation of G protein-coupled receptors. Curr Opin Neurobiol *10*, 365-9.

Turrigiano, G. G. (2008). The self-tuning neuron: synaptic scaling of excitatory synapses. Cell *135*, 422-35.

Tutor, A. S., Delpon, E., Caballero, R., Gomez, R., Nunez, L., Vaquero, M., Tamargo, J., Mayor, F., Jr. and Penela, P. (2006). Association of 14-3-3 proteins

to beta1-adrenergic receptors modulates Kv11.1 K+ channel activity in recombinant systems. Mol Biol Cell *17*, 4666-74.

Tzavara, E. T., Bymaster, F. P., Felder, C. C., Wade, M., Gomeza, J., Wess, J., McKinzie, D. L. and Nomikos, G. G. (2003). Dysregulated hippocampal acetylcholine neurotransmission and impaired cognition in M2, M4 and M2/M4 muscarinic receptor knockout mice. Mol Psychiatry *8*, 673-9.

Uetz, P., Dong, Y. A., Zeretzke, C., Atzler, C., Baiker, A., Berger, B., Rajagopala, S. V., Roupelieva, M., Rose, D., Fossum, E. and Haas, J. (2006). Herpesviral protein networks and their interaction with the human proteome. Science *311*, 239-42.

Van Criekinge, W. and Beyaert, R. (1999). Yeast Two-Hybrid: State of the Art. Biol Proced Online *2*, 1-38.

van Koppen, C. J. and Kaiser, B. (2003). Regulation of muscarinic acetylcholine receptor signaling. Pharmacol Ther *98*, 197-220.

Vargas, G. A. and Von Zastrow, M. (2004). Identification of a novel endocytic recycling signal in the D1 dopamine receptor. J Biol Chem *279*, 37461-9.

Vaynberg, J. and Qin, J. (2006). Weak protein-protein interactions as probed by NMR spectroscopy. Trends Biotechnol *24*, 22-7.

Vogler, O., Bogatkewitsch, G. S., Wriske, C., Krummenerl, P., Jakobs, K. H. and van Koppen, C. J. (1998). Receptor subtype-specific regulation of muscarinic acetylcholine receptor sequestration by dynamin. Distinct sequestration of m2 receptors. J Biol Chem *273*, 12155-60.

Voglmaier, S. M., Kam, K., Yang, H., Fortin, D. L., Hua, Z., Nicoll, R. A. and Edwards, R. H. (2006). Distinct endocytic pathways control the rate and extent of synaptic vesicle protein recycling. Neuron *51*, 71-84.

Vojtek, A. B., Hollenberg, S. M. and Cooper, J. A. (1993). Mammalian Ras interacts directly with the serine/threonine kinase Raf. Cell *74*, 205-14.

Volpicelli, L. A., Lah, J. J. and Levey, A. I. (2001). Rab5-dependent trafficking of the m4 muscarinic acetylcholine receptor to the plasma membrane, early endosomes, and multivesicular bodies. J Biol Chem *276*, 47590-8.

Voorn, P., Vanderschuren, L. J., Groenewegen, H. J., Robbins, T. W. and Pennartz, C. M. (2004). Putting a spin on the dorsal-ventral divide of the striatum. Trends Neurosci *27*, 468-74.

Vowels, J. J. and Payne, G. S. (1998). A dileucine-like sorting signal directs transport into an AP-3-dependent, clathrin-independent pathway to the yeast vacuole. EMBO J *17*, 2482-93.

Wang, H., Ng, K., Hayes, D., Gao, X., Forster, G., Blaha, C. and Yeomans, J. (2004). Decreased amphetamine-induced locomotion and improved latent inhibition in mice mutant for the M5 muscarinic receptor gene found in the human 15q schizophrenia region. Neuropsychopharmacology *29*, 2126-39.

Wang, H., Westin, L., Nong, Y., Birnbaum, S., Bendor, J., Brismar, H., Nestler, E., Aperia, A., Flajolet, M. and Greengard, P. (2009a). Norbin is an endogenous regulator of metabotropic glutamate receptor 5 signaling. Science *(in press)*.

Wang, H., Westin, L., Nong, Y., Birnbaum, S., Bendor, J., Brismar, H., Nestler, E., Aperia, A., Flajolet, M. and Greengard, P. (2009b). Norbin is an endogenous regulator of metabotropic glutamate receptor 5 signaling. Science.

Wang, X., Zeng, W., Soyombo, A. A., Tang, W., Ross, E. M., Barnes, A. P., Milgram, S. L., Penninger, J. M., Allen, P. B., Greengard, P. and Muallem, S. (2005). Spinophilin regulates Ca2+ signalling by binding the N-terminal domain of RGS2 and the third intracellular loop of G-protein-coupled receptors. Nat Cell Biol *7*, 405-11.

Wang, Y., Zhou, Y., Szabo, K., Haft, C. R. and Trejo, J. (2002). Down-regulation of protease-activated receptor-1 is regulated by sorting nexin 1. Mol Biol Cell *13*, 1965-76.

Wang, Z., Edwards, J. G., Riley, N., Provance, D. W., Jr., Karcher, R., Li, X. D., Davison, I. G., Ikebe, M., Mercer, J. A., Kauer, J. A. and Ehlers, M. D. (2008). Myosin Vb mobilizes recycling endosomes and AMPA receptors for postsynaptic plasticity. Cell *135*, 535-48.

Warner-Schmidt, J. L., Flajolet, M., Maller, A., Chen, E. Y., Qi, H., Svenningsson, P. and Greengard, P. (2009). Role of p11 in cellular and behavioral effects of 5-HT4 receptor stimulation. J Neurosci *29*, 1937-46.

Wei, M. L. (2006). Hermansky-Pudlak syndrome: a disease of protein trafficking and organelle function. Pigment Cell Res *19*, 19-42.

Weigert, R., Yeung, A. C., Li, J. and Donaldson, J. G. (2004). Rab22a regulates the recycling of membrane proteins internalized independently of clathrin. Mol Biol Cell *15*, 3758-70.

Weiner, D. M., Levey, A. I. and Brann, M. R. (1990). Expression of muscarinic acetylcholine and dopamine receptor mRNAs in rat basal ganglia. Proc Natl Acad Sci U S A *87*, 7050-4.

Wess, J., Blin, N., Mutschler, E. and Bluml, K. (1995). Muscarinic acetylcholine receptors: structural basis of ligand binding and G protein coupling. Life Sci *56*, 915-22.

Wess, J., Duttaroy, A., Zhang, W., Gomeza, J., Cui, Y., Miyakawa, T., Bymaster, F. P., McKinzie, L., Felder, C. C., Lamping, K. G., Faraci, F. M., Deng, C. and Yamada, M. (2003). M1-M5 muscarinic receptor knockout mice as novel tools to study the physiological roles of the muscarinic cholinergic system. Receptors Channels *9*, 279-90.

Wess, J., Eglen, R. M. and Gautam, D. (2007). Muscarinic acetylcholine receptors: mutant mice provide new insights for drug development. Nat Rev Drug Discov *6*, 721-33.

Wess, J., Liu, J., Blin, N., Yun, J., Lerche, C. and Kostenis, E. (1997). Structural basis of receptor/G protein coupling selectivity studied with muscarinic receptors as model systems. Life Sci *60*, 1007-14.

Wessler, I., Kilbinger, H., Bittinger, F., Unger, R. and Kirkpatrick, C. J. (2003). The non-neuronal cholinergic system in humans: expression, function and pathophysiology. Life Sci *72*, 2055-61.

Wessler, I., Kirkpatrick, C. J. and Racke, K. (1999). The cholinergic 'pitfall': acetylcholine, a universal cell molecule in biological systems, including humans. Clin Exp Pharmacol Physiol *26*, 198-205.

West, A. E., Neve, R. L. and Buckley, K. M. (1997a). Identification of a somatodendritic targeting signal in the cytoplasmic domain of the transferrin receptor. J Neurosci *17*, 6038-47.

West, A. E., Neve, R. L. and Buckley, K. M. (1997b). Targeting of the synaptic vesicle protein synaptobrevin in the axon of cultured hippocampal neurons: evidence for two distinct sorting steps. J Cell Biol *139*, 917-27.

Westphalen, R. I. and Hemmings, H. C., Jr. (2003). Selective depression by general anesthetics of glutamate versus GABA release from isolated cortical nerve terminals. J Pharmacol Exp Ther *304*, 1188-96.

Whistler, J. L., Enquist, J., Marley, A., Fong, J., Gladher, F., Tsuruda, P., Murray, S. R. and Von Zastrow, M. (2002). Modulation of postendocytic sorting of G protein-coupled receptors. Science *297*, 615-20.

Wilkin, M., Tongngok, P., Gensch, N., Clemence, S., Motoki, M., Yamada, K., Hori, K., Taniguchi-Kanai, M., Franklin, E., Matsuno, K. and Baron, M. (2008). Drosophila HOPS and AP-3 complex genes are required for a Deltex-regulated activation of notch in the endosomal trafficking pathway. Dev Cell *15*, 762-72.

Willets, J. M., Mistry, R., Nahorski, S. R. and Challiss, R. A. (2003). Specificity of g protein-coupled receptor kinase 6-mediated phosphorylation and regulation of single-cell m3 muscarinic acetylcholine receptor signaling. Mol Pharmacol *64*, 1059-68.

Wilson, S. J. and Smyth, E. M. (2006). Internalization and recycling of the human prostacyclin receptor is modulated through its isoprenylation-dependent interaction with the delta subunit of cGMP phosphodiesterase 6. J Biol Chem *281*, 11780-6.

Worby, C. A. and Dixon, J. E. (2002). Sorting out the cellular functions of sorting nexins. Nat Rev Mol Cell Biol *3*, 919-31.

Worzfeld, T., Wettschureck, N. and Offermanns, S. (2008). G(12)/G(13)-mediated signalling in mammalian physiology and disease. Trends Pharmacol Sci *29*, 582-9.

Wruck, C. J., Funke-Kaiser, H., Pufe, T., Kusserow, H., Menk, M., Schefe, J. H., Kruse, M. L., Stoll, M. and Unger, T. (2005). Regulation of transport of the angiotensin AT2 receptor by a novel membrane-associated Golgi protein. Arterioscler Thromb Vasc Biol *25*, 57-64.

Wu, G., Bogatkevich, G. S., Mukhin, Y. V., Benovic, J. L., Hildebrandt, J. D. and Lanier, S. M. (2000). Identification of Gbetagamma binding sites in the third intracellular loop of the M(3)-muscarinic receptor and their role in receptor regulation. J Biol Chem *275*, 9026-34.

Xia, C., Ma, W., Stafford, L. J., Liu, C., Gong, L., Martin, J. F. and Liu, M. (2003). GGAPs, a new family of bifunctional GTP-binding and GTPase-activating proteins. Mol Cell Biol *23*, 2476-88.

Xiao, B., Tu, J. C., Petralia, R. S., Yuan, J. P., Doan, A., Breder, C. D., Ruggiero, A., Lanahan, A. A., Wenthold, R. J. and Worley, P. F. (1998). Homer regulates the association of group 1 metabotropic glutamate receptors with multivalent complexes of homer-related, synaptic proteins. Neuron *21*, 707-16.

Xu, J. and Chuang, D. M. (1987). Muscarinic acetylcholine receptor-mediated phosphoinositide turnover in cultured cerebellar granule cells: desensitization by receptor agonists. J Pharmacol Exp Ther *242*, 238-44.

Xu, Y., Seet, L. F., Hanson, B. and Hong, W. (2001). The Phox homology (PX) domain, a new player in phosphoinositide signalling. Biochem J *360*, 513-30.

Yamada, M., Lamping, K. G., Duttaroy, A., Zhang, W., Cui, Y., Bymaster, F. P., McKinzie, D. L., Felder, C. C., Deng, C. X., Faraci, F. M. and Wess, J. (2001a). Cholinergic dilation of cerebral blood vessels is abolished in M(5) muscarinic acetylcholine receptor knockout mice. Proc Natl Acad Sci U S A *98*, 14096-101.

Yamada, M., Miyakawa, T., Duttaroy, A., Yamanaka, A., Moriguchi, T., Makita, R., Ogawa, M., Chou, C. J., Xia, B., Crawley, J. N., Felder, C. C., Deng, C. X. and Wess, J. (2001b). Mice lacking the M3 muscarinic acetylcholine receptor are hypophagic and lean. Nature *410*, 207-12.

Yan, Z., Song, W. J. and Surmeier, J. (1997). D2 dopamine receptors reduce N-type Ca2+ currents in rat neostriatal cholinergic interneurons through a membrane-delimited, protein-kinase-C-insensitive pathway. J Neurophysiol *77*, 1003-15.

Yan, Z. and Surmeier, D. J. (1997). D5 dopamine receptors enhance Zn2+-sensitive GABA(A) currents in striatal cholinergic interneurons through a PKA/PP1 cascade. Neuron *19*, 1115-26.

Yap, C. C., Wisco, D., Kujala, P., Lasiecka, Z. M., Cannon, J. T., Chang, M. C., Hirling, H., Klumperman, J. and Winckler, B. (2008). The somatodendritic endosomal regulator NEEP21 facilitates axonal targeting of L1/NgCAM. J Cell Biol *180*, 827-42.

Yasuda, R. P., Ciesla, W., Flores, L. R., Wall, S. J., Li, M., Satkus, S. A., Weisstein, J. S., Spagnola, B. V. and Wolfe, B. B. (1993). Development of antisera selective for m4 and m5 muscarinic cholinergic receptors: distribution of m4 and m5 receptors in rat brain. Mol Pharmacol *43*, 149-57.

Yeomans, J., Forster, G. and Blaha, C. (2001). M5 muscarinic receptors are needed for slow activation of dopamine neurons and for rewarding brain stimulation. Life Sci *68*, 2449-56.

Yu, H., Braun, P., Yildirim, M. A., Lemmens, I., Venkatesan, K., Sahalie, J., Hirozane-Kishikawa, T., Gebreab, F., Li, N., Simonis, N., Hao, T., Rual, J. F., Dricot, A., Vazquez, A., Murray, R. R., Simon, C., Tardivo, L., Tam, S., Svrzikapa, N., Fan, C., de Smet, A. S., Motyl, A., Hudson, M. E., Park, J., Xin, X., Cusick, M. E., Moore, T., Boone, C., Snyder, M., Roth, F. P., Barabasi, A. L., Tavernier, J., Hill, D. E. and Vidal, M. (2008). High-quality binary protein interaction map of the yeast interactome network. Science *322*, 104-10.

Zeitelhofer, M., Vessey, J. P., Xie, Y., Tubing, F., Thomas, S., Kiebler, M. and Dahm, R. (2007). High-efficiency transfection of mammalian neurons via nucleofection. Nat Protoc *2*, 1692-704.

Zeng, F. Y. and Wess, J. (1999). Identification and molecular characterization of m3 muscarinic receptor dimers. J Biol Chem *274*, 19487-97.

Zervos, A. S., Gyuris, J. and Brent, R. (1993). Mxi1, a protein that specifically interacts with Max to bind Myc-Max recognition sites. Cell *72*, 223-32.

Zhan, L., Liu, B., Jose-Lafuente, M., Chibalina, M. V., Grierson, A., Maclean, A. and Nasir, J. (2008). ALG-2 interacting protein AIP1: a novel link between D1 and D3 signalling. Eur J Neurosci *27*, 1626-33.

Zhang, H., Craciun, L. C., Mirshahi, T., Rohacs, T., Lopes, C. M., Jin, T. and Logothetis, D. E. (2003). PIP(2) activates KCNQ channels, and its hydrolysis underlies receptor-mediated inhibition of M currents. Neuron *37*, 963-75.

Zhang, H. and Sulzer, D. (2003). Glutamate spillover in the striatum depresses dopaminergic transmission by activating group I metabotropic glutamate receptors. J Neurosci *23*, 10585-92.

Zhang, H. and Sulzer, D. (2004). Frequency-dependent modulation of dopamine release by nicotine. Nat Neurosci *7*, 581-2.

Zhang, W., Basile, A. S., Gomeza, J., Volpicelli, L. A., Levey, A. I. and Wess, J. (2002a). Characterization of central inhibitory muscarinic autoreceptors by the use of muscarinic acetylcholine receptor knock-out mice. J Neurosci *22*, 1709-17.

Zhang, W., Yamada, M., Gomeza, J., Basile, A. S. and Wess, J. (2002b). Multiple muscarinic acetylcholine receptor subtypes modulate striatal dopamine release, as studied with M1-M5 muscarinic receptor knock-out mice. J Neurosci *22*, 6347-52.

Zhou, F. M., Wilson, C. J. and Dani, J. A. (2002a). Cholinergic interneuron characteristics and nicotinic properties in the striatum. J Neurobiol *53*, 590-605.

Zhou, H., Meyer, A., Starke, K., Gomeza, J., Wess, J. and Trendelenburg, A. U. (2002b). Heterogeneity of release-inhibiting muscarinic autoreceptors in heart atria and urinary bladder: a study with M(2)- and M(4)-receptor-deficient mice. Naunyn Schmiedebergs Arch Pharmacol *365*, 112-22.